Spring 5-15-2019

Glycan Precursor Transport in Cryptococcus neoformans

Lucy X. Li
Washington University in St. Louis

WASHINGTON UNIVERSITY IN ST. LOUIS

Division of Biology & Biomedical Sciences
Molecular Microbiology and Microbial Pathogenesis

Dissertation Examination Committee:
Tamara L. Doering, Chair
Stephen M. Beverley
Mario Feldman
Stuart A. Kornfeld
Amanda L. Lewis
Jennifer K. Lodge

Glycan Precursor Transport in *Cryptococcus neoformans*

by
Lucy X. Li

A dissertation presented to
The Graduate School
of Washington University in
partial fulfillment of the
requirements for the degree
of Doctor of Philosophy

May 2019
St. Louis, Missouri

Table of Contents

List of Figures vii
List of Tables ix
Acknowledgments x
Abstract of the Dissertation xiii
Chapter 1: Introduction 1
1.1 *Cryptococcus neoformans* and cryptococcosis 2
1.2 Glycans in *C. neoformans* 3
1.2.1 Capsule 3
1.2.2 Cell wall 5
1.2.3 Glycoproteins 6
1.2.4 Glycolipids 6
1.3 Glycan biosynthesis 7
1.3.1 Monosaccharides and activated sugars 8
1.3.2 Nucleotide sugar transporters 9
1.3.3 Glycosyltransferases 11
1.4 Aim of the present study 12
1.5 References 12
Chapter 2: UDP-glucuronic acid transport is required for cryptococcal virulence 20
2.1 Abstract 21
2.2 Introduction 21
2.3 Results 24
2.3.1 Identification of Uut1as a nucleotide sugar transporter candidate 24
2.3.2 Uut1 localizes to the ER 25
2.3.3 Uut1 is required for capsule synthesis 25
2.3.4 Uut1 is a UDP-glucuronic acid transproter 26
2.3.5 Loss of Uut1 causes defects in cell morphology and stress resistance 28
2.3.6 UDP-glucuronic acid transport is required for virulence 29
2.4 Discussion 30
2.5 Materials and methods 34

2.5.1 Sequence and phylogenetic analysis 34
2.5.2 Cell growth 35
2.5.3 *C. neoformans* strains and plasmids 36
2.5.4 Saccharomyes cerevisae localization 37
2.5.5 Capsule induction and visualization 37
2.5.6 GXM detection 37
2.5.7 Heterologous expression, reconsitution, and transport assays 38
2.5.8 Quantification of nucleotide sugars by mass spectrometry 38
2.5.9 Fungal gene expression 39
2.5.10 Electron microscopy 39
2.5.11 Cell wall staining 40
2.5.12 Macrophage assays 40
2.5.13 Animal studies 41
2.6 Acknowledgments 41
2.7 References 42
2.8 Figures 50
2.9 Supplementary materials 61
Chapter 3: Xylose donor transport is critical for fungal virulence 69
3.1 Abstract 70
3.2 Introduction 70
3.3 Results 73
3.3.1 Identification of cryptococccal UDP-xylose transporters 73
3.3.2 *UXT1* and *UXT2* sequence and expression 75
3.3.3 Uxt1 and Uxt2 localize to distinct subcellular compartments 76
3.3.4 Absence of *UXT1* and *UXT2* has pleiotropic effects on cell morphology and stress resistance 76
3.3.5 Lack of luminal UDP-Xyl alters interactions with host pahogcytes and virulence 77
3.4 Discussion 78
3.5 Materials and methods 82
3.5.1 Sequence and phylogenetic analysis 82
3.5.2 Cell growth 83

3.5.3 *C. neoformans* strains 84
3.5.4 Capsule induction and visualization 84
3.5.5 GXM ELISA 85
3.5.6 Glycan isolation and analysis 85
3.5.7 Heterologous expression, reconsitution, and transport assays 86
3.5.8 Quantification of nucleotide sugars by mass spectrometry 87
3.5.9 Protein localization 87
3.5.10 Fungal gene expression 88
3.5.11 Electron microscopy 89
3.5.12 Macrophage assays 89
3.5.13 Animal studies 90
3.6 Acknowledgments 91
3.7 References 92
3.8 Figures 97
3.9 Supplementary materials 104
Chapter 4: *Cryptococcus neoformans* evades pulmonary immunity by modulating xylose transport 120
4.1 Introduction 121
4.2 Results 122
4.2.1 UDP-Xyl transport is required for cryptococcal virulence and dissemination 122
4.2.2 Induction of a Th2 cytokine response is independent of cryptococcal xylosylation 123
4.2.3 Inducible bronchial-associated lymphoid tissue deveops following cryptococcal infection 124
4.2.4 Cryptococcal-induced iBALT recruits increased T and B cells at late time points 126
4.2.5 Survival of *uxt1*Δ *uxt2*Δ-infected mice is dependent on T cells 126
4.2.6 Lack of luminal xylose modification in *C. neoformans* stimulates DC activation 127
4.3 Discussion 128
4.4 Materials and methods 131
4.4.1 Fungal strains 131
4.4.2 Mice 131

4.4.3 Ethics statement 131
4.4.4 *C. neoformans* inoculation 132
4.4.5 Organ burden and cytokines 132
4.4.6 Immunofluorescence staining and histologic analysis 133
4.4.7 Flow analysis 133
4.4.8 Isolation of bone marrow derived cells 134
4.4.9 Dendritic cell assays 134
4.4.10 Statistical analysis 135
4.5 Acknowledgments 135
4.6 References 136
4.7 Figures 139
4.8 Supplementary materials 147
Chapter 5: Conclusions and future directions 149
5.1 Overview 150
5.2 Summary of major findings 151
5.2.1 Uut1 is a UDP-glucuronic acid transporter 151
5.2.2 Uxt1 and Uxt2 are UDP-xylose/UDP-galactofuranose transporters 152
5.2.3 *C. neoformans* xylose transport influences the host immune response 153
5.3 Open questions 154
5.3.1 Nucleotide sugar transporter structure and function relationship 154
5.3.2 Nucleotide sugar transporter regulation 155
5.3.3 Additional nucleotide sugar transporter candidates 157
5.3.4 Glycan repertoire of *C. neoformans* 158
5.4 Impact and closing remarks 159
5.5 References 161
Appendix A: *Cryptococcus neoformans UGT1* encodes a UDP-galactose/UDP-GalNAc transporter 163
Appendix B: Other nucleotide sugar transporter candidates 204
B.1 NST_G 205
B.2 NST_J 206
B.3 NST_L 206

B.4 NST_X 207
B.5 Future directions 209
B.6 References 209
B.7 Figures 211

List of Figures

Figure 2.1. Evolutionary conservation of UDP-GlcA transporters 50
Figure 2.2. Cryptococcal Uut1 colocalizes with the ER marker Kar2p/BiP, but not with the Golgi marker Sec7 51
Figure 2.3. The *uut1*Δ mutant does not produce capsule 52
Figure 2.4. Uut1 activity *in vitro* 54
Figure 2.5. UDP-GlcA metabolism 56
Figure 2.6. Transcription of *UUT1* increases during capsule induction 57
Figure 2.7. *uut1*Δ mutants exhibit defects in cell morphology and growth 58
Figure 2.8. Cells lacking Uut1 are more efficiently phagocytosed and killed by human cells than WT *C. neoformans* 59
Figure 2.9. *uut1*Δ is severely attenuated for virulence 60
Figure 2.S1. Predicted secondary structure of Uut1 61
Figure 2.S2. Anti-V5 immunoblot of proteoliposomes prepared from *S. cerevisiae* expressing vector alone (control) or V5-tagged Uut1 62
Figure 2.S3. Surface exposure of cell wall components 63
Figure 2.S4. GXM is not detectable within or around *uut1*Δ cells 64
Figure 2.S5. Growth of *uut1*Δ is restricted at 37°C and at 30°C under nutrient-limiting conditions 65
Figure 2.S6. The human UDP-GlcA transporter does not complement *uut1*Δ 66
Figure 2.S7. *uut1*Δ does not disseminate from the lung 67
Figure 3.1. Capsule characteristics of *uxt* mutants 97
Figure 3.2. Uxt1 and Uxt2 *in vitro* transport activities 98
Figure 3.3. Transcription of *UXT2* but not *UXT1* increases during capsule induction 100
Figure 3.4. Subcellular localization of Uxt1 and Uxt2 101
Figure 3.5. *uxt1*Δ and *uxt1*Δ *uxt2*Δ mutants exhibit growth and capsule defects 102
Figure 3.6. UDP-xylose transport is required for host interactions and virulence 103
Figure 3.S1. Conservation of cryptococcal nucleotide sugar transporter 104
Figure 3.S2. *uxt1*Δ *uxt2*Δ is recognized by xylose-independent capsule antibodies 106
Figure 3.S3. Uxt1- and Uxt2-mediated UDP-Gal*f* uptake into proteoliposomes 108
Figure 3.S4. *uxt1*Δ *uxt2*Δ growth is restricted at 37 °C 110
Figure 3.S5. orphological defects of *uxt1*Δ *uxt2*Δ 111
Figure 3.S6. *uxt1*Δ *uxt2*Δ is severely attenuated for virulence in C57BL/6 mice 113
Figure 3.S7. *uxt1*Δ *uxt2*Δ does not colonize extrapulmonary sites 114
Figure 3.S8. *UXT1* and *UXT2* transcription levels 115
Figure 3.S9. Nucleotide sugar uptake into Gmt1- and Gmt2- containing proteoliposomes 116
Figure 4.1. Fungal burden and cytokine responses in WT- and *uxt1*Δ *uxt2*Δ- infected mice 139
Figure 4.2. Inflammation and iBALT formation during *C. neoformans* infection 141

Figure 4.3. Increased T and B cell population in *uxt1*Δ *uxt2*Δ infection is required to prevent disease progression 143
Figure 4.4. Cytokine production by dendritic cells 145
Figure 4.S1. Representative data from the multi-color flow cytometry gating strategy used to quantify the indicated immune cell subsets 147
Figure A.1. Phylogenetic relationships of cryptococcal Ugt1 and human NSTs with known substrates 192
Figure A.2. Topology of *C. neoformans* Ugt1 as predicted by TMHMM server v 2.0 193
Figure A.3. The cryptococcal UDP-Gal transporter localizes with a Golgi marker and is functional in mammalian cells 194
Figure A.4. Ugt1 transports UDP-Gal and UDP-GalNAc 195
Figure A.5. Transcription of *UGT1* and *UGE1* increases during capsule induction 196
Figure A.6. *ugt1*Δ mutants show altered capsule and cellular morphology, and exhibit growth and mating defects 197
Figure A.7. N- and C- terminal Ugt1 truncations complement capsule and cellular morphology defects in *ugt1*Δ 198
Figure A.8. Cells lacking Ugt1 are more efficiently phagocytosed and killed by THP-1 cells than WT *C. neoformans* 199
Figure A.S1. Protein sequence alignment of *C. neoformans* Ugt1 with other UDP-Gal transporters 202
Figure A.S2. Cryptococcal Ugt1 colocalizes with a Golgi enzyme 203
Figure B.1. NST_G and NST_X deletion mutants are hypocapsular compared to WT 211
Figure B.2. Transcription of NST_G, NST_J, NST_L, and NST_X during capsule induction 211
Figure B.3. Intracellular survival of cells lacking NST_G resembles that of WT *C. neoformans*. 212
Figure B.4 Mice infected with nst_GΔ and nst_LΔ are delayed in time of death compared to those infected with WT cryptococci 212
Figure B.5. Uxt1- and Uxt2-mediated UDP-Gal*f* uptake into proteoliposomes 213
Figure B.6. nst_LΔ growth is not restricted at 37 °C 215
Figure B.7. Intracellular survival of cells lacking NST_L resembles that of WT *C. neoformans*. 216
Figure B.8. nst_XΔ growth is delayed in the presence of THP-1s 216
Figure B.9. nst_XΔ is cleared by 7 dpi in mice 217
Figure B.10. hCST partially rescues nst_XΔ growth on SDS 217
Figure B.11. Transport activity of hCST is not required to rescue nst_XΔ growth at 30 °C 218

List of Tables

Table 2.S1. Summary of GXM detection assays 68
Table 2.S2. Uut1 content of proteoliposomes used for transport assays 68
Table 3.S1. Methylation analysis of GXM for the indicated strains 118
Table 3.S2. Staining and stress sensitivity of *Cryptococcus neoformans* strains 118
Table 3.S3. Nucleotide sugar contents of *Cryptococcus neoformans* strains 119
Table 3.S4. Uxt1 and Uxt2 content of proteoliposomes used for transport assays 119
Table 4.S1. *C. neoformans* strains utilized in these studies 148
Table 4.S2. Flow analysis antibodies 148
Table A.1. *C. neoformans* strains used in these studies 200
Table A.2. Primers used for modification of or expression in *C. neoformans* 200
Table A.3. Ugt1 truncations and their ability to complement UDP-Gal transport 201
Table A.4. Primers used to generate truncation constructs for Lec8 expression 201
Table B.1. Capsule and cell wall phenotypes 219
Table B.2. Glycosyl composition analysis of GXM 219
Table B.3. Dot plating phenotypes 220

Acknowledgments

My deepest thanks to my advisor, Tamara Doering, for the guidance, encouragement, and advice that she has provided throughout my time as her student. I have learned more than I could have imagined—not just about science but also about how to communicate that understanding and how to approach problems and discover interesting questions. She has challenged me to be a better scientist and a more critical thinker, and I have her to thank for my successes.

I am also grateful to my thesis committee (Dr. Jennifer Lodge, Dr. Stephen Beverley, Dr. Mario Feldman, Dr. Stuart Kornfeld, and Dr. Amanda Lewis) for their insights and guidance. They have made my science more rigorous and me a better researcher.

Furthermore, I thank all the members, past and present, of the Doering laboratory that made graduate school more bearable and (on the rare occasion) fun: Daniel Agustinho, Holly Brown, Andrew Chang, Stacey Gish, Camaron Hole, Liza Miller, Felipe Santiago, and Matt Williams. I was especially lucky to share a bay with Felipe who provided insightful scientific suggestions and a healthy dose of common sense.

I am grateful to the friends that helped me to have a life outside of science and sustained me through graduate school: Yedda, Meghan, Andy, Alyssa, Ashley, Claire, Victoria, Melissa, and Sarah. A special acknowledgement goes to Yedda who has lent me a many a patient ear even when she was buried in experiments and in hours of piano practice. Our friendship has been full of music, mice, mischief, and ice cream!

Last but foremost, thank you to my parents, Jenny Zhang and Yabo Li, for all their love and unwavering support. They have always been there when I needed them most, and without them, I would not have gotten through graduate school. They have been my loudest cheerleaders, my biggest supporters, my willing (and unwilling) audience, and my voices of reason. Thank you

for imparting a sense of curiosity and wonder and instilling the motivation to work hard. Thank you for believing in me.

Lucy X. Li

Washington University in St. Louis

May 2019

Dedicated to my parents for their unwavering support.

ABSTRACT OF THE DISSERTATION

Glycan Precursor Transport in *Cryptococcus neoformans*

by

Lucy X. Li

Doctor of Philosophy in Biology and Biomedical Sciences

Molecular Microbiology and Microbial Pathogenesis

Washington University in St. Louis, 2019

Professor Tamara L. Doering, Chair

Glycans play diverse biological roles, ranging from structural and regulatory functions to mediating cellular interactions. For pathogens, they are also often required for virulence and survival in the host. Our interest in glycoconjugates stems from their role in the fungal pathogen *Cryptococcus neoformans*. This yeast colonizes the lungs and disseminates to the brain of immunocompromised individuals, where it causes a meningoencephalitis that is frequently lethal, killing almost 200,000 people each year. The major virulence factor of this yeast is a polysaccharide capsule that enables it to manipulate the host immune response and resist host antimicrobial defenses.

Synthesis of the capsular glycans and other critical glycoconjugates occurs primarily in the secretory compartment, although almost all activated precursors are made in cytosol. This topological problem is resolved by nucleotide sugar transporters (NSTs), which are thus required for such glycosylation. The identity and regulation of the complete set of cryptococcal NSTs, however, remain elusive. This major gap in our knowledge severely limits our understanding of and ability to manipulate critical biosynthetic processes in this important pathogen.

Here, we identified three novel NSTs and determined their kinetic profiles and roles in cryptococcal biology. Uut1 is a high-affinity ER-localized UDP-glucuronic acid (UDP-GlcA) transporter, and Uxt1 and Uxt2 are dual UDP-xylose (UDP-Xyl) transporters found in the Golgi apparatus and endoplasmic reticulum, respectively. Mutants lacking these proteins exhibited compositional changes in their glycoconjugates, including the capsule, increased sensitivity to stress, and altered interactions with phagocytes. UDP-GlcA and UDP-Xyl transport activities were also required for full virulence. Interestingly, UDP-Xyl transport was not required for persistence within the host, as the double *uxt1*Δ *uxt2*Δ mutant established a chronic infection of the lung and induced delayed formation of tertiary lymphoid tissue. Collectively, this work advanced our understanding of the localization and sequence of glycan biosynthetic events, and their relationship to virulence. It also set the stage for further studies of fundamental glycobiology, cryptococcal biology and pathogenesis, and potential antifungal agents.

Chapter 1: Introduction

Partially adapted from:

Unraveling synthesis and remodeling of the cryptococcal cell wall and capsule

Zhuo A. Wang,[*] Lucy X. Li,[*] and Tamara L. Doering ([*]co-first authors)

Glycobiology 2018, 28(10):719-730. doi: 10.1093/glycob/cwy030. PMID: 29648596.

1.1 *Cryptococcus neoformans* and cryptococcosis

Cryptococcus neoformans, an environmentally ubiquitous encapsulated fungus, causes serious respiratory disease in the setting of immune compromise, which often progresses to a lethal meningoencephalitis. Even with treatment, *C. neoformans* can establish a persistent infection due to inadequate primary therapy, development of fluconazole resistance, or the failure of antifungals to penetrate the infection space. Cryptococcal meningitis is responsible for 15% of AIDS-related mortality, making it the second most common cause of death in this population (1). Each year there are over a million cases of disease worldwide, resulting in almost 200,000 deaths (1-3).

Cryptococcosis is initially acquired by inhaling fungal cells or spores into the lower respiratory tract, where the infectious particles lodge within alveoli (4). There, alveolar macrophages are the first responders to and primary controllers of cryptococcal infection (5). In healthy individuals, phagocytosis of the fungi by these cells usually results in their death within the phagolysosome and the resolution of infection (6), but *C. neoformans* can also become latent and reactivate if the individual becomes immunosuppressed. The exact mechanism that enables development of latency remains an open question, although yeast cells appear to evade immune detection by remaining dormant (7). In immunocompromised patients, phagocytes also provide an intracellular niche for *C. neoformans* to replicate, which eventually leads to host cell lysis. This can promote fungal dissemination, which has a particular tropism for the brain, where it causes a life-threatening infection (8).

Glycans, like those of the cryptococcal capsule and cell wall, are attractive antifungal targets because they are often required by pathogens for virulence and survival in the host. They also play

a diverse set of essential biological roles, ranging from structural and regulatory functions to mediating cellular interactions (9). The newest class of antimycotic drugs exploits fungal dependence on glycans by inhibiting cell wall polysaccharide synthesis with rapid, broad fungicidal effect, but it unfortunately lacks clinical activity against *C. neoformans* (10). Our ability to manipulate these crucial determinants of fungal survival and pathogenesis in *C. neoformans* is limited by our lack of knowledge about how they are synthesized.

1.2 Glycans in *C. neoformans*

C. neoformans has an extensive glycoconjugate repertoire that is critically important for pathogenesis, encompassing a polysaccharide-based capsule and cell wall, in addition to typical eukaryotic glycoconjugates like glycoproteins and glycolipids. Although this glycan profile is often compared to the much less complex one of the distantly related model fungus, *Saccharomyces cerevisiae*, it exhibits marked genetic and metabolic differences. By defining cryptococcal glycosylation, we can develop novel therapeutic and diagnostic strategies that exploit its unique biology.

1.2.1 Capsule

The definitive virulence factor of *C. neoformans* is the polysaccharide capsule. Upon exposure to environmental stress (e.g. host conditions), the complex capsule polymers are synthesized and associate with the outer side of the cryptococcal cell wall to create a protective layer that impedes phagocytosis and immune mediator binding (11). Capsule material is also continually shed into the extracellular space where it suppresses the host immune response and interferes with normal cytokine release and leukocyte migration (12).

The unique capsule structure is mainly composed of the polysaccharides glucuronoxylomannan (GXM) and glucuronoxylomannogalactan (GXMGal), with trace amounts of mannoproteins. GXM (1,700-7,000 kDa) accounts for 90% of the capsule mass (13, 14), and consists of an α-1,3-linked mannose (Man) backbone substituted with single β-1,2 glucuronic acid (GlcA), and β-1,2 and β-1,4-xylose (Xyl) residues (13, 15). NMR analysis of capsule polymers has defined six distinct structural reporter groups of GXM that differ in the number of Xyl and 6-*O*-acetylation modifications on the Man backbone (13). The differences in the relative proportion of these structural motifs in different serotypes help produce the distinct antigenic properties of GXM from those strains (16).

GXMGal is relatively small (~100 kDa) in comparison to GXM and comprises the remaining 10% of the capsule mass. This glycan consists of an α-1,6 linked galactose (Gal) backbone modified with galactomannan side chains containing a variable number of β-linked GlcA and Xyl residues (17), and 80% of the Man residues bear either an *O*-2 or *O*-6-linked acetyl group (18). Rare galactofuranose (Gal*f*) modifications also decorate the Gal backbone (18-21).

Besides the two polysaccharides, mannoproteins (MPs) are a minor component of the capsule (<1% capsule mass). Hyaluronic acid, a polymer of GlcA and GlcNAc disaccharides, is also detected at the interface of the capsule and cell wall (22, 23), and several studies also suggest that sialic acid and hyaluronic acid may exist in the capsule (24), although their presence and possible roles in capsule remain unclear.

1.2.2 Cell wall

Fungal cell walls provide a critical protective barrier against extracellular stress and regulate cellular permeability (25). Mutants with defective cell walls are typically reduced in viability and often avirulent (26). The cryptococcal cell wall primarily consists of an extensive matrix of glucan (α- and β- linked), chitin, and chitosan associated with glycoproteins that is organized into a striated dense inner layer and a looser more particulate outer one (27).

Extended α-1,3- and β-1,6-glucan polymers constitute the majority of the cryptococcal cell wall (28). β-1,3-glucans comprise less than 10% of the cell wall polysaccharides, which contrasts with the extensive β-1,3-glucan content of cell walls in other yeast species (29). The glucans are further reinforced by covalent linkages to chitin polymers, which consist of linear chains of β-1,4-linked *N*-acetylglucosamine (GlcNAc). This helps to maintain cellular integrity and resist environmental stress. A large portion of the chitin is deacetylated to produce chitosan, which lends greater flexibility to the cell wall (30). The high chitosan level is another unique feature of *C. neoformans* cell walls.

Glycoproteins (Section 1.2.3), modified by *N*- and/or *O*-linked oligosaccharides, are also incorporated into this network of carbohydrate fibers. These proteins regulate cellular integrity by controlling porosity and mediate remodeling of this dynamic structure to accommodate cellular growth and division, and capsule synthesis (27). Over half of these proteins are modified by a glycosylphosphatidylinositol (GPI, Section 1.2.4) anchor in the endoplasmic reticulum (ER). They then either remain membrane associated or are transferred with part of the anchor to be co-

valently linked to cell wall glucans (31-33), some in only a transient fashion before being cleaved and released into the surrounding medium.

1.2.3 Glycoproteins

Glycan modifications found on cryptococcal proteins have not been completely characterized, but are high in mannose content and are structurally similar to those found in *S. cerevisiae. N*-glycans, which consist of an oligosaccharide core linked to asparagine residues, are the most common eukaryotic glycan modification on proteins (34). The basic mannose structures in *C. neoformans* are extended by the addition of short α1,6-Man(α1,2)-Man chains, and by the unusual incorporation of single β1,2- linked Xyl and Xyl-phosphate residues (35). Abrogating these outer chain processing events slightly attenuates virulence, potentially by altering host-fungus interactions (35).

O-glycans, in all yeasts and filamentous fungi studied so far, are synthesized by α-linkage of a mannose to serine or threonine followed by extension into a mannotriose (36). In *C. neoformans* additional Man and Xyl residues further modify this core structure (37). These *O*-glycans are critical for the stability, proper localization, and efficient function of secretory and membrane proteins, which impact numerous essential cellular processes (38).

1.2.4 Glycolipids

Glycolipids consist of one or more monosaccharides joined to a lipid by a glycosidic linkage and are classified by the nature of lipid moiety: glycosphingolipids contain a ceramide while glycoglycerolipids have a conserved diacylglycerol or related structure. Long considered integral

structural components of the cell membrane, the former are also key regulators of pathogenicity, and are required for cellular growth and resistance to alkaline conditions, and spore production and germination (39). The ceramide structure can vary in length, hydroxylation, and saturation (40), and there is a range of glycan components. Glucosylceramide (GlcCer), for instance, consists of a single glucose moiety covalently bound to a sphingoid backbone and fatty acid, and is critical for extracellular survival (41), while those sphingolipids bearing a mannose or inositol facilitate phagolysosome survival and replication (42-44). Glycoinositolphosphorylceramides (GIPCs), cryptococcal glycosphingolipids not present in mammals, span the range of relatively simple mannose-containing structures to more complex ones that also incorporate Xyl and Gal (45-47). They are essential mediators of proper cell cycle progression in non-acidic and elevated CO_2 environments, which are conditions that are present in the host (41).

GPIs are a distinct family of glycolipids that link proteins to the external leaflet of the plasma membrane. The structure consists of a conserved linear core of three Man and a non-acetylated glucosamine, which is covalently linked to an inositol phospholipid and the C-terminus of the polysaccharide (48). GPI modification modulates the movement, localization, and cleavage and release of the attached protein (49).

1.3 Glycan biosynthesis

Capsule polysaccharides and other cryptococcal glycoconjugates are assembled in the secretory pathway. However, nucleotide sugars, which donate individual sugar moieties to growing glycan structures, are synthesized primarily in the cytosol (50). Only a small fraction of cytosolic glycan precursors is consumed in that compartment, primarily for cell wall construction by plasma

membrane-bound glucan synthases and chitin synthase (27). The majority is translocated into the secretory pathway where glycosyltransferases facilitate the transfer of the sugar from the activated donor to modify nascent proteins and lipids, and form the protective capsule (34, 51).

1.3.1 Monosaccharides and activated sugars

Based on compositional studies of capsule glycans and glycoproteins, we know that GDP-Man, UDP-Gal, UDP-GlcA, UDP-Xyl and UDP-Gal*f* are required to synthesize complex polysaccharide structures in the secretory pathway. The synthetic pathways of these precursors are fairly well understood. In *C. neoformans* and other fungi, GDP-Man is synthesized through the sequential action of phosphomannose isomerase, phosphomannomutase, and GDP-Man pyrophosphorylase on fructose-6-phosphate (52). This sugar phosphate is also converted to UDP-GlcNAc through a series of transamination, *N*-acetylation, isomerization, and phosphorylation reactions. The other nucleotide sugars mentioned above are all generated from UDP-Glc, which is synthesized in two steps from glucose-6-phosphate by phosphoglucomutase followed by UDP-Glc pyrophosphorylase. Uge1, a UDP-glucose 4-epimerase, converts UDP-Glc to UDP-Gal, which may be further modified by UDP-galactopyranose mutase, Glf1, to produce UDP-Gal*f* (53). Lastly, UDP-Glc is also dehydrogenated by Ugd1 to generate UDP-GlcA; this in turn may be decarboxylated by Uxs1 to form UDP-Xyl (54, 55).

Disrupting synthesis of any of the nucleotide sugars mentioned above markedly alters the structure and composition of glycoconjugates in *C. neoformans*, with significant consequences. Deletion of *MAN1*, which encodes the phosphomannose isomerase (52), or of *UGD1*, which completely abrogates synthesis of UDP-GlcA and thus UDP-Xyl (56), inhibits capsule formation and

polysaccharide secretion, and causes morphological abnormalities. Deletion of *UXS1* specifically interrupts UDP-Xyl biosynthesis, and the mutant displays markedly reduced capsules as compared to wild type (56, 57). Mutants lacking Uge1 are, as would be expected, unable to synthesize GXMGal, but surprisingly, despite completely lacking 10% of the capsule material, they exhibit enlarged capsules (58). This supports a model where GXMGal participates in capsule polysaccharide organization, so that its absence yields a looser, and therefore more voluminous, structure. Mutants in these pathways, unsurprisingly, are all avirulent in mice (52, 56, 57, 59, 60), except for the mutant that lacks UDP-Gal*f* synthesis. NMR analysis of capsule glycans isolated from *glf1*Δ cells confirm the absence of Gal*f* in GXMGal despite no visible changes in capsule size or organization, and no detectable defects in virulence or survival (21), possibly because this sugar is only present at low levels.

1.3.2 Nucleotide sugar transporters

Although some UDP-Glc and UDP-GlcNAc is utilized in the cytosol for glucan and chitin synthesis, as mentioned above, most nucleotide sugars must gain access to the secretory pathway, where the majority of glycan biosynthesis reactions occur. The ER and Golgi membranes constitute physical barriers that prevent activated sugars from accessing biosynthetic enzymes. Nucleotide sugar transporters (NSTs) provide a solution to this topological problem, by translocating activated sugars into the secretory pathway in exchange for the corresponding nucleoside monophosphates (61-63). They are predicted to have an even number of transmembrane domains (6-10) with both termini present on the cytosolic side. The C-terminus appears to mediate homodimerization and protein stability (64), and the N-terminus may encode a localization signal. The cytosolic domains are usually responsible for binding a single type of nucleotide although a few

NSTs have been reported to recognize both UDP and GDP (65, 66). Transport activity is further restricted by interactions with the sugar portion of the activated donor (67, 68).

Identification of novel NSTs and determination of their precise biochemical function is limited by our inability to reliably predict NST specificity from primary sequences. A few limited NST sequence motifs have been associated with specific substrates (69), but NSTs with ~50% amino acid identity may still transport distinct substrates while others with ~20% identity may translocate the same one (70). Cells may also express several NSTs with overlapping specificity but non-identical substrate affinities and kinetics. Some transporters are highly selective for a specific substrate, while others transport as many as four nucleotide sugars (65, 68, 71-79). Further complicating the picture, association with glycan synthetic enzymes and subcellular localization may also influence the activity of a given transporter (80, 81). Determining NST substrate(s) thus requires biochemical demonstration of activity. All of these factors make it a challenge to determine the full complement of cryptococcal NSTs, impeding our ability to fully define critical glycan synthetic processes.

We initially identified ten NST candidates in the cryptococcal genome based on sequence analysis, but for the reasons above we could not assign substrates based on homology. Deletion of two candidates that were homologous to the *S. cerevisiae* GDP-Man transporter enabled identification of two functionally redundant GDP-Man transporters, Gmt1 and Gmt2 (32, 82). Cells deleted for only one of the corresponding genes still produce and display capsule although the capsule of *gmt1*Δ, but not *gmt2*Δ, is smaller than that of wild type. This result suggests that Gmt1 is the major transporter of the pair, although there is functional overlap. Loss of both genes disrupted

protein mannosylation and the accumulation of any detectable capsule material on the cell surface, similar to the phenotype of mutants incapable of synthesizing GDP-Man. There appears to be only a single UDP-Gal transporter in *C. neoformans* (58), which was assayed biochemically to exhibit the expected transport activity (83). Completely interrupting the transport of these two nucleotide sugars, either through double or single knockouts as appropriate, disrupted capsule polysaccharide production and left the mutant cells unable to cause disease (56, 58, 81, 83). Determining the specificity of the remaining seven NST candidates and their contribution to virulence and survival was the focus of my thesis work.

1.3.3 Glycosyltransferases

Once nucleotide sugars are transported into the luminal space, glycosyltransferases utilize the nucleotide sugars as donors to initiate and extend sugar polymers. Completed glycan structures are then trafficked to the proper cell compartment or surface, likely through the classical secretory pathway. Glycosyltransferases are generally specific for a particular sugar donor, acceptor, and type of linkage created (34). The complexity of cryptococcal glycan structures such as capsule polysaccharides suggests that a variety of glycosyltransferases are required for proper synthesis. However, we have only identified one glycosyltransferase implicated in capsule synthesis (84), although more than 70 glycosyltransferase candidates exist in the cryptococcal genome. Unfortunately, sequence analysis is an unreliable predictor of function for glycosyltransferases, and functional redundancy is common among this family of proteins. This increases the challenge of elucidating function through homology and genetic disruption.

1.4 Aim of the present study

At the time I began my thesis work, the only NSTs identified in *C. neoformans* were those for GDP-Man and UDP-Gal (58, 81-83). This failed to account for the precursors of acidic monosaccharides such as GlcA and sialic acid, or of other moieties like Xyl that are incorporated into protein- and lipid-linked glycans, and the capsule. I have investigated NST candidates identified by homology to known transporters in other organisms. I sought to demonstrate their transport activity and correlate those data with changes in glycoconjugate composition, as well as ascertain the role of these NSTs in growth, stress resistance, and resistance to internalization and clearance. For some transporters I also analyzed the host response to understand changes in disease dynamics as measured by virulence and organ burden. Together this work aimed to advance our understanding of glycan biosynthesis to address critical questions of fundamental glycobiology and cryptococcal pathogenesis.

1.5 References

1. Rajasingham R, *et al.* (2017) Global burden of disease of HIV-associated cryptococcal meningitis: an updated analysis. *Lancet Infect Dis*.

2. Kwon-Chung KJ, *et al.* (2014) *Cryptococcus neoformans* and *Cryptococcus gattii*, the etiologic agents of cryptococcosis. *Cold Spring Harb Perspect Med* 4(7):a019760.

3. Denning DW (2016) Minimizing fungal disease deaths will allow the UNAIDS target of reducing annual AIDS deaths below 500 000 by 2020 to be realized. *Philos Trans R Soc Lond B Biol Sci* 371(1709).

4. Ellis DH & Pfeiffer TJ (1990) Ecology, life cycle, and infectious propagule of *Cryptococcus neoformans*. *Lancet* 336(8720):923-925.

5. McQuiston TJ & Williamson PR (2012) Paradoxical roles of alveolar macrophages in the host response to Cryptococcus neoformans. *J Infect Chemother* 18(1):1-9.

6. Levitz SM, *et al.* (1999) Cryptococcus neoformans resides in an acidic phagolysosome of human macrophages. *Infect Immun* 67(2):885-890.

7. Garcia-Hermoso D, Janbon G, & Dromer F (1999) Epidemiological evidence for dormant *Cryptococcus neoformans* infection. *J Clin Microbiol* 37(10):3204-3209.

8. Feldmesser M, Kress Y, Novikoff P, & Casadevall A (2000) Cryptococcus neoformans is a facultative intracellular pathogen in murine pulmonary infection. *Infect Immun* 68(7):4225-4237.

9. Cummings RD & Doering TL (2009) Fungi. *Essentials of Glycobiology*, eds Varki A, Cummings RD, Esko JD, Freeze HH, Stanley P, Bertozzi CR, Hart GW, & Etzler MECold Spring Harbor (NY)), 2nd Ed.

10. Balkovec JM, *et al.* (2014) Discovery and development of first in class antifungal caspofungin (CANCIDAS(R))--a case study. *Nat Prod Rep* 31(1):15-34.

11. Doering TL (2009) How sweet it is! Cell wall biogenesis and polysaccharide capsule formation in *Cryptococcus neoformans*. *Annu Rev Microbiol* 63:223-247.

12. Vecchiarelli A, *et al.* (2013) Elucidating the immunological function of the *Cryptococcus neoformans* capsule. *Future Microbiol* 8(9):1107-1116.

13. Cherniak R, Valafar H, Morris LC, & Valafar F (1998) *Cryptococcus neoformans* chemotyping by quantitative analysis of 1H nuclear magnetic resonance spectra of glucuronoxylomannans with a computer-simulated artificial neural network. *Clin Diagn Lab Immunol* 5(2):146-159.

14. McFadden DC, De Jesus M, & Casadevall A (2006) The physical properties of the capsular polysaccharides from *Cryptococcus neoformans* suggest features for capsule construction. *J Biol Chem* 281(4):1868-1875.

15. Turner SH, Cherniak R, Reiss E, & Kwon-Chung KJ (1992) Structural variability in the glucuronoxylomannan of *Cryptococcus neoformans* serotype A isolates determined by 13C NMR spectroscopy. *Carbohydr Res* 233:205-218.

16. Fries BC, Goldman DL, Cherniak R, Ju R, & Casadevall A (1999) Phenotypic switching in Cryptococcus neoformans results in changes in cellular morphology and glucuronoxylomannan structure. *Infect Immun* 67(11):6076-6083.

17. Heiss C, Klutts JS, Wang Z, Doering TL, & Azadi P (2009) The structure of *Cryptococcus neoformans* galactoxylomannan contains beta-D-glucuronic acid. *Carbohydr Res* 344(7):915-920.

18. Previato JO, *et al.* (2017) Distribution of the O-acetyl groups and beta-galactofuranose units in galactoxylomannans of the opportunistic fungus *Cryptococcus neoformans*. *Glycobiology* 27(6):582-592.

19. Vaishnav VV, Bacon BE, O'Neill M, & Cherniak R (1998) Structural characterization of the galactoxylomannan of *Cryptococcus neoformans* Cap67. *Carbohydr Res* 306(1-2):315-330.

20. De Jesus M, Nicola AM, Rodrigues ML, Janbon G, & Casadevall A (2009) Capsular localization of the *Cryptococcus neoformans* polysaccharide component galactoxylomannan. *Eukaryot Cell* 8(1):96-103.

21. Heiss C, *et al.* (2013) Unusual galactofuranose modification of a capsule polysaccharide in the pathogenic yeast *Cryptococcus neoformans*. *J Biol Chem*.

22. Jong A, *et al.* (2007) Identification and characterization of *CPS1* as a hyaluronic acid synthase contributing to the pathogenesis of *Cryptococcus neoformans* infection. *Eukaryot Cell* 6(8):1486-1496.

23. Chang YC, Jong A, Huang S, Zerfas P, & Kwon-Chung KJ (2006) CPS1, a homolog of the *Streptococcus pneumoniae* type 3 polysaccharide synthase gene, is important for the pathobiology of *Cryptococcus neoformans*. *Infect Immun* 74(7):3930-3938.

24. Gahrs W, Tigyi Z, Emody L, & Makovitzky J (2009) Polarization optical analysis of the surface structures of various fungi. *Acta Histochem* 111(4):308-315.

25. Free SJ (2013) Fungal cell wall organization and biosynthesis. *Adv Genet* 81:33-82.

26. Gilbert NM, Lodge JK, & Specht CA (2011) The cell wall of *Cryptococcus*. *Cryptococcus, from human pathogen to model yeast* eds Heitman J, Kozel TR, Kwon-Chung J, Perfect J, & Casadevall A (ASM Press, Washington, D.C), p 620.

27. Gilbert NM, Lodge JK, & Specht CA (2011) The Cell Wall of *Cryptococcus*. *Cryptococcus From Human Pathogen to Model Yeast*, eds Heitman J, Kozel TR, Kwon-Chung KJ, Perfect J, & Casadevall A (ASM Press, Washington), pp 67-79.

28. Bose I, Reese AJ, Ory JJ, Janbon G, & Doering TL (2003) A yeast under cover: the capsule of *Cryptococcus neoformans*. *Eukaryot Cell* 2(4):655-663.

29. Bose I & Doering TL (2011) Efficient implementation of RNA interference in the pathogenic yeast *Cryptococcus neoformans*. *J Microbiol Methods* 86(2):156-159.

30. Banks IR, *et al.* (2005) A chitin synthase and its regulator protein are critical for chitosan production and growth of the fungal pathogen *Cryptococcus neoformans*. *Eukaryot Cell* 4(11):1902-1912.

31. Rodrigues ML & Djordjevic JT (2012) Unravelling secretion in *Cryptococcus neoformans*: more than one way to skin a cat. *Mycopathologia* 173(5-6):407-418.

32. Wang ZA, *et al.* (2014) The dual GDP-mannose transporters of Cryptococcus neoformans and their role in biology and virulence. *Eukaryot Cell*.

33. Pittet M & Conzelmann A (2007) Biosynthesis and function of GPI proteins in the yeast *Saccharomyces cerevisiae*. *Biochim Biophys Acta* 1771(3):405-420.

34. Rini J, Esko J, & Varki A (2009) Glycosyltransferases and Glycan-processing Enzymes. *Essentials of Glycobiology*, eds Varki A, Cummings RD, Esko JD, Freeze HH, Stanley P, Bertozzi CR, Hart GW, & Etzler MECold Spring Harbor (NY)), 2nd Ed.

35. Park JN, *et al.* (2012) Unraveling unique structure and biosynthesis pathway of N-linked glycans in human fungal pathogen *Cryptococcus neoformans* by glycomics analysis. *J Biol Chem* 287(23):19501-19515.

36. Gemmill TR & Trimble RB (1999) Overview of N- and O-linked oligosaccharide structures found in various yeast species. *Biochim Biophys Acta* 1426(2):227-237.

37. Lee DJ, Bahn YS, Kim HJ, Chung SY, & Kang HA (2015) Unraveling the novel structure and biosynthetic pathway of O-linked glycans in the Golgi apparatus of the human pathogenic yeast *Cryptococcus neoformans*. *J Biol Chem* 290(3):1861-1873.

38. Loibl M & Strahl S (2013) Protein O-mannosylation: what we have learned from baker's yeast. *Biochim Biophys Acta* 1833(11):2438-2446.

39. Del Poeta M, Nimrichter L, Rodrigues ML, & Luberto C (2014) Synthesis and biological properties of fungal glucosylceramide. *PLoS Pathog* 10(1):e1003832.

40. Levery SB, Toledo MS, Doong RL, Straus AH, & Takahashi HK (2000) Comparative analysis of ceramide structural modification found in fungal cerebrosides by electrospray tandem mass spectrometry with low energy collision-induced dissociation of Li+ adduct ions. *Rapid Commun Mass Spectrom* 14(7):551-563.

41. Rittershaus PC, *et al.* (2006) Glucosylceramide synthase is an essential regulator of pathogenicity of *Cryptococcus neoformans*. *J Clin Invest* 116(6):1651-1659.

42. Fan W, Kraus PR, Boily MJ, & Heitman J (2005) *Cryptococcus neoformans* gene expression during murine macrophage infection. *Eukaryot Cell* 4(8):1420-1433.

43. Shea JM, Kechichian TB, Luberto C, & Del Poeta M (2006) The cryptococcal enzyme inositol phosphosphingolipid-phospholipase C confers resistance to the antifungal effects of macrophages and promotes fungal dissemination to the central nervous system. *Infect Immun* 74(10):5977-5988.

44. Luberto C, *et al.* (2001) Roles for inositol-phosphoryl ceramide synthase 1 (*IPC1*) in pathogenesis of *C. neoformans*. *Genes Dev* 15(2):201-212.

45. Dickson RC & Lester RL (1999) Yeast sphingolipids. *Biochim Biophys Acta* 1426(2):347-357.

46. Lester RL & Dickson RC (1993) Sphingolipids with inositolphosphate-containing head groups. *Adv Lipid Res* 26:253-274.

47. Castle SA, *et al.* (2008) Beta1,2-xylosyltransferase Cxt1p is solely responsible for xylose incorporation into *Cryptococcus neoformans* glycosphingolipids. *Eukaryot Cell* 7(9):1611-1615.

48. Klutts JS, Yoneda A, Reilly MC, Bose I, & Doering TL (2006) Glycosyltransferases and their products: cryptococcal variations on fungal themes. *FEMS Yeast Res* 6(4):499-512.

49. Ferguson MAJ, Kinoshita T, & Hart GW (2009) Glycosylphosphatidylinositol Anchors. *Essentials of Glycobiology*, eds Varki A, Cummings RD, Esko JD, Freeze HH, Stanley P, Bertozzi CR, Hart GW, & Etzler MECold Spring Harbor (NY)), 2nd Ed.

50. Freeze HH & Elbein AD (2009) Glycosylation Precursors. *Essentials of Glycobiology*, eds Varki A, Cummings RD, Esko JD, Freeze HH, Stanley P, Bertozzi CR, Hart GW, & Etzler MECold Spring Harbor (NY)), 2nd Ed.

51. Yoneda A & Doering TL (2006) A eukaryotic capsular polysaccharide is synthesized intracellularly and secreted via exocytosis. *Mol Biol Cell* 17(12):5131-5140.

52. Wills EA, *et al.* (2001) Identification and characterization of the *Cryptococcus neoformans* phosphomannose isomerase-encoding gene, *MAN1*, and its impact on pathogenicity. *Mol Microbiol* 40(3):610-620.

53. Beverley SM, *et al.* (2005) Eukaryotic UDP-galactopyranose mutase (*GLF* gene) in microbial and metazoal pathogens. *Eukaryot Cell* 4(6):1147-1154.

54. Bar-Peled M, Griffith CL, & Doering TL (2001) Functional cloning and characterization of a UDP- glucuronic acid decarboxylase: the pathogenic fungus *Cryptococcus neoformans* elucidates UDP-xylose synthesis. *Proc Natl Acad Sci U S A* 98(21):12003-12008.

55. Bar-Peled M, Griffith CL, Ory JJ, & Doering TL (2004) Biosynthesis of UDP-GlcA, a key metabolite for capsular polysaccharide synthesis in the pathogenic fungus *Cryptococcus neoformans*. *Biochem J* 381(Pt 1):131-136.

56. Griffith CL, Klutts JS, Zhang L, Levery SB, & Doering TL (2004) UDP-glucose dehydrogenase plays multiple roles in the biology of the pathogenic fungus *Cryptococcus neoformans*. *J Biol Chem* 279(49):51669-51676.

57. Moyrand F, Klaproth B, Himmelreich U, Dromer F, & Janbon G (2002) Isolation and characterization of capsule structure mutant strains of *Cryptococcus neoformans*. *Mol Microbiol* 45(3):837-849.

58. Moyrand F, Fontaine T, & Janbon G (2007) Systematic capsule gene disruption reveals the central role of galactose metabolism on *Cryptococcus neoformans* virulence. *Mol Microbiol* 64(3):771-781.

59. Moyrand F & Janbon G (2004) *UGD1*, encoding the C*ryptococcus neoformans* UDP-glucose dehydrogenase, is essential for growth at 37 degrees C and for capsule biosynthesis. *Eukaryot Cell* 3(6):1601-1608.

60. Moyrand F, Lafontaine I, Fontaine T, & Janbon G (2008) *UGE1* and *UGE2* regulate the UDP-glucose/UDP-galactose equilibrium in *Cryptococcus neoformans*. *Eukaryot Cell* 7(12):2069-2077.

61. Abeijon C, Mandon EC, & Hirschberg CB (1997) Transporters of nucleotide sugars, nucleotide sulfate and ATP in the Golgi apparatus. *Trends Biochem Sci* 22(6):203-207.

62. Berninsone P, Eckhardt M, Gerardy-Schahn R, & Hirschberg CB (1997) Functional expression of the murine Golgi CMP-sialic acid transporter in *Saccharomyces cerevisiae*. *J Biol Chem* 272(19):12616-12619.

63. Berninsone PM & Hirschberg CB (2000) Nucleotide sugar transporters of the Golgi apparatus. *Curr Opin Struct Biol* 10(5):542-547.

64. Gao XD & Dean N (2000) Distinct protein domains of the yeast Golgi GDP-mannose transporter mediate oligomer assembly and export from the endoplasmic reticulum. *J Biol Chem* 275(23):17718-17727.

65. Ebert B, *et al.* (2015) Identification and characterization of a Golgi-localized UDP-xylose transporter family from *Arabidopsis*. *Plant Cell* 27(4):1218-1227.

66. Suda T, *et al.* (2004) Molecular cloning and characterization of a human multisubstrate specific nucleotide-sugar transporter homologous to *Drosophila fringe connection*. *J Biol Chem* 279(25):26469-26474.

67. Aoki K, Ishida N, & Kawakita M (2003) Substrate recognition by nucleotide sugar transporters: further characterization of substrate recognition regions by analyses of UDP-galactose/CMP-sialic acid transporter chimeras and biochemical analysis of the substrate specificity of parental and chimeric transporters. *J Biol Chem* 278(25):22887-22893.

68. Aoki K, Ishida N, & Kawakita M (2001) Substrate recognition by UDP-galactose and CMP-sialic acid transporters. Different sets of transmembrane helices are utilized for the

specific recognition of UDP-galactose and CMP-sialic acid. *J Biol Chem* 276(24):21555-21561.

69. Gao XD, Nishikawa A, & Dean N (2001) Identification of a conserved motif in the yeast golgi GDP-mannose transporter required for binding to nucleotide sugar. *J Biol Chem* 276(6):4424-4432.

70. Guillen E, Abeijon C, & Hirschberg CB (1998) Mammalian Golgi apparatus UDP-N-acetylglucosamine transporter: molecular cloning by phenotypic correction of a yeast mutant. *Proc Natl Acad Sci U S A* 95(14):7888-7892.

71. Segawa H, Soares RP, Kawakita M, Beverley SM, & Turco SJ (2005) Reconstitution of GDP-mannose transport activity with purified *Leishmania* LPG2 protein in liposomes. *J Biol Chem* 280(3):2028-2035.

72. Caffaro CE, *et al.* (2008) A single *Caenorhabditis elegans* Golgi apparatus-type transporter of UDP-glucose, UDP-galactose, UDP-N-acetylglucosamine, and UDP-N-acetylgalactosamine. *Biochemistry* 47(14):4337-4344.

73. Norambuena L, *et al.* (2002) Transport of UDP-galactose in plants. Identification and functional characterization of AtUTr1, an *Arabidopsis thaliana* UDP-galactose/UDP-glucose transporter. *J Biol Chem* 277(36):32923-32929.

74. Segawa H, Kawakita M, & Ishida N (2002) Human and *Drosophila* UDP-galactose transporters transport UDP-N-acetylgalactosamine in addition to UDP-galactose. *Eur J Biochem* 269(1):128-138.

75. Ashikov A, *et al.* (2005) The human solute carrier gene SLC35B4 encodes a bifunctional nucleotide sugar transporter with specificity for UDP-xylose and UDP-N-acetylglucosamine. *J Biol Chem* 280(29):27230-27235.

76. Rautengarten C, *et al.* (2017) The elaborate route for UDP-arabinose delivery into the Golgi of plants. *Proc Natl Acad Sci U S A* 114(16):4261-4266.

77. Saez-Aguayo S, *et al.* (2017) UUAT1 is a Golgi-localized UDP-uronic acid transporter that modulates the polysaccharide composition of *Arabidopsis* Seed Mucilage. *Plant Cell* 29(1):129-143.

78. Rautengarten C, *et al.* (2016) The *Arabidopsis* Golgi-localized GDP-L-fucose transporter is required for plant development. *Nat Commun* 7:12119:12119.

79. Rautengarten C, *et al.* (2014) The Golgi localized bifunctional UDP-rhamnose/UDP-galactose transporter family of *Arabidopsis*. *Proc Natl Acad Sci U S A* 111(31):11563-11568.

80. Maszczak-Seneczko D, Sosicka P, Majkowski M, Olczak T, & Olczak M (2012) UDP-N-acetylglucosamine transporter and UDP-galactose transporter form heterologous complexes in the Golgi membrane. *FEBS Lett* 586(23):4082-4087.

81. Wang ZA, *et al.* (2014) *Cryptococcus neoformans* dual GDP-mannose transporters and their role in biology and virulence. *Eukaryot Cell* 13(6):832-842.

82. Cottrell TR, Griffith CL, Liu H, Nenninger AA, & Doering TL (2007) The pathogenic fungus *Cryptococcus neoformans* expresses two functional GDP-mannose transporters with distinct expression patterns and roles in capsule synthesis. *Eukaryot Cell* 6(5):776-785.

83. Li LX, *et al.* (2017) *Cryptococcus neoformans UGT1* encodes a UDP-Galactose/UDP-GalNAc transporter. *Glycobiology* 27(1):87-98.

84. Klutts JS & Doering TL (2008) Cryptococcal xylosyltransferase 1 (Cxt1p) from *Cryptococcus neoformans* plays a direct role in the synthesis of capsule polysaccharides. *J Biol Chem* 283(21):14327-14334.

Chapter 2: UDP-glucuronic acid transport is required for cryptococcal virulence

From:

UDP-glucuronic acid transport is required for virulence of *Cryptococcus neoformans*

Lucy X. Li, Carsten Rautengarten, Joshua L. Heazlewood, and Tamara L. Doering

mBio. 2018, 9(1), pii: e02319-17. doi: 10.1128/mBio.02319-17. PMID: 29382737

2.1 Abstract

Glycans play diverse biological roles, ranging from structural and regulatory functions to mediating cellular interactions. For pathogens, they are also often required for virulence and survival in the host. In *Cryptococcus neoformans,* an opportunistic pathogen of humans, the acidic monosaccharide glucuronic acid (GlcA) is a critical component of multiple essential glycoconjugates. One of these glycoconjugates is the polysaccharide capsule, a major virulence factor that enables this yeast to modulate the host immune response and resist antimicrobial defenses. This allows cryptococci to colonize the lung and brain, leading to hundreds of thousands of deaths each year worldwide. Synthesis of most glycans, including capsule polysaccharides, occurs in the secretory pathway. However, the activated precursors for this process, nucleotide sugars, are made primarily in the cytosol. This topological problem is resolved by the action of nucleotide sugar transporters (NSTs). We discovered that Uut1 is the sole UDP-GlcA transporter in *C. neoformans,* and is unique among NSTs for its narrow substrate range and high affinity for UDP-GlcA. Mutant cells deleted for *UUT1* lack capsule polysaccharides and are highly sensitive to environmental stress. As a result, the deletion mutant is internalized and cleared by phagocytes more readily than wild-type cells and is completely avirulent in mice. These findings expand our understanding of the requirements for capsule synthesis and cryptococcal virulence and elucidate a critical protein family.

2.2 Introduction

UDP-glucuronic acid (UDP-GlcA) is a critical precursor for essential glycoconjugates across biological kingdoms, ranging from mammalian glycosaminoglycans and plant cell wall polysaccharides to bacterial capsule glycoglycerolipids (1-3). Aberrant UDP-GlcA synthesis or subcellu-

lar localization leads to severe impairments such as Schneckenbecken dysplasia in humans (4) and virulence defects in bacterial pathogens (5-7).

Our interest in UDP-GlcA stems from its role in the fungal pathogen *Cryptococcus neoformans*. This opportunistic yeast colonizes the lungs and disseminates to the brain of immunocompromised individuals, where it causes a meningoencephalitis that is responsible for roughly two hundred thousand deaths per year (8-10). UDP-GlcA is a key biosynthetic precursor of cryptococcal polysaccharides. These complex polysaccharides associate with the cell wall to form the cryptococcal capsule, which provides a physical barrier against host immune defenses. These polysaccharides are also shed into the extracellular space (11), where they impede host defenses by interfering with phagocytosis and clearance of the yeast, inhibiting the production of proinflammatory cytokines, depleting complement components, and reducing leukocyte migration to sites of inflammation (12).

The capsule consists of two complex polysaccharides, glucuronoxylomannan (GXM) and glucuronoxylomannogalactan (GXMGal). GXM, which constitutes 90% of the capsule by mass, is a repeating polymer with a mannose (Man) backbone that is partially acetylated and is substituted with monosaccharide side chains of glucuronic acid (GlcA) and xylose (Xyl) (13). The remaining 10% of the capsule mass consists of GXMGal, which is a linear galactose (Gal) polymer bearing both single galactofuranose (Gal*f*) residues and galactomannan side chains substituted with a variable number of GlcA and Xyl residues (14-16). Overall, GlcA comprises approximately 16% and 7% of the GXM and GXMGal residues, respectively, and is responsible for their acidic nature.

Both GXM and GXMGal, like most other eukaryotic glycans, are believed to be assembled in the secretory pathway (17). However, nucleotide sugars, which donate individual sugar moieties to growing glycan structures, are synthesized primarily in the cytosol (18). The ER and Golgi membranes, therefore, constitute physical barriers that prevent substrate access to biosynthetic enzymes. Nucleotide sugar transporters (NSTs) provide a solution to this topological problem, by translocating activated sugars into the luminal space in exchange for the corresponding nucleoside monophosphates (19, 20). In this way, NSTs enable luminal glycan biosynthesis.

Predicted protein sequence is not a reliable predictor of NST substrate specificity. For example, NSTs with almost 50% amino acid identity have been reported to transport distinct substrates, while others with only 20% identity appear to translocate the same one (21). Further complicating the picture, individual NSTs range from highly specific proteins that recognize a single substrate to less restrictive ones that transport up to four substrates, and NSTs with overlapping but non-identical substrate affinities can be found in a single cell (22-28). Finally, associated glycan synthetic enzymes and subcellular localization may also influence the activity of a given NST (29, 30). All of these factors make it a challenge to identify and characterize the full complement of NSTs in a cell type of interest, impeding our ability to fully define critical glycan synthetic processes.

Mutant *C. neoformans* strains incapable of synthesizing UDP-GlcA do not produce capsule or cause disease in mice, demonstrating the importance of GlcA in cryptococcal biology and pathogenesis (31, 32). Despite this, the NST(s) responsible for transporting its donor, UDP-GlcA, has never been identified in *C. neoformans*. Here we show that *C. neoformans* Uut1 is a UDP-GlcA

transporter by using an *in vitro* assay to directly demonstrate its activity. We also characterize its specificity and kinetic properties. We further show that cells lacking Uut1 exhibit marked growth defects and metabolic abnormalities, which correlate with greater phagocytosis by host macrophages and quicker clearance of infection *in vitro* and *in vivo.* Uut1 is thus a critical protein for cryptococcal biosynthetic processes and is required for multiple aspects of *C. neoformans* virulence.

2.3 Results

2.3.1 Identification of Uut1 as a nucleotide sugar transporter candidate

To identify the cryptococcal UDP-GlcA transporter, we first used BLASTP to search the *C. neoformans* genome for predicted proteins with homology to known UDP-GlcA transporters. Although we found no homologs of the transporters from *Caenorhabditis elegans, Homo sapiens,* or *Drosophila melanogaster*, we did find a predicted ortholog of the *Arabidopsis thaliana* transporter UUAT1 (33), which we termed Uut1 (CNAG_06230). Similar to other NSTs, Uut1 is predicted to have an even number of transmembrane domains (here 10) such that the N- and C-termini are on the same side of the membrane, likely in the cytosol (Fig. 2.S1). Phylogenetic analysis of Uut1 places it closest to UUAT1 (Fig. 2.1), and more distant from other UDP-GlcA transporters and from known cryptococcal NSTs. Notably, Uut1 and UUAT1 share only 16% amino acid identity, although as discussed above, homology is a poor predictor of substrate specificity in this family of proteins.

2.3.2 Uut1 localizes to the ER

If Uut1 is indeed a nucleotide sugar transporter that supplies precursors for polysaccharide synthesis, we expect it to reside in the secretory pathway. To test this we took advantage of existing markers and facile imaging methods in the model yeast *S. cerevisiae*, and expressed FLAG-Uut1 under a copper inducible promoter in that system. Immunofluorescence (IF) staining showed that the tagged protein colocalized with an ER marker (Kar2p/BiP) but not with the late Golgi marker Sec7 (34) (Fig. 2.2; see discussion). A KXKXX motif near the C terminus (Fig. 2.S1) may be involved in this localization. Such motifs mediate the retrieval of type I transmembrane proteins from downstream membranes to the ER (35, 36), although the Uut1 sequence (Fig. 2.S1) is atypical in that it is followed by three additional amino acids.

2.3.3 Uut1 is required for capsule synthesis

To define the role of Uut1 in cryptococcal biology, we deleted the corresponding gene (*UUT1*). Even when the resulting mutant was grown in capsule-inducing conditions (see Materials and methods), we detected no capsule by negative staining (Fig. 2.3A) or by staining with fluorophore-conjugated anti-GXM antibodies (Fig. 2.3B). We also detected no GXM shed into the growth medium by enzyme-linked immunosorbent assay (ELISA; Fig. 2.3C) or by immunoblotting (Fig. 2.3D), and the mutant cells appeared clumpy compared to wild type (Fig. 2.3A, Fig. 2.3B). All of these phenotypes were consistent with those of the acapsular strain *cap59*Δ and were reversed when the deletion was complemented with the wild-type gene at the original locus (Fig. 2.3, *UUT1*). We obtained similar results for capsule staining, GXM shedding ELISA, and GXM immunoblotting with additional antibodies (Table 2.S1). As far as we can determine, therefore, cells lacking Uut1 are completely acapsular.

2.3.4 Uut1 is a UDP-glucuronic acid transporter

The absence of capsule on cells lacking Uut1 suggested that this putative nucleotide transporter translocates a major capsule substrate(s). The components of GXM and GXMGal are Man, Gal, Xyl, Gal*f*, and GlcA. We previously identified two transporters of GDP-Man (30, 37), and there is a known UDP-Gal transporter (38, 39), so we hypothesized that those were less likely to be substrates of Uut1. Additionally, even completely abrogating synthesis of UDP-Xyl or UDP-Gal*f* yields hypo- or normo- capsular cells, respectively (15, 32, 40), rather than the acapsular cells observed in the *uut1*D mutant; this argued against these capsule donors as Uut1 substrates. This reasoning left UDP-GlcA as the best candidate substrate, which was further supported by the observation that cells unable to synthesize UDP-GlcA are acapsular (31, 32).

To test our hypothesis that Uut1 transports UDP-GlcA, we directly assayed its activity *in vitro*. For these studies we first prepared microsomes from *S. cerevisiae* heterologously expressing V5-tagged Uut1. We then reconstituted the microsomal protein in proteoliposomes, which were pre-loaded with UMP or GMP to serve as antiport substrates. After confirmation of Uut1-V5 expression by immunoblotting (Fig. 2.S2), the proteoliposomes were incubated with a mixture of nucleotide sugars, subjected to gel filtration to remove any that were not imported, and analyzed by liquid chromatography-tandem mass spectrometry (LC-MS/MS). UDP-GlcA was the only cryptoccal nucleotide sugar that was transported over background by Uut1-bearing proteoliposomes pre-loaded with UMP (Fig. 2.4A). This transport was saturable with time and substrate concentration (Fig. 2.4C, Fig. 2.4D), and had an apparent K_M of 0.6 ± 0.1 μM and V_{max} of 1.1 ± 0 nM s^{-1} (mean ± SEM from four independent experiments) with a turnover rate of 0.08 s^{-1}. We also observed minor transport of UDP-galacturonic acid and UDP-arabinofuranose, but those substrates

have never been reported in *C. neoformans* and are not detectable in our analyses (see below). We observed no transport of any assayed nucleotide sugar when the proteoliposomes were pre-loaded with GMP (Fig. 2.4B).

We next wondered whether eliminating UDP-GlcA transport would alter cellular nucleotide sugar metabolism. UDP-GlcA is synthesized from UDP-Glc by UDP-Glc dehydrogenase (Ugd1), and may be decarboxylated by UDP-Xyl synthase (Uxs1) to produce UDP-Xyl; this product inhibits Ugd1 to regulate the pathway (Fig. 2.5A). Our measurements of nucleotide sugar content (see Materials and methods) showed that the level of UDP-Glc in *uut1*Δ cells was about 4-fold higher than in WT cells (Fig. 2.5B). The levels of UDP-GlcA and UDP-Xyl, in contrast, were not significantly different between mutant and WT cells (Fig. 2.5B).

We next examined the cellular level of UDP-GlcA when *C. neoformans* was incubated for 24 hours under conditions that induce capsule synthesis, which we expected to require increased UDP-GlcA. Surprisingly, the overall concentration of UDP-GlcA remained constant in these conditions (4 ± 2 pmol/mg wet weight; mean ± SD from four independent experiments). Consistent with this observation, transcriptome sequencing (RNA-seq) studies showed no change in *UGD1* transcription over this interval (Fig. 2.6). However, under the same conditions *UUT1* expression was upregulated 28-fold (Fig. 2.6). It thus appears that the increased demand for UDP-GlcA is satisfied by greater transport in the context of adequate cytosolic pools.

2.3.5 Loss of Uut1 causes defects in cell morphology and stress resistance

GXM and GXMGal are the only *C. neoformans* glycans known to contain glucuronic acid, although not all cryptococcal glycoconjugates have been extensively profiled. Furthermore, the UDP-GlcA synthase mutant, *ugd1*Δ, exhibits profound cellular defects that cannot be solely attributed to the absence of capsule (31, 32). We therefore assayed additional characteristics of cells lacking Uut1.

We had already noticed that *ugd1*Δ mutant cells appeared smaller and less spherical than WT cells and exhibited the aggregation typical of acapsular strains (Fig. 2.3A). Closer examination of *uut1*Δ by transmission electron microscopy (TEM) confirmed these observations, and revealed the absence of the distinct morphological layers in the cell wall (Fig. 2.7A) that are normally present in WT cells (11, 41-43). The mutant cell wall also appeared less organized (Fig. 2.7A) and showed altered exposure of mannans as detected by ConA binding, although dyes recognizing other components of the cell wall bound the two strains similarly (Fig. 2.S3). Furthermore, the cell membrane appeared to make irregular contact with the internal surface of the cell wall, and the cells contained large vacuoles and abnormal intracellular inclusions, often associated with the plasma membrane, whether they were grown in rich or nutrient-deficient media (Fig. 2.7A, Fig. 2.S4). The contents of vacuoles or membranous inclusions were not recognized by anti-GXM antibody in immunoelectron microscopy studies (Fig. 2.S4).

In addition to marked abnormalities in cell morphology, the *uut1*Δ mutant was highly susceptible to a range of stresses. It demonstrated temperature sensitive growth (shown for solid and liquid media in Fig. 2.7B and Fig. 2.S5, respectively), which was exacerbated by nutrient limitation

(Fig. 2.S5). Mutant cells also grew poorly in the presence of SDS or high salt (Fig. 2.7B). Heterologous expression of the human UDP-GlcA transporter, UGTrel7, did not restore growth under any of these conditions (Fig. 2.S6).

Since pigment production correlates with resistance to environmental stress (44-46), we assayed the ability of the mutant strain to produce melanin on medium containing the precursor L-3,4-dihydroxyphenylalanine (L-DOPA). We observed no melanization, however, even after 7 days of growth (Fig. 2.7C). In all phenotypic studies the complement restored growth or melanization to WT levels.

2.3.6 UDP-glucuronic acid transport is required for virulence

We next tested whether the observed mutant phenotypes would translate into aberrant interactions with host cells. Using an automated imaging method (47), we found that differentiated human monocytic cells (THP-1 cells) internalized the *uut1*Δ mutant at significantly higher rates than they internalized the WT, independent of serum opsonization (Fig. 2.8A). The mutant was also more susceptible to killing after internalization: host phagocytes completely cleared *uut1*Δ by 24 h, in contrast to stable levels of WT and the complemented strain (*UUT1*; Fig 2.8B).

Our data suggested that *uut1*Δ would poorly evade recognition and clearance by the host immune system and was unlikely to survive under host nutrient and temperature conditions. To test this *in vivo*, we inoculated mice with WT, *uut1*Δ, or *UUT1* intranasally, to mimic the natural route of infection. The *uut1*Δ mutant was cleared from the lungs by 15 days post infection (dpi; Fig. 2.9A), with no fungi detected in the brain or spleen at that time (Fig. 2.S7). The WT or the com-

plemented strain, in contrast, caused the mice to succumb to infection by three weeks post inoculation (Fig. 2.9B).

2.4 Discussion

We have discovered the first fungal nucleotide sugar transporter that translocates UDP-GlcA. This protein, Uut1, is critical for *C. neoformans* virulence, likely due to its role in providing a key precursor for synthesis of the polysaccharide capsule and potentially other glycoconjugates, and it is also notable for its substrate specificity. Importantly, Uut1 has less than 12% identity at the protein level with its human counterpart, which also does not compensate for deficiencies in the fungal mutant (Fig. 2.S6).

Similar to other NSTs, Uut1 is localized to the secretory pathway. Our immunofluorescence studies suggest that this protein occurs mainly in the ER (Fig. 2.6), like the human transporter (UGTrel7) and in contrast to the more closely-related, yet Golgi-localized, plant transporter (UUAT1) (33, 48). This is surprising, because we expect formation of mannose polymers to precede the addition of GlcA, and the mannose donor enters the secretory pathway in the Golgi apparatus (30, 49, 50). It may be that luminal UDP-GlcA progresses through the secretory pathway. Alternatively, the distribution of protein upon heterologous expression in *S. cerevisiae* may not accurately reflect the native localization, for example because of expression level or the lack of potential cryptococcal interaction partners. Furthermore, even if much of the protein is retrieved to the ER, perhaps to serve transport-independent functions, some fraction may remain in the Golgi apparatus (spatially separated from late Golgi proteins like Sec7) and carry out transport

there. Further analysis to determine localization of the cryptococcal transporter must await the development of reliable subcellular imaging methods for *C. neoformans.*

Uut1 is unique, however, in its specificity for UDP-GlcA among cryptococcal nucleotide sugars. Other known proteins that translocate UDP-GlcA also transport additional substrates *in vivo*: UGTrel7 and UUAT1 transport UDP-GalNAc and UDP-GalA, respectively (33, 48), while the *Drosophila* and *C. elegans* transporters, UST74c and SQV-7, recognize an even wider range of UDP-sugars (22, 51). Another notable feature of Uut1 is its affinity for UDP-GlcA, which is significantly above that of plant or human transporters; K_M of 0.6 μM compared to 1.5 mM for UUAT1 and 4 μM for UGTrel7 (33, 48). This low K_M relative to the measured cellular UDP-GlcA concentrations (Fig. 2.5B) suggests that Uut1 functions at a constant rate in both rich and nutrient-deficient media. Meeting increased demand for UDP-GlcA in the secretory pathway, for example in capsule-inducing conditions, thus requires more Uut1, which is achieved by upregulation at the transcriptional level (Fig. 2.6). The higher rates of UDP-GlcA transport out of the cytosol could then reduce UDP-Xyl production and consequent inhibition of Ugd1, balancing the system and maintaining stable UDP-GlcA levels (Fig. 2.5 and reported values above). In the absence of Uut1, there is likely an elevated pool of cytosolic UDP-GlcA due to the absence of transport and subsequent consumption, which leads to slightly increased UDP-Xyl production in that compartment and consequent feedback inhibition on Ugd1. Thus, total UDP-Glc, but not UDP-GlcA or UDP-Xyl, was significantly higher in *uut1*Δ cells than in WT cells.

Uut1 and the human transporter UGTrel7 overlap in subcellular localization, and both translocate UDP-GlcA, yet UGTrel7 does not rescue the *uut1*Δ mutant phenotype. At 550 amino acids, Uut1

is also roughly 70% longer than UGTrel7 and other NSTs, mainly due to a unique extended N-terminal cytosolic domain (Fig. 2.S1) that is absent from the human and plant transporters and dispensable for transport activity (Fig. 2.4, Fig. 2.S2). It may be that this domain interacts with cryptococcal synthetic machinery to efficiently channel substrates into the luminal compartment or performs other functions specific to Uut1. Further studies of this unusual protein may elucidate functional differences that could be exploited for therapeutic intervention.

Cells lacking the donor of Xyl, an abundant capsule component, display capsule although the fibers are short and deformed (32, 40). Since GlcA is less abundant than Xyl in capsule polysaccharides, we originally expected to observe a similar phenotype in *uut1*Δ cells. We were therefore surprised to observe that these cells completely lacked capsule (Fig. 2.3, Fig. 2.S4). These unexpected results suggest that GlcA modification is a prerequisite for Xyl addition. This model is consistent with the greater variability in GXM and GXMGal of capsule Xyl residues compared to GlcA, and their more distal position in GXMGal (11). An acapsular phenotype could also result if GlcA incorporation is required for the extension of GXM's mannose backbone or to inhibit the degradation of unmodified mannose polymers.

Another possible explanation for the lack of capsule on *uut1*Δ cells is that GlcA modification is required for export of GXM and/or GXMGal, either directly by interacting with trafficking machinery or indirectly by enabling additional modifications (e.g. Xyl incorporation) (76-78) required for recognition. The mutant cells do contain unusual intracellular inclusions (Fig. 2.7, Fig. 2.S4), although their contents were not recognized by anti-GXM antibody (Fig. 2.S4). (The possibility remains that aberrant polymers are made but are not recognized by the anti-GXM anti-

bodies we tested, although none of these antibodies are reported to require GlcA for binding (52, 53).) Finally, GlcA modification could be required for function of a protein involved in capsule synthesis (see below).

We observed numerous defects in the growth and morphology of cells lacking Uut1, including cell wall disorganization and abnormal plasma membranes (Fig. 2.7, Fig. 2.S3). This suggests a role for GlcA modification beyond the capsule. Although GlcA has not been detected thus far in surveys of cryptococcal protein-linked glycans or glycolipids (54-57), the levels might be below the limits of detection of the methods used. Glucuronidation could also potentially occur in additional contexts (e.g., the cytosol). Further detailed characterization of cryptococcal glyconconjugates may elucidate such mechanisms.

The lack of a GlcA donor in the secretory pathway drastically influences cryptococcal interactions with the host. The resulting absence of the polysaccharide capsule may expose normally hidden immunogenic components (Fig. 2.S3) (58), while aberrant glycosylation may also create novel immunoreactive epitopes. Both of these could lead to the increased recognition and internalization of *uut1*Δ by macrophages that we observe (Fig. 2.8). Internalized *uut1*Δ cells are also rapidly cleared both *in vitro* (Fig. 2.8) and *in vivo* (Fig. 2.9), likely facilitated by the reduced ability of *uut1*Δ to resist environmental stress. These observations suggest processes involving UDP-GlcA synthesis as a potential target for intervention, which might exploit the unique features of key proteins like Uut1 and the novel biology of the pathogen.

Our discovery of a highly specific, high-affinity fungal UDP-GlcA transporter has provided novel insights into cryptococcal biology. These studies have advanced our understanding of the localization and sequence of glycan biosynthetic events, and supported the hypothesis that GlcA is incorporated into structures other than capsule, and that it plays integral roles in maintaining cellular homeostasis. This work thus sets the stage for future studies in both cryptococcal pathogenesis and fundamental glycobiology.

2.5 Materials and methods

2.5.1 Sequence and phylogenetic analysis

uut1 was identified by BLASTP searches against *C. neoformans* predicted proteins (Broad Institute; *Cryptococcus neoformans var. grubii* H99 database) using known UDP-GlcA transporters from *Arabidopsis thaliana* (NP_196036.1), *Caenorhabditis elegans* (NP_495436.1, AT5G04160), *Homo sapiens* (NP_055954.1.), and *Drosophila melanogaster* (NP_524126.1). Multiple sequence alignment (MUSCLE; (59)), phylogenetic analysis (PhyML; (60)), and tree rendering (TreeDyn; (61)) of Uut1, characterized UDP-GlcA transporters (listed above), and other known cryptococcal NSTs was done using the online Phylogeny.fr program (http://www.phylogeny.fr/index.cgi) with default settings (62, 63). The putative protein topology of Uut1 was predicted using the Constrained Consensus TOPology prediction server (CCTOP; Institute of Enzymology, Budapest, Hungary; (64, 65)) and visualized using Protter (http://wlab.ethz.ch/ protter/start/) (66). The predicted ER localization signal was identified using LocSigDB (http://genome.unmc.edu/ LocSig DB/) (67).

2.5.2 Cell growth

C. neoformans strains were grown at 30 °C in YPD medium (1% wt/vol BactoYeast Extract, 2% wt/vol BactoPeptone, 2% wt/vol dextrose) with shaking (230 rpm) unless otherwise noted.

For phenotypic analysis, cells from overnight (O/N) cultures (16 – 18 hours) were washed in sterile phosphate buffered saline (PBS), resuspended at 10^6 cells/mL in PBS, and 5 μL aliquots of five-fold serial dilutions were plated and grown at 30°C or 37°C as indicated. Conditions tested included YPD plates containing 0.01% SDS, 1.2 M NaCl, 1.2 M KCl, Tris pH 8.8, 1.5 M sorbitol, 0.05% Congo red (CR), or 2% calcofluor white (CFW). Samples were also tested on YNB medium (0.67% wt/vol yeast nitrogen base without amino acids, 2% wt/vol glucose, 2% wt/vol agar, 25 mM sodium succinate pH 4.0) supplemented with 0.5 mM hydrogen peroxide (H_2O_2) or sodium nitrite ($NaNO_2$) to test oxidative and nitrosative stress sensitivity, respectively. Cell-associated melanin production was assayed by plating 5 μL of a 10^6 cells/mL solution on agar plates containing 8 mg/mL KH_2PO_4, 2 mg/mL glucose, 2 mg/mL L-glycine, 1 μg/mL D-biotin, 1 μg/mL thiamine, 0.92 mg/mL $MgSO_4$ 7 H_2O, and 0.4 mg/mL L-3,4-dihydrohyphenylalanine (L-DOPA; Sigma-Aldrich).

To determine growth rates of various strains, cells from O/N cultures were washed in sterile PBS and resuspended at 10^5 cells/mL in 30 mL of YPD, YNB, DMEM, or RPMI at 30°C or 37°C as indicated. Triplicate samples were taken at regular intervals and counted with a hemocytometer.

2.5.3 *C. neoformans* strains and plasmids

To generate the *uut1*Δ mutant, we replaced *UUT1* in the KN99α wild-type (WT) strain with a nourseothricin (NAT) resistance marker, using a split marker strategy (68). Transformants of interest were identified by resistance to NAT and validated by PCR verification of gene replacement. We used a similar strategy to replace the NAT deletion cassette with *UUT1* (amplified from KN99α cDNA) or *UGTREL7* (amplified from a pMKIT-neo hUGTrel7-HA plasmid (48)), in tandem with a geneticin (G418) resistance marker. Transformants resistant to G418 and sensitive to NAT were verified by PCR.

2.5.4 *S. cerevisiae localization*

UUT1 was amplified from KN99α cDNA, cloned into the copper-inducible expression vector pYEScupFLAG*K* (26), and transformed into *S. cerevisiae* strain Sec7x3GFP (from Dr. Benjamin S. Glick, University of Chicago) using lithium acetate. After O/N growth in synthetic complete (SC) medium minus uracil (URA), cultures were adjusted to 0.5 mM $CuSO_4$ and cultured for 1 h. The cells were fixed in 1% paraformaldehyde for 30 min, washed, resuspended in a 0.1 M KPO_4 (pH 6.5)/1.2 M sorbitol buffer, and then incubated for 15 min in buffer supplemented with β-mercaptoethanol (2% wt/vol) and zymolyase (100μg/mL; Sigma-Aldrich). Fifteen microliter aliquots buffer-washed cells were then spotted onto polylysine-coated slides (Electron Microscopy Sciences), incubated for 10 min and immediately plunged first into methanol for 5 min and then acetone for 30 sec. The samples were blocked with 5% goat serum in PBS for 30 min and stained O/N at 4°C with anti-FLAG (mouse antibody diluted 1:1000; Invitrogen) and anti-Kar2p/BiP antibody (rabbit antibody diluted 1:1000; from Dr. Jeff Brodsky, University of Pittsburgh). Finally, cells were incubated for 2 h with AlexaFluor 594-tagged goat anti-mouse IgG (Thermo

Fisher Scientific), AlexaFluor 488-tagged goat anti-rabbit IgG (Thermo Fisher Scientific), and DAPI (Thermo Fisher Scientific), and viewed with a ZEISS Axioskop2 MOT Plus microscope (Carl Zeiss Microscopy, LLC). Where not specified, all steps were performed at room temperature (RT).

2.5.5 Capsule induction and visualization

Cultures of *C. neoformans* grown in YPD O/N were collected by centrifugation (3000 x g, 5 min), washed twice with sterile PBS. The cells were then resuspended in DMEM at 10^6 cells/mL in T-75 tissue culture flasks or 24-well plates and incubated at 37°C with 5% CO_2 for 24 h to induce production of capsule. Induced cells were then collected, washed, and resuspended in PBS, mixed with 1.5 parts India ink (Chartpak, Inc.), and viewed with a ZEISS Axioskop2 MOT Plus microscope (Carl Zeiss Microscopy, LLC).

2.5.6 GXM detection

Cell wall-associated and shed GXM were visualized by fluorescence microscopy and immunoblotting, respectively. To visualize capsule on cells, the strains were induced as described above for 24 h, fixed for 1 h in 3.7% formaldehyde, washed in PBS, and then incubated for 1 h with 1 mg/mL of anti-GXM monoclonal antibody (mAb) 3C2, 2H1, 3O2, 339, or F12D2 (from Dr. Thomas R. Kozel, University of Nevada School of Medicine) conjugated to AlexaFluor 488. Stained cells were washed twice with PBS, resuspended in PBS, and examined on a ZEISS Axioskop 2 MOT Plus microscope. All samples from each experiment were imaged with identical acquisition settings. To analyze shed GXM, strains were induced for 90 min or 24 h before cells were removed by centrifugation. The supernatant fractions were then denatured with heat (60 °C

for 5 min), resolved on agarose gels, transferred onto a positively charged nylon membrane, and immunoblotted with 1 μg/ml anti-GXM mAb 3C2, 2H1, F12D2, or 339 as described in (69). The GXM content of the supernatant fractions was quantified by ELISA as described in reference 70 using mAb 339 and F12D2.

2.5.7 Heterologous expression, reconstitution, and transport assays

The *UUT1* coding region was synthesized into pUC57-Amp by Genewiz, amplified by PCR without the native stop codon, and introduced into the pENTR/SD/D-TOPO vector (Life Technologies) according to the manufacturer's protocols to generate pENTR-*UUT1*. Recombination of the entry clone with destination vector pYES-DEST52 (Life Technologies) using LR clonase II (Life Technologies) produced a C-terminal His/V5 epitope fusion that was verified by sequencing before transformation into *S. cerevisiae* strain INVSc1 (Thermo Fisher Scientific). To verify heterologous protein expression, 2.5 μg of the proteoliposomes were resolved by SDS-PAGE and analyzed by immunoblotting with anti-V5 antibody (Thermo Fisher Scientific) as previously described (71). UDP-GlcA transport was measured at the UDP-GlcA concentrations and times indicated, and kinetic parameters were calculated by nonlinear regression using the Prism 6 application (GraphPad Software). Measured Uut1 content (Table 2.S2) was used to determine turnover rate.

2.5.8 Quantification of nucleotide sugars by mass spectrometry

Nucleotide sugars were extracted from approximately 50 mg of ground cells (wet weight) according to previous methods (72). LC-MS/MS was performed using porous graphitic carbon as the stationary phase on an 1100 series HPLC system (Agilent Technologies) and a 4000 QTRAP

LC-MS/MS system (Sciex) equipped with a TurboIonSpray ion source using methods previously described (73). Four biological replicates were analyzed, each in duplicate.

2.5.9 Fungal gene expression

Wild-type cells cultured in YPD were induced for capsule as described above and sampled at 0, 1.5, 3, 8, and 24 h for RNA isolation and sequencing. See reference (74) for details.

2.5.10 Electron microscopy

Strains were grown in YPD medium or under capsule-inducing conditions, collected by centrifugation (3,000 x g, 5min), fixed for 1 h at RT with 2% glutaraldehyde (Polysciences Inc.) in 100 mM phosphate buffer (pH 7.2), and then incubated for 1 h in 1% osmium tetraoxide (OsO_4; Polysciences Inc.). Following dehydration with ethanol and propylene oxide, cells were embedded in Eponate 12 resin (Tel Pella Inc.), and 70-90 nm sections were cut with a UCT ultramicrotome (Leica Microsystems Inc.). Sections were stained with uranyl acetate and lead citrate for visualization with a JEOL 1200EX transmission electron microscope (JEOL Inc.).

For immunoelectron microscopy, cells were fixed and labeled as in (17). Briefly, induced cells were fixed in glutaraldehyde as above, washed in citrate buffer (pH 6.0), and treated with lysing enzymes from *Trichoderma harzianum (*Sigma-Aldrich) in the same buffer for 30 min before being washed in 0.1 M phosphate buffer (pH 7.0), and post-fixed in 1% OsO_4. Ethanol-substituted samples were then substituted in propylene oxide and embedded in Eponate 12 resin. Sections were blocked with 5% fetal bovine serum (FBS; Thermo Fisher Scientific) in PIPES buffer (pH 7.0) for 30 min, labeled with the anti-GXM mAb 3C2 for 1 h, washed in blocking

buffer, and incubated with 12 nm gold-conjugated goat anti-mouse IgG (Jackson Immuno Research). Sections were then washed in PIPES buffer and water, stained with uranyl acetate and lead citrate, and viewed with a JEOL JEM-1400Plus 120kV Transmission Electron Microscope (JEOL Ltd.).

2.5.11 Cell wall staining

For eosin Y staining, O/N cultures were washed, diluted to 10^7 cells/mL in McIlvaine's buffer (pH 6.0), and incubated with 250 μg/mL eosin Y for 15 min. For the other dyes, the cells were washed, diluted to 10^7 cells/mL in PBS, and stained for 15 min with 100 μg/mL CFW (fluorescent brightner 28, Sigma), 30 μg/mL ConA-FITC (Concanavalin A, Sigma), or 1:10,000 dilution Pontamine (Pontamine fast scarlet 4B, Bayer Corp.). The cells were then washed in PBS and imaged with a ZEISS Axioskop2 MOT Plus microscope.

2.5.12 Macrophage assays

Macrophage phagocytosis and survival of fungal strains was quantified as in reference 39. Briefly, cells were grown in YPD medium, collected by centrifugation, washed, and opsonized with human serum before incubation with differentiated THP-1 macrophages for 1 h. To measure fungal uptake by phagocytes, host cell cytosol and nuclei and fungal walls were stained, and samples were imaged on a Cytation3 plate reader (BioTek) and analyzed using IN Cell Developer Toolbox 1.9.2 (GE Healthcare Life Sciences). For survival assays, samples were washed twice with PBS, lysed either immediately or after a 24 h incubation, and the lysate plated on YPD agar for counts of colony forming units (CFU). Assay results for the *uut1*Δ mutant were compared to

those for wild-type and complemented strains by one-way analysis of variance (ANOVA) with Tukey's *post-hoc* test.

2.5.13 Animal studies

Fungal strains to be tested were cultured O/N in YPD medium, washed in sterile PBS, and diluted to 10^6 cells/mL in sterile PBS. Four- to 6-week-old female A/JCr mice (National Cancer Institute) were then intranasally inoculated with 50 µL aliquots of each strain. Groups of three mice infected with the WT strain and three mice infected with the *uut1*Δ mutant were sacrificed at 6, 12, and 15 days post-inoculation. Initial inocula and organ (lung, brain, spleen) homogenates were plated for CFU, and organ burden was analyzed by Student's t-test. Additional groups of eight mice were infected with WT, *uut1*Δ, and *UUT1* strains, weighed daily, and sacrificed once they lost >20% of their body weight relative to peak weight or at day 50. Survival curves were compared using a log rank test in GraphPad Prism. All studies were performed in compliance with institutional guidelines for animal experimentation.

2.6 Acknowledgements

This work was supported by National Institutes of Health grants R21 AI109623, R01 GM066303, R01 AI78795, and R01 AI087794 (to TLD) and a Mizutani Foundation for Glycoscience grant #160151 (to JLH and CR). LXL was partly supported by a National Research Science award (T32 GM007200), a Sondra Schlesinger Graduate Fellowship (Washington University St Louis Microbiology Department), and a National Institute of Allergy and Infectious Diseases award (F30 AI120339). JLH was supported by an ARC Future Fellowship (FT130101165). The substrates from Carbosource Services (Athens, GA) were supported in part by NSF-RCN

grant 0090281. Immunoelectron microscopy studies were performed at the Washington University Center for Cellular Imaging (WUCCI), supported by Washington University School of Medicine, the Children's Discovery Institute of Washington University, St. Louis Children's Hospital (CDI-CORE-2015-505), and the National Institute for Neurological Disorders and Stroke (NS086741).

We thank Matthew Williams for help with the mouse and growth curve experiments, Cara Griffith for initially identifying this sequence, Dr. Zeke Maier and Dr. Stacey Gish for expression analysis, Dr. Felipe T. Santiago for immunoelectron microscopy imaging, and members of the Doering laboratory for helpful discussions. We also thank Dr. Wandy Beatty (Washington University School of Medicine) for TEM, Robyn Roth (Washington University Center for Cellular Imaging Core) for immunoelectron microscopy, Dr. Benjamin S. Glick (University of Chicago) for the *S. cerevisiae* strain expressing Sec7-3xGFP, Dr. Jeff Brodsky (University of Pittsburgh) for α-Kar2p/BiP antibody, Dr. Joe Heitman (Duke University) for strain KN99α, Dr. Jennifer Lodge (Washington University School of Medicine) for plasmid pMH12-T, Dr. Masatoshi Muraoka (Rinshoken) for hUGTrel7 plasmid, and Dr. Thomas R. Kozel (University of Nevada School of Medicine) for the anti-GXM monoclonal antibodies.

2.7 References

1. Sugahara K & Kitagawa H (2000) Recent advances in the study of the biosynthesis and functions of sulfated glycosaminoglycans. *Curr Opin Struct Biol* 10(5):518-527.

2. Holzl G & Dormann P (2007) Structure and function of glycoglycerolipids in plants and bacteria. *Prog Lipid Res* 46(5):225-243.

3. Reboul R, *et al.* (2011) Down-regulation of UDP-glucuronic acid biosynthesis leads to swollen plant cell walls and severe developmental defects associated with changes in pectic polysaccharides. *J Biol Chem* 286(46):39982-39992.

4. Hiraoka S, *et al.* (2007) Nucleotide-sugar transporter SLC35D1 is critical to chondroitin sulfate synthesis in cartilage and skeletal development in mouse and human. *Nat Med* 13(11):1363-1367.

5. Dougherty BA & van de Rijn I (1993) Molecular characterization of hasB from an operon required for hyaluronic acid synthesis in group A *Streptococci.* Demonstration of UDP-glucose dehydrogenase activity. *J Biol Chem* 268(10):7118-7124.

6. Arrecubieta C, Lopez R, & Garcia E (1994) Molecular characterization of *cap3A*, a gene from the operon required for the synthesis of the capsule of *Streptococcus pneumoniae type 3*: sequencing of mutations responsible for the unencapsulated phenotype and localization of the capsular cluster on the pneumococcal chromosome. *J Bacteriol* 176(20):6375-6383.

7. Chang KW, Weng SF, & Tseng YH (2001) UDP-glucose dehydrogenase gene of *Xanthomonas campestris* is required for virulence. *Biochem Biophys Res Commun* 287(2):550-555.

8. Kwon-Chung KJ, *et al.* (2014) *Cryptococcus neoformans* and *Cryptococcus gattii*, the etiologic agents of cryptococcosis. *Cold Spring Harb Perspect Med* 4(7):a019760.

9. Denning DW (2016) Minimizing fungal disease deaths will allow the UNAIDS target of reducing annual AIDS deaths below 500 000 by 2020 to be realized. *Philos Trans R Soc Lond B Biol Sci* 371(1709).

10. Rajasingham R, *et al.* (2017) Global burden of disease of HIV-associated cryptococcal meningitis: an updated analysis. *Lancet Infect Dis* 17(8):873-881.

11. Doering TL (2009) How sweet it is! Cell wall biogenesis and polysaccharide capsule formation in *Cryptococcus neoformans*. *Annu Rev Microbiol* 63:223-247.

12. Vecchiarelli A, *et al.* (2013) Elucidating the immunological function of the *Cryptococcus neoformans* capsule. *Future Microbiol* 8(9):1107-1116.

13. Cherniak R, Valafar H, Morris LC, & Valafar F (1998) *Cryptococcus neoformans* chemotyping by quantitative analysis of 1H nuclear magnetic resonance spectra of glucuronoxylomannans with a computer-simulated artificial neural network. *Clin Diagn Lab Immunol* 5(2):146-159.

14. Heiss C, Klutts JS, Wang Z, Doering TL, & Azadi P (2009) The structure of *Cryptococcus neoformans* galactoxylomannan contains beta-D-glucuronic acid. *Carbohydr Res* 344(7):915-920.

15. Heiss C, *et al.* (2013) Unusual galactofuranose modification of a capsule polysaccharide in the pathogenic yeast *Cryptococcus neoformans*. *J Biol Chem* 288(16):10994-11003.

16. Previato JO, *et al.* (2017) Distribution of the O-acetyl groups and beta-galactofuranose units in galactoxylomannans of the opportunistic fungus *Cryptococcus neoformans*. *Glycobiology* 27(6):582-592.

17. Yoneda A & Doering TL (2006) A eukaryotic capsular polysaccharide is synthesized intracellularly and secreted via exocytosis. *Mol Biol Cell* 17(12):5131-5140.

18. Freeze HH & Elbein AD (2009) Glycosylation Precursors. *Essentials of Glycobiology*, eds Varki A, Cummings RD, Esko JD, Freeze HH, Stanley P, Bertozzi CR, Hart GW, & Etzler ME. Cold Spring Harbor (NY)), 2nd Ed.

19. Abeijon C, Mandon EC, & Hirschberg CB (1997) Transporters of nucleotide sugars, nucleotide sulfate and ATP in the Golgi apparatus. *Trends Biochem Sci* 22(6):203-207.

20. Berninsone P, Eckhardt M, Gerardy-Schahn R, & Hirschberg CB (1997) Functional expression of the murine Golgi CMP-sialic acid transporter in *Saccharomyces cerevisiae*. *J Biol Chem* 272(19):12616-12619.

21. Guillen E, Abeijon C, & Hirschberg CB (1998) Mammalian Golgi apparatus UDP-N-acetylglucosamine transporter: molecular cloning by phenotypic correction of a yeast mutant. *Proc Natl Acad Sci USA* 95(14):7888-7892.

22. Berninsone P, Hwang HY, Zemtseva I, Horvitz HR, & Hirschberg CB (2001) SQV-7, a protein involved in *Caenorhabditis elegans* epithelial invagination and early embryogenesis, transports UDP-glucuronic acid, UDP-N- acetylgalactosamine, and UDP-galactose. *Proc Natl Acad Sci USA* 98(7):3738-3743.

23. Norambuena L, *et al.* (2002) Transport of UDP-galactose in plants. Identification and functional characterization of AtUTr1, an *Arabidopsis thaliana* UDP-galactose/UDP-glucose transporter. *J Biol Chem* 277(36):32923-32929.

24. Segawa H, Kawakita M, & Ishida N (2002) Human and *Drosophila* UDP-galactose transporters transport UDP-N-acetylgalactosamine in addition to UDP-galactose. *Eur J Biochem* 269(1):128-138.

25. Aoki K, Ishida N, & Kawakita M (2003) Substrate recognition by nucleotide sugar transporters: further characterization of substrate recognition regions by analyses of UDP-galactose/CMP-sialic acid transporter chimeras and biochemical analysis of the substrate specificity of parental and chimeric transporters. *J Biol Chem* 278(25):22887-22893.

26. Ashikov A, *et al.* (2005) The human solute carrier gene SLC35B4 encodes a bifunctional nucleotide sugar transporter with specificity for UDP-xylose and UDP-N-acetylglucosamine. *J Biol Chem* 280(29):27230-27235.

27. Segawa H, Soares RP, Kawakita M, Beverley SM, & Turco SJ (2005) Reconstitution of GDP-mannose transport activity with purified *Leishmania* LPG2 protein in liposomes. *J Biol Chem* 280(3):2028-2035.

28. Caffaro CE, *et al.* (2008) A single *Caenorhabditis elegans* Golgi apparatus-type transporter of UDP-glucose, UDP-galactose, UDP-N-acetylglucosamine, and UDP-N-acetylgalactosamine. *Biochemistry* 47(14):4337-4344.

29. Maszczak-Seneczko D, Sosicka P, Majkowski M, Olczak T, & Olczak M (2012) UDP-N-acetylglucosamine transporter and UDP-galactose transporter form heterologous complexes in the Golgi membrane. *FEBS Lett* 586(23):4082-4087.

30. Wang ZA, *et al.* (2014) *Cryptococcus neoformans* dual GDP-mannose transporters and their role in biology and virulence. *Eukaryot Cell* 13(6):832-842.

31. Moyrand F & Janbon G (2004) *UGD1*, encoding the C*ryptococcus neoformans* UDP-glucose dehydrogenase, is essential for growth at 37 degrees C and for capsule biosynthesis. *Eukaryot Cell* 3(6):1601-1608.

32. Griffith CL, Klutts JS, Zhang L, Levery SB, & Doering TL (2004) UDP-glucose dehydrogenase plays multiple roles in the biology of the pathogenic fungus *Cryptococcus neoformans*. *J Biol Chem* 279(49):51669-51676.

33. Saez-Aguayo S, *et al.* (2017) UUAT1 is a Golgi-localized UDP-uronic acid transporter that modulates the polysaccharide composition of *Arabidopsis* Seed Mucilage. *Plant Cell* 29(1):129-143.

34. Losev E, *et al.* (2006) Golgi maturation visualized in living yeast. *Nature* 441(7096):1002-1006.

35. Jackson LP, Lewis M, Kent HM, Edeling MA, Evans PR, Duden R, & Owen DJ (2012) Molecular basis for recognition of dilysine trafficking motifs by COPI. *Dev Cell* 23:1255-1262.

36. Ma W & Goldberg J (2013) Rules for the recognition of dilysine retrieval motifs by coa-tomer. *EMBO J* 32:926-937.

37. Cottrell TR, Griffith CL, Liu H, Nenninger AA, & Doering TL (2007) The pathogenic fungus *Cryptococcus neoformans* expresses two functional GDP-mannose transporters with distinct expression patterns and roles in capsule synthesis. *Eukaryot Cell* 6(5):776-785.

38. Moyrand F, Fontaine T, & Janbon G (2007) Systematic capsule gene disruption reveals the central role of galactose metabolism on *Cryptococcus neoformans* virulence. *Mol Microbiol* 64(3):771-781.

39. Li LX, *et al.* (2017) *Cryptococcus neoformans UGT1* encodes a UDP-Galactose/UDP-GalNAc transporter. *Glycobiology* 27(1):87-98.

40. Moyrand F, Klaproth B, Himmelreich U, Dromer F, & Janbon G (2002) Isolation and characterization of capsule structure mutant strains of *Cryptococcus neoformans*. *Mol Microbiol* 45(3):837-849.

41. Reese AJ & Doering TL (2003) Cell wall alpha-1,3-glucan is required to anchor the *Cryptococcus neoformans* capsule. *Mol Microbiol* 50(4):1401-1409.

42. Gilbert NM, Lodge JK, & Specht CA (2011) The Cell Wall of *Cryptococcus*. *Cryptococcus From Human Pathogen to Model Yeast*, eds Heitman J, Kozel TR, Kwon-Chung KJ, Perfect J, & Casadevall A (ASM Press, Washington), pp 67-79.

43. Santiago-Tirado FH, Peng T, Yang M, Hang HC, & Doering TL (2015) A Single Protein S-acyl Transferase Acts through Diverse Substrates to Determine Cryptococcal Morphology, Stress Tolerance, and Pathogenic Outcome. *PLoS Pathog* 11(5):e1004908.

44. Zhu X & Williamson PR (2004) Role of laccase in the biology and virulence of *Cryptococcus neoformans*. *FEMS Yeast Res* 5(1):1-10.

45. Nosanchuk JD & Casadevall A (2006) Impact of melanin on microbial virulence and clinical resistance to antimicrobial compounds. *Antimicrob Agents Chemother* 50(11):3519-3528.

46. Panepinto JC & Williamson PR (2006) Intersection of fungal fitness and virulence in *Cryptococcus neoformans*. *FEMS Yeast Res* 6(4):489-498.

47. Srikanta D, Yang M, Williams M, & Doering TL (2011) A sensitive high-throughput assay for evaluating host-pathogen interactions in *Cryptococcus neoformans* infection. *PLoS One* 6(7):e22773.

48. Muraoka M, Kawakita M, & Ishida N (2001) Molecular characterization of human UDP-glucuronic acid/UDP-N-acetylgalactosamine transporter, a novel nucleotide sugar transporter with dual substrate specificity. *FEBS Lett* 495(1-2):87-93.

49. Dean N, Zhang YB, & Poster JB (1997) The *VRG4* gene is required for GDP-mannose transport into the lumen of the Golgi in the yeast, *Saccharomyces cerevisiae*. *J Biol Chem* 272:31908-31914.

50. Gao XD & Dean N (2000) Distinct protein domains of the yeast Golgi GDP-mannose transporter mediate oligomer assembly and export from the endoplasmic reticulum. *J Biol Chem* 275:17718–17727.

51. Goto S, *et al.* (2001) UDP-sugar transporter implicated in glycosylation and processing of Notch. *Nat Cell Biol* 3(9):816-822.

52. Belay T, Cherniak R, Kozel TR, & Casadevall A (1997) Reactivity patterns and epitope specificities of anti-*Cryptococcus neoformans* monoclonal antibodies by enzyme-linked immunosorbent assay and dot enzyme assay. *Infect Immun* 65(2):718-728.

53. Kozel TR, *et al.* (2003) Antigenic and biological characteristics of mutant strains of *Cryptococcus neoformans* lacking capsular O acetylation or xylosyl side chains. *Infect Immun* 71(5):2868-2875.

54. Heise N, *et al.* (2002) Molecular analysis of a novel family of complex glycoinositolphosphoryl ceramides from *Cryptococcus neoformans*: structural differences between encapsulated and acapsular yeast forms. *Glycobiology* 12(7):409-420.

55. Biondo C, *et al.* (2005) Characterization of two novel cryptococcal mannoproteins recognized by immune sera. *Infect Immun* 73(11):7348-7355.

56. Turner KM, Wright LC, Sorrell TC, & Djordjevic JT (2006) N-linked glycosylation sites affect secretion of cryptococcal phospholipase B1, irrespective of glycosylphosphatidylinositol anchoring. *Biochim Biophys Acta* 1760(10):1569-1579.

57. Park JN, *et al.* (2012) Unraveling unique structure and biosynthesis pathway of N-linked glycans in human fungal pathogen *Cryptococcus neoformans* by glycomics analysis. *J Biol Chem* 287(23):19501-19515.

58. Voelz K & May RC (2010) Cryptococcal interactions with the host immune system. *Eukaryot Cell* 9(6):835-846.

59. Edgar RC (2004) MUSCLE: multiple sequence alignment with high accuracy and high throughput. *Nucleic Acids Res* 32(5):1792-1797.

60. Guindon S & Gascuel O (2003) A simple, fast, and accurate algorithm to estimate large phylogenies by maximum likelihood. *Syst Biol* 52(5):696-704.

61. Chevenet F, Brun C, Banuls AL, Jacq B, & Christen R (2006) TreeDyn: towards dynamic graphics and annotations for analyses of trees. *BMC Bioinformatics* 7:439.

62. Dereeper A, *et al.* (2008) Phylogeny.fr: robust phylogenetic analysis for the non-specialist. *Nucleic Acids Res* 36(Web Server issue):W465-469.

63. Dereeper A, Audic S, Claverie JM, & Blanc G (2010) BLAST-EXPLORER helps you building datasets for phylogenetic analysis. *BMC Evol Biol* 10:8.

64. Dobson L, Remenyi I, & Tusnady GE (2015) CCTOP: a Consensus Constrained TOPology prediction web server. *Nucleic Acids Res* 43(W1):W408-412.

65. Dobson L, Remenyi I, & Tusnady GE (2015) The human transmembrane proteome. *Biol Direct* 10:31.

66. Omasits U, Ahrens CH, Muller S, & Wollscheid B (2014) Protter: interactive protein feature visualization and integration with experimental proteomic data. *Bioinformatics* 30(6):884-886.

67. King BR & Guda C (2007) ngLOC: an n-gram-based Bayesian method for estimating the subcellular proteomes of eukaryotes. *Genome Biol* 8(5):R68.

68. Fu J, Hettler E, & Wickes BL (2006) Split marker transformation increases homologous integration frequency in *Cryptococcus neoformans*. *Fungal Genet Biol* 43(3):200-212.

69. Yoneda A & Doering TL (2008) Regulation of *Cryptococcus neoformans* capsule size is mediated at the polymer level. *Eukaryot Cell* 7(3):546-549.

70. Percival A, Thorkildson P, & Kozel TR (2011) Monoclonal antibodies specific for immunorecessive epitopes of glucuronoxylomannan, the major capsular polysaccharide of *Cryptococcus neoformans*, reduce serotype bias in an immunoassay for cryptococcal antigen. *Clin Vaccine Immunol* 18(8):1292-1296.

71. Rautengarten C, *et al.* (2016) The Arabidopsis Golgi-localized GDP-L-fucose transporter is required for plant development. *Nature Communications* 7.

72. Ito J, *et al.* (2014) Analysis of plant nucleotide sugars by hydrophilic interaction liquid chromatography and tandem mass spectrometry. *Analytical Biochemistry* 448:14-22.

73. Rautengarten C, *et al.* (2014) The Golgi localized bifunctional UDP-rhamnose/UDP-galactose transporter family of Arabidopsis. *Proceedings of the National Academy of Sciences of the United States of America* 111(31):11563-11568.

74. Maier EJ, *et al.* (2015) Model-driven mapping of transcriptional networks reveals the circuitry and dynamics of virulence regulation. *Genome Res* 25(5):690-700.

75. Salas SD, Bennett JE, Kwon-Chung KJ, Perfect JR, & Williamson PR (1996) Effect of the laccase gene *CNLAC1*, on virulence of *Cryptococcus neoformans*. *J Exp Med* 184(2):377-386.

76. Klutts JS, Levery SB, & Doering TL (2007) A beta-1,2-xylosyltransferase from *Cryptococcus neoformans* defines a new family of glycosyltransferases. *J Biol Chem* 282(24):17890-17899.

77. Castle SA, *et al.* (2008) Beta1,2-xylosyltransferase Cxt1p is solely responsible for xylose incorporation into *Cryptococcus neoformans* glycosphingolipids. *Eukaryot Cell* 7(9):1611-1615.

78. Klutts JS & Doering TL (2008) Cryptococcal xylosyltransferase 1 (Cxt1p) from *Cryptococcus neoformans* plays a direct role in the synthesis of capsule polysaccharides. *J Biol Chem* 283(21):14327-14334.

2.8 Figures

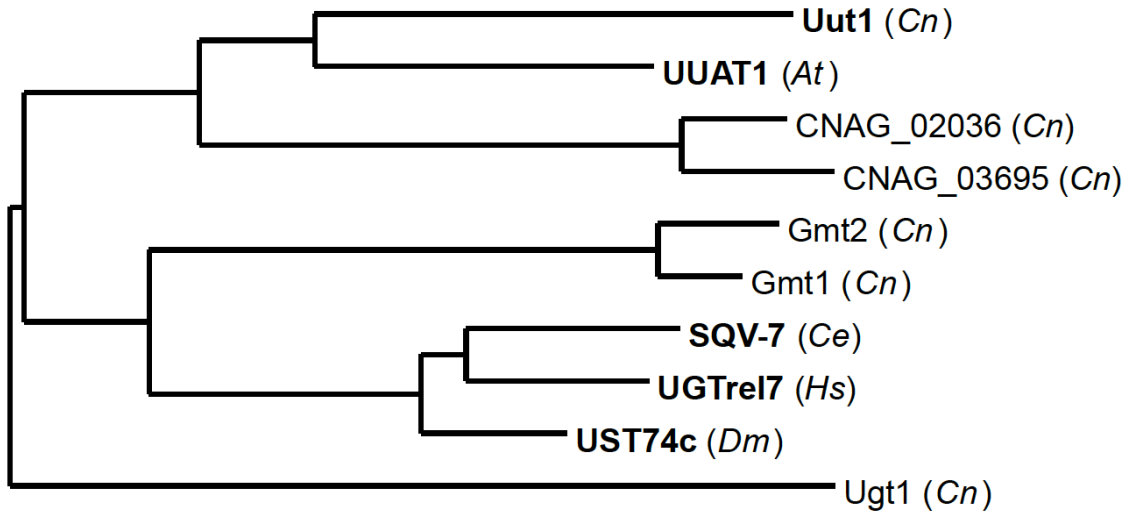

Figure 2.1. Evolutionary conservation of UDP-GlcA transporters. Phylogenetic relationships of *C. neoformans* (*Cn*) nucleotide sugar transporters (NSTs) and other UDP-GlcA transporters (shown in boldface type) from *Caenorhabditis elegans* (*Ce*), *Homo sapiens* (*Hs*), *Drosophila melanogaster* (*Dm*), and *Arabidopsis thaliana* (*At*). Tree reconstruction was performed with the Phylogeny.fr web server (62, 63) using MUSCLE, PhyML, and TreeDyn software. Branch lengths are drawn to scale.

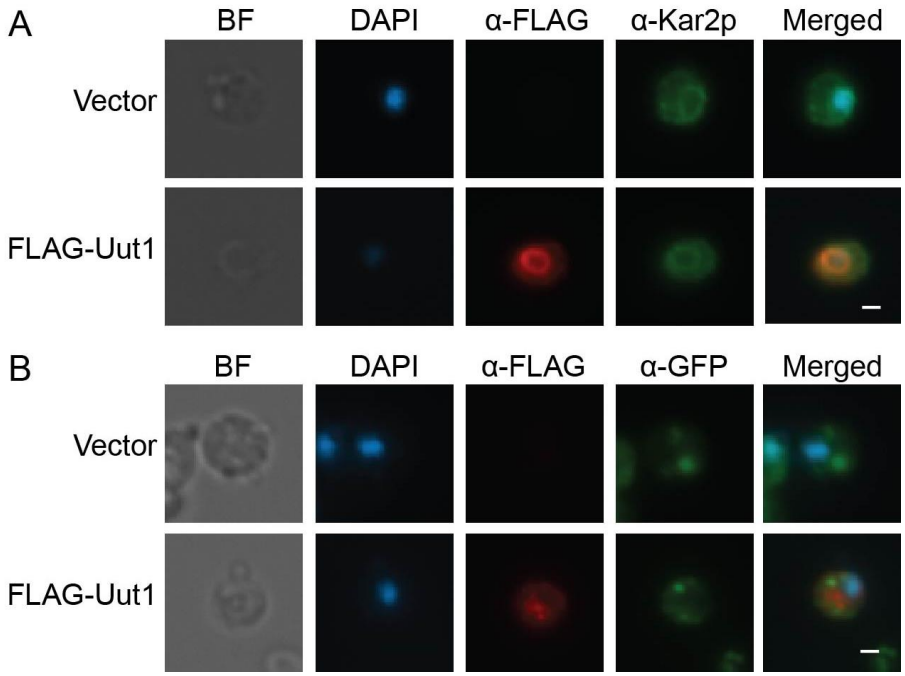

Figure 2.2. Cryptococcal Uut1 colocalizes with the ER marker Kar2p/BiP (A), but not with the late Golgi marker Sec7 (B). Sec7-3xGFP *S. cerevisiae* cells transformed with vector alone (Vector) or vector expressing FLAG-tagged Uut1 (FLAG-Uut1) were stained with DAPI and probed with the indicated antibodies. Bright field (BF), single-channel, and merged images are shown, all images have the same magnification (bars, 1 μm). The colors indicate the following: blue, DAPI; red, anti-FLAG (α-FLAG); green, anti-GFP (α-GFP) and anti-Kar2p/BiP (α-Kar2p/BiP). Images are representative of three independent immunofluorescence experiments.

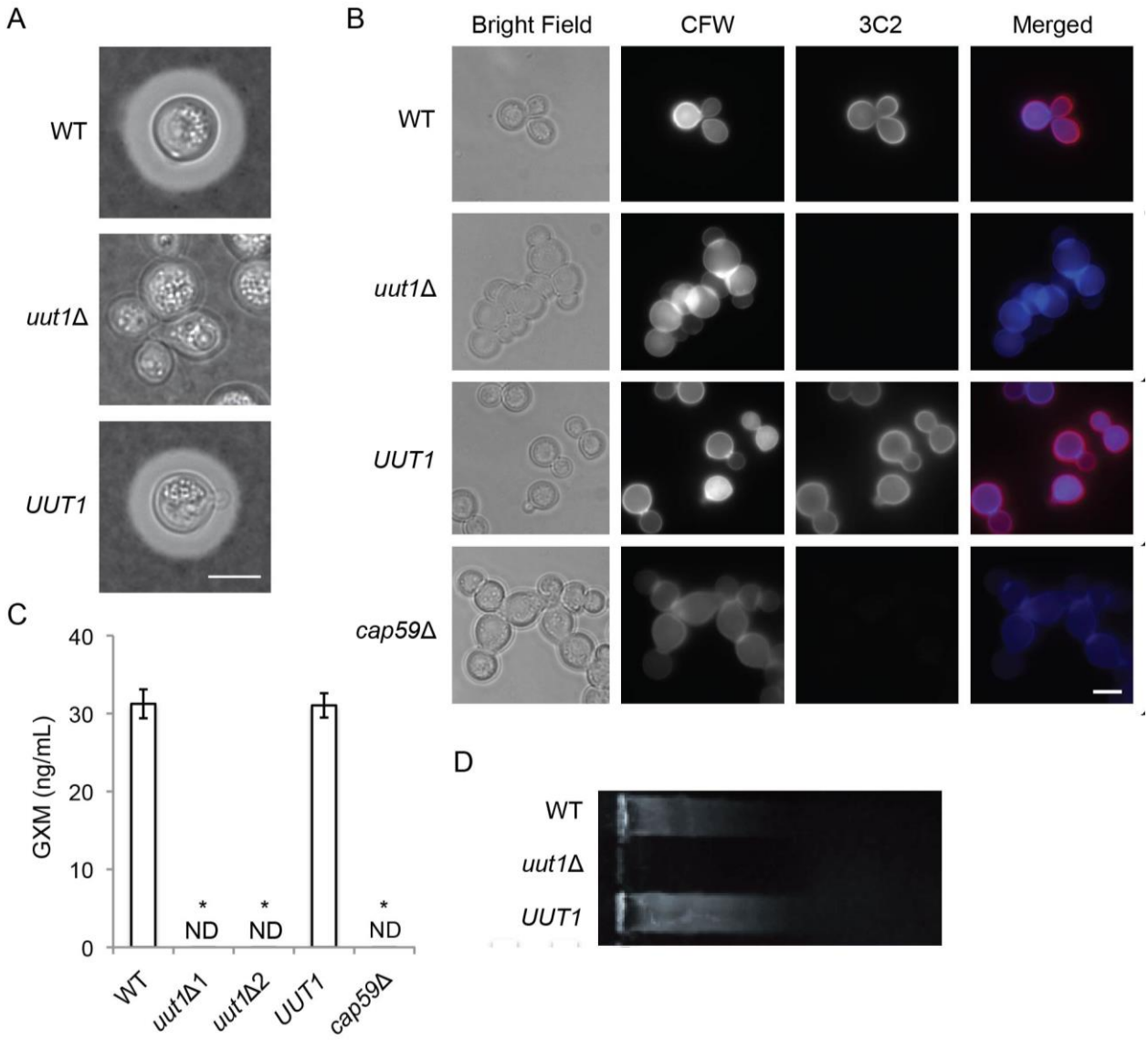

Figure 2.3. The *uut1*Δ mutant does not produce capsule. (A) Wild-type (WT), *uut1*Δ, and complemented *uut1*Δ (*UUT1*) strains were cultured under capsule-inducing conditions (see Materials and methods) for 24 h and then visualized by light microscopy after negative staining with India ink. Bar = 5 μm. (B) Cells from the indicated strains were incubated with calcofluor white (CFW; blue) to stain the cell wall, and mAb 3C2 (red) to visualize the capsule. Bright field, single-channel gray scale, and merged images are shown. Bar = 5 μm. (C) Shed capsule polysaccharide, from two independent deletions and control strains, was quantitated by ELISA (see Materi-

als and methods). Values are means ± SEM from three independent experiments. Values that are significantly different ($P < 0.01$) by one-way ANOVA and Tukey's posthoc test from the value for the WT strain are indicated by an asterisk. ND, not detected. (D) Conditioned medium from the indicated strains was resolved on an agarose gel, transferred to a nylon membrane, and analyzed by immunoblotting with anti-GXM mAb 3C2 as in reference 69.

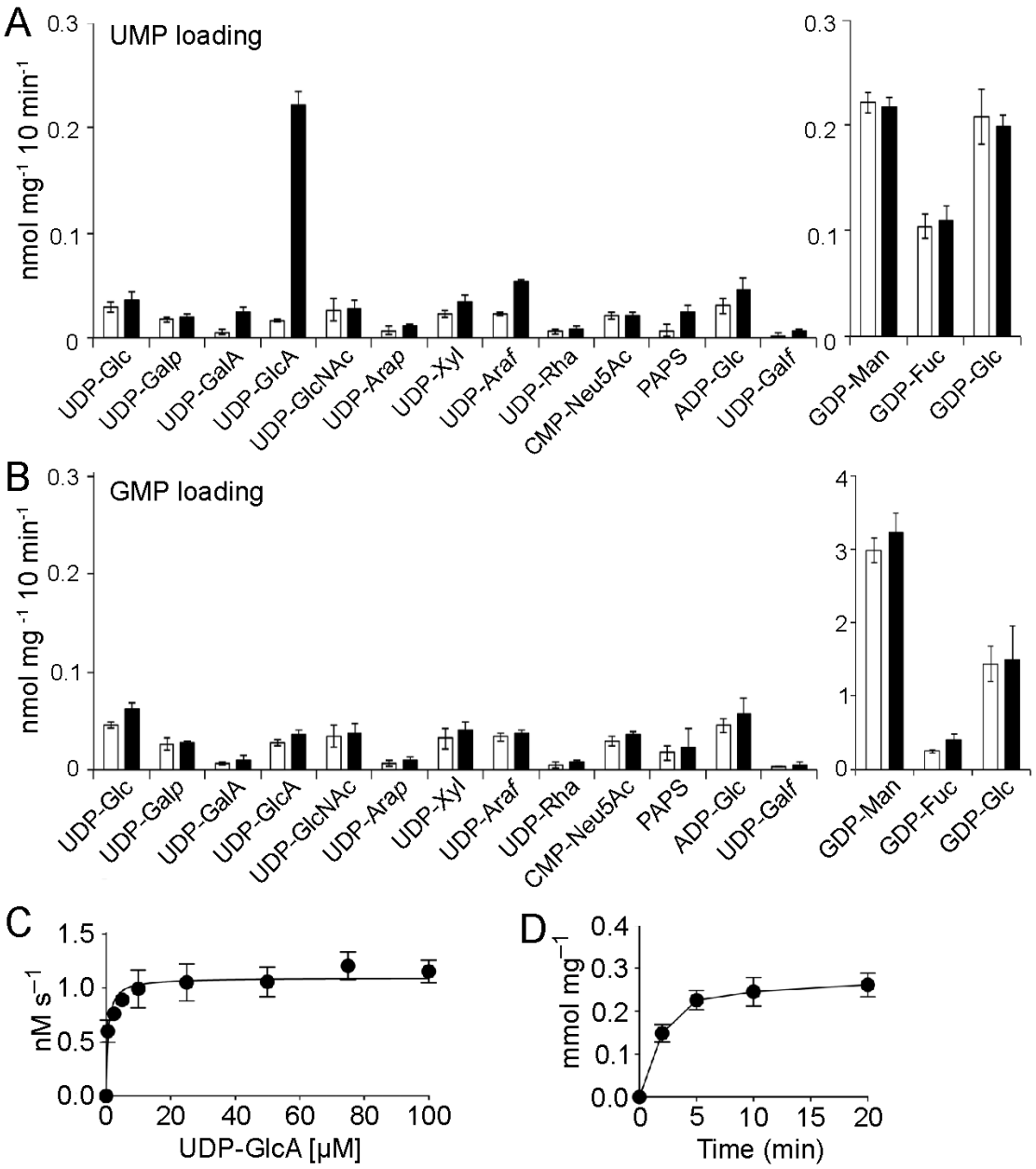

Figure 2.4. Uut1 activity *in vitro*. (A, B) Substrate and exchange substrate specificity of Uut1. Proteoliposomes from cells without Uut1 (white bars) or with Uut1 (black bars), preloaded with 30 mM UMP (A) or 30 mM GMP (B), were incubated for 10 min with a mixture of the indicated nucleotide sugars, each at 50 µM. Data were normalized to the total protein content of the proteoliposome preparations. (C) Proteoliposomes from cells expressing Uut1, preloaded with 10 mM UMP, were incubated with UDP-GlcA at the indicated concentrations for 2 min and UDP-GlcA

transport was measured as described in Materials and methods. (D) Proteoliposomes, preloaded as described for panel C, were assayed with 50 μM UDP-GlcA for the times shown. Values are normalized to the Uut1 content of the proteo-liposome preparations (Table 2.S2). All values shown are the means ± SEMs from four independent experiments.

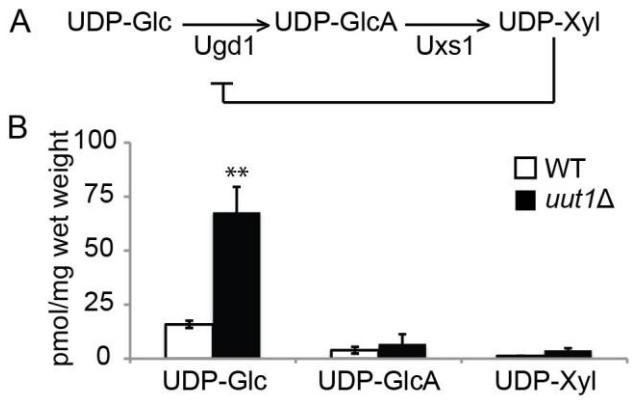

Figure 2.5. UDP-GlcA metabolism. (A) UDP-GlcA synthesis and regulation. (B) Nucleotide sugar concentrations in the *uut1*Δ mutant (black bars) compared to the WT control (white bars). Values are the averages ± SEMs of four independent replicates. Values that are significantly different ($P \leq 0.01$) by two-tailed Student's *t* test are indicated by two asterisks.

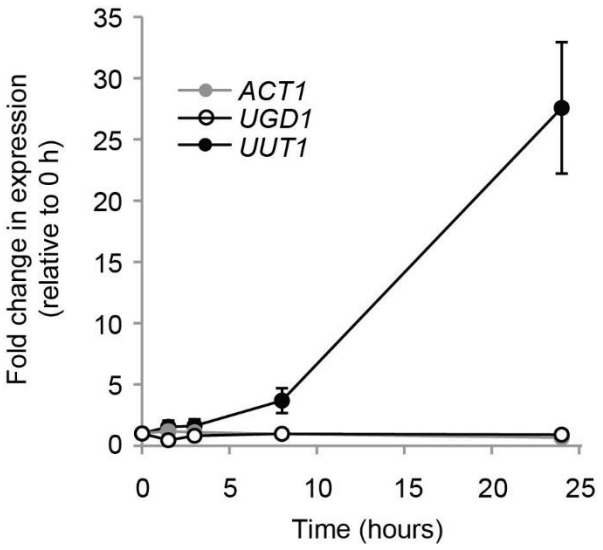

Figure 2.6. Transcription of *UUT1* increases during capsule induction. The number of reads from RNA-Seq data (mean ± SD) during capsule induction (see Materials and methods) were normalized to their levels at t = 0, which were as follows: 125691 ± 8645 for *UUT1*; 1761976 ± 108920 for *UGD1*; and 4495647 ± 279579 for *ACT1* (included as a control). Values shown are compiled from three independent experiments, each with RNA prepared from three biological replicates as in reference 74.

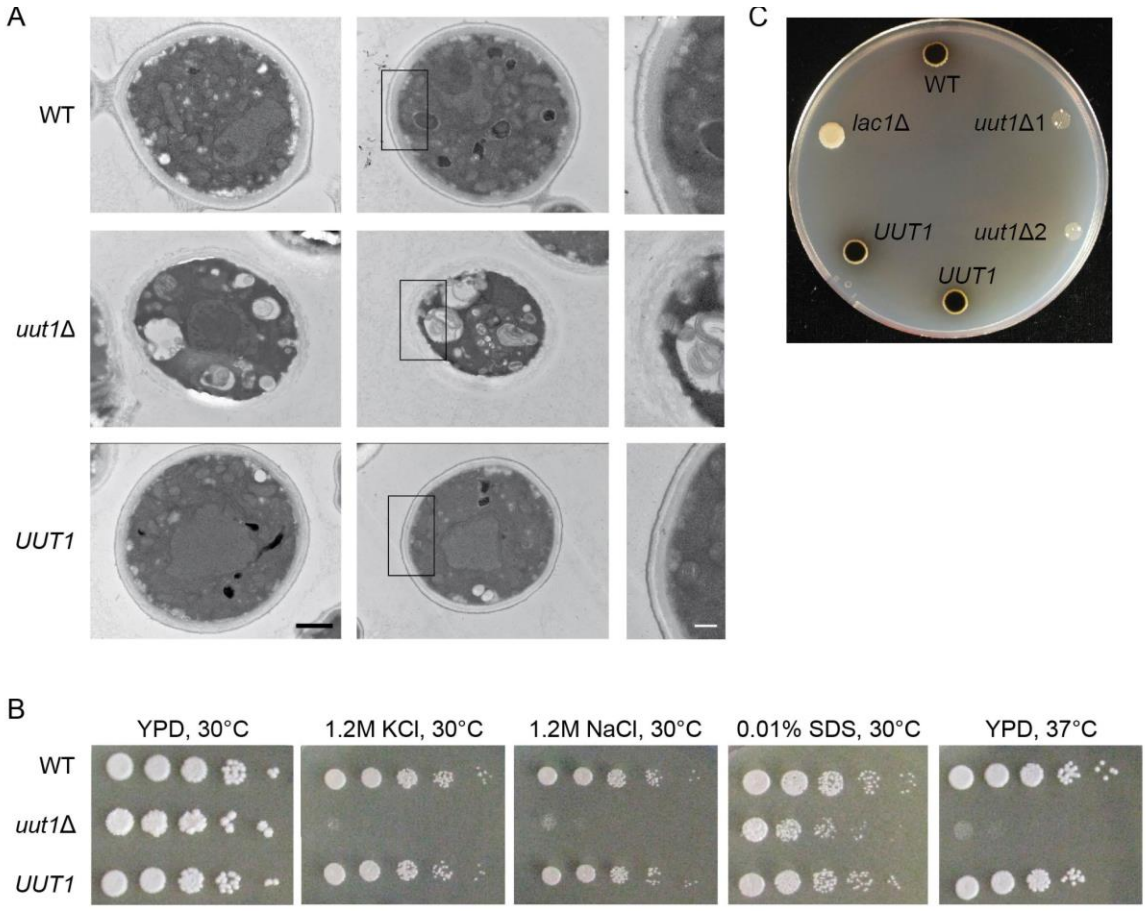

Figure 2.7. *uut1*Δ mutants exhibit defects in cell morphology and growth. (**A**) Electron micrographs of WT, *uut1*Δ, and *UUT1* strains grown in rich medium (left and middle columns, bar = 1 μm) with enlarged insets (right column, bar = 0.25 μm). (**B**) Melanization of the indicated strains after growth on L-DOPA plates (see Materials and methods). *lac1*Δ cells do not melanize (75). (**C**) The indicated strains were grown overnight at 30°C in YPD medium, and 5-μl volumes of serial dilutions (10-fold starting at 10^6 cells/mL) were spotted and grown on YPD or minimal medium under the conditions shown. Images of the 30 °C and 37 °C plates were taken 2 and 3 days after inoculation, respectively.

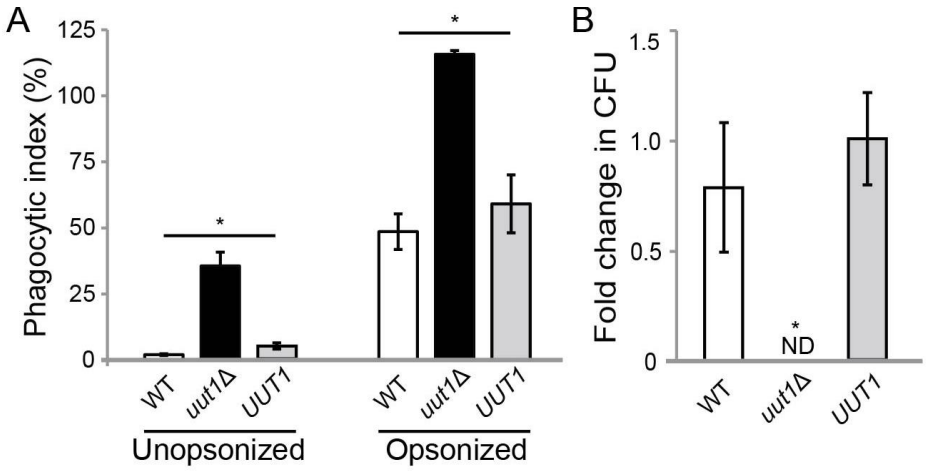

Figure 2.8. Cells lacking Uut1 are more efficiently phagocytosed and killed by human cells than wild-type *C. neoformans*. (A) Phagocytic index (engulfed fungi per 100 host cells) for fungi with or without serum opsonization. (B) Fold change in CFU (comparing results at 24 h to results at 1 h) after internalization of opsonized fungi by THP-1 cells. Data are the means ± SEMs for three biological replicates. Values that are significantly different ($P < 0.05$) by one-way ANOVA and Tukey's posthoc test are indicated by an asterisk. ND, not detected.

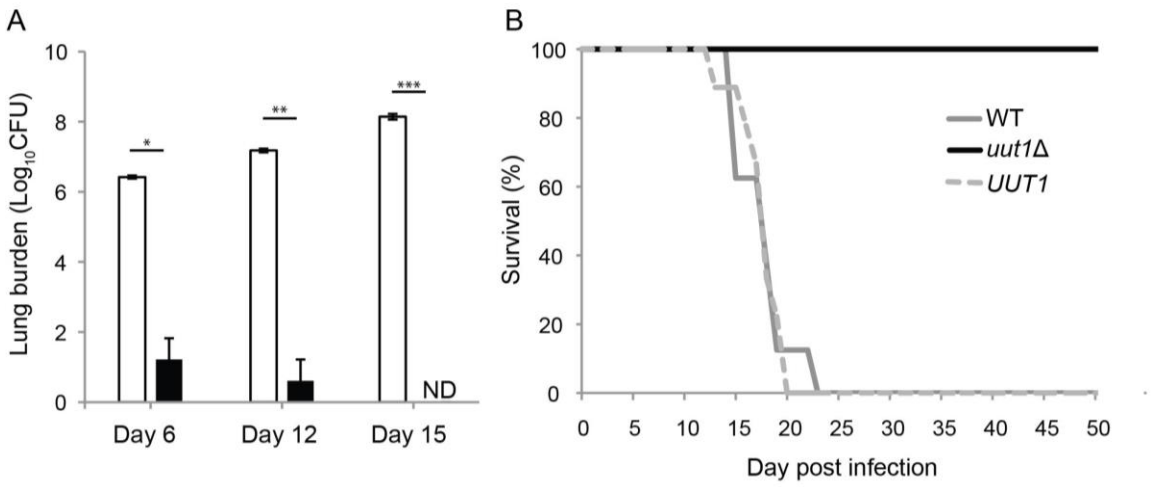

Figure 2.9. *uut1*Δ is severely attenuated for virulence. (A) Lung CFU of mice infected intranasally with 5 x 10^4 cells of WT (white bars) or the *uut1*Δ mutant (black bars). Values that are significantly different by two-tailed Student's *t* test are indicated by bars and asterisks as follows: *, $P < 0.05$; **, $P < 0.01$; ***, $P < 0.001$. ND, not detected. (B) Survival of mice infected as in panel A with the indicated strains (8 or 9 mice per strain).

2.9 Supplementary materials

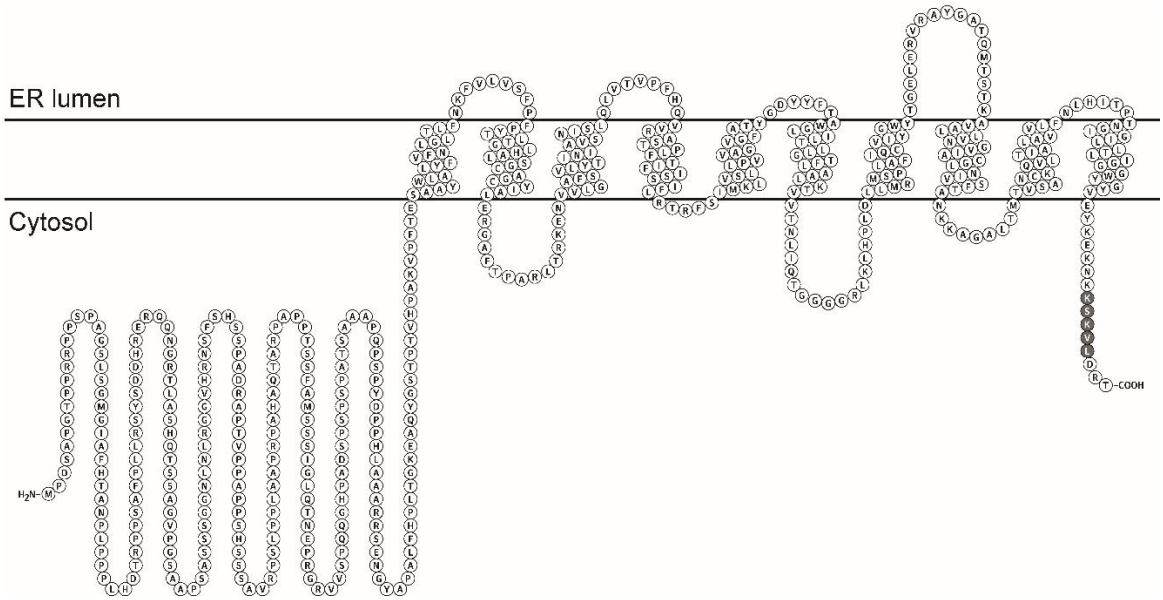

Figure 2.S1. Predicted secondary structure of Uut1 (550 amino acids), showing an extended N-terminal domain (amino acids 1 to 244), 10 predicted transmembrane domains, and a predicted ER localization signal (KXKXX motifs; dark grey) near the C terminus.

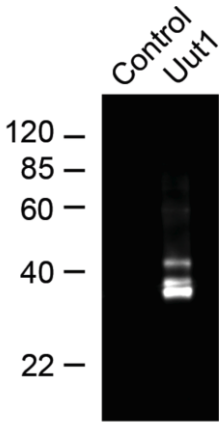

Figure 2.S2. Anti-V5 immunoblot of proteoliposomes prepared from *S. cerevisiae* expressing vector alone (control) or V5-tagged Uut1; 2.5 μg of total protein was loaded into each lane. The positions of the molecular mass standards (in kDa) are shown to the left of the gel. In *S. cerevisiae*, the expressed and active polypeptide is cleaved prior to amino acid 200.

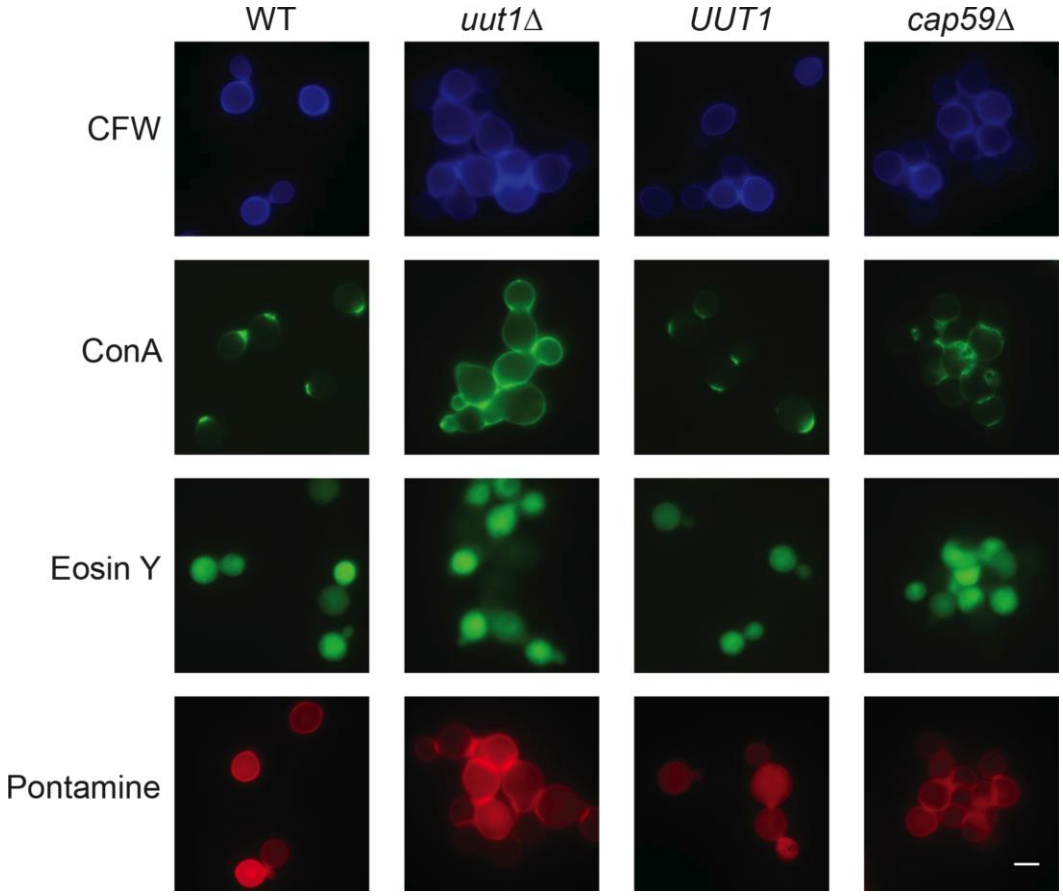

Figure 2.S3. Surface exposure of cell wall components. WT, *uut1*Δ, *UUT1*, and *cap59*Δ strains were grown and stained with CFW (binds chitin), concanavalin A (binds mannoproteins), eosin Y (binds chitosan), and Pontamine (binds unspecified cell wall components). The images shown are representative of two independent experiments. Bar = 5 μm.

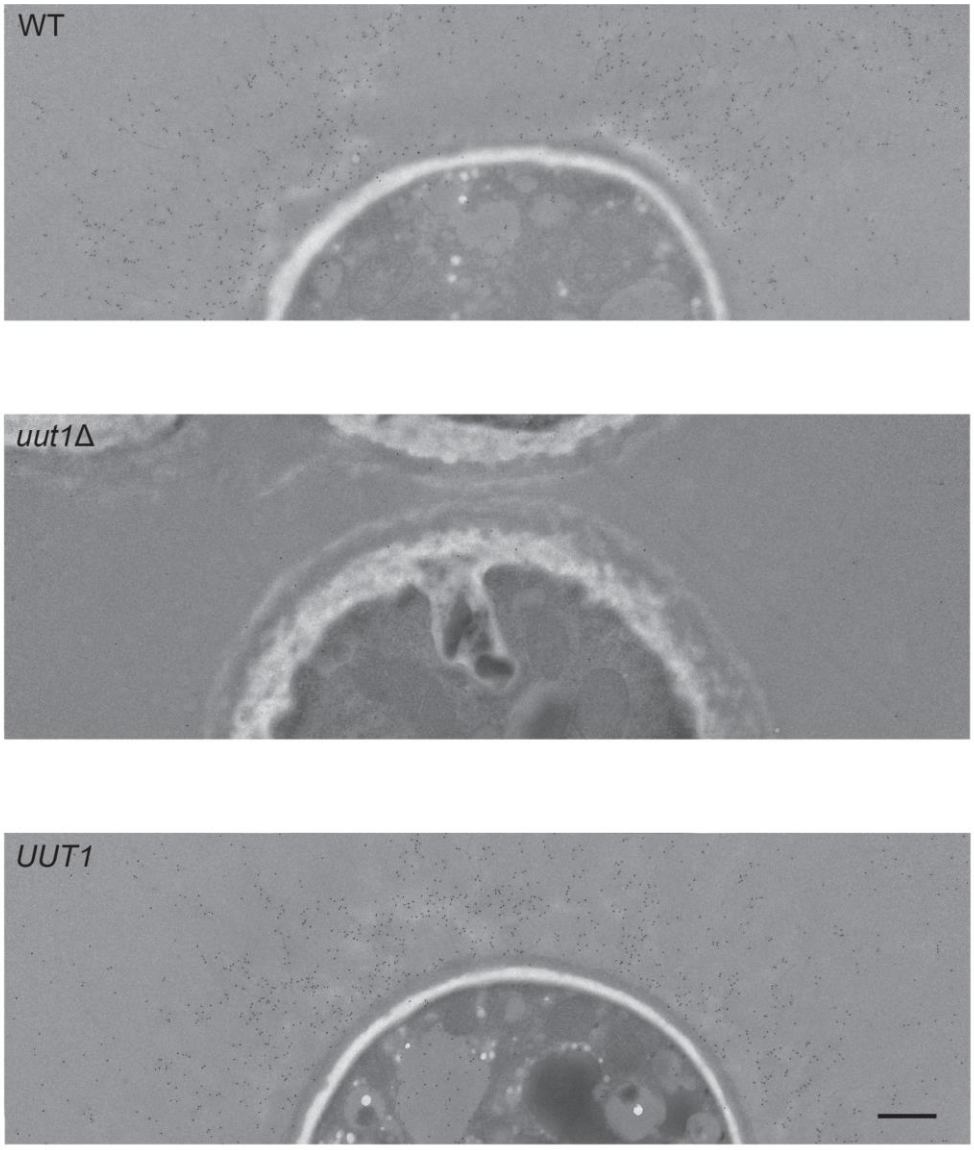

Figure 2.S4. GXM is not detected within or around *uut1*Δ cells, in contrast to the abundant labeling of this capsule component on WT and complemented controls. Shown are electron micrographs of WT, *uut1*Δ, and *UUT1* strains grown for 24 h in nutrient-deficient media, which induces capsule production. Sections were labeled with anti-GXM mAb 3C2 and 12-nm gold-conjugated anti-mouse antibody, which appears as black dots. Bar = 500 nm.

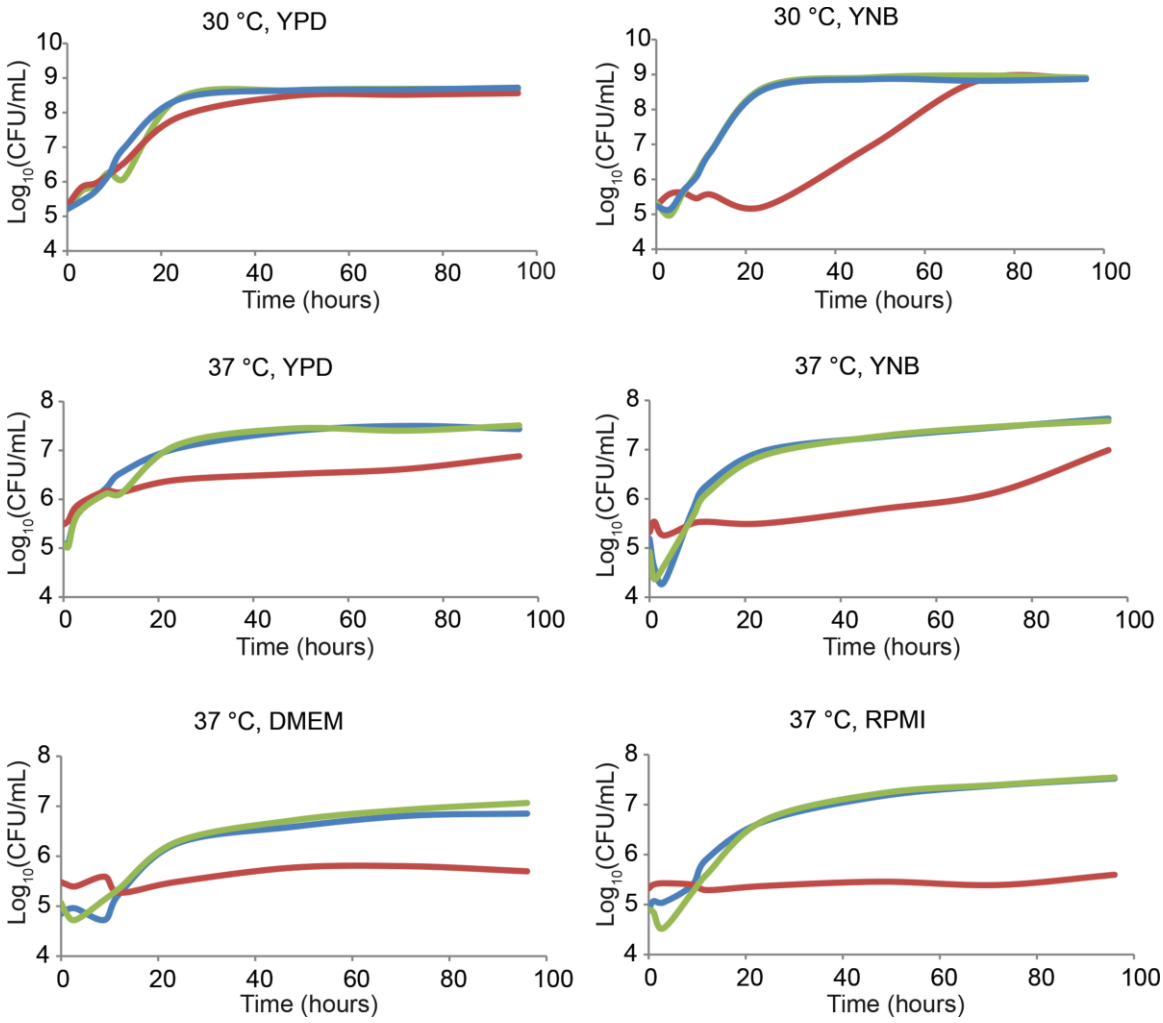

Figure 2.S5. Growth of *uut1*Δ mutant (red) is restricted at 37 °C and at 30 °C under nutrient-limiting conditions (either the yeast medium YNB or mammalian tissue culture media DMEM and RPMI 1640) compared to wild type (blue) and the complemented mutant (green). Strains were grown overnight at 30 °C in YPD medium, diluted to 10^5 cells per mL in the media indicated, and incubated at 30 or 37 °C with shaking. The results shown are the averages of three measurements.

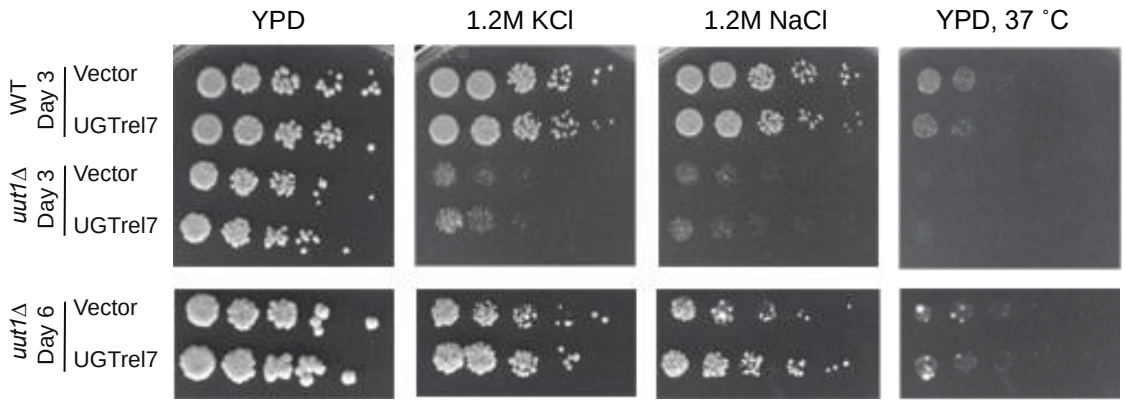

Figure 2.S6. The human UDP-GlcA transporter does not complement *uut1*Δ. *uut1*Δ and WT strains transformed with vector alone (vector) or vector expressing His-tagged UGTrel7 were grown overnight at 30°C in YPD with G418, and 5 μL of serial dilutions (10-fold starting at 10^6 cells per mL) were spotted and grown as indicated on medium containing G418. Images of the WT and *uut1*Δ strains were taken three and six days later as indicated.

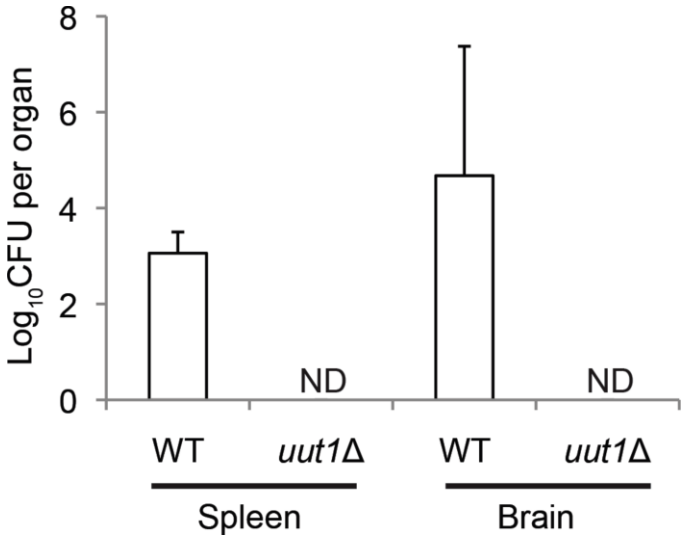

Figure 2.S7. *uut1*Δ does not disseminate from the lung. Brain and spleen CFU at day 15 post infection. Data shown is the mean ± SD for 3 mice.

Table 2.S1. Summary of GXM detection assays.

	ELISA (ng/mL, mean ± SEM)		GXM blotting				Capsule staining
mAb / Strain	339	F12D2	2H1	3O2	339	F12D2	2H1
WT	31.9 ± 0.3	113.3 ± 12.9	+	+	+	+	+
*uut1*Δ	0 ± 0	0 ± 0	-	-	-	-	-
UUT1	25.2 ± 3.2	69.8 ± 7.7	+	+	+	+	+
*cap59*Δ	0 ± 0	0 ± 0	-	-	-	-	-

Table 2.S2. Uut1 content of proteoliposomes used for transport assays.

	Molecular Mass (Da)	fmol*/5 µg	ng/5 µg	Total protein (%)
Uut1	63195.7	79.7 ± 4.1[†]	5.0 ± 0.3[†]	0.1 ± 0.0[†]

*Amount was estimated using LC-MS/MS (MRM) quantitation of a C-terminal peptide (SRGPFEGKPIPNPLLGLDSTR) and interpreted based on the molecular mass (including V5-tag and 6-His tags) estimated using the Compute pI/Mw tool at ExPASy (http://web.expasy.org/).

[†]Values represent the mean ± SD of three independent experiments.

Chapter 3: Xylose donor transport is critical for fungal virulence

From:

Xylose donor transport is critical for fungal virulence

Lucy X. Li, Carsten Rautengarten, Joshua L. Heazlewood, and Tamara L. Doering

Plos Pathogens. 2018, 14(1):e1006765. doi: 10.1371/journal.ppat.1006765. PMID: 29346417

3.1 Abstract

Cryptococcus neoformans, an AIDS-defining opportunistic pathogen, is the leading cause of fungal meningitis worldwide and is responsible for hundreds of thousands of deaths annually. Cryptococcal glycans are required for fungal survival in the host and for pathogenesis. Most glycans are made in the secretory pathway, although the activated precursors for their synthesis, nucleotide sugars, are made primarily in the cytosol. Nucleotide sugar transporters are membrane proteins that solve this topological problem, by exchanging nucleotide sugars for the corresponding nucleoside phosphates. The major virulence factor of *C. neoformans* is an anti-phagocytic polysaccharide capsule that is displayed on the cell surface; capsule polysaccharides are also shed from the cell and impede the host immune response. Xylose, a neutral monosaccharide that is absent from model yeast, is a significant capsule component. Here we show that Uxt1 and Uxt2 are both transporters specific for the xylose donor, UDP-xylose, although they exhibit distinct subcellular localization, expression patterns, and kinetic parameters. Both proteins also transport the galactofuranose donor, UDP-galactofuranose. We further show that Uxt1 and Uxt2 are required for xylose incorporation into capsule and protein; they are also necessary for *C. neoformans* to cause disease in mice, although surprisingly not for fungal viability in the context of infection. These findings provide a starting point for deciphering the substrate specificity of an important class of transporters, elucidate a synthetic pathway that may be productively targeted for therapy, and contribute to our understanding of fundamental glycobiology.

3.2 Introduction

Glycans are critical for the normal development, growth, and viability of organisms across all kingdoms of life. The extensive glycoconjugate repertoire of *Cryptococcus neoformans*, a ubiq-

uitous environmental fungus, enables this pathogen to cause serious respiratory disease in the setting of immune compromise. This pulmonary infection often progresses to a lethal meningoencephalitis, even with treatment, leading to several hundred thousand deaths each year (1-3).

The major virulence factor of *C. neoformans*, a polysaccharide capsule, acts as a physical barrier against host defenses when associated with the cell wall and as an immune modulator when shed into the extracellular space (4, 5). This material consists primarily of two complex polysaccharides, glucuronoxylomannan (*GXM*) and glucuronoxylomannanogalactan (GXMGal) (4). The more abundant capsule component, GXM, is a linear mannose (Man) polymer with single glucuronic acid (GlcA) and xylose (Xyl) side chains (6). The second polysaccharide, GXMGal, consists of a galactose backbone modified with single galactofuranose (Gal*f*) residues and galactomannan side chains bearing a variable number of GlcA and Xyl residues (7-9).

Beyond the capsule, *C. neoformans* glycoconjugates include proteins with *N*- and *O*-linked glycans that resemble the corresponding mannose structures of the model yeast *Saccharomyces cerevisiae*, although they are further modified with Xyl or Xyl-phosphate residues (10-13). Cryptococcal glycosphingolipids range from simple mannose modification of lipids to more complex structures that also incorporate galactose (Gal) and Xyl (14), and the cryptococcal cell wall consists of glucans, chitin, chitosan, and mannoproteins, many of which bear GPI anchors (15). These glycans play integral structural and regulatory roles to facilitate fungal survival and pathogenesis (16).

Consistent with the abundant glycosylation of *C. neoformans*, a significant portion of its genetic

machinery and metabolic energy is dedicated to glycan synthesis. These synthetic reactions typically occur in the secretory pathway, although they rely on nucleotide sugar donors that are synthesized in the cytosol (17). The charged donors enter the luminal space via nucleotide sugar transporters (NSTs), which exchange activated sugars for the corresponding nucleoside monophosphates (18, 19). NSTs thus mediate a limiting step in glycan biosynthesis and are consequently required for cryptococcal viability and pathogenicity (20-22).

Our focus is on defining glycan synthesis in *C. neoformans*, motivated by its unique biology and critical role in a deadly disease. Cryptococcal NSTs comprise a key subset of this machinery, which has stimulated us to identify these proteins and their functions. This effort is complicated by the observations that NST homology is not always a reliable predictor of substrate specificity and that NSTs may be functionally redundant. Individual NSTs also range from highly specific single-substrate transporters to more promiscuous, multi-substrate proteins (23-28). NST substrate specificity may also be modulated by localization to a particular cellular compartment and/or association with other glycan biosynthetic enzymes (21, 29).

In prior work, protein structure predictions and homology facilitated identification of the cryptococcal NSTs responsible for GDP-Man (21, 30) and UDP-Gal (20, 22) transport. We have now used product analysis and mass spectrometry-based assays to discover Uxt1 and Uxt2, which both transport UDP-Xyl although they exhibit distinct subcellular localization, expression patterns, and kinetic parameters. Cells without these two proteins lack Xyl in all analyzed glycoconjugates, and exhibit growth defects and metabolic abnormalities that are present to a lesser extent

in single mutant strains. We further made the unexpected finding that transporter function is required for virulence in a mouse model of disease but not for persistence in that context.

3.3 Results

3.3.1 Identification of cryptococcal UDP-xylose transporters

In examining the cryptococcal genome for genes encoding putative NSTs, we discovered a pair of sequences (CNAG_02036 and CNAG_03695) that encoded closely related proteins (57% identity at the amino acid level; Fig. 3.S1A). We were interested in these sequences because the level of identity could indicate functional redundancy to ensure transport of a key glycan precursor, or, in the absence of shared activity, could shed light on mechanisms of substrate specificity.

To assess the biological role of the novel protein pair we had identified, we generated single and double deletion strains. We first tested whether these mutations affected the major cryptococcal virulence factor, its polysaccharide capsule. Composition analysis of capsule GXM showed complete loss of Xyl from the double mutant, while single mutants were less affected (Fig 3.1A). This suggested that both proteins transported the Xyl precursor UDP-Xyl, so we designated them as UDP-Xyl transporters 1 and 2 (Uxt1 and Uxt2). *uxt1*Δ GXM had only 20% of the Xyl found in WT material, while *uxt2*Δ exhibited no defect in composition. Consistent with these results, linkage analysis of GXM mannose residues showed a dramatic shift to less substitution of the mannose backbone in the double mutant, with a slightly lesser shift in *uxt1*Δ (Table 3.S1).

To further examine the mutant capsules, we used a Xyl-dependent monoclonal antibody to GXM (31). This antibody, F12D2, labeled both single mutant strains, but not the *uxt1*Δ *uxt2*Δ strain

(Fig. 3.1B). In this respect the double mutant resembled *uxs1*Δ, a strain that does not synthesize UDP-Xyl (32). Both *uxt1*Δ *uxt2*Δ and *uxs1*Δ still bind Xyl-independent anti-GXM monoclonal antibodies (Fig. 3.S2, Table 3.S2).

We next used an unbiased approach to directly measure UDP-Xyl transport activity and assay for additional transport substrates. To do this, we prepared microsomes from *S. cerevisiae* heterologously expressing Uxt1 and Uxt2 (Fig. 3.2A). When these were preloaded with UMP we observed import of UDP-Xyl (Fig. 3.2B-D), consistent with our composition studies and antibody binding results. Transport of UDP-Xyl by both proteins was saturable with substrate (Fig. 3.2E) and time (Fig. 3.2F). Uxt1 had an apparent K_M of 1.0 ± 0.2 μM and V_{max} of 20.4 ± 0.6 nM s^{-1} (mean ± SEM of n = 4) with a turnover rate of 0.9 s^{-1}, while Uxt2 exhibited lower affinity and catalytic efficiency with an apparent K_M of 2.2 ± 0.5 μM, V_{max} of 2.2 ± 0.1 nM s^{-1}, and a turnover rate of 0.4 s^{-1}. These K_M values were consistent with the estimated μM physiological concentration of UDP-Xyl (Table 3.S3).

We further observed transport of UDP-Gal*f*, the donor of a known capsule component, although assessment of its transport kinetics was hindered by its instability, which necessitates simultaneous synthesis and assay. We also observed transport of UDP-Ara*p* and UDP-Ara*f* (Fig. 3.2C, Fig. 3.2D, Fig. 3.S3) although arabinose has never been reported in *C. neoformans*. Neither of these donor molecules were detected in our nucleotide sugar analyses (Table 3.S3).

Surprisingly, Uxt2 was almost as efficient in using GMP as UMP as an antiport substrate for UDP-Xyl and UDP-Gal*f*. In contrast we observed minimal transport activity over control when

Uxt1-bearing proteoliposomes were preloaded with GMP (Fig. 3.2G, Fig. 3.S3E). Although Uxt1 and Uxt2 have similar activity, they are clearly not functionally identical at the enzymatic level.

3.3.2 *UXT1* and *UXT2* sequence and expression

We wondered how Uxt1 and Uxt2, the first reported fungal UDP-Xyl/UDP-Gal*f* transporters, compared to other NSTs with similar substrate specificities. Phylogenetic analysis with known transporters of UDP-Xyl and UDP-Ara*f* placed Uxt1 and Uxt2 closest to the *A. thaliana* UDP-Ara*f* transporters (UAfT1-4) even though, as mentioned above, arabinose has never been detected in *C. neoformans* (Fig. 3.S1B). Interestingly, Uxt1 and Uxt2 were more divergent from known UDP-Xyl transporters, such as those from human and *A. thaliana* (Fig. 3.S1B), which may be of therapeutic relevance.

Our biochemical and phylogenetic studies did not explain why *C. neoformans* has two transporters for UDP-Xyl and UDP-Gal*f* and raised the question of whether they have distinct roles *in vivo*. To define the physiological roles of Uxt1 and Uxt2, we first examined the expression of *UXT1* and *UXT2* under nutrient rich and deficient (capsule-inducing) conditions; the latter was tested because of the central role capsule plays in virulence and the differences we had noted in capsule composition. We found that *UXT1* expression was not affected by capsule induction, while *UXT2* had a lower basal level of expression in rich media (0 h) that was upregulated 15-fold upon capsule induction (Fig. 3.3).

3.3.3 Uxt1 and Uxt2 localize to distinct subcellular compartments

When we expressed FLAG-tagged Uxt1 and Uxt2 in *S. cerevisiae* to assess their subcellular localization, we found that Uxt2 localized to the ER (Fig. 3.4A). In contrast, Uxt1 exhibited a Golgi distribution (Fig. 3.4B), consistent with its predicted N-terminal ER export signal (two diacidic motifs). Swapping the N-terminal cytosolic domains of the two proteins caused each to shift to the other secretory compartment (Fig. 3.4, bottom row of each panel).

3.3.4 Absence of *UXT1* and *UXT2* has pleiotropic effects on cell morphology and stress resistance

We wondered if the observed differences in protein expression and localization had phenotypic consequences beyond alterations in GXM. All of the mutants grew normally at 37 °C, except for a modest increase in the doubling time of *uxt1*Δ *uxt2*Δ, which was further exacerbated by nutrient limitation (Fig. 3.S4). We saw no changes in growth when these strains were challenged with stressors that target the cell wall, consistent with their wild-type patterns of cell wall staining (Table 3.S2). At this temperature, however, *uxt1*Δ *uxt2*Δ growth was abolished by SDS (that of *uxt1*Δ was slightly inhibited), and the growth of both of these strains was slightly inhibited by high salt (Fig. 3.5A).

Both of the single *uxt* mutants showed normal capsule thickness (Fig. 3.5B; Fig. 3.S5A), cell diameter (Fig. 3.5B, Fig. 3.S5B), and GXM shedding (Fig. 3.S5C). The *uxt1*Δ cells, however, aggregated more than wild type (Fig. 3.5B), and differed from wild-type cells in capsule organization, despite the similarity in overall capsule radius: individual fibers seemed thicker and appeared to form a sparser network over the cell surface (Fig. 3.5C, Fig. 3.S5D). The capsule

changes were more striking in *uxt1*Δ *uxt2*Δ cells; these showed significantly thinner capsules (Fig. 3.S5A) and reduced GXM shedding (Fig. 3.S5C). Their capsule fibers also appeared shorter and coarser than those of *uxt1*Δ, resembling those of *uxs1*Δ cells, which do not synthesize UDP-Xyl (Fig. 3.5C, Fig. 3.S5D).

The observed differences in capsule did not explain the increased sensitivity of *uxt1*Δ and *uxt1*Δ *uxt2*Δ to stress, because even acapsular cells grow normally under these conditions (33, 34). We hypothesized that this sensitivity instead results from reduced Xyl in other glycoconjugates, such as protein-linked glycans. In support of this idea, the Xyl content of soluble glycoproteins isolated from *uxt1*Δ and *uxt2*Δ was 15% and 90% of their respective complements. We detected no Xyl in samples purified from *uxt1*Δ *uxt2*Δ or the control *uxs1*Δ.

3.3.5 Lack of luminal UDP-xylose alters interactions with host phagocytes and virulence

We wondered whether the stress sensitivity and altered glycoconjugate xylosylation of the *uxt* mutants would translate into aberrant interactions with host cells. Since host macrophages are critical for determining the outcome of cryptococcal infection (35), we investigated the ability of our mutants to interact with bone marrow macrophages (BMM) *in vitro*. We found that the level of internalization by BMMs was inversely related to the degree of xylosylation: *uxt1*Δ *uxt2*Δ was taken up more readily than WT cells while *uxt1*Δ exhibited an intermediate phenotype (Fig. 3.6A). Notably, while WT and the single deletion strains replicated ~2-fold over 24 h after internalization by BMM, the level of *uxt1*Δ *uxt2*Δ did not change (Fig. 3.6B). This reflected both de-

creased replication and increased clearance, which negated the small growth that occurred (Fig. 3.6C).

The altered host interactions we observed *in vitro* suggested a potential defect in pathogenicity of the *uxt* strains. Studies using an inhalational model to mimic the natural route of infection showed that *uxt2*Δ and, more surprisingly, *uxt1*Δ, caused disease with normal kinetics (Fig. 3.6D) and organ burdens (Fig. 3.6E, Fig. 3.S7). In contrast, *uxt1*Δ *uxt2*Δ was attenuated for virulence in both A/JCr and C57BL/6 mice (Fig. 3.6D, Fig. 3.S6). More detailed studies using A/JCr mice showed that the double mutant was unexpectedly detectable in the lungs out to 100 days post infection (dpi), when the experiment was terminated (Fig. 3.6E). Despite the persistent pulmonary burden, *uxt1*Δ *uxt2*Δ failed to disseminate from the lungs; it was never detected in the spleen and was only transiently detected in the brain (Fig. 3.S7).

3.4 Discussion

C. neoformans encodes an unusual pair of highly homologous UDP-Xyl/UDP-Gal*f* transporters, which together are critical for virulence. Uxt1 and Uxt2 are unique for their high affinity for UDP-Xyl (Fig. 3.2), with K_M values almost two orders of magnitude lower than those of the *Arabidopsis* UDP-Xyl transporters (36). Despite transporting the same nucleotide sugars, the two proteins are not completely functionally redundant, likely due to differences in expression, enzyme kinetics, and localization.

Beyond nucleotide sugars known to occur in *C. neoformans*, *in vitro* Uxt1 and Uxt2 also transport UDP-Ara*p* and UDP-Ara*f* (Fig. 3.2), potentially enabled by the similar structures of

Xyl and Ara (D-Xyl and L-Ara are epimers). While the NSTs most closely related to Uxt1 and Uxt2 (*At* UAfT1-4) are highly specific for UDP-Ara*f* (37), the substrate range of the cryptococcal proteins most closely resembles that of plant UDP-Xyl transporters (UXT1-3; (36)) despite their sequence divergence (Fig. 3.S1B). These observations highlight the importance of using rigorous biochemical analysis to test functional assumptions based on homology.

Since UDP-Ara is not found in cryptococcal cells and abrogating UDP-Gal*f* synthesis does not alter cryptococcal growth or virulence (8), the phenotypes associated with loss of Uxt1 and Uxt2 likely result from disruption of UDP-Xyl transport into the secretory compartment. Notably, capsule material was still produced (Fig. 3.5), even when no Xyl was detected in GXM because both transporters were absent (Fig. 3.1A). This suggests that Xyl incorporation is not required for GXM backbone synthesis or elongation, or for incorporation of GlcA. However, lack of the Xyl donor did reduce the amount of shed capsule material by over 75% (Fig. 3.S5C). Since Xyl constitutes only 20-30% of the capsule mass, loss of this moiety alone does not explain this reduction. Instead, it may be a direct effect of the reduced Xyl incorporation, if these side chains are needed for capsule recognition by synthetic or trafficking machinery, or an indirect effect, for example if synthetic enzymes must be xylosylated to function efficiently. Lack of UDP-Xyl transport also yielded thinner capsules (Fig. 3.5B, Fig. 3.S5A) with abnormal fiber morphology (Fig. 3.5C, Fig. 3.S5D); this presumably results from the lack of Xyl substitution, which may be required for proper stabilization and organization of capsule polysaccharides.

Why does *C. neoformans* express two UDP-Xyl transporters? Judging by the severity of mutant phenotypes (Fig. 3.5) and the gene expression levels (Fig. 3.3), Uxt1 is the major transporter of

the pair, but loss of both is required to eliminate Xyl incorporation (Fig. 3.1). These data exclude the possibility of a third UDP-Xyl transporter of any significance, while highlighting the unequal contribution of these two proteins. One factor in this inequity is likely the higher affinity and catalytic efficiency for UDP-Xyl transport of Uxt1 compared to Uxt2 (Fig. 3.2). Another is probably their distinct regulatory patterns, with *UXT1* expressed constitutively, while *UXT2* expression levels is upregulated in response to greater glycan biosynthetic demands (Fig. 3.3). Curiously, expression of the two genes was not optimally regulated to enable compensation in the single mutants: expression of *UXT1* did not change in response to the loss of *UXT2* even in capsule-inducing conditions, and the normal *UXT2* induction was muted in the absence of *UXT1* (Fig. 3.S8). Future studies will address this regulatory relationship.

The distinct roles of Uxt1 and Uxt2 also potentially reflect their association with other glycan synthetic proteins, such as glycosyltransferases. We found no evidence of association with specific xylosyltransferase(s), as for example preferential loss of β-1,2 or β-1,4 linked Xyl in the GXM of either mutant (Table 3.S1). However, the full cryptococcal glycan repertoire is not known; future studies may enable us to identify specific protein or lipid modifications enabled by each enzyme. Another factor in the dominant role of Uxt1 is likely its localization to the Golgi (Fig. 3.4B), the probable site of capsule and protein xylosylation (10, 11, 14), in contrast to the ER localization of Uxt2 (Fig. 3.4A). The latter is intriguing, as this compartment is upstream of most glycan synthesis. It is possible that Uxt2 has transport-independent functions, or that it supplies novel synthetic processes that have yet to be described. These will be exciting areas for future investigation.

The increased sensitivity to stress (Fig. 3.5A) and greater uptake by host phagocytes (Fig. 3.6A) of *uxt1*Δ were insufficient to alter its behavior in animal infection (Fig. 3.6D). We expected the highly impaired double mutant *uxt1*Δ *uxt2*Δ, which cannot transport UDP-Xyl into the secretory pathway, to behave like strains that cannot synthesize UDP-Xyl (*uxs1*Δ), which are avirulent and completely cleared by 7 days post-infection (38). Surprisingly, this mutant persisted in the lungs (Fig. 3.6E), suggesting either a cytosolic role for UDP-Xyl or a UDP-Xyl-independent role for Uxs1; these possibilities remain to be investigated.

The double mutant population increased very slowly in both A/JCr and C57BL/6 mice, likely due to its slower growth rate under stress (Fig. 3.6C, Fig. 3.S4) and reduced ability to resist host defenses (Fig. 3.6A, Fig. 3.6B). Xyl modifications have been identified as immunodominant epitopes in antibody responses to allergens and pathogens (39, 40), and the absence of Xyl modifications in *uxt1*Δ *uxt2*Δ did increase immune detection and clearance of the pathogen *in vitro* (Fig. 3.6A, Fig. 3.6B). The mutant also remained confined to the lungs of A/JCr mice (Fig. 3.S7) and was slow to cause lethal meningoencephalitis in C57BL/6 mice (Fig. 3.S6). This may reflect an inability to disseminate or to efficiently establish infection at distal sites, or may be the result of active restriction by the immune system. Notably, phagocytes have a multifaceted role in cryptococcal infection, potentially aiding and/or inhibiting fungal survival and dissemination depending on the circumstance (35). Elucidating the complex interplay between Uxt mutants and the infected host will be the focus of future work. Further studies may also uncover facets of this infection that could be exploited for therapeutic intervention and potentially inform vaccine design.

C. neoformans is unusual among yeast for its extensive utilization of Xyl, in capsule polysaccharides, *N*- and *O*-linked glycans (including a unique Xyl-phosphate modification), and glycolipids. By elucidating UDP-Xyl transport, we have expanded our understanding of this aspect of cryptococcal glycan biosynthesis, including the sequence and localization of capsule synthetic events, and of NSTs as a protein family. We have identified the first fungal UDP-Xyl/UDP-Gal*f* transporters and also set the stage for studies of an unusual mutant that may help elucidate mechanisms of cryptococcal pathogenesis and host response.

3.5 Materials and methods

3.5.1 Sequence and phylogenetic analysis

Uxt1 and Uxt2 were identified by BLASTP searches of known NSTs against *C. neoformans* predicted proteins (Broad Institute; *Cryptococcus neoformans var. grubii* H99 database); the closest related sequence was that of the *Aspergillus fumigatus* UDP-Gal*f* transporter (ACR56866.1). The online Phylogeny.fr program (http://www.phylogeny.fr/version2_cgi/index.cgi) with default settings (41, 42) was used for multiple sequence alignment (MUSCLE; (43)), phylogenetic analysis (PhyML; (44)), and tree rendering (TreeDyn; (45)) of Uxt1 and Uxt2 and other NSTs. These included transporters of UDP-Gal*f* (*Aspergillus fumigatus*, *Af*), UDP-Xyl (*Homo sapiens*, *Hs*, UXT NP_116215.1; *Arabidopsis thaliana*, *At*, UXT1 NP_850120.3 (At2g28315), *At* UXT2 NP_180604.4 (At2g30460), and *At* UXT3 NP_172172.2 (At1g06890)), and UDP-arabinofuranose (*At* UAfT1 NP_568469.1, At5g25400; *At* UAfT2 NP_196684.1, At5g11230; *At* UAfT3 NP_194965.1, At4g32390; *At* UAfT4 NP_180122.1, At2g25520), as well as other cryptococcal (*Cn*) NSTs.

Sequence alignment between Uxt1 and Uxt2 was analyzed using T-coffee (http://tcoffee.crg.cat/apps/tcoffee/do:regular) and formatted using Boxshade (http:// www.ch.embnet.org/software/BOX_form.html). The protein sequences were analyzed for predicted localization signals using LocSigDB (http://genome.unmc.edu/ LocSigDB/; (46)).

3.5.2 Cell growth

C. neoformans strains were grown in YPD medium (1% wt/vol BactoYeast Extract, 2% wt/vol BactoPeptone, 2% wt/vol dextrose) at 30 °C with shaking (230 rpm) unless otherwise noted. For phenotypic analysis, cells were grown overnight (O/N), washed in sterile phosphate buffered saline (PBS), and diluted to 10^6 cells/mL in PBS. 4 μL aliquots of serial 5-fold dilutions were plated and grown at 30 or 37 °C as indicated. The stress conditions tested included YPD containing 0.01% SDS, 1.2 M NaCl, 1.2 M KCl, Tris pH 8.8, 1.5 M Sorbitol, 0.05% Congo Red (CR), or 2% Calcofluor White (CFW). To test oxidative and nitrosative stress sensitivity, dilutions were spotted onto solid YNB medium (0.67% w/v yeast nitrogen base without amino acids, 2% wt/vol glucose, 2% wt/vol agar, 25 mM sodium succinate, pH 4.0) supplemented with 0.5 mM hydrogen peroxide (H_2O_2) or 0.5 mM sodium nitrite ($NaNO_2$). To assess cell-associated melanin production, 5 μL of a 10^6 cells/mL solution was plated on agar plates containing 8 mg/mL KH_2PO_4, 2 mg/mL glucose, 2 mg/mL L-glycine, 1 μg/mL D-biotin, 1μg/mL thiamine, 0.92 mg/mL $MgSO_4$ $7H_2O$, and 0.4 mg/mL L-3,4-dihydrohyphenylalanine (L-DOPA; Sigma-Aldrich). To assay growth, cells were cultured O/N; washed in sterile PBS; resuspended at 10^5 cells/mL in 30 mL of YPD, YNB, DMEM, or RPMI; and incubated at 37 °C for 120 h, with triplicate samples counted by hemocytometer at various times.

3.5.3 *C. neoformans* strains

We replaced *UXT1* in KN99α (WT) with a nourseothricin (NAT) resistance marker using a split marker strategy (47). Transformants of interest were identified by resistance to NAT and validated by PCR verification of gene replacement. We used a similar strategy to complement the *uxt1* deletion strain at the endogenous locus by replacing the deletion cassette with *UXT1* in tandem with a G418 resistance marker. Transformants resistant to G418 and sensitive to NAT were verified by PCR and assessed for reversal of mutant phenotypes (see Results). We generated *uxt2*Δ and *UXT2* with an identical approach, using G418 and NAT markers in the deletion and complement constructs, respectively. To obtain an *uxt1*Δ *uxt2*Δ double mutant, we crossed the single mutants on V8 agar plates (48). Double mutants were selected for by resistance to both drugs and verified by PCR amplification.

3.5.4 Capsule induction and visualization

O/N cultures of *C. neoformans* were collected by centrifugation, washed twice with sterile PBS, diluted to 10^6 cells/mL in DMEM and incubated at 37 °C in 5% CO_2 for 24 h in T-75 tissue culture flasks or 24-well plates. The cells were then washed and resuspended in PBS, mixed with 1.5 parts India Ink, and viewed by light microscopy with a ZEISS Axioskop2 MOT Plus microscope (Carl Zeiss Microscopy, LLC).

For antibody detection of cell wall-associated GXM, strains were induced as above for 24 h, fixed for 1 h in 3.7% formaldehyde, washed in PBS, and then incubated for 1 h at room temperature (RT) with 1 mg/mL of anti-GXM monoclonal antibody (mAb) F12D2 or 302 (from Dr. Thomas R. Kozel, University of Nevada School of Medicine) conjugated to AlexaFlour 488.

Stained cells were washed twice with PBS, resuspended in PBS, and examined on a ZEISS Axioskop 2 MOT Plus microscope.

3.5.5 GXM ELISA

GXM content of supernatant fractions from cell cultures was quantified by ELISA according to previous methods (49), using anti-GXM mAb 339 (from Dr. Thomas R. Kozel, University of Nevada School of Medicine).

3.5.6 Glycan isolation and analysis

GXM was isolated from strains of interest by selective precipitation of culture supernatants with hexadecyltrimethylammonium bromide (CTAB) as detailed in (11). For isolation of soluble glycoproteins, O/N cultures were diluted into YPD and grown to 10^7 cells/mL. 2 x 10^7 cells per strain were collected, washed in Tris-EDTA buffer (100 mM Tris pH 8.5, 0.1 mM EDTA pH 8.0), and resuspended in 40 mL Tris-EDTA buffer with protease inhibitors. Samples were then subjected to 15 cycles of bead beating (3 min) alternating with 3 min on ice, which yielded ~75% cell lysis (as judged by microscopy). All subsequent steps were performed at 4 °C. Lysates were collected, pooled with three 10 mL rinses of the beads, and subjected to a clearing spin (1000 x g; 25 min). Supernatant fractions were then transferred to fresh tubes, adjusted to a final concentration of 1% CHAPS, incubated with rocking for 2 h, and subjected to ultracentrifugation (75000 x g; 45 min). The CHAPS extract was then dialyzed (8000 M_r) against 2 L of 50 mM NH_4HCO_3 with three buffer changes over 48 h, lyophilized, and washed with 80% acetone to reduce detergent and polymeric contaminants.

For compositional analysis, per-*O*-trimethylsilyl (TMS) derivatives of monosaccharide methyl glycosides were produced from the GXM samples by acidic methanolysis using methods described in (50, 51). Glycosyl composition was then determined by combined gas chromatography/mass spectrometry (GC/MS) on an Agilent 7890A GC interfaced to a 5975C MSD (mass selective detector, electron impact ionization mode; Agilent Technologies) with a Supelco EC-1 fused silica capillary column (30 m × 0.25 mm ID; Sigma-Aldrich). For linkage analysis, GXM samples were permethylated, depolymerized, reduced, and acetylated as described in (7). The resultant partially methylated alditol acetates (PMAAs) were then analyzed as above but using a 30 m Supelco SP-2331 bonded phase fused silica capillary column (Sigma-Aldrich).

3.5.7 Heterologous expression, reconstitution, and transport assays

The *UXT1*, *UXT2*, *GMT1*, and *GMT2* coding regions were amplified from WT cDNA and introduced into the pENTR/SD/D-TOPO vector (Life Technologies) according to the manufacturer's protocols to generate pENTR-*UXT1*, pENTR-*UXT2*, pENTR-*GMT1*, and pENTR-*GMT2*. Recombination of each entry clone with destination vector pYES-DEST52 (Life Technologies) using LR clonase II (Life Technologies) produced a C-terminal His/V5 epitope fusion that was verified by sequencing before transformation into *S. cerevisiae* strain INVSc1 (Thermo Fisher Scientific). Heterologous expression, reconstitution into proteoliposomes, and transport assays were performed as previously described in reference (52). UDP-Gal*f* was prepared from UDP-galactopyranose (UDP-Galp) according to reference (53). Protein expression and incorporation was verified by polyacrylamide gel electrophoreses and immunoblot analysis of 2.5 µg of microsomes or proteoliposomes using anti-V5 antibody (Thermo Fisher Scientific), also as previously described in reference (52). Kinetic parameters were calculated by non-linear regression using

the Prism 6 application (GraphPad). The assay was validated, and its sensitivity confirmed using the well-characterized GDP-Man transporters Gmt1 and Gmt2 (Fig. 3.S9A). Both proteins transported GDP-Man and smaller amounts of other GDP-sugars in exchange for GMP and, significantly less efficiently, UMP (Fig. 3.S9D, Fig. 3.S9E).

3.5.8 Quantification of nucleotide sugars by mass spectrometry

Nucleotide sugars were extracted from approximately 50 mg of ground cells (wet weight) as previously described in reference (54). Four biological replicates were processed per strain and condition, and then analyzed in duplicate by LC-MS/MS using porous graphitic carbon as the stationary phase on an 1100 series HPLC system (Agilent Technologies) and a 4000 QTRAP LC/MS/MS system (Sciex) equipped with a TurboIonSpray ion source as in reference (55). Results in pmol mg^{-1} wet weight were converted to concentrations using a cell volume of 47.7 μm^3 (based on the average radius of 10^7 cells, measured by cellometer (Nexcolom Bioscience LLC; n = 3)) and a mass of 4.35 x 10^{-8} mg/cell (based on weighing a known number of cells; n = 3).

3.5.9 Protein localization

For expression in *S. cerevisiae*, *UXT1* and *UXT2* were amplified from WT cDNA, cloned into the copper-inducible expression vector pYEScupFLAG*K* (26), and transformed using lithium acetate into *S. cerevisiae* strain Sec7-3xGFP (from Dr. Benjamin S. Glick, University of Chicago). To generate N-terminal swaps of Uxt1 and Uxt2, we amplified both genes from the start codon to the beginning of the first predicted transmembrane domain (*UXT1* bp 1-135, *UXT2* bp 1-180) and from the first transmembrane domain until the stop codon (*UXT1* bp 136-1032; *UXT2* bp 181-1068), using WT cDNA as a template. We then PCR amplified to fuse the N-terminal

region of *UXT1* to the transmembrane region of *UXT2* and vice versa, cloned each construct into pYEScupFLAG*K*, and transformed into *S. cerevisiae* Sec7-3xGFP as above. All constructs were verified by sequencing.

For localization, cultures were grown O/N in synthetic complete media without uracil (SC-URA), adjusted to OD 0.5 and 0.5 mM $CuSO_4$, and cultured for an additional hour. The cells were then fixed for 30 min in 1% paraformaldehyde, washed and resuspended in 0.1M KPO_4/1.2 M sorbitol, and incubated for 15 min in the same buffer containing β-mercaptoethanol and zymolase (100 μg/mL). 15 μL of the cells were then spotted onto polylysine-coated slides (Electron Microscopy Sciences), incubated for 10 min, and plunged into methanol for 5 min followed by acetone for 30 sec. The samples were blocked with 5% goat serum in PBS for 30 min, and stained O/N at 4 °C with anti-FLAG (Mouse, 1:1000; Invitrogen) and anti-Kar2p/BiP antibody (Rabbit, 1:1000; from Dr. Jeff Brodsky, University of Pittsburgh). Finally, cells were incubated for 2 h with AlexaFluor 594-tagged goat anti-mouse IgG, AlexaFluor 488-tagged goat anti-rabbit IgG (Thermo Fisher Scientific), and DAPI (Thermo Fisher Scientific), and viewed with a ZEISS Axioskop2 MOT Plus microscope.

3.5.10 Fungal gene expression

Wild-type cells cultured O/N in YPD were placed in DMEM capsule-inducing conditions and sampled at 0, 1.5, 3, 8, and 24 h for RNA isolation and sequencing as in (56). Additional samples were collected at 0 and 24 h for qPCR analysis. Levels of *UXT1*, *UXT2*, and the reference gene *ACT1* were quantified using the CFX96 Real Time System (BioRad). All sample reactions contained 1 μL cDNA (100 ng), 4 μL of each primer (200 nM), and 10 μL SYBR Select Master Mix

(Applied Biosystems). qRT-PCR was performed in triplicate for each sample and non-template controls (for each set of primers) using 15 min activation and denaturation at 95 °C followed by 40 cycles of 15 sec at 95 °C, 30 sec at 60 °C, and 30 sec at 72 °C. Baseline and threshold values were determined for all reactions using CFX manager software (BioRad) and exported to Microsoft Excel for additional analysis using the ΔC_q method.

3.5.11 Electron microscopy

Strains were induced for capsule (as above), collected by centrifugation, fixed for 1 h at RT with 2% glutaraldehyde (Polysciences Inc.) in 100 mM phosphate buffer (pH 7.2), and incubated for 1 h in 1% osmium tetraoxide (Polysciences Inc.). Cells were then dehydrated with ethanol and propylene oxide and embedded in Eponate 12 resin (Tel Pella Inc.). 70 to 90 nm sections were cut with an UCT ultramicrotome (Leica Microsystems Inc.) and stained with uranyl acetate and lead citrate for visualization with a JOEL 1200EX transmission electron microscope (JOEL Ltd).

3.5.12 Macrophage assays

Bone marrow macrophages (BMMs) from the femurs and tibiae of C57BL/6 mice (Jackson Laboratory) was incubated for one week at 37°C and 5% CO2 in BMM medium (20% FBS, 30% L-cell supernatant, 1% Penicillin-Streptomycin in RPMI), which was refreshed 4 and 6 days after plating. Cells were harvested on day 7 by incubation in ice-cold PBS for 10 min and by positive selection using biotinylated α-F4/80 antibody (eBioscience) and anti-biotin conjugated magnetic beads (Miltenyi Biotec). BMMs were then plated in 24-well plates at 3.5 x 10^5 cells/mL of R10 media, and incubated O/N at 37 °C and 5% CO_2. On the following day, log-phase fungi were collected by centrifugation, washed, and opsonized with mouse serum (40 %) for 30 min at

37 °C. The strains were then washed with PBS, resuspended at 3.5 x 10^4 cells/mL in DMEM, and incubated with macrophages for 1 h. Samples were washed twice with PBS, and lysed using water either immediately or after 24 h incubation in DMEM at 37 °C and 5% CO_2. For CFU quantification, the lysates and initial inocula were plated on YPD agar. Results were analyzed using one-way analysis of variance (ANOVA) with Tukey's *post-hoc* test. For assays distinguishing parental and daughter cells, fungi were also stained with Oregon Green 488 dye (2 μg/mL; ThermoFisher) in 0.1 M sodium bicarbonate (pH 8.0) for 1 h at room temperature prior to opsonization and then treated as described above. Following lysis, cells were stained with calcofluor white (2 mg/mL PBS) for 30 min before flow analysis with a BD LSRFortessa X-20 using OneComp eBeads (eBioscience) for compensation controls. Data were analyzed using FlowJo (Treestar) and compared using Student's t-tests.

3.5.13 Animal studies

Fungal strains were cultured O/N in YPD, washed, and diluted to 10^6 cells/mL in sterile PBS. 50 μL aliquots of each strain were inoculated intranasally into groups of eight 6- to 8-week-old female A/JCr (National Cancer Institute) or C57BL/6 (Jackson Laboratory) mice. Infected mice were weighed daily and sacrificed if they lost >20% relative to peak weight, or on day 49, 63, or 100 post infection, whichever came first. Lung, brain, and spleen homogenates were harvested and plated for CFU at time of death or indicated time points, and organ burdens were analyzed by ANOVA with Tukey's *post-hoc* test.

All animal studies were approved by the Washington University Institutional Animal Care and Use Committee (Protocol 20140184). All research involving animals was carried out in strict ac-

cordance with the “Guide for the Care and Use of Laboratory Animals” published by the National Research Council and endorsed by the Association for the Assessment and Accreditation of Laboratory Animal Care.

3.6 Acknowledgements

This work was funded by National Institutes of Health grants R21 AI109623, R01 GM066303, and R01 AI087794 to TLD, and a Mizutani Foundation for Glycoscience grant to JLH and CR (160151). LXL was partly supported by a National Research Science Award (T32 GM007200), a Sondra Schlesinger Graduate Fellowship (Washington University St. Louis Microbiology Department), and a National Institute of Allergy and Infectious Diseases award (F30 AI120339). JLH was supported by an ARC Future Fellowship (FT130101165). Substrates from Carbosource Services (Athens, GA) were supported in part by a NSF-RCN grant (0090281). Glycan compositional and linkage analyses at the Complex Carbohydrate Research Center (Athens, GA) were supported by the Chemical Sciences, Geosciences and Biosciences Division, Office of Basic Energy Sciences, U.S. Department of Energy grants DE-FG02-93ER20097 and DE-FG02-96ER20220.

We thank the members of the Doering laboratory for insightful discussions and assistance with experiments (Cara Griffith for initial gene identification; Dr. Zeke Maier and Dr. Stacey Gish for transcriptional analysis; Matthew Williams for mouse studies; and Dr. Camaron Hole for macrophage experiments). We also thank Dr. Wandy Beatty (Washington University School of Medicine) for TEM, Dr. Jeff Brodsky (University of Pittsburgh) for αKar2p/BiP antibody, Dr. Benjamin S. Glick (University of Chicago) for the Sec7-3xGFP *S. cerevisiae* strain, Dr. Joe Heitman

(Duke University) for *C. neoformans* KN99α, Dr. Thomas R. Kozel (University of Nevada School of Medicine) for anti-GXM mAbs, and Dr. Jennifer Lodge (Washington University School of Medicine) for plasmid pMH12-T.

3.7 References

1. Kwon-Chung KJ, *et al.* (2014) *Cryptococcus neoformans* and *Cryptococcus gattii*, the etiologic agents of cryptococcosis. *Cold Spring Harb Perspect Med* 4(7):a019760.

2. Denning DW (2016) Minimizing fungal disease deaths will allow the UNAIDS target of reducing annual AIDS deaths below 500 000 by 2020 to be realized. *Philos Trans R Soc Lond B Biol Sci* 371(1709).

3. Rajasingham R, *et al.* (2017) Global burden of disease of HIV-associated cryptococcal meningitis: an updated analysis. *Lancet Infect Dis*.

4. Doering TL (2009) How sweet it is! Cell wall biogenesis and polysaccharide capsule formation in *Cryptococcus neoformans*. *Annu Rev Microbiol* 63:223-247.

5. Vecchiarelli A, *et al.* (2013) Elucidating the immunological function of the *Cryptococcus neoformans* capsule. *Future Microbiol* 8(9):1107-1116.

6. Cherniak R, Valafar H, Morris LC, & Valafar F (1998) *Cryptococcus neoformans* chemotyping by quantitative analysis of 1H nuclear magnetic resonance spectra of glucuronoxylomannans with a computer-simulated artificial neural network. *Clin Diagn Lab Immunol* 5(2):146-159.

7. Heiss C, Klutts JS, Wang Z, Doering TL, & Azadi P (2009) The structure of *Cryptococcus neoformans* galactoxylomannan contains beta-D-glucuronic acid. *Carbohydr Res* 344(7):915-920.

8. Heiss C, *et al.* (2013) Unusual galactofuranose modification of a capsule polysaccharide in the pathogenic yeast *Cryptococcus neoformans*. *J Biol Chem* 288(16):10994-11003.

9. Previato JO, *et al.* (2017) Distribution of the O-acetyl groups and beta-galactofuranose units in galactoxylomannans of the opportunistic fungus *Cryptococcus neoformans*. *Glycobiology* 27(6):582-592.

10. Klutts JS, Levery SB, & Doering TL (2007) A beta-1,2-xylosyltransferase from *Cryptococcus neoformans* defines a new family of glycosyltransferases. *J Biol Chem* 282(24):17890-17899.

11. Klutts JS & Doering TL (2008) Cryptococcal xylosyltransferase 1 (Cxt1p) from *Cryptococcus neoformans* plays a direct role in the synthesis of capsule polysaccharides. *J Biol Chem* 283(21):14327-14334.

12. Park JN, *et al.* (2012) Unraveling unique structure and biosynthesis pathway of N-linked glycans in human fungal pathogen *Cryptococcus neoformans* by glycomics analysis. *J Biol Chem* 287(23):19501-19515.

13. Lee DJ, Bahn YS, Kim HJ, Chung SY, & Kang HA (2015) Unraveling the novel structure and biosynthetic pathway of O-linked glycans in the Golgi apparatus of the human pathogenic yeast *Cryptococcus neoformans*. *J Biol Chem* 290(3):1861-1873.

14. Castle SA, *et al.* (2008) Beta1,2-xylosyltransferase Cxt1p is solely responsible for xylose incorporation into *Cryptococcus neoformans* glycosphingolipids. *Eukaryot Cell* 7(9):1611-1615.

15. Gilbert NM, Lodge JK, & Specht CA (2011) The Cell Wall of *Cryptococcus*. *Cryptococcus From Human Pathogen to Model Yeast*, eds Heitman J, Kozel TR, Kwon-Chung KJ, Perfect J, & Casadevall A (ASM Press, Washington), pp 67-79.

16. Rittershaus PC, *et al.* (2006) Glucosylceramide synthase is an essential regulator of pathogenicity of *Cryptococcus neoformans*. *J Clin Invest* 116(6):1651-1659.

17. Cummings RD & Doering TL (2009) Fungi. *Essentials of Glycobiology*, eds Varki A, Cummings RD, Esko JD, Freeze HH, Stanley P, Bertozzi CR, Hart GW, & Etzler MECold Spring Harbor (NY)), 2nd Ed.

18. Abeijon C, Mandon EC, & Hirschberg CB (1997) Transporters of nucleotide sugars, nucleotide sulfate and ATP in the Golgi apparatus. *Trends Biochem Sci* 22(6):203-207.

19. Berninsone P, Eckhardt M, Gerardy-Schahn R, & Hirschberg CB (1997) Functional expression of the murine Golgi CMP-sialic acid transporter in *Saccharomyces cerevisiae*. *J Biol Chem* 272(19):12616-12619.

20. Moyrand F, Fontaine T, & Janbon G (2007) Systematic capsule gene disruption reveals the central role of galactose metabolism on *Cryptococcus neoformans* virulence. *Mol Microbiol* 64(3):771-781.

21. Wang ZA, *et al.* (2014) *Cryptococcus neoformans* dual GDP-mannose transporters and their role in biology and virulence. *Eukaryot Cell* 13(6):832-842.

22. Li LX, *et al.* (2017) *Cryptococcus neoformans UGT1* encodes a UDP-Galactose/UDP-GalNAc transporter. *Glycobiology* 27(1):87-98.

23. Berninsone P, Hwang HY, Zemtseva I, Horvitz HR, & Hirschberg CB (2001) SQV-7, a protein involved in *Caenorhabditis elegans* epithelial invagination and early

embryogenesis, transports UDP-glucuronic acid, UDP-N- acetylgalactosamine, and UDP-galactose. *Proc Natl Acad Sci U S A* 98(7):3738-3743.

24. Segawa H, Kawakita M, & Ishida N (2002) Human and *Drosophila* UDP-galactose transporters transport UDP-N-acetylgalactosamine in addition to UDP-galactose. *Eur J Biochem* 269(1):128-138.

25. Aoki K, Ishida N, & Kawakita M (2003) Substrate recognition by nucleotide sugar transporters: further characterization of substrate recognition regions by analyses of UDP-galactose/CMP-sialic acid transporter chimeras and biochemical analysis of the substrate specificity of parental and chimeric transporters. *J Biol Chem* 278(25):22887-22893.

26. Ashikov A, *et al.* (2005) The human solute carrier gene SLC35B4 encodes a bifunctional nucleotide sugar transporter with specificity for UDP-xylose and UDP-N-acetylglucosamine. *J Biol Chem* 280(29):27230-27235.

27. Segawa H, Soares RP, Kawakita M, Beverley SM, & Turco SJ (2005) Reconstitution of GDP-mannose transport activity with purified *Leishmania* LPG2 protein in liposomes. *J Biol Chem* 280(3):2028-2035.

28. Caffaro CE, *et al.* (2008) A single *Caenorhabditis elegans* Golgi apparatus-type transporter of UDP-glucose, UDP-galactose, UDP-N-acetylglucosamine, and UDP-N-acetylgalactosamine. *Biochemistry* 47(14):4337-4344.

29. Maszczak-Seneczko D, Sosicka P, Majkowski M, Olczak T, & Olczak M (2012) UDP-N-acetylglucosamine transporter and UDP-galactose transporter form heterologous complexes in the Golgi membrane. *FEBS Lett* 586(23):4082-4087.

30. Cottrell TR, Griffith CL, Liu H, Nenninger AA, & Doering TL (2007) The pathogenic fungus *Cryptococcus neoformans* expresses two functional GDP-mannose transporters with distinct expression patterns and roles in capsule synthesis. *Eukaryot Cell* 6(5):776-785.

31. Kozel TR, *et al.* (2003) Antigenic and biological characteristics of mutant strains of *Cryptococcus neoformans* lacking capsular O acetylation or xylosyl side chains. *Infect Immun* 71(5):2868-2875.

32. Bar-Peled M, Griffith CL, & Doering TL (2001) Functional cloning and characterization of a UDP-glucuronic acid decarboxylase: the pathogenic fungus *Cryptococcus neoformans* elucidates UDP-xylose synthesis. *Proc Natl Acad Sci USA* 98: 12003–12008.

33. Moyrand F & Janbon G (2004) *UGD1*, encoding the C*ryptococcus neoformans* UDP-glucose dehydrogenase, is essential for growth at 37 degrees C and for capsule biosynthesis. *Eukaryot Cell* 3(6):1601-1608.

34. O'Meara TR, *et al.* (2014) The *Cryptococcus neoformans* Rim101 transcription factor directly regulates genes required for adaptation to the host. *Mol Cell Biol* 34(4):673-684.

35. Leopold Wager CM, Hole CR, Wozniak KL, & Wormley FL, Jr. (2016) Cryptococcus and Phagocytes: Complex Interactions that Influence Disease Outcome. *Front Microbiol* 7:105.

36. Ebert B, *et al.* (2015) Identification and characterization of a Golgi-localized UDP-xylose transporter family from *Arabidopsis*. *Plant Cell* 27(4):1218-1227.

37. Rautengarten C, *et al.* (2017) The elaborate route for UDP-arabinose delivery into the Golgi of plants. *Proc Natl Acad Sci USA* 114(16):4261-4266.

38. Gish SR, *et al.* (2016) Computational analysis reveals a key regulator of Cryptococcal virulence and determinant of host response. *MBio* 7(2):e00313-00316.

39. van Ree R, *et al.* (2000) Beta(1,2)-xylose and alpha(1,3)-fucose residues have a strong contribution in IgE binding to plant glycoallergens. *J Biol Chem* 275(15):11451-11458.

40. Mickum ML, Prasanphanich NS, Heimburg-Molinaro J, Leon KE, & Cummings RD (2014) Deciphering the glycogenome of schistosomes. *Front Genet* 5:262.

41. Dereeper A, *et al.* (2008) Phylogeny.fr: robust phylogenetic analysis for the non-specialist. *Nucleic Acids Res* 36:W465-469.

42. Dereeper A, Audic S, Claverie JM, & Blanc G (2010) BLAST-EXPLORER helps you building datasets for phylogenetic analysis. *BMC Evol Biol* 10:8.

43. Edgar RC (2004) MUSCLE: multiple sequence alignment with high accuracy and high throughput. *Nucleic Acids Res* 32(5):1792-1797.

44. Guindon S & Gascuel O (2003) A simple, fast, and accurate algorithm to estimate large phylogenies by maximum likelihood. *Syst Biol* 52(5):696-704.

45. Chevenet F, Brun C, Banuls AL, Jacq B, & Christen R (2006) TreeDyn: towards dynamic graphics and annotations for analyses of trees. *BMC Bioinformatics* 7:439.

46. King BR & Guda C (2007) ngLOC: an n-gram-based Bayesian method for estimating the subcellular proteomes of eukaryotes. *Genome Biol* 8(5):R68.

47. Fu J, Hettler E, & Wickes BL (2006) Split marker transformation increases homologous integration frequency in *Cryptococcus neoformans*. *Fungal Genet Biol* 43(3):200-212.

48. Kwon-Chung KJ, Edman JC, & Wickes BL (1992) Genetic association of mating types and virulence in *Cryptococcus neoformans*. *Infect Immun* 60(2):602-605.

49. Percival A, Thorkildson P, & Kozel TR (2011) Monoclonal antibodies specific for immunorecessive epitopes of glucuronoxylomannan, the major capsular polysaccharide of *Cryptococcus neoformans*, reduce serotype bias in an immunoassay for cryptococcal antigen. *Clin Vaccine Immunol* 18(8):1292-1296.

50. York W, Darvill A, McNeil M, Stevenson T, & Albersheim P (1985) Isolation and characterization of plant cell walls and cell-wall components. *Methods Enzymol* 118:3-40.

51. Merkle RK & Poppe I (1994) Carbohydrate composition analysis of glycoconjugates by gas-liquid chromatography/mass spectrometry. *Methods Enzymol* 230:1-15.

52. Rautengarten C, *et al.* (2016) The Arabidopsis Golgi-localized GDP-L-fucose transporter is required for plant development. *Nature Communications* 7.

53. Lee R, Monsey D, Weston A, Duncan K, Rithner C, et al. (1996) Enzymatic synthesis of UDP-galactofuranose and an assay for UDP-galactopyranose mutase based on high-performance liquid chromatography. *Anal Biochem* 242: 1–7.

54. Ito J, *et al.* (2014) Analysis of plant nucleotide sugars by hydrophilic interaction liquid chromatography and tandem mass spectrometry. *Analytical Biochemistry* 448:14-22.

55. Rautengarten C, *et al.* (2014) The Golgi localized bifunctional UDP-rhamnose/UDP-galactose transporter family of Arabidopsis. *Proc Natl Acad Sci USA* 111(31):11563-11568.

56. Maier EJ, *et al.* (2015) Model-driven mapping of transcriptional networks reveals the circuitry and dynamics of virulence regulation. *Genome Res* 25(5):690-700.

57. Huffnagle GB, Boyd MB, Street NE, & Lipscomb MF (1998) IL-5 is required for eosinophil recruitment, crystal deposition, and mononuclear cell recruitment during a pulmonary *Cryptococcus neoformans* infection in genetically susceptible mice (C57BL/6). *J Immunol* 160: 2393–2400.

3.8 Figures

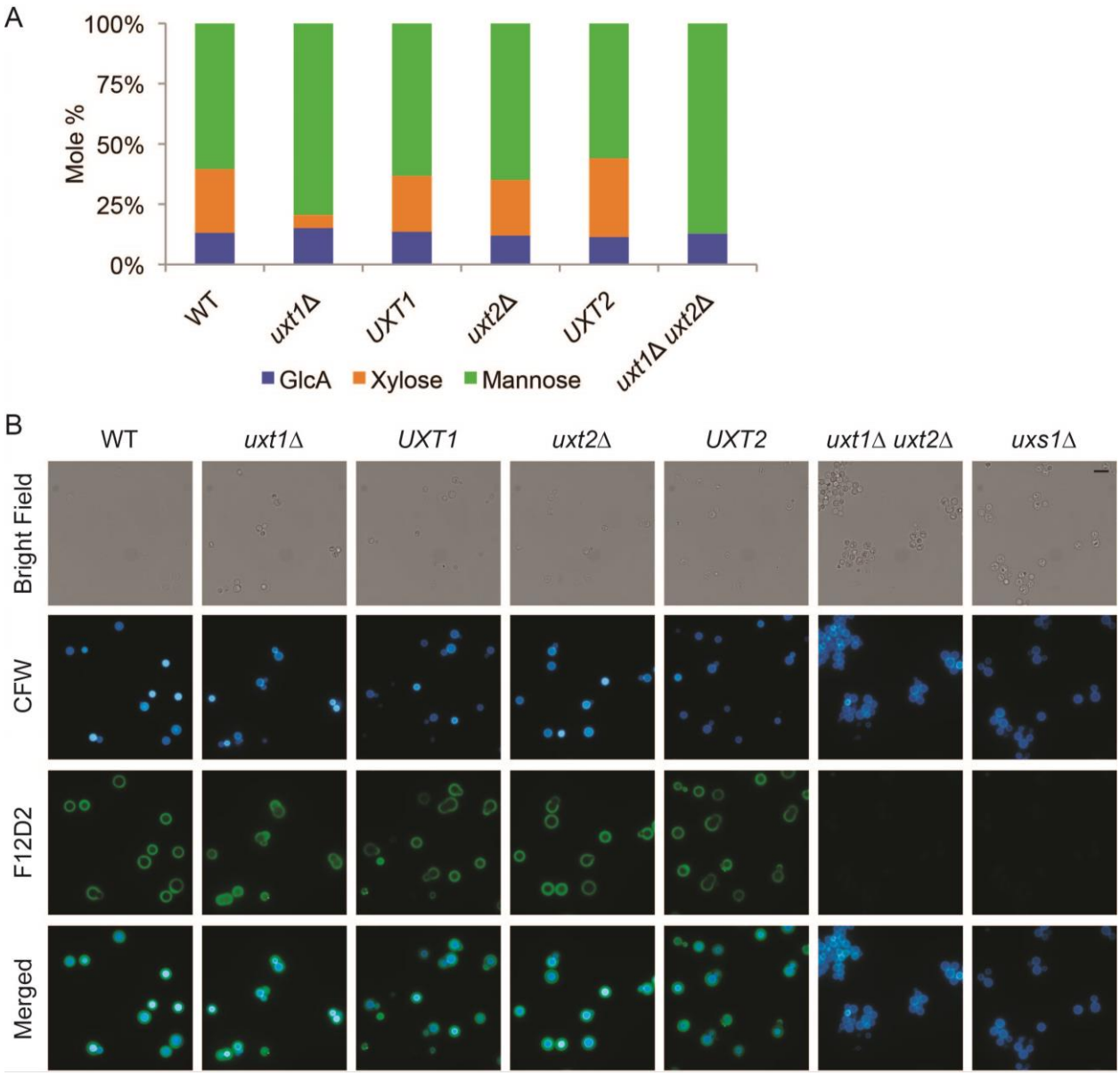

Figure 3.1. Capsule characteristics of *uxt* mutants. (A) Glycan composition of GXM. (B) Cell wall and capsule staining with Calcofluor white (CFW; blue) and anti-GXM mAb F12D2 (green), respectively. Bright field, single channel, and merged images are shown; scale bar = 10 μm.

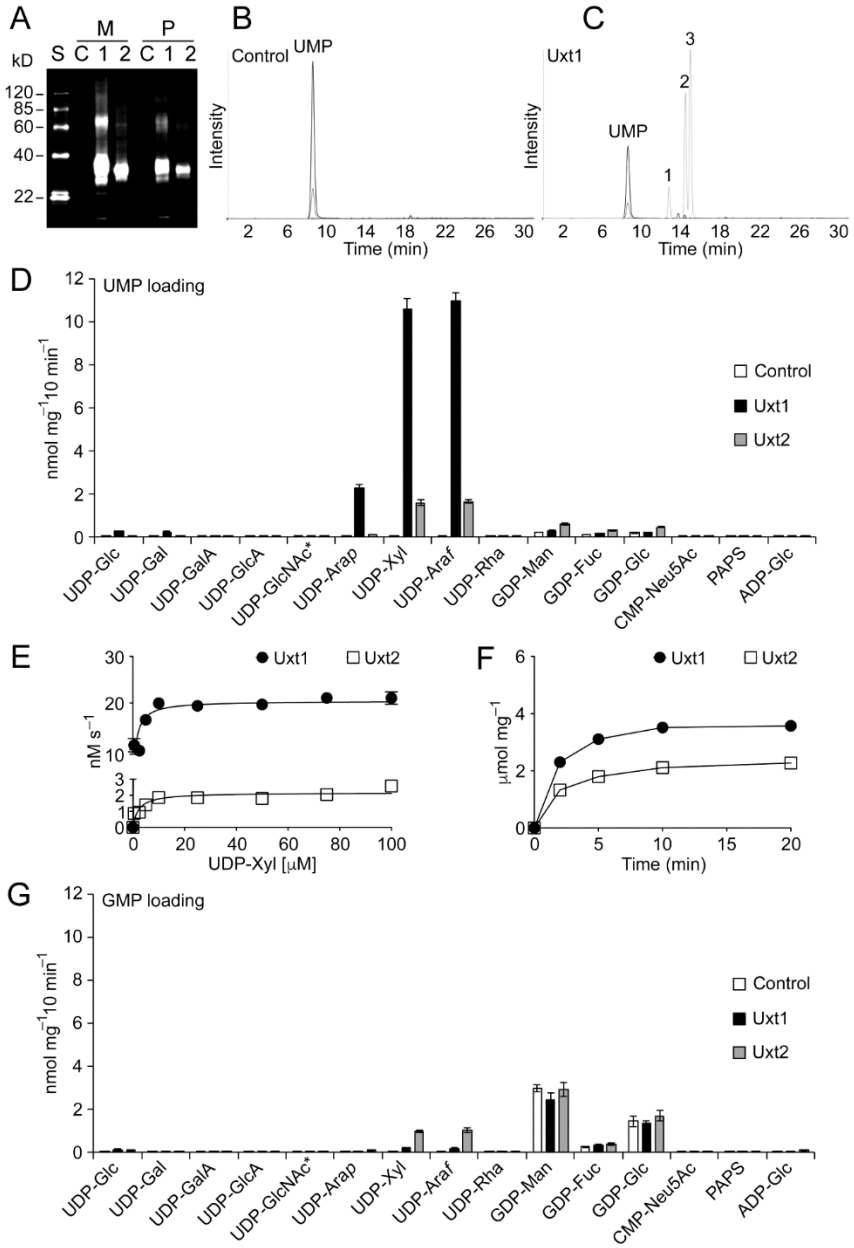

Figure 3.2. Uxt1 and Uxt2 *in vitro* transport activities. (A) Immunoblot analysis of microscomes (M) and proteoliposomes (P) prepared from *S. cerevisiae* expressing vector alone (Control) or V5-tagged Uxt1 or Uxt2 (2.5 μg protein per lane; S, standards; C, control; 1, Uxt1; 2, Uxt2). (B and C) Representative LC-MS/MS spectra of proteoliposomes prepared from (B) control or (C) Uxt1-expressing *S. cerevisiae* cells, preloaded with 30 mM UMP, and incubated with a mixture

of 16 nucleotide / nucleotide sugar substrates (50 μM each, 10 min, 37 °C); Peak 1, UDP-Ara*p*; Peak 2, UDP-Xyl; Peak 3, UDP-Ara*f*. (D) Nucleotide sugar uptake into proteoliposomes pre-loaded with 30 mM UMP. Values were normalized to the total protein content of the proteoliposome preparations. Data represent the mean ± SD of n = 4 assays. *, mixture of UDP-GalNAc and UDP-GlcNAc. (E and F) Proteoliposomes preloaded with 10 mM UMP were incubated for 2 min with UDP-Xyl (E) at variable concentrations (0 - 100 μM) or (F) for the indicated times with 50 μM UDP-Xyl. Values were normalized to the actual NST content in proteoliposome preparations (Table 3.S4). Data are the mean ± SEM of n = 4 assays. (G) Nucleotide sugar uptake into proteoliposomes preloaded with 30 mM GMP analyzed as in (D).

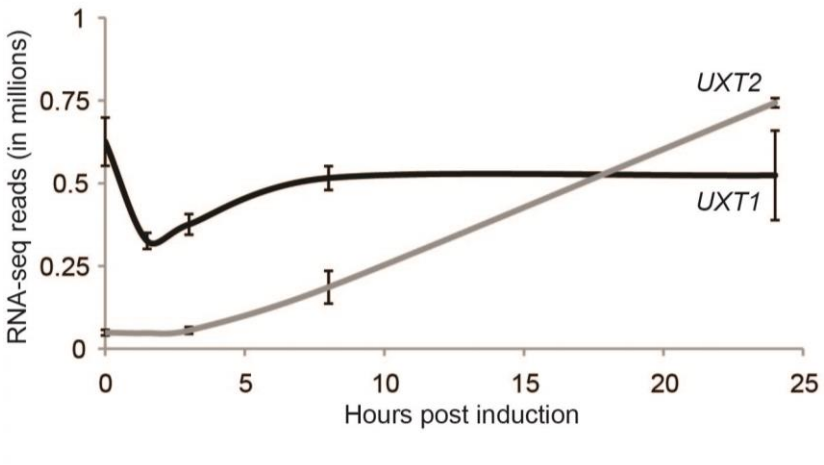

Figure 3.3. Transcription of *UXT2* but not *UXT1* increases during capsule induction. Reads from RNA-Seq data (mean ± SD) during capsule induction (see Materials and methods) were compiled from three independent experiments, each with RNA prepared from three biological replicates as in (56).

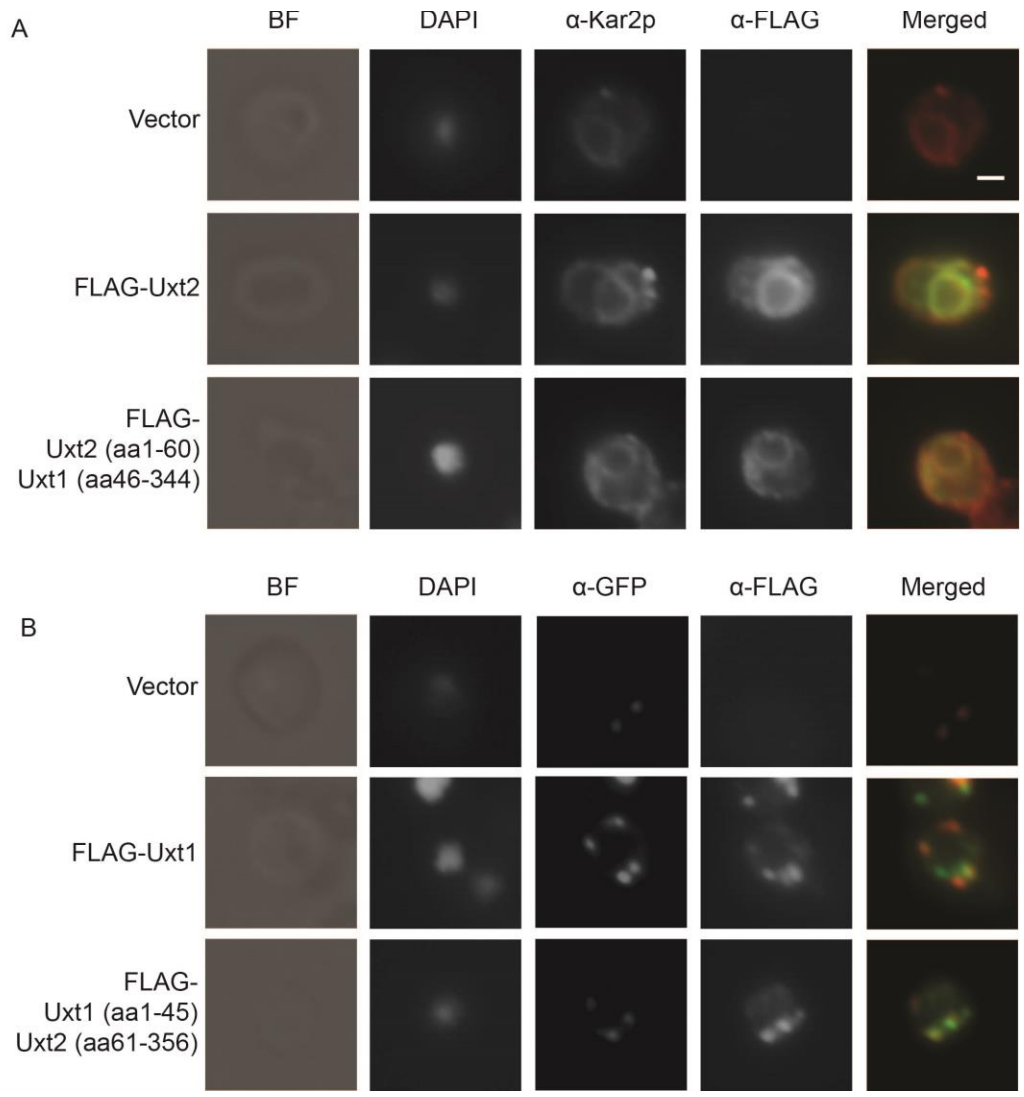

Figure 3.4. Subcellular localization of Uxt1 and Uxt2. Sec7-3xGFP *S. cerevisiae* cells transformed with vector alone (Vector) or vector expressing FLAG-tagged Uxt1, Uxt2, or chimeras of Uxt1 and Uxt2 were stained with DAPI and probed with the indicated antibodies. Bright field, single channel, and merged images are shown (scale bars, 1 μm). Blue, DAPI; red, α-Kar2p/BiP to mark the ER (A) or α-GFP to localize the Golgi marker Sec7 (B); green, α-FLAG. Images are representative of three independent studies.

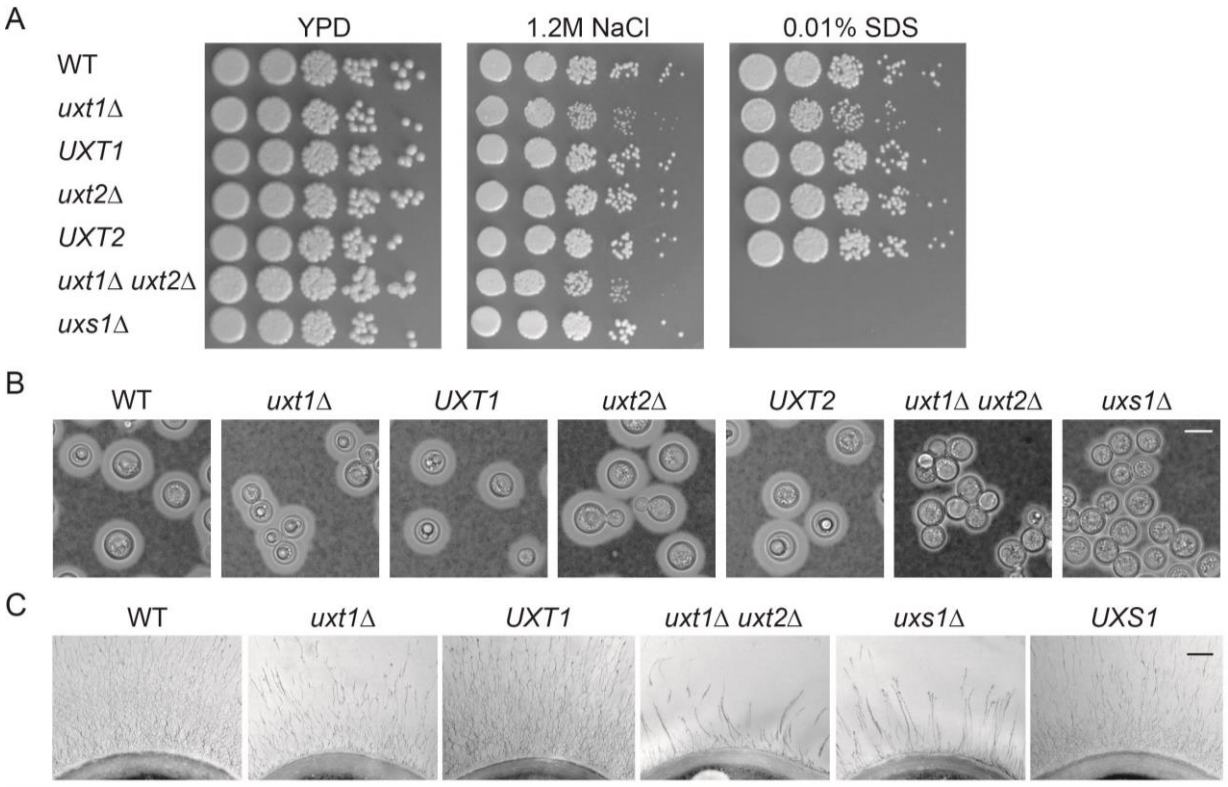

Figure 3.5. *uxt1*Δ and *uxt1*Δ *uxt2*Δ mutants exhibit growth and capsule defects. (A) 5-fold serial dilutions of the indicated strains, grown on the indicated media at 37 °C and photographed after three days. *uxs1*Δ is included as a control. (B and C) The indicated strains were placed in capsule-inducing conditions (see Materials and methods) for 24 h, and then visualized by light microscopy after negative staining with India ink (B, scale bar = 5 μm) or by electron microscopy (C, scale bar = 0.5 μm). Additional EM images are provided in Fig. 3.S5D.

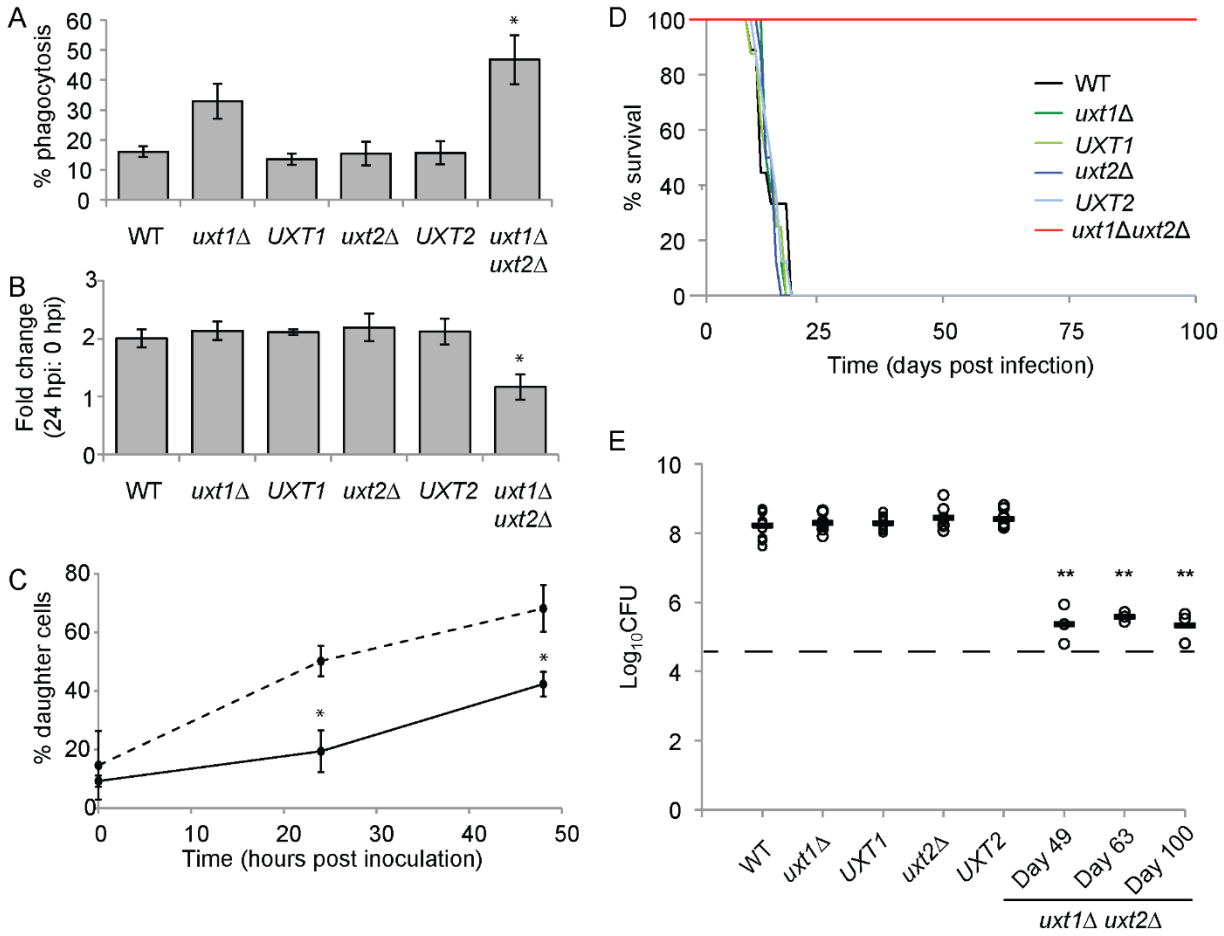

Figure 3.6. UDP-Xyl transport is required for host interactions and virulence. (A) Percent phagocytosis (engulfed fungi/initial inoculum) of opsonized fungi. (B) Fold-change in colony-forming units (CFU) 24 h:0 h after internalization. (C) Proportion of daughter cells in the population of WT (dashed line) and *uxt1*Δ *uxt2*Δ (black line) cells incubated with BMMs for 0, 24, and 48 h. Data are the mean ± SEM of three independent experiments. *, $p < 0.05$ by (A, B) one-way ANOVA with Tukey's post hoc test or (C) Student t-test. (D) Survival of A/JCr mice after intranasal inoculation with 5×10^4 cells of the indicated strains (n = 8-9). (E) Lung CFU of infected mice at the time of death (for WT, *uxt1*Δ, *uxt2*Δ, and complemented mutants; n = 8) or at the indicated time points (for *uxt1*Δ *uxt2*Δ; n = 3). Open circles, individual mice; black bar, mean; dashed line, initial inoculum. **, $p < 0.01$ by one-way ANOVA with Tukey's post hoc test.

3.9 Supplementary materials

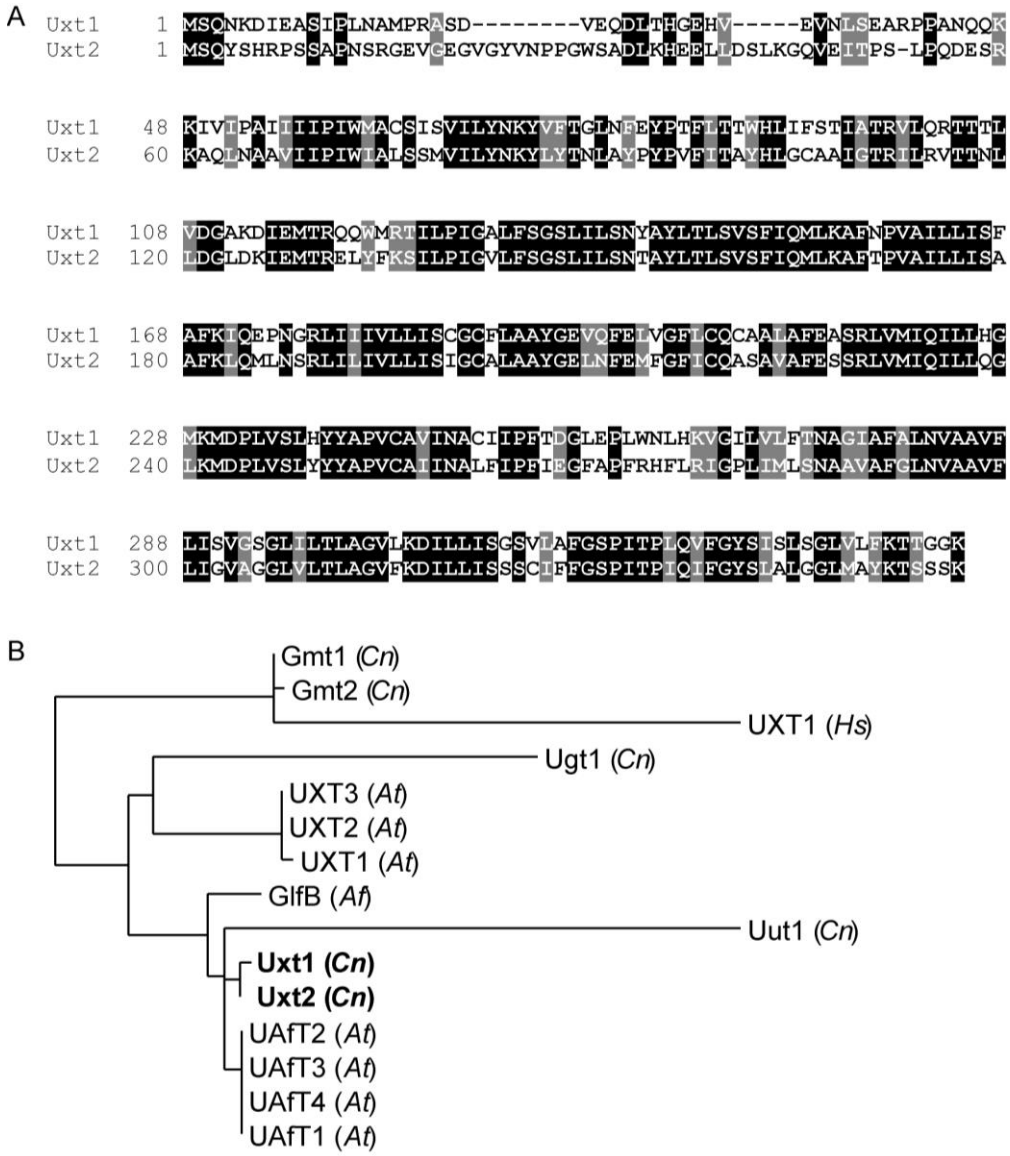

Figure 3.S1. Conservation of cryptococcal nucleotide sugar transporters. (A) Protein sequence alignment of Uxt1 and Uxt2 (CNAG_02036 and CNAG_03695) with conserved residues highlighted (black, identical residues; grey, conserved substitutions). (B) Phylogenetic relationships of *C. neoformans* (*Cn*) NSTs (including Uxt1 and Uxt2, in bold), and UDP-Xyl, UDP-Gal*f*, and UDP-Ara*p* transporters from other organisms (*Hs, Homo sapiens*; *Af, Aspergillus fumigatus*; *At,*

Arabidopsis thaliana) using MUSCLE, PhyML, and TreeDyn software (see Materials and methods). Branch lengths are drawn to scale.

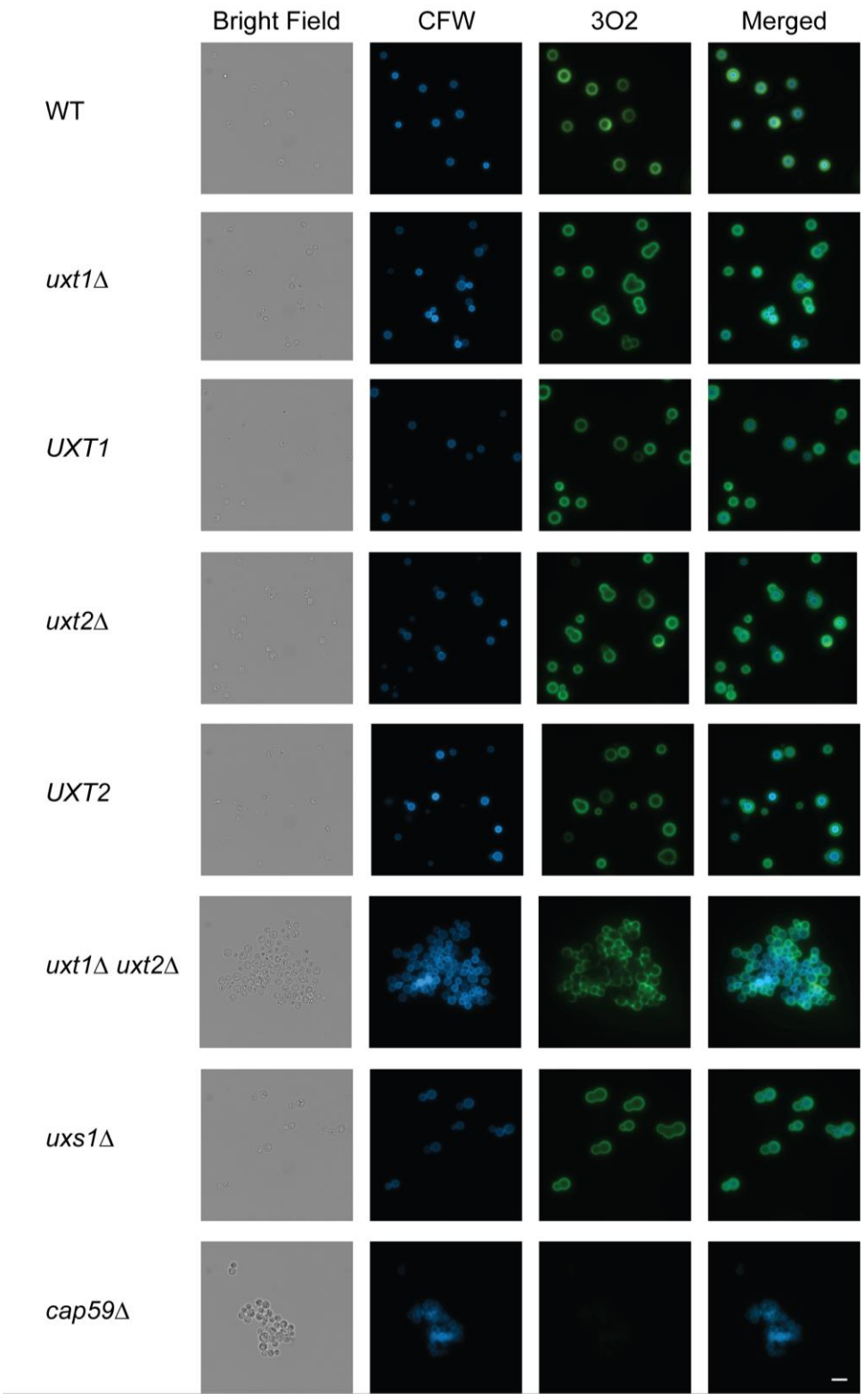

Figure 3.S2. *uxt1*Δ *uxt2*Δ is recognized by Xyl-independent capsule antibodies. Cells from the indicated strains were incubated with calcofluor white (CFW; blue) to stain the cell wall and an-

ti-GXM mAb 302 to visualize the capsule (green). Bright field, single channel, and merged images are shown; scale bar = 10 μm. *cap59*Δ is an acapsular strain included as a control.

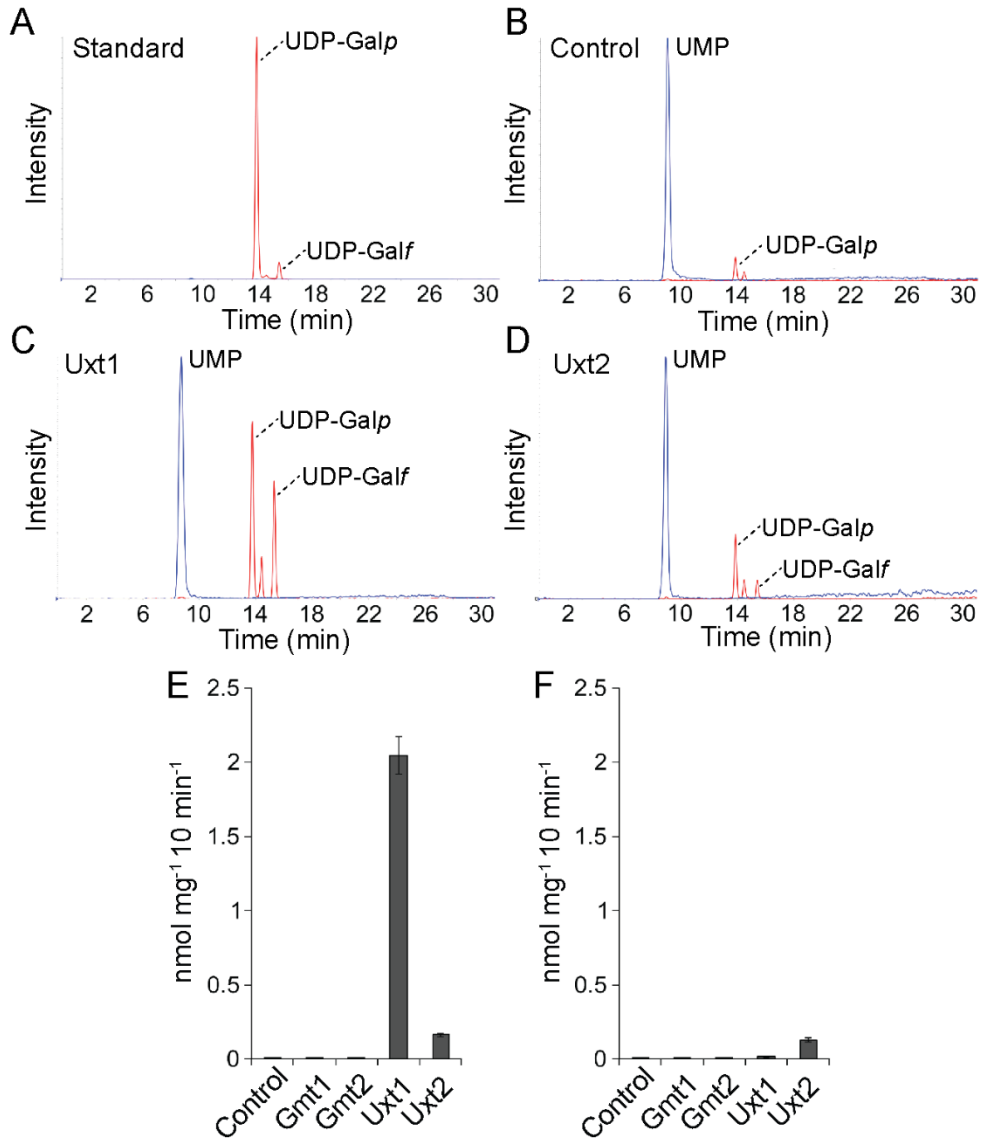

Figure 3.S3. Uxt1- and Uxt2-mediated UDP-Gal*f* uptake into proteoliposomes. (A) LC-MS/MS analysis of UDP-Gal*f* prepared from UDP-Gal*p* utilizing *E. coli* UDP-galactopyranose mutase (GLF). (B - D) Proteoliposomes prepared from *S. cerevisiae* expressing vector alone (B), Uxt1 (C), or Uxt2 (D) were preloaded with 30 mM UMP, and analyzed by LC-MS/MS after a 10 min incubation with 700 μM UDP-Gal*p* and 10 μg purified GLF. Based on mass and retention time, the minor peak between UDP-Gal*p* and UDP-Gal*f* is likely UDP-Glc, presumably present in the reaction starting material. (E and F) Quantification of nucleotide sugar uptake into proteolipo-

somes preloaded with 30 mM UMP (E) or 30 mM GMP (F). Amounts were calculated using a UDP-Gal*p* standard and normalized to the total protein content of the proteoliposome preparations, and the mean ± SD of four assays are plotted. All assays were performed at 37 °C.

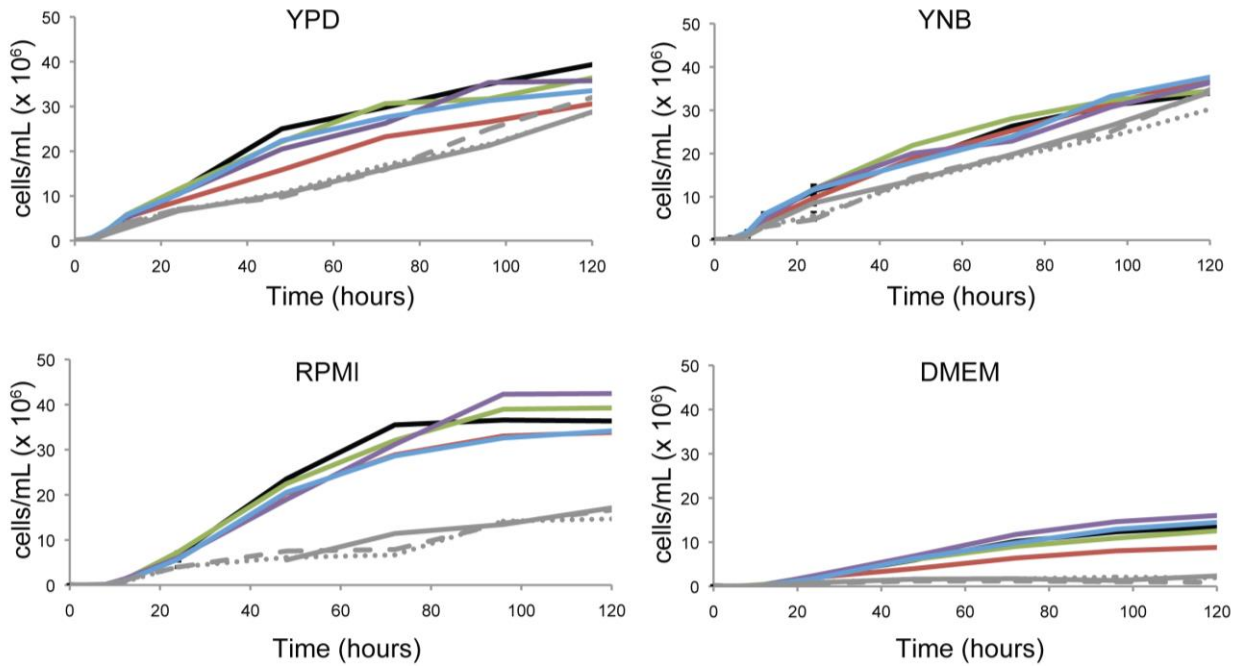

Figure 3.S4. *uxt1*Δ *uxt2*Δ growth is restricted at 37 °C. The indicated *C. neoformans* strains were grown overnight at 30 °C in YPD, diluted to 10^5 cells/mL in the media indicated, and incubated at 37 °C with 5% CO_2. The results shown are the averages of three measurements. Black, WT; red, *uxt1*Δ; green, *UXT1*; purple, *uxt2*Δ; blue, *UXT2*; grey, *uxt1*Δ *uxt2*Δ (continuous and dashed lines, representing three independently obtained double deletion strains).

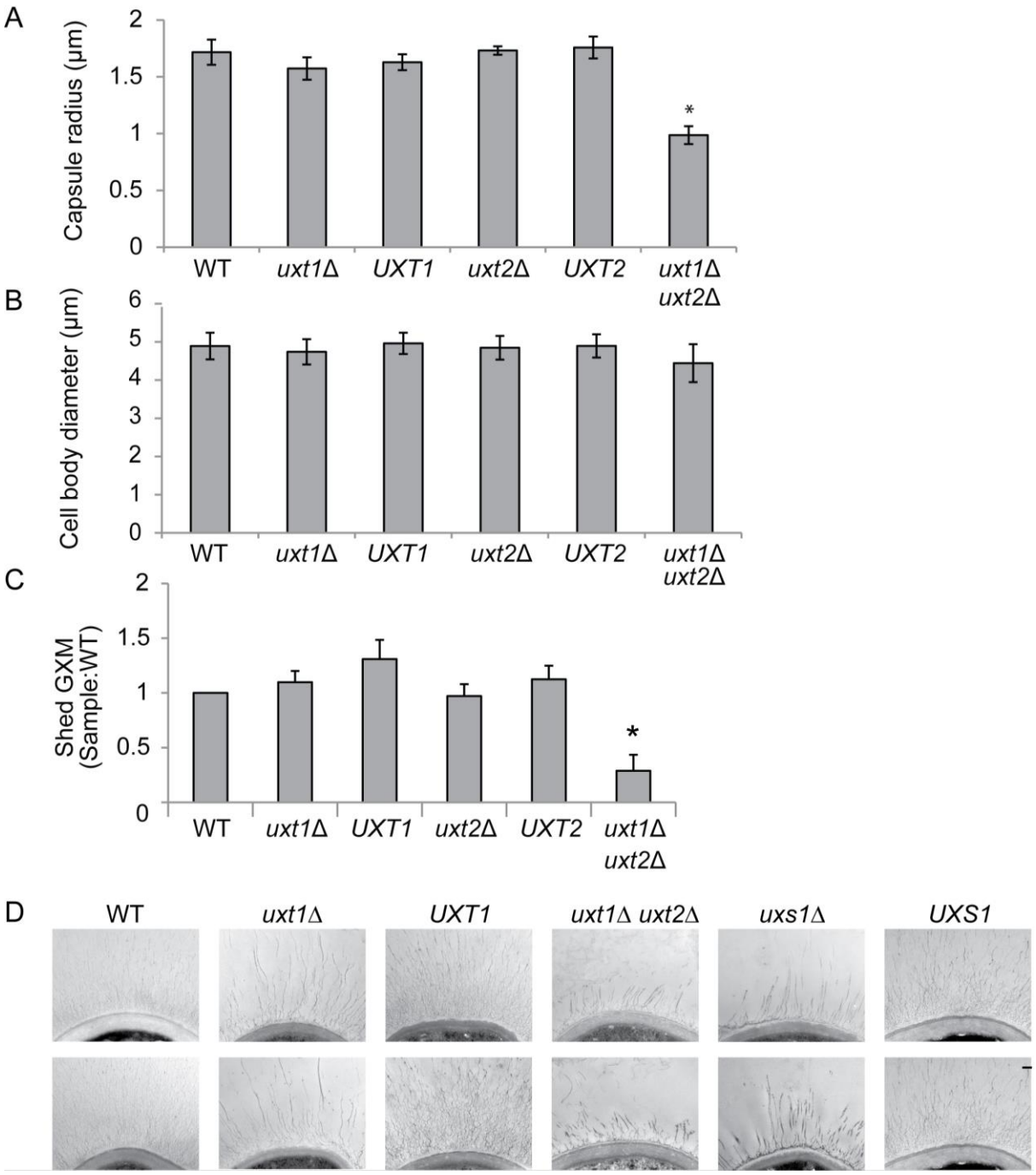

Figure 3.S5. Morphological defects of *uxt1*Δ *uxt2*Δ. Induced cells were stained with India Ink, and the radius of the capsule (A) and diameter of the cell body (B) were measured using ImageJ (100 cells counted per strain; mean ± SEM of three biological replicates). (C) GXM shed from equal numbers of each of the indicated strains was quantitated by ELISA (see Materials and

methods). Data is the mean ± SEM of three independent experiments. *, $p < 0.05$, one-way ANOVA with Tukey's *post-hoc* test. (D) Electron micrographs of the indicated strains induced for capsule as in Fig. 5. Two representative images are displayed for each strain. Scale bar = 0.5 μm.

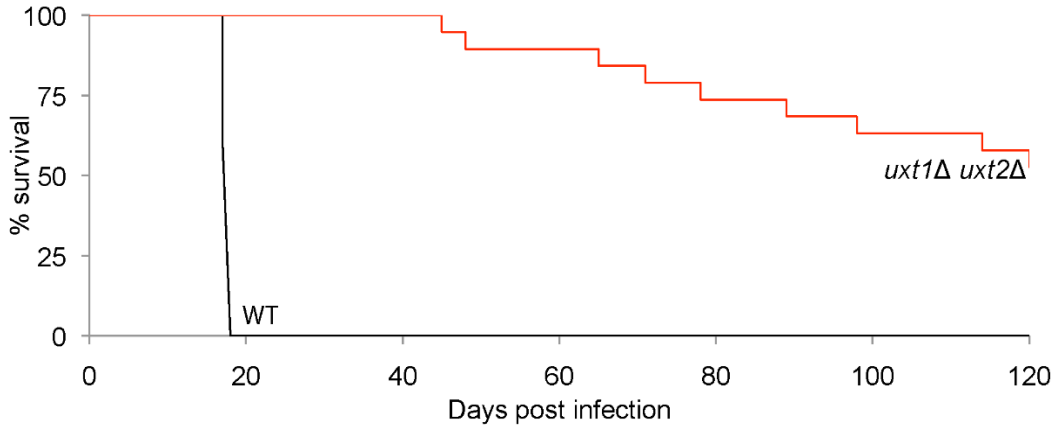

Figure 3.S6. *uxt1*Δ *uxt2*Δ is severely attenuated for virulence in C57BL/6 mice. Survival of C57BL/6 mice after intranasal inoculation with 5 × 104 cells of WT (n = 5) or *uxt1*Δ *uxt2*Δ (n = 19). C57BL/6 mice naturally skew towards a non-protective Th2-type response, which increases their susceptibility to cryptococcal infection compared to A/JCr mice (57).

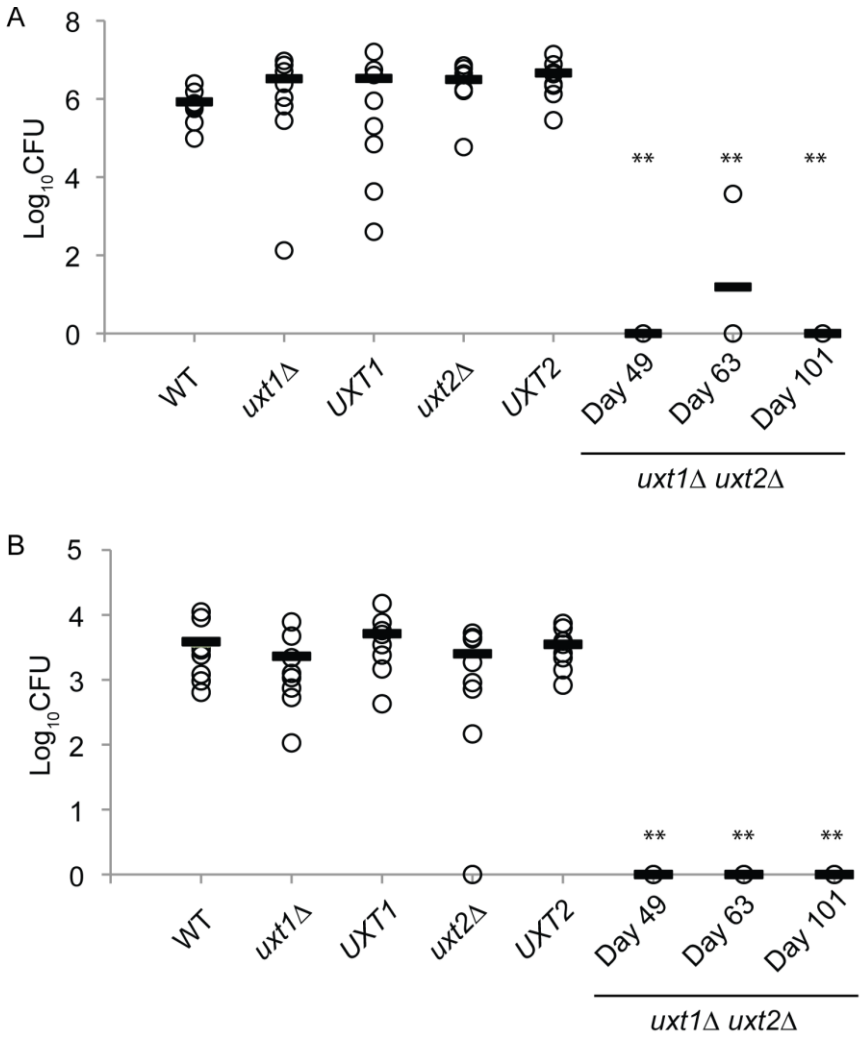

Figure 3.S7. *uxt1*Δ *uxt2*Δ does not colonize extrapulmonary sites. Brain (A) and spleen (B) CFUs of infected A/JCr mice at the time of death (for WT, *uxt1*Δ, *uxt2*Δ, and complemented mutants; n = 8) or at the indicated time points (for *uxt1*Δ *uxt2*Δ; n = 3). Open circles, individual mice; black bar, mean; dashed line, initial inoculum. **, $p < 0.01$ by one-way ANOVA with Tukey's post hoc test.

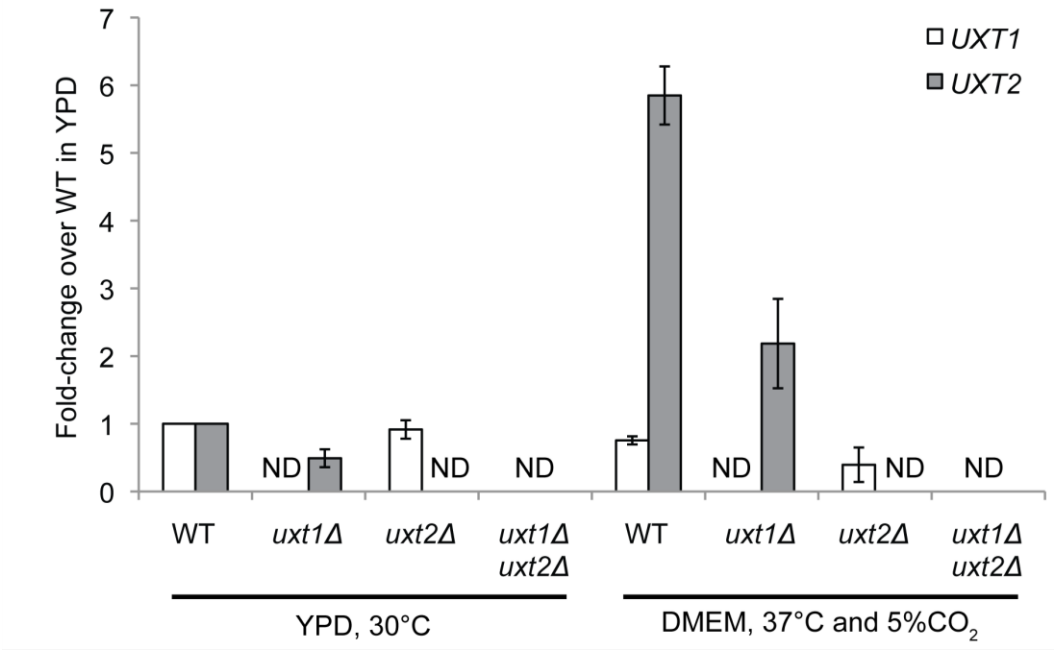

Figure 3.S8. *UXT1* and *UXT2* transcription levels. Expression of *UXT1* and *UXT2* measured by qRT-PCR with RNA prepared from the indicated strains after growth in nutrient rich (YPD) or capsule-inducing conditions (DMEM, 37 °C and 5% CO_2). Values are normalized to the WT sample grown in YPD and are the mean ± SEM of six biological replicates.

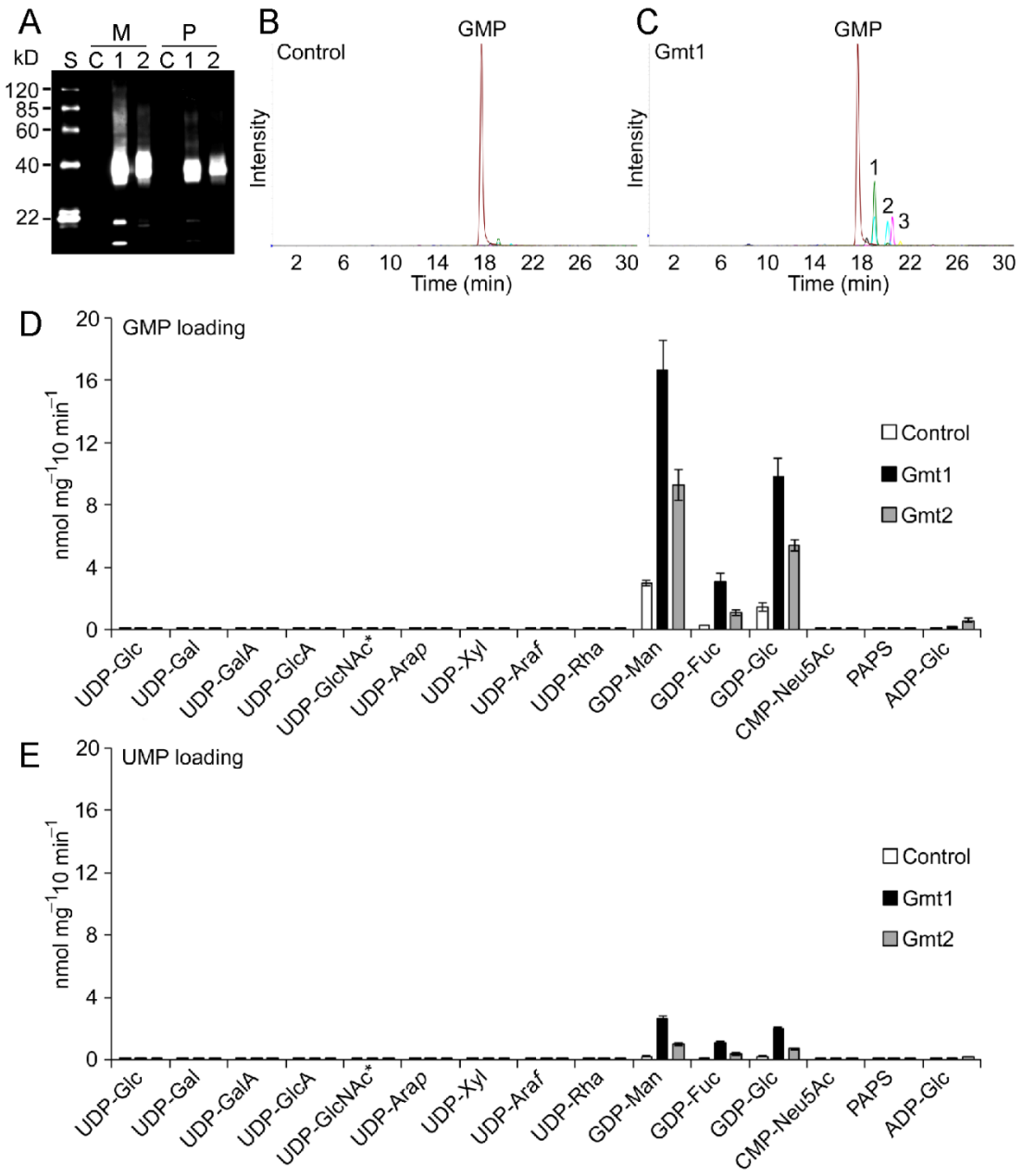

Figure 3.S9. Nucleotide sugar uptake into Gmt1- and Gmt2- containing proteoliposomes. (A) Immunoblot analysis of microsome (M) and proteoliposome (P) preparations from *S. cerevisiae* expressing vector only (Control) or V5-tagged Gmt1 or Gmt2 (2.5 μg protein per lane; S, molecular weight standards; C, control; 1, Gmt1; 2, Gmt2). (B and C) Representative LC-MS/MS spectra of GMP-preloaded proteoliposomes (B, Control; C, Gmt1) incubated for 10 min at 37 °C

with a mixture of 16 nucleotide/nucleotide sugar substrates, each 50 mM. Peak 1, GDP-Man; Peak 2, GDP-Glc; Peak 3, GDP-fucose (D and E) Quantification of nucleotide sugar uptake into proteoliposomes preloaded with (D) 30 mM GMP or (E) 30 mM UMP. Data were normalized to the total protein content of the proteoliposome preparations and show the mean ± SD of four assays. These results are consistent with prior studies (21, 30) and yield new information about Gmt substrate specificity.

Table 3.S1. Methylation analysis of GXM for the indicated strains.[a]

	WT	*uxt1*Δ	*UXT1*	*uxt2*Δ	*UXT2*	*uxt1*Δ *uxt2*Δ
t-Man	0.4	0.1	0.1	0.3	0.1	0.5
3-Man	42	66	47	51	39	80[b]
2,3-Man	53	33	48	45	54	18
3,4-Man	0.8	0.4	0.6	0.8	1.4	0.8
2,3,4-Man	3.4	0.4	4.5	2.5	4.1	0.0

[a] Values reported as percent of total mannose linkages to facilitate comparison.
[b] This product primarily reflects backbone substitution with GlcA.

Table 3.S2. Staining and stress sensitivity of *Cryptococcus neoformans* strains.

	Anti-GXM mAbs		Cell wall staining[a]				Cell growth[b]				
Strain	2H1	3C2	CFW	ConA	EosinY	Pont	YPD	2% CFW	0.05% CR	0.01% SDS	1.5 M Sorbitol
WT	+	+	+	+	+	+	+	+	+	+	+
*uxt1*Δ	+	+	+	+	+	+	+	+	+	+	+
UXT1	+	+	+	+	+	+	+	+	+	+	+
*uxt2*Δ	+	+	+	+	+	+	+	+	+	+	+
UXT2	+	+	+	+	+	+	+	+	+	+	+
*uxt1*Δ *uxt2*Δ	-	-	+	+	+	+	+	+	+	+	+
*uxs1*Δ	-	-	NT[c]	NT	NT	NT	+	+	+	+	+

[a] The indicated strains were stained with anti-GXM mAbs 2H1 or 3C2, CFW (binds chitin), ConA (binds mannoproteins), Eosin Y (binds chitosan), or Pontamine (binds unspecified cell wall components) as in Materials and methods.
[b] All growth conditions were assayed at 30°C.
[c] NT, not tested

Table 3.S3. Nucleotide sugar contents of *Cryptococcus neoformans* strains.[a]

Compound	Wild type	*uxt1*Δ	*UXT1*	*uxt2*Δ	*UXT2*	*uxt1*Δ *uxt2*Δ	*uxs1*Δ
UDP-α-D-Xyl	1 ± 0[b]	3 ± 1	2 ± 1	1 ± 0	1 ± 0	6 ± 3	ND[c, d]
UDP-α-D-Glc	16 ± 2	55 ± 17	26 ± 7	23 ± 6	21 ± 6	46 ± 21	50 ± 9
UDP-α-D-GlcA	4 ± 1	4 ± 2	5 ± 1	6 ± 1	5 ± 2	0 ± 0	400 ± 105[c]
UDP-α-D-Gal	1 ± 0	4 ± 3	2 ± 1	1 ± 1	1 ± 1	3 ± 3	4 ± 3

[a] Levels of UDP-α-D-Gal*f*, UDP-α-D-Ara*p*, and UDP-α-D-Ara*f* were below the limit of detection.
[b] Values are given in pmol mg^{-1} wet weight and represent the average of $n = 4$ (± SEM). Estimated cell volume was used to convert values to μM (see Materials and methods for details).
[b] ANOVA, $p \leq 0.01$.
[c] ND, below limit of detection.

Table 3.S4. Uxt1 and Uxt2 content of proteoliposomes used for transport assays.

	Molecular Mass (Da)	fmol[a]/5 μg	ng/5 μg	Total protein (%)
Uxt1	42442.2	501.8 ± 2.0[b]	21.3 ± 0.1[b]	0.43 ± 0.00[b]
Uxt2	43535.4	116.2 ± 5.9[b]	5.1 ± 0.3[b]	0.10 ± 0.01[b]

[a] Amount was estimated using LC-MS/MS (MRM) quantitation of a C-terminal peptide (SRGPFEGKPIPNPLLGLDSTR) and interpreted based on the molecular mass (including V5-tag and 6-His tags) estimated using the Compute pI/Mw tool at ExPASy (http://web.expasy.org/).

[b] Values represent the mean ± SD of n = 3.

Chapter 4: *Cryptococcus neoformans* evades pulmonary immunity by modulating xylose transport

From:

Cryptococcus neoformans evades pulmonary immunity by modulating xylose transport

Lucy X. Li, Camaron R. Hole, Javier Rangel-Moreno, Shabaana A. Khader, and

Tamara L. Doering

(manuscript in preparation)

4.1 Introduction

Cryptococcus neoformans is a ubiquitous environmental fungus that causes pneumonia and meningitis. This opportunistic pathogen infects over a million individuals each year, with overall mortality exceeding 20% (1-3). Patient immune status is the main determinant of infection outcome, highlighting the importance of host immune responses in the control of cryptococcosis.

C. neoformans infection begins when the organism is inhaled, followed by its proliferation in the lungs. This pulmonary infection may then disseminate to the brain, where it causes a frequently lethal meningoencephalitis. In the lungs, *C. neoformans* first interacts with host phagocytes, including macrophages and dendritic cells, which can engulf the fungus and present antigen to initiate the adaptive immune response. The protective immune response to *C. neoformans*, however, is primarily T cell mediated. Specifically, T helper cell type 1 (Th1) responses are protective against *C. neoformans* (4), although T helper type 17 (Th17) responses may also play a role by facilitating pathogen clearance at mucosal surfaces (5-7). In contrast, Th2 responses are associated with a non-protective immune response leading to fungal growth and dissemination to the CNS (8, 9). The induction of these non-protective responses is not well understood, but cryptococcal glycans may contribute to this process (10).

Glycan structures facilitate antigen recognition, immune activation, or immune regulation in multiple organisms (11). In *C. neoformans* the major virulence factor, a polysaccharide capsule, modulates the immune response by multiple mechanisms (12, 13). The capsule is composed of primarily of two large polysaccharides, glucuronoxylomannan (GXM) and glucuronoxylomannogalactan (GXMGal) (14, 15). One major component of both polymers is xylose (Xyl),

which comprises almost one fourth of the polysaccharide capsule mass (16). Xylose also occurs in cryptococcal glycolipids (17) and as both Xyl and Xyl-phosphate modifications of protein-linked glycans (18-20). We demonstrate here that Xyl plays an important role in the immune recognition of, and response to, *C. neoformans*.

The incorporation of Xyl into cryptococcal glycan structures occurs in the secretory pathway, via enzyme reactions that use the substrate molecule UDP-Xyl. This xylose donor is imported into the synthetic compartment by two transporters, termed Uxt1 and Uxt2 (21). A mutant strain that lacks both transporters (*uxt1*Δ *uxt2*Δ) exhibits defects in glycosylation, including incomplete synthesis of capsule polysaccharides, and is avirulent in mouse models of infection. Surprisingly, this strain persists in the lungs of infected mice, despite its avirulence. In pursuing the mechanism of this persistence, we observed the formation of inducible bronchus associated lymphoid tissue (iBALT) in the lungs of both *uxt1*Δ *uxt2*Δ and wild-type (WT) infected mice, although the characteristics of this tissue differed. In the mutant strain, where mice experience a long-term asymptomatic infection rather than a rapid and lethal one, iBALT formation was delayed. However, once formed, the iBALT appeared better organized and successfully controlled the infection, unlike the case when mice were infected with fully xylosylated WT *C. neoformans*. Together, our results suggest that luminal Xyl modifications of cryptococcal glycoconjugates inhibit the immune recognition and activation that are required to control infection.

4.2 Results

4.2.1 UDP-xylose transport is required for cryptococcal virulence and dissemination

We previously observed that a *C. neoformans* strain lacking UDP-Xyl transporters (*uxt1*Δ *uxt2*Δ) was highly attenuated in virulence compared to the WT parental strain KN99α, yet persisted in the lungs of asymptomatic mice for at least 100 days after infection (21). To probe the mechanism responsible for this chronic infection, we first examined the kinetics of fungal burden in mice after intranasal inoculation with each strain. In A/JCr mice infected intranasally with WT fungi, we observed a rapid and significant rise in pulmonary fungal burden (Fig. 4.1A), along with significant dissemination to the spleen (Fig. 4.1B) and brain (Fig. 4.1C); these mice typically succumb to infection roughly 18 days post-infection (dpi). In contrast, the pulmonary burden in *uxt1*Δ *uxt2*Δ-infected mice increased only gradually from initial inoculum levels to a modest peak at 63 dpi (Fig. 4.1A). Colony-forming units in the lung then gradually declined, with clearance in 30% of the mice by 189 dpi (Fig. 4.1A). This infection was not limited to the lungs, although only a fraction of the mice had measurable *uxt1*Δ *uxt2*Δ cells in the spleen (Fig. 4.1B) and brain (Fig. 4.1C) at any time during infection. Furthermore, this limited dissemination was only observed at the times of highest lung burden (63 and 126 dpi), with no fungi detected in distal sites by 189 dpi (Fig. 4.1B, Fig. 4.1C). These results suggest that the A/JCr mice would eventually clear the *uxt1*Δ *uxt2*Δ infection.

4.2.2 Induction of a Th2 cytokine response is independent of cryptococcal xylosylation

We next sought to identify the mechanism(s) responsible for the protracted, although ultimately successful, host clearance of *uxt1*Δ *uxt2*Δ infection. As summarized above, protection against *C. neoformans* is generally associated with a Th1-type immune response, characterized by the production of interleukin (IL)-2, IL-12, interferon gamma (IFN-γ), and tumor necrosis factor alpha

(TNF-α). In contrast a Th2-type immune response to cryptococcal infection (characterized by the production of IL-4, IL-5, IL-10, and IL-13) is generally detrimental (22) and is associated with dissemination to the central nervous system (4, 22).

We hypothesized that the increased survival of mice infected with the mutant cryptococci reflected an alteration in the immune response elicited by pulmonary infection. To test this hypothesis, we analyzed cytokine levels over time in lung homogenates from mice infected with WT or *uxt1*Δ *uxt2*Δ (Fig. 4.1). Infection with the WT strain induced a strong Th2-type response with significant induction of IL-4 and IL-5 over the 15 days prior to sacrifice (Fig. 4.1D, Fig. 4.1E). In contrast, while infection with *uxt1*Δ *uxt2*Δ elicited a more quiescent cytokine response in the comparable early stages of infection. Furthermore, by the time of peak fungal burden in *uxt1*Δ *uxt2*Δ-infected mice (day 63, Fig. 4.1A), there was a significant increase in the T cell polarizing cytokine, IL-12p40, over the level observed in naïve lungs (Fig. 4.1F). IL-12p40 levels subsequently slowly decreased, along with fungal burden (Fig. 4.1F). Levels of IFNγ and TNFα (Fig. 4.1G, Fig. 4.1H) were showed little difference from those in the lungs of naïve mice, although IL-17a trended higher at the point of peak infection (Fig. 4.1I). Overall, while WT infection induced non-protective Th2 responses, infection with *uxt1*Δ *uxt2*Δ failed to do so (even at peak fungal burden), while exhibiting sustained induction of IL-12p40 and an increase in IL-17a.

4.2.3 Inducible bronchial-associated lymphoid tissue develops following cryptococcal infection

The differences we observed in fungal burden and cytokine levels between mutant and WT infection suggested alterations in the immune response at the cellular level. To test this, we per-

formed quantitative histopathology on lungs from WT-infected mice at day 15 and *uxt1*Δ *uxt2*Δ-infected mice on days 15 and 189. The mutant-infected animals showed significantly reduced lung inflammation at both time points (Fig. 4.2A), consistent with the more quiescent cytokine response reported above (Fig. 4.1). We also noted lymphocytic accumulations proximal to the basal side of the bronchial epithelium in both mouse populations (Fig. 4.2B). The lymphoid populations within these structures were organized into B cell germinal centers surrounded by CD3+ T cell cuffs ($B220^{Lo}$; Fig. 4.2C). These inflammatory foci were consistent with inducible bronchus-associated lymphoid tissue (iBALT) (23).

iBALT is a tertiary lymphoid tissue that forms in the lung. Its structure resembles that of secondary lymphoid organs like lymph nodes, consisting of two zones: the B cell follicle and the T cell zone (24). The B cell follicle contains follicular B cells and is associated with the production of CXCL13. It is surrounded by a zone of T cells that contains CD4 and CD8 T cells as well as dendritic cells (DCs) (24). At 15 days after infection with WT cryptococci, we observed numerous highly developed iBALT structures, with clear B cell follicles surrounded by T cells (Fig. 4.2C, Fig. 4.2D). In contrast, *uxt1*Δ *uxt2*Δ infected animals exhibited significantly fewer, less well-developed, B cell follicles at the same time point (Fig. 4.2C, Fig. 4.2D). By 189 dpi, however, *uxt1*Δ *uxt2*Δ-induced iBALT were well-organized structures that, although still less abundant than the 15 dpi WT iBALT (Fig. 4.2D), were larger (Fig. 4.2E) and even contained IgG+ plasma cells (Fig. 4.2C). Early in *uxt1*Δ *uxt2*Δ infection the reduced formation of these iBALT structures was accompanied by increased peri-vascular cuffing of T cells (Fig. 4.2F) and lower production of CXCL13 (Fig. 4.2G, Fig. 4.2H), which is required for iBALT structure formation and organization (23). By a late time point in this protracted developmental process,

however, reduced T cell cuffing (Fig. 4.2F) and increased CXCL13 expression (Fig. 4.2G, Fig. 4.1H) were evident.

4.2.4 Cryptococcal-induced iBALT recruits increased T and B cells at late time points

To further define the host immune response to *uxt1*Δ *uxt2*Δ, we used flow cytometry to characterize leukocyte populations in the lungs of mice infected with WT or *uxt1*Δ *uxt2*Δ cells. By 12 to15 dpi the fraction of leukocytes that were B (Fig. 4.3A) or T cells ($CD4^+$ and $CD8^+$; Fig. 4.3B, Fig. 4.3C) in *uxt1*Δ *uxt2*Δ-infected mice significantly exceeded those of WT-infected mice and continued to rise as infection progressed. The total numbers of cells in these populations remained elevated through 126 dpi (Fig. 4.3A-C, right), although they subsequently declined, consistent with the decreased average T cell cuff size of iBALT at 189 versus 15 dpi (Fig. 4.2F).

4.2.5 Survival of *uxt1*Δ *uxt2*Δ-infected mice is dependent on T cells

To test the role of T and B cells in the prolonged survival of *uxt1*Δ *uxt2*Δ-infected mice, we examined whether ablation of these cell types altered the course of infection. For these studies we used mouse lines in the C57BL/6 background, so this strain was included as a control; these mice are less resistant to *C. neoformans* than the A/JCr mice used above (25), as shown by their eventual susceptibility to *uxt1*Δ *uxt2*Δ infection (Fig. 4.3D, solid black line). We found that *Rag1*-/- mice were significantly more susceptible to *uxt1*Δ *uxt2*Δ infection than controls, succumbing by 55 dpi (Fig. 4.3D; solid blue line).

Since *Rag1*-/- mice lack both T and B cells, we also infected mice deficient in either T cells (*TCRβ* -/-) or B cells (*μMT*). B cell deficient mice exhibited a more protracted course of disease than *Rag1*-/-, succumbing over an 85-day period (Fig. 4.3D, solid green line). Mice lacking T cells alone, however, succumbed to *uxt1*Δ *uxt2*Δ infection with kinetics similar to those of the *Rag1*-/- mice (Fig. 4.3D, solid red line). In contrast, all mice inoculated with WT *C. neoformans* succumbed by 20 dpi (Fig. 4.3D; dashed lines). *Rag1*-/- and *TCRβ*-/- mice still succumbed slightly faster than C57BL/6 and μMT mice, (Fig. 4.3D). Together, these data show that T cells are the prominent cell type responsible for the increased survival of *uxt1*Δ *uxt2*Δ-infected mice, although B cells may play a role in protection.

4.2.6 Lack of luminal xylose modification in *C. neoformans* stimulates DC activation

DCs are critical for induction of a protective immune response against *C. neoformans* (26), and DC activation and cytokine production are required for iBALT formation and maintenance (24). During iBALT formation, antigen-triggered activation of DCs and their consequent cytokine production is responsible for T and B cell recruitment (24); this could potentially induce both the observed increase in these cell populations and the protective effect of the T cells during cryptococcal infection. We tested DC interactions with WT cells, which exhibit Xyl modification of antigens, and *uxt1*Δ *uxt2*Δ cryptococci, which lack these modifications. We also tested single *uxt*Δ mutants: *uxt1*Δ shows an intermediate level of Xyl utilization while *uxt2*Δ is similar to WT (21). In these assays, we measured the ability of heat-killed fungi to stimulate DC production of pro-inflammatory cytokines, comparing WT, *uxt1*Δ *uxt2*Δ, single *uxt* mutants, *uxs1*Δ (which lacks all Xyl modification because it cannot synthesize UDP-Xyl), and an acapsular control

strain (*cap59*Δ) which has been shown to induce a potent DC response (27). We found that BMDCs co-incubated with *uxt1*Δ *uxt2*Δ cells released high levels of IL-1β, IL-6, and TNF-α, similar to levels following treatment with a completely acapsular control strain, *cap59*Δ (Fig. 4.4A-C). In contrast, individual *uxt* mutants and *uxs1*Δ induced IL-1β and IL-6 levels similar to those induced by WT fungi (close to background levels; Fig. 4.4A, Fig. 4.4B). TNF-α similarly showed the greatest response upon challenge with *uxt1*Δ *uxt2*Δ, with levels like those induced by an acapsular strain, although some increase was also noted with other xylose-deficient strains (*uxt1*Δ and *uxs1*Δ). These results suggest that early interaction with DCs and consequent induction of proinflammatory cytokines are regulated by Xyl expression in Cryptococcus.

4.3 Discussion

Here we report that iBALT forms during *C. neoformans* infection, although this process does not prevent mice from succumbing to the disease. Notably, the iBALT observed in our experimental infections resembles subpleural nodules that have been reported in cryptococcosis patients (28), although further histological examination would be necessary to support this relationship. The only other fungus reported to induce iBALT is *Pneumocystis* (23).

When we infected mice with mutant fungi unable to use Xyl for luminal glycoconjugate synthesis (*uxt1*Δ *uxt2*Δ), we observed a delay in the organization of the iBALT structures and in fungal accumulation. When *uxt1*Δ *uxt2*Δ burden did peak, it was accompanied by a rise in IL-12p40 (Fig. 4.1F), a cytokine normally required for inducing a protective response against *C. neoformans* (29), which may have facilitated resolution of the *uxt1*Δ *uxt2*Δ infection. A change in IL-12p40 level might reflect an increase in either IL-23 or IL-12 (30), which stimulate a Th17 or

Th1 type response, respectively; the former is required for iBALT formation (23). Since we saw no difference in IFN-γ levels, IL-12p40 is more likely associated with a Th17 response. We did observe a trend towards increased IL-17 levels when *uxt1*Δ *uxt2*Δ burden was the highest, which was absent in WT-infection.

DCs reacted more strongly to *uxt1*Δ *uxt2*Δ than to WT *in vitro*, releasing greater amounts of pro-inflammatory cytokines (Fig. 4.4A-C). These may directly or indirectly lead to the increased recruitment of T and B cells in *uxt1*Δ *uxt2*Δ infection (Fig. 4.3A-C), which are subsequently organized into germinal centers (Fig. 4.2). Such differences in development may confer distinct properties on the iBALT induced by WT and *uxt1*Δ *uxt2*Δ, influencing their ability to respond to *C. neoformans*.

We expected that the highly immunostimulatory behavior of *uxt1*Δ *uxt2*Δ *in vitro* reflected its lack of Xyl modifications on secreted glycoconjugates, a consequence of the lack of UDP-Xyl transport into the secretory compartment. We were surprised, therefore, that mutants unable to synthesize UDP-Xyl (*uxs1*Δ), which similarly lack Xyl modifications on secreted glycoconjugates, did not phenocopy this broad and robust DC response. This suggests that Uxs1 itself is required for the strong response seen in the absence of xylosylation in the secretory pathway. It may be that this protein plays additional roles unrelated to glycosylation, or that the stimulatory component is dependent on cytosolic UDP-Xyl, rather than UDP-Xyl that has been transported into the secretory pathway.

Unlike encapsulated strains, mutants lacking capsule induce the upregulation of multiple genes involved in cytokine responses as well as in antigen processing and presentation by DCs (31). Interestingly, the cytokine levels induced in DC by the *uxt1*Δ *uxt2*Δ mutant were similar to those induced by the acapsular mutant *cap59*Δ (Fig. 4.4A-C). Xyl may thus be critical for the immune suppressive effects normally exerted by capsule material. The mechanisms behind the robust DC activation seen in these two mutants, including the cellular receptors and fungal components responsible, remain to be determined.

Control of *uxt1*Δ *uxt2*Δ infection requires both T and B cells (Fig. 4.3D), which suggests that iBALT formation may play a key role in restricting disease. Even in the absence of T and B cells, however, mutant-infected mice still survived more than twice as long as WT-infected animals (Fig. 4.3D); this may be due to slower growth of the mutant, which we have previously observed (21).

We have found that *C. neoformans* infection induces iBALT formation, although this is insufficient to protect against wild-type fungal infection. Inoculation with a *uxt1*Δ *uxt2*Δ strain, however, induced similar lymphoid structures, which do appear to restrict infection despite delayed organization in this context. *In vitro*, these mutants induced DCs to release much higher levels of proinflammatory cytokines than WT fungi. This is presumably a consequence of the lack of surface Xyl modification, suggesting a role for this residue in the immunosuppressive character of capsule polysaccharides or other surface exposed or secreted glycoconjugates. By influencing the dynamics of the inflammatory process, we may be able exploit this response to help control infection and use this information to help guide novel therapies.

4.4 Materials and methods

4.4.1 Fungal strains

C. neoformans strains (Table 4.S1) were grown at 30 °C in YPD medium (1% [wt/vol] yeast extract, 2% [wt/vol] peptone, 2% [wt/vol] dextrose) with shaking (230 rpm) or on YPD agar plates (YPD medium with 2% [wt/vol] agar) supplemented with the following antibiotics as appropriate: 100 μg/ml nourseothricin (NAT; Werner BioAgents) or Geneticin (G418; Invitrogen).

4.4.2 Mice

C57BL/6J and A/JCr mice were from Jackson Laboratory. *Rag1*-/-, *TCRβ*-/-, and μMT mice (all on C57BL/6 background) were generously provided by Dr. Michael Diamond (Washington University School of Medicine) and Dr. Wayne Yokoyama (Washington University School of Medicine); breeders were originally purchased from Jackson Laboratory. All mice were 6- to 8-weeks old at the time of infection. A/JCr mice were female; male and female mice were used for the other strains with gender and age matched C57BL/6 controls.

4.4.3 Ethics statement

All animal protocols were reviewed and approved by the Animal Studies Committee of the Washington University School of Medicine and conducted according to National Institutes of Health guidelines for housing and care of laboratory animals.

4.4.4 *C. neoformans* inoculation

Fungal strains were cultured overnight (O/N) and diluted to 10^6 cells/mL in sterile PBS. Mice were intranasally inoculated with a 50 μL aliquot, and then weighed daily. Infected mice were sacrificed if they lost >20% relative to peak weight or at specified time points. At the time of sacrifice, mice were perfused intracardially with 10 mL sterile PBS, and organs were processed as described below for fungal burden, flow analysis, and cytokine measurements.

4.4.5 Organ burden and cytokines

Brain and spleen homogenates were harvested and plated for CFU at the specified time points. 50 μL aliquots of the left lung homogenates (V_T = 1 mL) were similarly plated for CFUs. The remaining sample was assayed for pulmonary cytokine levels using the Bio-Plex Protein Array System (Bio-Rad Laboratories). Briefly, the lung homogenates were mixed with an equal volume of PBS/0.1% Triton 100x/2x protease inhibitor (Pierce EDTA-free protease inhibitor; Thermo Scientific), vortexed for 3 seconds, and clarified by centrifugation (2500 x g, 10 min). Supernatant fractions were then assayed using the Bio-Plex Pro Mouse Cytokine 23-Plex (Bio-Rad Laboratories) for the presence of IL-1α, IL-1β, IL-2, IL-3, IL-4, IL-5, IL-6, IL-9, IL-10, IL-12 (p40), IL-12 (p70), IL-13, IL-17A, granulocyte colony stimulating factor (G-CSF), granulocyte monocyte colony stimulating factor (GM-CSF), interferon-γ (IFN-γ), CXCL1/keratinocyte-derived chemokine (KC), CCL2/monocyte chemotactic protein-1 (MCP-1), CCL3/macrophage inflammatory protein-1α (MIP-1α), CCL4/MIP-1β, CCL5/regulated upon activation normal T cell expressed and secreted (RANTES), and tumor necrosis factor-α (TNF-α).

4.4.6 Immunofluorescence staining and histologic analysis

Mice were perfused with sterile PBS, and the lungs inflated with 10% formalin. Lung tissue was then fixed O/N in 10% formalin, and submitted to the Washington University Developmental Biology Histology Core for paraffin-embedding, sectioning, and staining with H&E. Immunofluorescence staining for germinal center B cells (APC-conjugated rat anti-mouse CD45R/B220, clone RA3-6B2, BD Biosciences), T cell cuffing (CD3-ε, clone M-20, Santa Cruz Biotechnology), and CXCL13-producing cells (goat α-mouse CXCL13, AF470, R&D Systems) was performed as in reference 23. Images were collected with a Zeiss Axioplan2 microscope, and lung structures were quantitated in a blinded manner using the outline tool in Zeiss Axiovision.

4.4.7 Flow analysis

The right lung of individual mice was enzymatically digested (in 5 mL RPMI with 1 mg/mL collagenase type IV) at 37 °C with shaking (230 rpm) for 30 min, and then sequentially passed through sterile 70 and 40 µm pore nylon strainers (BD Biosciences, San Jose, CA). Red blood cells in the samples were lysed by treatment for 3 min on ice with 5 mL ammonium-chloride-potassium lysing buffer (8.024 g/L NH_4Cl, 1.001 g/L $KHCO_3$, and 2.722 mg/L EDTA•Na_2 $2H_2O$) followed by the addition of 2 volumes of PBS. The remaining cells were pelleted (1000 x g, 5 min, 4 °C), washed twice with PBS, diluted to 10^6 cells/mL in PBS, and stained with LIVE/DEAD fixable blue dead cell stain (1:1000; Thermo Scientific). Following incubation in the dark for 30 min at 4 °C, cells were washed with PBS and FACS buffer (2% fetal bovine serum in PBS) before resuspension in FACS buffer. Samples were then treated with CD16/CD32 (1:500; Fc Block™; BD Biosciences) for 5 min and incubated for 30 min with optimal concentrations of fluorochrome-conjugated antibodies (Table 4.S2) diluted in Brilliant Stain Buffer (BD

Biosciences). After three washes with FACS buffer, the cells were fixed in 2% formaldehyde/FACS buffer. For data acquisition, >50,000 events were collected on a BD LSRFortessa X-20 flow cytometer (BD Biosciences), and the data were analyzed with FlowJo V10 (Fig. 4.S1; TreeStar). The absolute number of cells in each leukocyte subset was determined by multiplying the absolute number of $CD45^+$ cells by the percentage of cells stained by fluorochrome-labeled antibodies for each cell population analyzed.

4.4.8 Isolation of bone marrow derived cells

Bone marrow was flushed from the femurs and tibiae of C57BL/6 mice using RPMI. Cells were collected (1000 x g, 5 min, 4 °C), resuspended in RPMI, and counted by hemocytometer. To prepare bone marrow derived dendritic cells (BMDCs), 2 x 10^6 bone marrow cells were plated in 10 mL R10 medium (10% FBS, 0.4% Penicillin-Streptomycin, 2 mM L-glutamate, 50 μM 2-β-mercaptoethanol in RPMI) supplemented with 1 ng/mL GM-CSF, and incubated at 37 °C and 5% CO_2. Medium was changed 3 and 6 days after plating, and cells were harvested on day 8. BMDCs were enriched by depletion of BMMs using biotinylated α-F4/80 antibody (eBioscience) and anti-biotin conjugated magnetic beads (Miltenyi Biotec). The BMDCs in the flow through were positively selected using α-CD11c magnetic beads according to the manufacturer's protocol (Miltenyi Biotec).

4.4.9 Dendritic cell assays

To assay the ability of fungal strains to activate the BMDCs, *C. neoformans* strains of interest were grown O/N, washed in PBS, and incubated at 65 °C for 15 min to heat kill (HK) the fungi. BMDCs and HK fungi (10^6 cells of each) were then co-incubated for 24 h, sedimented, and the

supernatant fractions transferred to 1.5 mL centrifuge tubes containing 10 μL of 100x protease inhibitor (ThermoScientific) for measurement of IL-1β, IL-6, and TNF-α levels by ELISA according to the manufacturer's protocol (R&D Systems).

4.4.10 Statistical analysis

Each experiment was performed a minimum of two times. Statistical analyses were conducted using GraphPad Prism version 6.0f (GraphPad Software). All studies comparing two groups were analyzed with a Student's t-test. Those with three or more groups were compared using an ordinary one-way ANOVA with Tukey's *post-hoc* test. $p < 0.05$ was considered statistically significant.

4.5 Acknowledgements

This work was funded by National Institutes of Health (NIH) grants R21 AI109623 and R01 AI102882 to TLD. LXL was partly supported by a National Research Science Award (T32 GM007200), a Sondra Schlesinger Graduate Fellowship (Washington University St. Louis Microbiology Department), and a National Institute of Allergy and Infectious Diseases award (NIAID; F30 AI120339). CRH was partly funded by a NIAID T32 training grant (AI007172). SAK and JR-M were supported by NIH grant R01 AI111914.

We thank the members of the Doering laboratory for helpful discussions and assistance with experiments. We also thank Dr. Thomas R. Kozel (University of Nevada School of Medicine) for the anti-GXM monoclonal antibody, Dr. Michael Diamond and Dr. Wayne Yokoyama (Washington University School of Medicine) for immune deficient mouse lines.

4.6 References

1. Kwon-Chung KJ, *et al*. (2014) *Cryptococcus neoformans* and *Cryptococcus gattii*, the etiologic agents of cryptococcosis. *Cold Spring Harb Perspect Med* 4(7):a019760.

2. Denning DW (2016) Minimizing fungal disease deaths will allow the UNAIDS target of reducing annual AIDS deaths below 500 000 by 2020 to be realized. *Philos Trans R Soc Lond B Biol Sci* 371(1709).

3. Rajasingham R, *et al*. (2017) Global burden of disease of HIV-associated cryptococcal meningitis: an updated analysis. *Lancet Infect Dis* 17(8):873-881.

4. Wozniak KL & Levitz SM. T cell and dendritic cell immune responses to Cryptococcus. In: Heitman J, Kozel TR, Kwon-Chung KJ, Perfect JR, Casadeval A, editors. *Cryptococcus*. Washington, DC: ASM Press; 2011. p. p 387-96.

5. Zhang Y, *et al*. (2009) Robust Th1 and Th17 immunity supports pulmonary clearance but cannot prevent systemic dissemination of highly virulent *Cryptococcus neoformans* H99. *Am J Pathol.* 175(6):2489-500.

6. Wozniak KL, Hardison SE, Kolls JK, & Wormley FL (2011) Role of IL-17A on resolution of pulmonary *C. neoformans* infection. *PloS One*. 6(2):e17204

7. Murdock BJ, Huffnagle GB, Olszewski MA, & Osterholzer JJ (2013) Interleukin-17A enhances host defense against cryptococcal lung infection through effects mediated by leukocyte recruitment, activation, and gamma interferon production. *Infect immun* 82(3):937-48.

8. Schulze B, *et al*. (2014) CD4(+) FoxP3(+) regulatory T cells suppress fatal T helper 2 cell immunity during pulmonary fungal infection. *E J Immunol* 44(12):3596-604.

9. Wiesner DL, Smith KD, Kotov DI, Nielsen JN, Bohjanen PR, & Nielsen K (2016) Regulatory T cell induction and retention in the lungs drives suppression of detrimental type 2 Th cells during pulmonary cryptococcal infection. *J Immunol* 196(1):365-74.

10. Wiesner DL, *et al*. (2015) Chitin recognition via chitotriosidase promotes pathologic type-2 helper T cell responses to cryptococcal infection. *PLoS Pathog* 11(3):e1004701.

11. Wolfert MA & Boons GJ (2013) Adaptive immune activation: glycosylation does matter. *Nat Chem Biol* 9(12):776-84.

12. Zaragoza O, Rodrigues ML, De Jesus M, Frases S, Dadachova E, & Casadevall A (2009) The capsule of the fungal pathogen *Cryptococcus neoformans*. *Adv Appl Microbiol* 68:133-216.

13. Yauch LE, Lam JS, & Levitz SM (2006) Direct inhibition of T-cell responses by the *Cryptococcus* capsular polysaccharide glucuronoxylomannan. *PLoS Pathog* 2(11):e120.

14. Agustinho DP, Miller LC, Li LX & Doering TL (2018) Peeling the onion: the outer layers of *Cryptococcus neoformans*. *Mem Inst Oswaldo Cruz* 113(7):e180040.

15. Wang ZA, Li LX & Doering TL (2018) Unraveling synthesis of the cryptococcal cell wall and capsule. *Glycobiology* 28(10):719-30.

16. Cherniak R, Valafar H, Morris LC & Valafar F (1998) *Cryptococcus neoformans* chemotyping by quantitative analysis of 1H nuclear magnetic resonance spectra of glucuronoxylomannans with a computer-simulated artificial neural network. *Clin Diagn Lab Immunol* 5(2):146-59.

17. Castle SA, *et al*. (2008) Beta1,2-xylosyltransferase Cxt1p is solely responsible for xylose incorporation into *Cryptococcus neoformans* glycosphingolipids. *Eukaryot Cell* 7(9):1611-5.

18. Klutts JS, Levery SB & Doering TL (2007) A beta-1,2-xylosyltransferase from *Cryptococcus neoformans* defines a new family of glycosyltransferases. *J Biol Chem* 282(24):17890-9.

19. Park JN, Lee DJ, Kwon O, Oh DB, Bahn YS, & Kang HA (2012) Unraveling unique structure and biosynthesis pathway of N-linked glycans in human fungal pathogen *Cryptococcus neoformans* by glycomics analysis. *J Biol Chem* 287(23):19501-15.

20. Lee DJ, Bahn YS, Kim HJ, Chung SY, & Kang HA (2015) Unraveling the novel structure and biosynthetic pathway of O-linked glycans in the Golgi apparatus of the human pathogenic yeast *Cryptococcus neoformans*. *J Biol Chem* 290(3):1861-73.

21. Li LX, Rautengarten C, Heazlewood JL, & Doering TL (2018) Xylose donor transport is critical for fungal virulence. *PLoS Pathog* 14(1):e1006765.

22. Koguchi Y & Kawakami K (2002) Cryptococcal infection and Th1-Th2 cytokine balance. *Int Rev Immunol* 21(4-5):423-38.

23. Eddens T, *et al*. (2017) Pneumocystis-driven inducible bronchus-associated lymphoid tissue formation requires Th2 and Th17 immunity. *Cell Rep* 18(13):3078-90.

24. Hwang JY, Randall TD & Silva-Sanchez A (2016) Inducible bronchus-associated lymphoid tissue: taming inflammation in the lung. *Front Immunol* 7:258.

25. Huffnagle GB, Boyd MB, Street NE & Lipscomb MF (1998) IL-5 is required for eosinophil recruitment, crystal deposition, and mononuclear cell recruitment during a pulmonary *Cryptococcus neoformans* infection in genetically susceptible mice (C57BL/6). *J Immunol* 160(5):2393-400.

26. Leopold Wager CM, Hole CR, Wozniak KL & Wormley FL, Jr (2016) Cryptococcus and phagocytes: complex interactions that influence disease outcome. *Front Microbiol* 7:105.

27. Grijpstra J, Tefsen B, van Die I & de Cock H (2009) The *Cryptococcus neoformans* cap10 and cap59 mutant strains, affected in glucuronoxylomannan synthesis, differentially activate human dendritic cells. *FEMS Immunol Med Microbiol* 57(2):142-50.

28. Haugen RK & Baker RD (1954) The pulmonary lesions in cryptococcosis with special reference to subpleural nodules. *Am J Clin Pathol* 24(12):1381-90.

29. Decken K, *et al*. (1998) Interleukin-12 is essential for a protective Th1 response in mice infected with *Cryptococcus neoformans*. *Infect Immun.* 66(10):4994-5000.

30. Marks E, *et al*. (2017) Regulation of IL-12p40 by HIF controls Th1/Th17 responses to prevent mucosal inflammation. *Mucosal Immunol* 10(5):1224-36.

31. Lupo P, *et al*. (2008) The presence of capsule in *Cryptococcus neoformans* influences the gene expression profile in dendritic cells during interaction with the fungus. *Infect Immun* 76(4):1581-9.

32. Nielsen K, Cox GM, Wang P, Toffaletti DL, Perfect JR & Heitman J (2003) Sexual cycle of *Cryptococcus neoformans var. grubii* and virulence of congenic a and alpha isolates. *Infect Immun* 71:4831-4841.

33. Gish SR, *et al*. (2016) Computational analysis reveals a key regulator of Cryptococcal virulence and determinant of host response. *mBio* 7:e00313-00316.

34. Moyrand F & Janbon, G (2004) UGD1, encoding the *Cryptococcus neoformans* UDP-glucose dehydrogenase, is essential for growth at 37 degrees C and for capsule biosynthesis. *Eukaryot Cell* 3:1601-1608.

4.7 Figures

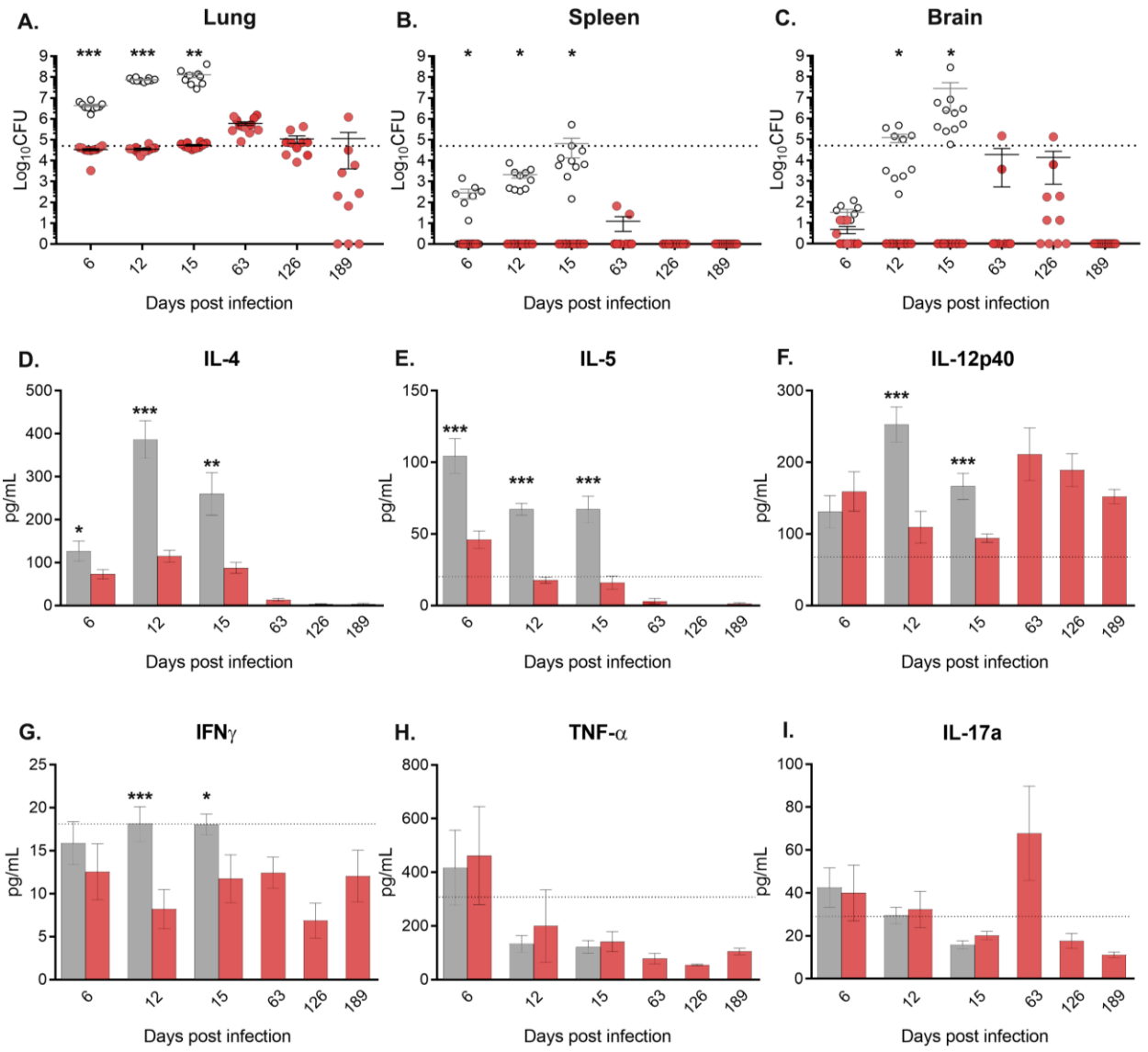

Figure 4.1. Fungal burden and cytokine responses in WT and *uxt1*Δ *uxt2*Δ mice. (A-C) Tissue homogenates of infected A/JCr mice were plated for CFUs at the indicated dpi (open circles, WT; red circles, *uxt1*Δ *uxt2*Δ; dashed line, initial inoculum). (D-I) Cytokines in lung homogenates at the indicated dpi (dashed line, naïve; gray bars, WT; red bars, *uxt1*Δ *uxt2*Δ). For all panels, data shown is for individual mice from two independent experiments (n = 5 per group per

experiment), plotted with the mean ± SEM. *, $p < 0.05$; **, $p < 0.01$; ***, $p < 0.005$ by Student's t-test comparing wild type to mutant.

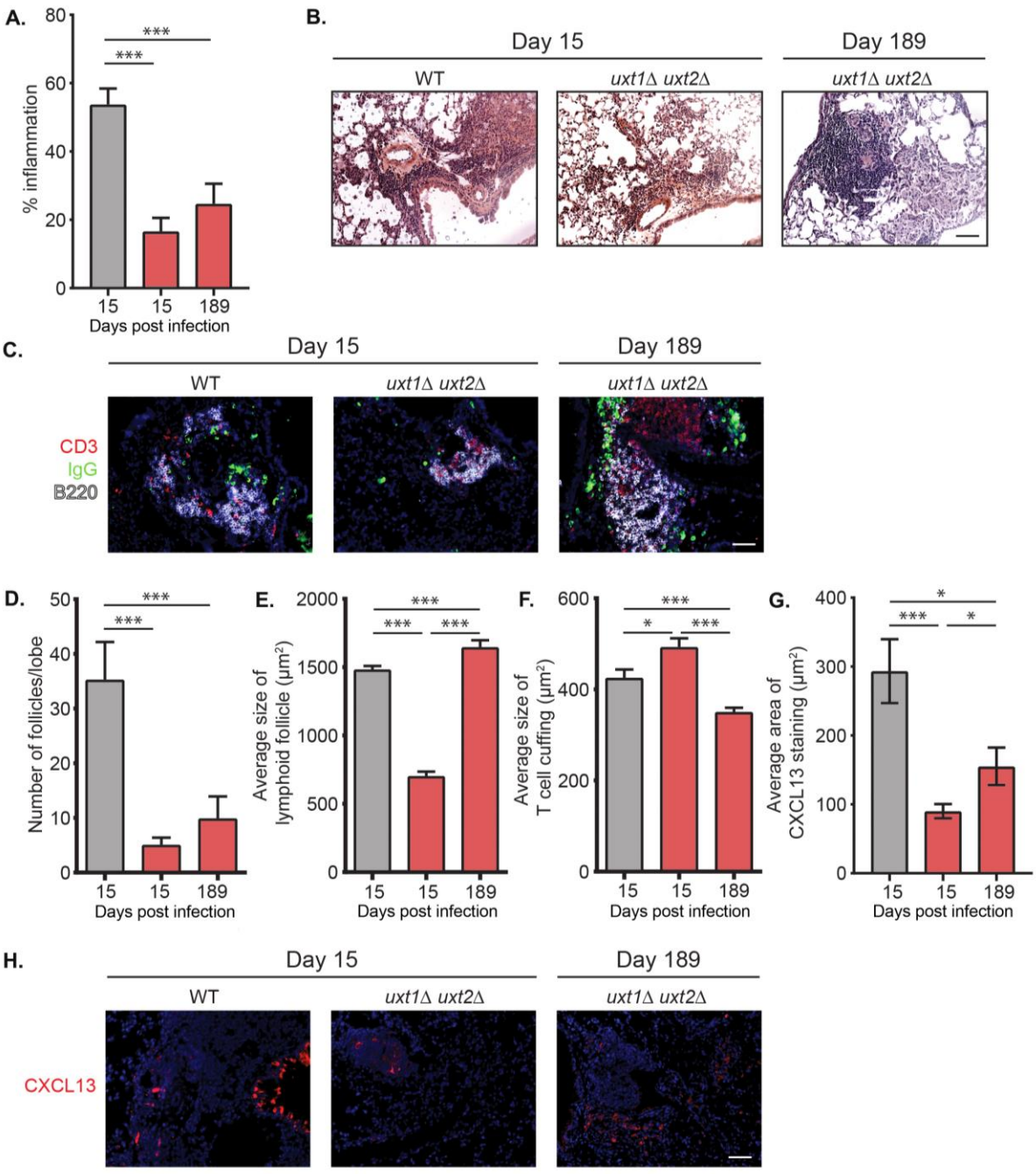

Figure 4.2. Inflammation and iBALT formation during *C. neoformans* infection. (A) Quantification of inflammation and (B) iBALT development during *C. neoformans* infection. Representative micrographs of H & E stained lung sections at 15 and 189 dpi are shown. Scale bar = 100 μm. (C) Immunofluorescent staining of B cells (B220+), T cells (CD3+), and plasma cells

(IgG+) in the lungs of infected A/JCr mice. Scale bar = 50 μm. (D-F) Quantification of iBALT structures in A/JCr mice infected with WT and *uxt1*Δ *uxt2*Δ. (G, H) Immunofluorescent staining and quantification of CXCL13 (red) expression; nuclei are stained with DAPI (blue). Scale bar = 50 μm. Plots show the mean ± SEM (n = 4-5; two independent experiments). *, $p < 0.05$; ***, $p < 0.005$ by Student's t-test.

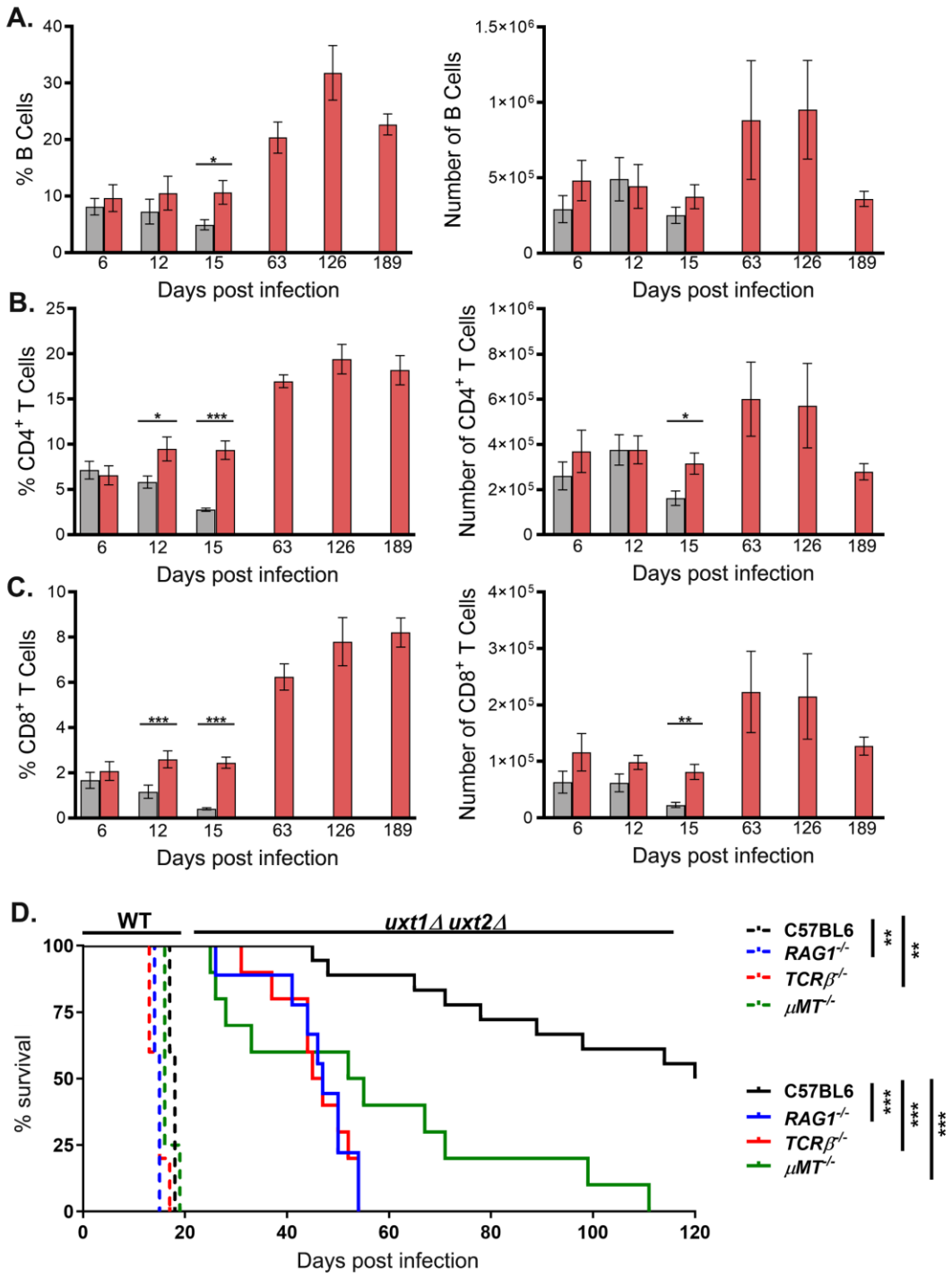

Figure 4.3. Increased T and B cell population in *uxt1*Δ *uxt2*Δ infection is required to prevent disease progression. (A) B cell, (B) CD4+ T cell, and (C) CD8+ T cell populations in the lungs of infected mice were quantified by flow analysis (gray, WT; red, *uxt1*Δ *uxt2*Δ). Data shown are

mean ± SEM of 10 mice from two independent experiments. *, $p < 0.05$; **, $p < 0.01$; ***, $p < 0.005$ by Student's t-test. (D) Survival of mice after intranasal inoculation with 5×10^4 cells of WT (n = 5) or *uxt1*Δ *uxt2*Δ (n = 10). Data shown are from two independent experiments. **, $p < 0.01$; ***, $p < 0.005$ by the log-rank test.

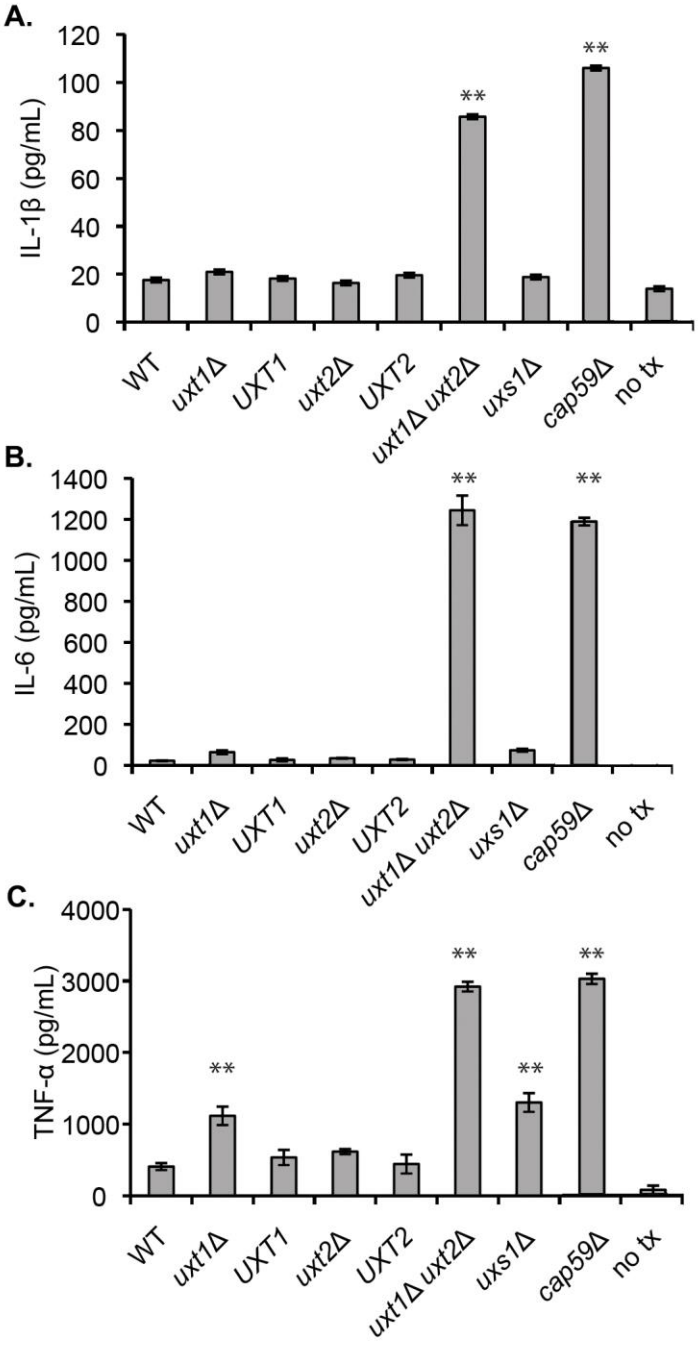

Figure 4.4. Cytokine production by dendritic cells. DCs were co-incubated for 24 h with heat-killed cells from the indicated strains. Levels of (B) IL-1β, (C) IL-6, and (D) TNF-α in the supernatant were then quantified by ELISA (no tx, no treatment). Data shown is the mean ± SD (n

= 3) of one representative experiment of five similar independent experiments. **, $p < 0.01$ by one-way ANOVA with Tukey's post hoc test.

4.8 Supplementary materials

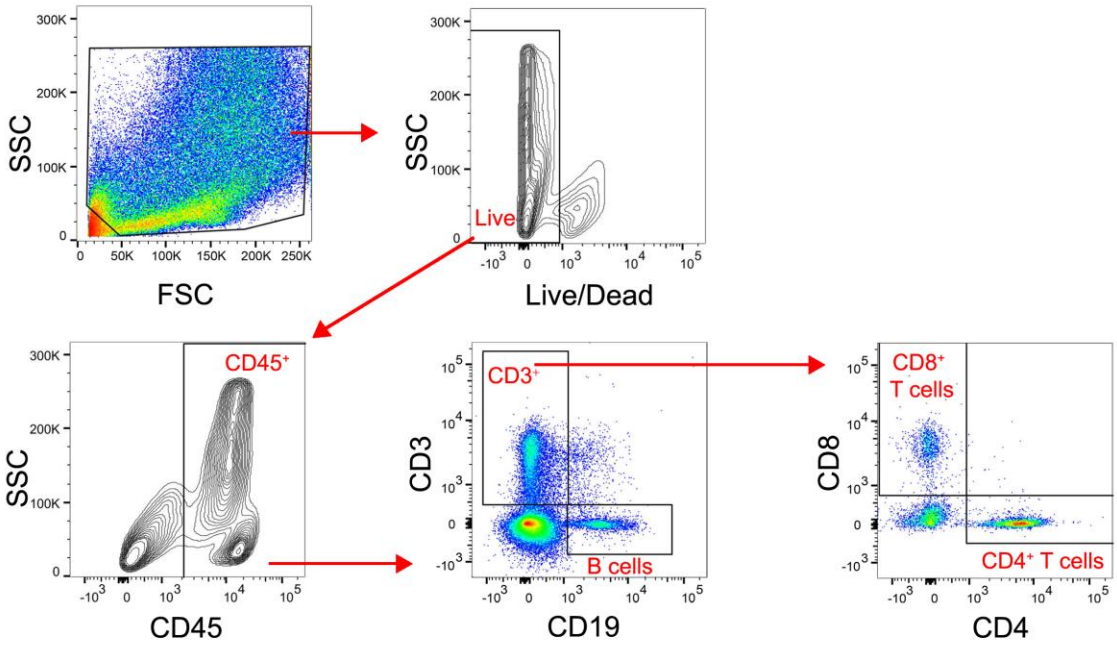

Figure S1. Representative data from the multi-color flow cytometry gating strategy used to quantify the indicated immune cell subsets.

Table 4.S1. *C. neoformans* strains utilized in these studies

C. neoformans strain[a]	Origin
KN99α	(32)
*uxt1*Δ	(21)
UXT1	(21)
*uxt2*Δ	(21)
UXT2	(21)
*uxt1*Δ *uxt2*Δ	(21)
*uxs1*Δ	(33)
*cap59*Δ	(34)

[a] All mutant strains are derived from KN99α

Table 4.S2. Flow analysis antibodies

Antigen	Clone	Fluorophore	Dilution	Company
CD3	17-A2	APC-Cy7	1:250	BioLegend
CD4	GK1.5	BUV737	1:500	BD Biosciences
CD8a	53-6.7	BV650	1:125	BD Biosciences
CD1/CD32 FC Block	2.4G2	(not applicable)	1:500	BD Biosciences
CD19	1D3	BV786	1:125	BD Biosciences
CD45	30-F11	Pacific Blue	1:250	BioLegend

Chapter 5:
Conclusions and future directions

5.1 Overview

Cryptococcus neoformans is an opportunistic fungal pathogen that infects over one million people and kills almost 200,000 individuals worldwide each year. Current treatments are inadequate with high rates of morbidity, mortality, and relapse following infection despite expensive and toxic antifungal interventions. Cryptococcal glycans are indispensable for an amazing diversity of basic metabolic functions, and are also crucial determinants of survival and pathogenesis, making them attractive therapeutic targets. Defining *C. neoformans* glycan biosynthetic pathways will allow us to potentially disrupt their function during the course of infection.

Synthesis of glycoconjugates requires activated donor molecules, which are generally made in the cytosol and then transported by NSTs into the ER and/or Golgi, where most glycosylation reactions occur. Glycan biosynthesis is thus completely dependent on the activity of these transporters to move select substrates across hydrophobic membrane barriers in exchange for nucleoside monophosphates. In prior work, GDP-Man transport was attributed to Gmt1 and Gmt2 (1, 2), and UDP-Gal appeared to be transported by Ugt1 (3). This did not, however, account for the donors of additional moieties such as GlcA and Xyl that are incorporated into the capsule. This major gap in our knowledge severely limited our understanding of and ability to manipulate critical biosynthetic processes in this important pathogen. My thesis project was designed to address this gap.

5.2 Summary of major findings

5.2.1 Uut1 is a UDP-glucuronic acid transporter

Uut1 (CNAG_06230) is an ER-localized UDP-GlcA transporter (Fig 2.2; Fig. 2.4). Unique among NSTs for its narrow substrate range and high affinity for UDP-GlcA (Fig. 2.4), it is also the sole transporter of this precursor in *C. neoformans.* UDP-GlcA transport by Uut1 was saturable with time and substrate concentration (Fig. 2.4), and had an apparent K_M of 0.6 ± 0.1 μM and V_{max} of 1.1 ± 0 mM s^{-1} (mean ± SEM of n = 4) with a turnover rate of 0.08 s^{-1}.

To investigate the physiological role of Uut1, we examined the *uut1* deletion mutant for changes in glycoconjugate composition. Although GlcA has only been detected in the side chains of capsule polysaccharides, loss of *UUT1* surprisingly abrogated capsule production and appeared to alter cell shape (Fig. 2.3). The cell membrane of the mutant also seemed to make irregular contact with the internal surface of the cell wall. The wall itself exhibited altered exposure of mannans (Fig. 2.S3) and lacked the distinct morphological layers (Fig. 2.7), which are normally present in WT cells (4-7). In addition to marked abnormalities in cell morphology, *uut1*Δ was highly susceptible to elevated temperature, nutrient limitation, and environmental stressors (Fig. 2.7 and Fig. 2.S5), phenotypes which were not rescued by heterologous expression of the human UDP-GlcA transporter, UGTrel7 (Fig. 2.S6). As a result of these defects, the deletion mutant was internalized and cleared by phagocytes more readily than wild-type cells (Fig. 2.8) and was completely avirulent in mice (Fig. 2.9).

Together these data indicate that Uut1 is a functionally significant UDP-GlcA-specific transporter and suggest that GlcA is a key modification of glycoconjugates beyond the capsule. It also

seems that the extension of capsule polymers requires GlcA modification, either directly (e.g. because it participates in recognition by glycosyltransferases) or indirectly (e.g. because it influences the localization or activity of glycoactive enzymes).

5.2.2 Uxt1 and Uxt2 are UDP-xylose/UDP-galactofuranose transporters

Uxt1 (CNAG_02036) and Uxt2 (CNAG_03695) are dual UDP-Xyl/UDP-Gal*f* transporters (Fig. 3.2, Fig. 3.S3). Although the two proteins share 57% amino acid identity (Fig. 3.S1A), Uxt1 displayed higher affinity and catalytic efficiency for UDP-Xyl (Fig. 3.2E-F) and exhibited stricter antiport substrate requirements (Fig. 3.2G). We also detected significant transport of UDP-Ara*p* and UDP-Ara*f* by both NSTs (Fig. 3.2D), but arabinose has never been reported in *C. neoformans* and is not detectable in our analyses, so we did not pursue this activity.

In addition to the differences in kinetic parameters, *UXT1* and *UXT2* demonstrated distinct patterns of expression (Fig. 3.3) and of localization (Fig. 3.4). These differences raised the question of whether Uxt1 and Uxt2 are functionally redundant *in vivo*. Deletion of *UXT1,* but not *UXT2,* markedly reduced the mole % of Xyl in capsule polysaccharides and in glycoproteins, although complete abrogation of Xyl incorporation into both glycoconjugates required the deletion of both genes (Fig. 3.1A). Uxt1 thus seems to be the major UDP-Xyl transporter, although there are still significant contributions by Uxt2.

Loss of UDP-Xyl transport lengthened mutant doubling time (Fig. 3.S4), altered capsule fiber morphology (Fig. 3.5C, Fig. 3.S5D), and reduced capsule size (Fig. 3.S5A) and GXM shedding (Fig. 3.S5C) with respect to WT. The mutants also exhibited increased sensitivity to high salt and

SDS (Fig. 3.5A). Together, these defects contributed to the increased phagocytosis and clearance of *uut1*Δ by host phagocytes *in vitro* (Fig. 3.6A-C). When inoculated into mice, the double mutant was avirulent (Fig. 3.6D) although mutant cells persisted in the lungs until the experiment was terminated at 100 dpi (Fig. 3.6E). These data (Chapter 3) support the critical importance of the UDP-Xyl transport mediated by Uxt1 and Uxt2.

5.2.3 *C. neoformans* xylose transport influences the host immune response

UDP-Xyl transport was required for cryptococcal virulence and dissemination. Although WT-infected mice succumbed by 15 dpi, *uxt1*Δ *uxt2*Δ-infected mice remained asymptomatic despite detectable pulmonary burdens (Fig. 4.1A). In these mice fungi were detected at distal sites only transiently, coinciding with the peaks in lung burden at day 63 and 126 dpi (Fig. 4.1A-C). By 189 dpi the mutant was cleared from 30% of the mice (Fig. 4.1A-C), which suggested that the remaining mice would eventually resolve the *uxt1*Δ *uxt2*Δ infection.

Early in infection, *uxt1*Δ *uxt2*Δ stimulated a more quiescent cytokine response with a milder Th2 cytokine skew than WT (Fig. 4.1D-I). When mutant burden peaked at day 63, there was a significant increase in the Th1/Th17 cytokine IL-12p40 as compared to naïve levels at day 63, and levels subsequently dropped with the fungal burden as the mice began to resolve the infection (Fig. 4.1F), although the level of inflammation was still lower than that in WT-infected mice (Fig. 4.2A). Infection with either strain, however, induced formation of lymphoid structures proximal to the basal side of the bronchial epithelium (Fig. 4.2B). These lymphoid aggregates were organized into a germinal center with a T cell cuff, consistent with inducible bronchus-associated lymphoid tissue (iBALT; Fig. 4.2C). The structures involved a smaller area and were

slower to form in *uxt1*Δ *uxt2*Δ-infected lungs as compared to WT-infection (Fig. 4.2D-G), which correlated with the overall lower fungal burden in the former.

In *uxt1*Δ *uxt2*Δ infection, but not WT, we observed a rise in the population of B (Fig. 4.3A) and T ($CD4^+$ and $CD8^+$; Fig. 4.3B-C) cells within the lung, with both cell populations required to control infection (Fig. 4.3D). During iBALT formation, T and B cell recruitment is triggered by antigen activation of and cytokine production by DCs (8). BMDCs co-incubated with *uxt1*Δ *uxt2*Δ, but not WT, released high levels of IL-1β (Fig. 4.4A), IL-6 (Fig. 4.4B), and TNF-α (Fig. 4.4C). These increases in cytokine production may have led to the greater T and B cell populations that we observed. This may also have caused functional differences that resulted in the reduced morbidity associated with *uxt1*Δ *uxt2*Δ infection although iBALT was induced by both strains.

5.3 Open questions

While the work presented in this thesis has advanced our understanding of nucleotide sugar transport in *C. neoformans*, there are still many questions about NSTs that remain unanswered. Below I explore several unresolved questions that arose during my study of Uut1, Uxt1, and Uxt2, and discuss possible approaches and outcomes.

5.3.1 Nucleotide sugar transporter structure and function relationship

There are no sequences known to confer specificity for a particular nucleotide sugar(s) although NSTs are able to discriminate between these activated donors. While a GDP-Man motif was proposed (9), Gmts have proven to be promiscuous GDP-sugar transporters (Fig. 3.S9). Domain

swaps between the CMP-sialic acid and UDP-Gal transporters have also only defined broad regions required for substrate recognition (10).

Since we have identified the substrates and kinetic parameters of Uut1 and the Uxts, we can now compare NSTs from multiple phyla that share their substrates, in conjunction with *in silico* analysis of nucleotide sugar and NST docking. The conserved residues that are predicted to interact favorably with the substrate(s) may provide the structural basis for substrate preferences and differences among NSTs, which could be validated by directed mutagenesis. Uut1 might be especially useful in these studies as it exhibits high affinity and specificity for UDP-GlcA despite sharing less than 20% identity with the *A. thaliana* and *H. sapiens* UDP-GlcA transporters. The UDP-Xyl transporters will also be an interesting tool for interrogating these question as they are ~60% identical at the amino acid level and recognize the same activated donors, but have non-identical kinetic parameters and nucleoside monophosphate requirements. They are also less than 20% identical to the *A. thaliana*, *H. sapiens*, and *A. fumigatus* transporters that share all or a subset of the same nucleotide sugar substrates.

5.3.2 Nucleotide sugar transporter regulation

Work by our lab and others has generated a network map of the complex interactions between cryptococcal transcription factors (TF) and their downstream targets, under conditions including capsule induction (11-13). Using these data we have examined the expression of the genes encoding predicted NSTs and made predictions of possible TFs interactions, but we have not systematically studied their regulation. Further examination of the upstream regions for TF binding sites will expand our knowledge of NST regulation and possible transcriptional coordination of

glycosylation machinery. This may help explain why *UXT2* was not upregulated to WT-levels in the absence of *UXT1*, and why the expression of *UXT1* was unresponsive to the loss of *UXT2* (Fig.3.S8).

Aside from this transcriptional regulation of NSTs, there are also likely mechanisms of post-translational control. Cryptococcal NSTs are notable for their unique long N-terminal domains. There are ~250 amino acids between the start codon of Uut1 and the beginning of the first transmembrane domain, and ~300 amino acids in the same region of Ugt1, in comparison to < 20 amino acid N-terminal cytosolic regions for comparable transporters in other systems. Uxt1 and Uxt2 have shorter N-termini (~50 amino acids), but they are still several times longer than those of the *A. thaliana* UDP-Xyl transporters. The Ugt1 N-terminus was not absolutely required for substrate recognition and transport (3), but it may modulate the efficiency of those processes or additional downstream glycosylation reaction(s); the requirement for this domain has not yet been tested for any other cryptococcal NSTs.

The solvent-exposed regions of the NSTs might impact downstream glycosylation reaction(s) by mediating interactions with capsule-associated glycosyltransferases to efficiently channel substrates into the luminal compartment, influencing oligomerization-based regulation, or modulating binding of regulatory proteins. Distinct complexes of glycoactive enzymes may be recruited depending on environmental cues, for example preferential association with capsule-specific glycosyltransferases under capsule-inducing conditions. These differences might explain the poor ability of human NSTs that share the same *in vitro* transport activity to complement cryptococcal NST mutants. We can directly interrogate this hypothesis by expressing chimeric fusion

proteins that include these regions. This approach may furthermore offer insights into the functional differences between Uxt1 and Uxt2 since the majority of their divergent residues reside prior to the second transmembrane domain. We can potentially distinguish the contributions of these innate enzymatic properties (Fig. 3.2) from the distinct expression patterns (Fig. 3.3) by placing Uxt1 and Uxt2 (and the fusions constructs) under the reciprocal promoters. Future work addressing the role(s) of particular regions in cryptococcal NSTs might also include interrogating protein interactions with these domains by co-immunoprecipitation with mass spectrometry analysis; being sure to validate any detected interactions with complementary approaches including more quantitative ones.

5.3.3 Additional nucleotide sugar transporter candidates

Alongside *UUT1* and the *UXT*s, we identified four other genes encoding putative NSTs (G, J, L, and X) in our initial analysis of the cryptococcal genome. I examined their contribution to survival and pathogenesis, and also made significant efforts to ascertain their biochemical function (described in Appendix B). None of them, however, transported any of the 16 nucleotide sugars assayed (as in Fig. 2.4; Joshua Heazlewood, personal communication), and none of the corresponding mutants had detectable changes in GXM composition (Table B.1, Table B.2) although $nst_G\Delta$ and $nst_X\Delta$ produced smaller capsules than WT cells (Fig. B.1).

These four proteins may not be NSTs but may instead transport molecules that are structurally similar to nucleotide sugars. NST_G, for example, clades with triose phosphate transporters. We may be able to adapt our *in vitro* transport assay to test a broad range of sugar phosphates. Alternatively, we could determine the ability of these NST candidates to complement cell lines defi-

cient for known transporters. We are particularly interested in identifying the substrates of NST_G, NST_L, and NST_X, since the loss of the corresponding genes reduced or completely abolished cryptococcal virulence (Fig. B.4, Fig. B.9).

5.3.4 Glycan repertoire of *C. neoformans*

Compositional analysis of glycans in *C. neoformans* has elucidated the monosaccharide components of each class of cryptococcal glycoconjugate. The crude preparations utilized in these studies, however, may overlook minor, but critical, sugars. We furthermore lack information about the glycans decorating specific proteins or lipids.

The pleiotropic effects of deleting *UUT1* suggested that GlcA is incorporated into structures other than the capsule, although that is the only *C. neoformans* glycoconjugate reported to contain GlcA. It may be that the GlcA content in other glycans is below the limit of detection, while still being functionally significant. Prior glycoprotein profiling efforts have utilized lower-resolution HPLC studies or MALDI-TOF analyses that obtained multiple unassigned peaks (14, 15). Additional studies with MALDI-TOF may prove more fruitful if aided by comparison of WT glycoprotein (examining *N*- and *O*-linked glycans separately) or glycolipid profiles to those of *uut1*Δ and *uxt1*Δ *uxt2*Δ. Our previous work provides precedent for using mutants with Xyl-deficient capsule polysaccharides to assist with structural analysis (16, 17).

We can also identify and characterize cryptococcal glucuronyltransferases for evidence of GlcA in non-capsule glycans; no enzyme of this type is known in *C. neoformans* to date. For example, the presence of transferases specific for GlcA linkages other than β1,2 and β1,4 (normally found

in GXM and GXMGal), might suggest that polysaccharides other than capsule incorporate GlcA. This would have the added benefit of expanding our understanding of the cryptococcal glycosyltransferase repertoire, of which only two xylosyltransferases have been elucidated. These efforts might also help to link the *uut1*Δ stress and growth phenotypes to specific glycoproteins and glycolipid defects.

Glycosylation could also potentially occur in additional contexts (e.g. the cytosol). Exposure to cells with perturbed UDP-Xyl synthesis (*uxs1*Δ) and UDP-Xyl transport (*uxt1*Δ *uxt2*Δ), for example, clearly leads to distinct cytokine responses in dendritic cells. This difference between cells that totally lack UDP-Xyl and those that have it only in the cytosol suggests that either Uxs1 has synthesis-independent functions or that UDP-Xyl is utilized within the cytosol (i.e. directly donating Xyl to a nascent cellular component or being further modified). The downstream product of this cytosolic process is then immunogenic in the absence of luminal xylosylation. Further detailed characterization of glycoconjugates in *ugd1*Δ and *uxs1*Δ alongside the aforementioned transporter mutants may help identify the responsible cellular component(s).

5.4 Impact and closing remarks

At the outset of my thesis work, we had a good understanding of nucleotide sugar metabolism, but knew little about how these critical precursors traffic within the cell. GDP-Man transport was attributed to Gmt1 and Gmt2, and there was only circumstantial evidence that Ugt1 transported UDP-Gal (1, 2, 18). There were no proteins identified that could transport precursors of additional moieties such as GlcA, Xyl, or potentially sialic acid that are incorporated into the capsule.

Through my thesis work, I have doubled the number of known transporters and characterized an equal number of putative NST candidates. I determined that Uut1 is a highly specific, high affinity UDP-GlcA transporter, and obtained evidence that GlcA is incorporated into structures other than capsule. I also showed that Uxt1 and Uxt2 are UDP-Xyl/UDP-Gal*f* transporters with only partial functional redundancy, exhibiting distinct localization and expression patterns, and kinetic profiles. Finally, I established that Ugt1 is actually a dual UDP-Gal/UDP-GalNAc transporter using a biochemical approach (3). Importantly, all of these transporters play key roles in cryptococcal survival and pathogenesis.

We have now defined a transporter for the activated donor of every monosaccharide reported in cryptococcal glycoconjugates made in the secretory pathway of *C. neoformans*, including its major virulence factor, and assigned activity to four proteins of previously unknown function. This work has advanced our understanding of the localization and sequence of glycan biosynthetic events, which have not been fully characterized in *C. neoformans*. These data have also expanded our knowledge of NSTs as a protein family, enabling comparisons across phyla, which will set the stage for future mechanistic and phylogenetic studies. Together these studies furthered our efforts to completely describe the cellular machinery that assembles the glycan-rich surfaces of *C. neoformans*, and to determine how these components are involved in interactions with and modulation of host immunity. Unique features of the essential fungal NSTs identified in this work and from future efforts have the potential to be exploited for novel therapies.

5.5 References

1. Wang ZA, *et al.* (2014) *Cryptococcus neoformans* dual GDP-mannose transporters and their role in biology and virulence. *Eukaryot Cell* 13(6):832-842.

2. Cottrell TR, Griffith CL, Liu H, Nenninger AA, & Doering TL (2007) The pathogenic fungus *Cryptococcus neoformans* expresses two functional GDP-mannose transporters with distinct expression patterns and roles in capsule synthesis. *Eukaryot Cell* 6(5):776-785.

3. Li LX, *et al.* (2017) *Cryptococcus neoformans UGT1* encodes a UDP-Galactose/UDP-GalNAc transporter. *Glycobiology* 27(1):87-98.

4. Reese AJ & Doering TL (2003) Cell wall alpha-1,3-glucan is required to anchor the *Cryptococcus neoformans* capsule. *Mol Microbiol* 50(4):1401-1409.

5. Doering TL (2009) How sweet it is! Cell wall biogenesis and polysaccharide capsule formation in *Cryptococcus neoformans*. *Annu Rev Microbiol* 63:223-247.

6. Gilbert NM, Lodge JK, & Specht CA (2011) The Cell Wall of *Cryptococcus*. *Cryptococcus From Human Pathogen to Model Yeast*, eds Heitman J, Kozel TR, Kwon-Chung KJ, Perfect J, & Casadevall A (ASM Press, Washington), pp 67-79.

7. Santiago-Tirado FH, Peng T, Yang M, Hang HC, & Doering TL (2015) A Single Protein S-acyl Transferase Acts through Diverse Substrates to Determine Cryptococcal Morphology, Stress Tolerance, and Pathogenic Outcome. *PLoS Pathog* 11(5):e1004908.

8. Hwang JY, Randall TD, & Silva-Sanchez A (2016) Inducible Bronchus-Associated Lymphoid Tissue: Taming Inflammation in the Lung. *Front Immunol* 7:258.

9. Gao XD, Nishikawa A, & Dean N (2001) Identification of a conserved motif in the yeast golgi GDP-mannose transporter required for binding to nucleotide sugar. *J Biol Chem* 276(6):4424-4432.

10. Aoki K, Ishida N, & Kawakita M (2001) Substrate recognition by UDP-galactose and CMP-sialic acid transporters. Different sets of transmembrane helices are utilized for the specific recognition of UDP-galactose and CMP-sialic acid. *J Biol Chem* 276(24):21555-21561.

11. Gish SR, *et al.* (2016) Computational analysis reveals a key regulator of Cryptococcal virulence and determinant of host response. *MBio* 7(2):e00313-00316.

12. Maier EJ, *et al.* (2015) Model-driven mapping of transcriptional networks reveals the circuitry and dynamics of virulence regulation. *Genome Res* 25(5):690-700.

13. Haynes BC, *et al.* (2011) Toward an integrated model of capsule regulation in *Cryptococcus neoformans*. *PLoS Pathog* 7(12):e1002411.

14. Lee DJ, Bahn YS, Kim HJ, Chung SY, & Kang HA (2015) Unraveling the novel structure and biosynthetic pathway of O-linked glycans in the Golgi apparatus of the human pathogenic yeast *Cryptococcus neoformans*. *J Biol Chem* 290(3):1861-1873.

15. Park JN, *et al.* (2012) Unraveling unique structure and biosynthesis pathway of N-linked glycans in human fungal pathogen *Cryptococcus neoformans* by glycomics analysis. *J Biol Chem* 287(23):19501-19515.

16. Heiss C, *et al.* (2013) Unusual galactofuranose modification of a capsule polysaccharide in the pathogenic yeast *Cryptococcus neoformans*. *J Biol Chem* 288(16):10994-11003.

17. Previato JO, *et al.* (2017) Distribution of the O-acetyl groups and beta-galactofuranose units in galactoxylomannans of the opportunistic fungus *Cryptococcus neoformans*. *Glycobiology* 27(6):582-592.

18. Moyrand F, Fontaine T, & Janbon G (2007) Systematic capsule gene disruption reveals the central role of galactose metabolism on *Cryptococcus neoformans* virulence. *Mol Microbiol* 64(3):771-781.

Appendix A:
Cryptococcus neoformans UGT1 encodes a UDP-galactose/UDP-GalNAc transporter

From:

Cryptococcus neoformans UGT1 encodes a UDP-galactose/UDP-GalNAc transporter

Lucy X. Li, Angel Ashikov, Hong Liu, Cara L. Griffith, Hans Bakker, and Tamara L. Doering

Glycobiology 2017 Jan 1; 27(1) 87–98 doi: 10.1093/glycob/cww078

Abstract

Cryptococcus neoformans, an opportunistic fungal pathogen, produces a glycan capsule to evade the immune system during infection. This definitive virulence factor is composed mainly of complex polysaccharides, which are made in the secretory pathway by reactions that utilize activated nucleotide sugar precursors. Although the pathways that synthesize these precursors are known, the identity and regulation of the nucleotide sugar transporters (NSTs) responsible for importing them into luminal organelles remain elusive. The UDP-galactose transporter, Ugt1, was initially identified by homology to known UGTs and glycan composition analysis of *ugt1*Δ mutants. However, sequence is an unreliable predictor of NST substrate specificity, cells may express multiple NSTs with overlapping specificities, and NSTs may transport multiple substrates. Determining NST activity thus requires biochemical demonstration of function. We showed that Ugt1 transports both UDP-galactose and UDP-N-acetylgalactosamine *in vitro*. Deletion of *UGT1* resulted in growth and mating defects along with altered capsule and cellular morphology. The mutant was also phagocytosed more readily by macrophages than wild-type cells and cleared more quickly *in vivo* and *in vitro*, suggesting a mechanism for the lack of virulence observed in mouse models of infection.

Introduction

Cryptococcus neoformans is an opportunistic fungal pathogen that is ubiquitous in the environment. It infects over a million people worldwide each year and kills over 600,000 of them, disproportionately affecting resource-limited areas (1). Cryptococcosis is initially acquired by inhalation of fungal cells or spores into the lower respiratory tract (2). This leads to a primary pulmonary infection, which is normally controlled by alveolar macrophages. In immunocompromised individuals, however, fungi can proliferate and disseminate throughout the host, with a particular tropism for the brain.

The principal virulence factor of *C. neoformans* is a polysaccharide capsule, which helps it evade the host immune response. This structure surrounds the yeast cell wall, which as in other fungi is made of glucans, chitin, and mannoproteins (3). The capsule is composed of two polysaccharides, glucuronoxylomannan (GXM) and glucuronoxylomannogalactan (GXMGal), with trace amounts of mannoproteins (4). These polymers, which are synthesized intracellularly (5), become associated with the outer surface of the cryptococcal cell wall (6), forming a protective layer that impedes phagocytosis and immune mediator binding (7). This structure is highly responsive to environmental conditions, becoming particularly large during infection of mammalian hosts (3). Capsule polysaccharides are also continually shed from the yeast, and act in suppression of the host immune response (7). Understanding the pathways that produce the capsule and other essential glycoconjugates is central to developing strategies to effectively disrupt their function and combat this lethal pathogen.

GXM typically constitutes ~90% of the capsule mass (3). It is a repeating polymer, made up of a mannose backbone with glucuronic acid (GlcA) and xylose (Xyl) side chains (8) (all sugars are pyranose forms unless otherwise indicated). GXMGal, which makes up the remaining 10% of the capsule mass, consists of a galactan backbone modified with galactomannan side chains bearing a variable number of Xyl and GlcA residues (9); the backbone may also be modified with single galactofuranose (Gal*f*) residues (10). Mutants lacking either or both capsular polysaccharides are avirulent (11, 12).

C. neoformans dedicates a significant portion of its genetic machinery and metabolic energy to synthesizing capsule and other cellular glycoconjugates, including protein-linked glycans (13-15), cell wall components (6, 16-19), and glycolipids (20-23). These compounds are essential for maintaining cellular homeostasis and establishing infection. Synthesis of many glycoconjugates relies on activated donor molecules, such as nucleotide sugars, from which individual sugar moieties are transferred to a growing glycan structure. Nucleotide sugars are generally made in the cytosol and then transported into the secretory organelles (endoplasmic reticulum and/or Golgi apparatus) where most glycan biosynthesis occurs (24). Nucleotide sugar transporters (NSTs) mediate transport of these highly charged compounds by importing them in exchange for the corresponding nucleotide monophosphates via an antiport mechanism (25, 26). This makes the nucleotide sugars available for use by the luminal glycosyltransferase enzymes that synthesize capsule polymers or other glycans.

The capsule polysaccharides are composed of galactose (Gal), Gal*f*, GlcA, Man, and Xyl; this suggests that their synthesis requires the corresponding donors, which are UDP-Gal, UDP-Gal*f*,

UDP-GlcA, GDP-Man, and UDP-Xyl. The enzymatic pathways required for synthesis of these compounds in *C. neoformans* have been elucidated (27-32), but the identity and regulation of most of the NSTs that translocate them into the secretory pathway remain elusive. Only transport of the mannose donor, GDP-mannose, has been demonstrated biochemically (33).

Strains deficient in UDP-Gal synthesis have aberrant capsule, likely due to perturbed GXMGal production, and are completely avirulent, emphasizing the critical role of this nucleotide sugar (32). A UDP-Gal transporter, Ugt1, was initially identified by homology to known UDP-Gal transporters (12), which are found ubiquitously in eukaryotes. However, sequence identity does not tell the whole story of NST substrate specificity (34). For example, cells may express several NSTs with overlapping specificities but non-identical substrate affinities. Some transporters are highly selective for a specific substrate, while others transport as many as four distinct nucleotide sugars (35-41). Finally, transport activity may also be influenced by association with glycan synthetic enzymes and by subcellular localization (42). Although the absence of galactose in total capsular polysaccharide and whole cell preparations from *ugt1*Δ mutants (12) provides indirect evidence that UDP-galactose is a Ugt1 substrate, defining NST activity requires biochemical demonstration of function.

Here we directly interrogated the biochemical activity of Ugt1, motivated by the central role of galactose in cryptococcal virulence and the gaps in our knowledge of *C. neoformans* NSTs (12). We found that Ugt1 transports both UDP-Gal and UDP-N-acetylgalactosamine (GalNAc) *in vitro* and that this function does not depend on the extended cytosolic termini of the protein. Furthermore, cells lacking Ugt1 exhibit growth and mating defects, along with altered capsule and

cellular morphology. Finally, the mutant was phagocytosed more readily by macrophages and cleared more quickly *in vivo* and *in vitro*. Our studies define the biochemical role of this important protein and suggest mechanisms for the reduced virulence of cells lacking this transporter.

Results

C. neoformans strains are classified into four serotypes: A and D are associated with cryptococcosis in immunocompromised populations, while B and C are associated with disease in otherwise healthy individuals. We initially identified *UGT1* in serotype A, which is the most prevalent serotype and causes most of the mortality from this disease (43), and subsequently identified homologs with 92-95% identity at the protein level in the other serotypes (protein accession numbers XP_012048733, KIR46271, KIR59644, and XP_568024 for serotypes A through D, respectively). Phylogenetic analysis of the serotype D *UGT1* sequence together with characterized human NSTs places Ugt1 in the SLC35A subfamily, along with its human counterpart (Fig. A.1). Similar to other transporters, it is predicted to have an even number of transmembrane domains (here ten) with cytosolic N- and C- termini (Fig. A.2). The predicted cytosolic termini are unique and unusually long (Fig. A.2), at least five times longer than those of other known UDP-Gal transporters with no significant sequence similarity (not shown). The NST domain of Ugt1 (aa 299-558) also shares less than 50% identity to those proteins (Fig. A.S1).

We next investigated Ugt1 localization by comparing staining of episomally expressed Ugt1-HA to that of a known Golgi xylosyltransferase, Cxt1p, which we have tagged with myc (14). When we probed doubly-tagged cryptococci with both anti-HA and anti-myc antibodies, we observed

co-staining of large perinuclear puncta, suggesting Golgi localization of Ugt1 (Fig. A.S2). This localization is consistent with a role for this protein in providing raw materials for glycan synthesis to processes occurring in the secretory pathway. Because the inherent challenges of immunostaining this yeast limit image quality, we also localized HA-tagged human and cryptococcal Ugt1 in MDCKII cells. In this higher resolution analysis both proteins colocalized with the Golgi marker giantin (Fig. A.3A), supporting our *C. neoformans* results.

The mammalian Lec8 cell line is deficient in UDP-Gal transport (44, 45). We used transient transfection to assess whether the cryptococcal transporter could complement this defect, using *Griffonia simplicifolia* lectin (GSII) as a reporter. This lectin binds terminal GlcNAc residues, which are masked in normal cells by galactose added in the secretory pathway. In cells lacking UDP-Gal transport this galactose modification is absent, so the lectin is able to bind to the cell surfaces. Expression of cryptococcal Ugt1 reversed this binding (Fig. A.3B). Notably, the subset of transiently transfected cells that did not express exogenous protein still bound the lectin (Fig. A.3B), serving as an internal control. This staining pattern was mirrored by expression of the human UDP-Gal transporter, strongly supporting shared biochemical activity of the two proteins.

To directly measure the activity of the cryptococcal transporter we used heterologous expression in *S. cerevisiae*. When we assessed the transport of a panel of radiolabeled nucleotide sugars *in vitro*, Golgi vesicles from cells expressing cryptococcal Ugt1 demonstrated transport of UDP-Gal, as predicted by homology, as well as somewhat lower transport of UDP-GalNAc (Fig. A.4). We did not detect transport over background of other capsule precursors (UDP-Xyl or UDP-GlcA), UDP-GlcNAc, or UDP-Glc.

We had noted the unusual length of the N- and C-terminal cytosolic tails of Ugt1 and wondered whether they were required for its transport activity. To test this we used transient transfection to determine which of a series of Ugt1 truncation variants (Fig. A.2) could complement the deficient UDP-Gal transport of CHOP8 cells, which are derived from Lec8 cells (see Materials and methods). We detected activity by co-transfection with DNA encoding a rat β 1,3-glucuronyltransferase, such that the combination could support the synthesis of GlcUAβ1,3Gal epitopes; these are recognized by the antibody L2-412 (46, 47). As shown in Table A.3, all of the cytosolic tail truncations that we tested (Fig. A.2) retained activity; function was only disrupted when the truncation was extended beyond the first transmembrane domain.

Because galactose is a major component of one capsule polysaccharide, GXMGal, we examined the expression of *UGT1* and other genes related to galactose metabolism under growth conditions that induce capsule synthesis. RNA-seq analysis indicated that both *UGT1* and *UGE1*, a gene encoding a UDP-glucose epimerase (which catalyzes the interconversion of UDP-glucose and UDP-Gal), are upregulated several fold under these conditions (Fig. A.5), consistent with a role for both proteins in capsule synthesis. A *UGE1* paralog, *UGE2*, remains at basal levels during capsule induction (Fig. A.5); the corresponding mutant also has no defects in capsule synthesis or virulence (32). Other genes involved in UDP-Gal metabolism (galactokinase and galactose-1-phosphate uridylyltransferase) showed no change or less two-fold reduction in expression over the same time course of induction (data not shown).

We next directly examined the effect of deleting *UGT1* on capsule morphology. When we grew cells in non capsule-inducing conditions (the rich yeast medium YPD), both wild-type and mu-

tant cells had thin capsules, which were minimally discernible by negative staining (Fig. A.6A, first column). Capsules of both strains were also similarly enlarged when the cells were grown in our standard capsule-inducing conditions (DMEM at 37°C and 5% CO_2; Fig. A.6A, second column), which were also used for the expression profiling above. Because serotype A cells lacking *UGT1* had previously been reported to be hypercapsular (12), which we did not observe in the DMEM conditions, we tested other inducing media. We found that *ugt1*Δ cells grown in 10% Sabouraud's media were hypercapsular compared to wild-type cells (Fig. A.6A, third column). The capsule fibers of mutant cells grown in this medium were also markedly longer by electron microscopy (Fig. A.6A fourth column); these phenotypes were reversed by complementation of the mutant. In all conditions, the mutant cells tended to aggregate, which suggested altered surface properties independent of capsule formation.

Cryptococcal glycans have not been exhaustively analyzed, but galactose is a known component of cryptococcal glycolipids (48) and capsule polysaccharides, and may occur in other glycoconjugates as well. For this reason we tested other characteristics of cells lacking Ugt1. We noted that *ugt1*Δ cells were significantly more sensitive than wild type to Congo Red dye, suggesting a cell wall defect (Fig. 6B). This strain was also sensitive to H_2O_2 (Fig. A.6B), in addition to high temperature and SDS (properties previously reported for the corresponding serotype A mutant (12), which we verified for serotype D (not shown)). The mutant cells were also defective in mating, failing to form filaments and spores when co-cultured on solid media with cells of the opposite mating type (Fig. A.6C). In all cases the wild-type phenotypes were restored in the complemented mutant.

We wondered whether the extended termini of Ugt1, which were not required for transport activity (Table A.3), might influence cell phenotypes. To test this, we episomally complemented *ugt1*Δ with wild type *UGT1*, or *UGT1* modified so its product lacked either the N- or C-terminus, all under control of the constitutive actin promoter. All three construct-expressing strains restored wild-type resistance to stress but also exhibited larger capsules than wild-type cells. Interestingly, the full length and C-terminally truncated *UGT1* produced considerably larger capsules than wild-type cells (1.8- and 1.6-fold greater than WT, respectively; Fig. A.7A). They also demonstrated greater growth on NaCl but not on any of the other conditions tested (Fig. A.7B) (see Discussion).

The observed changes in surface properties and reduced ability to resist stress of the mutant strongly suggested that its interactions with host cells would be aberrant. To test this, we first used an automated high throughput imaging method (49) to quantify the early interactions between a human monocytic cell line (THP-1) and each strain. As in previous work, unopsonized fungi were poorly phagocytosed. For opsonized samples, we found that when the yeast had been cultured in rich medium (YPD or Sabouraud's broth), *ugt1*Δ was engulfed at significantly higher rates than wild type (Fig. A.8A). This was independent of capsule size, as wild-type and mutant cells both produce minimal capsule in YPD (Fig. A.6A). In contrast, after culturing in conditions where wild type and mutant displayed equally large capsules (Fig. A.6A, DMEM), phagocytosis of all strains was similar (Fig. A.8A). We also tested the relative survival of internalized fungi during a 24-hour period. We found that the mutant cell population increased more slowly than wild-type or complemented strains within host phagocytes, reflecting poor growth and/or increased destruction by the host cells (Fig. A.8B).

The combination of defects we observed in *ugt1*Δ suggested that this strain would do poorly in an infected host, as previously observed in a model based on tail vein infection (12). We tested this in mice infected intranasally, which mimics the natural route of infection. In this model *ugt1*Δ was completely cleared from the lungs by 7 days after inoculation, in contrast to wild type and complement infected mice (average $\log_{10}$CFU/mL at 7dpi: WT, 2.76; *ugt1*Δ, 0; *UGT1*, 2.33). This rapid clearance of the mutant supports the key role of Ugt1 in cryptococcal biology.

Discussion

C. neoformans encodes a single functional UDP-Gal/UDP-GalNAc transporter, which is homologous to UGTs found across multiple phyla (e.g. *H. sapiens*, C. *elegans*, *S. pombe, A. thaliana*; Fig. A.S1). This protein is predicted to have ten transmembrane segments with N- and C-terminal tails in the cytosol (Fig. A.2) and is localized to the Golgi apparatus (Fig. A.3A, Fig. A.S2), consistent with other transporters in this family. Alignment of Ugt1 and known transporters, however, did not reveal any common motif that would potentially confer UDP-Gal or UDP-GalNAc specificity (Fig. A.S1).

We demonstrated that cryptococcal Ugt1 transports UDP-Gal both indirectly, through complementation of Lec8 cells (Fig. A.3B), and directly, by performing transport assays in a heterologous system (Fig. A.4). Of the other potential substrates tested (Fig. A.4), we only observed transport of UDP-GalNAc. Human and *Drosophila* UGTs similarly recognize this combination of substrates, although only the human and cryptococcal UGTs transport UDP-Gal more efficiently than UDP-GalNAc (Fig. A.4 and ref (37)). Galactose is an abundant component of cryptococcal capsule and is also known to be incorporated into some of its glycolipids. GalNAc, in

contrast, has not been detected in any cryptococcal glycans to date, but this does not preclude the possibility that small amounts are incorporated into these structures, particularly as the synthetic machinery for UDP-GalNAc is encoded in the cryptococcal genome.

Specific recognition of multiple substrates with the same nucleotide portion is common among NSTs, with the nucleotide binding specificity mediated by the cytosolic domains (25). The cryptococcal Ugt1 is noteworthy for having unusually long cytosolic tails, which stimulated us to pursue their function. The first transmembrane helix of human SLC35A2 is required for UDP-Gal transport (50); we similarly found that the first transmembrane domain of the cryptococcal protein was needed for transport in mammalian cells, although both cytosolic tails were dispensable (Fig. A.2 and Table A.3). In *C. neoformans*, episomal expression of *Ugt1* truncations that spared the transmembrane domains also restored wild-type capsule and stress resistance to *ugt1*Δ (Fig. A.7), supporting the dispensability of the cytosolic domains for transport activity. Notably, constitutive episomal expression of full length Ugt1 (or the C-terminal truncation) yielded capsules that were larger than those of wild-type cells (Fig. A.7A) and appeared to confer an increased salt tolerance (Fig. A.7B). One potential explanation of these findings is that Ugt1 overexpression impacts the quantity or composition and structure of cellular glycoconjugates, perhaps through greater incorporation of galactose, producing larger capsules and modulating stress resistance pathways. The inability of N-terminal mutants to produce capsules as large as mutants expressing full length and C-terminal Ugt1 thus suggests that, while the N-terminus is not absolutely required for substrate recognition and transport, it may modulate the efficiency of those processes or additional downstream glycosylation reaction(s). The N-terminus of Ugt1 might impact these processes by mediating interactions with capsule-associated glycosyltransferases,

influencing oligomerization-based regulation, or regulating binding of regulatory proteins (51). It will be of interest in the future to further elucidate the role of these domains.

When we examined the transcriptional profile of *C. neoformans* under conditions that induce capsule production, and thus presumably UDP-Gal utilization, we observed that *UGT1* and *UGE1* expression are significantly upregulated within 8 hours (Fig. A.5). Other genes implicated in galactose metabolism demonstrated less than a two-fold change in either direction, perhaps not surprising since strains were grown with glucose as the primary carbon source. *C. neoformans* thus seems to satisfy the greater demand for UDP-Gal imposed under inducing conditions by increasing UDP-Gal synthesis in conjunction with transport into the proper luminal compartment.

Once UDP-Gal is translocated into the secretory pathway, the galactose moiety is incorporated into glycoconjugates made in that compartment. These probably include GXMGal, as we previously localized a glycosyltransferase required for GXMGal synthesis to the Golgi compartment (52, 53). Consistent with this finding, GXMGal synthesis is completely abrogated in cells lacking *UGT1* (12). Paradoxically, capsules of cells lacking *UGT1* are enlarged (Fig. A.6A), consistent with prior reports (12). It may be that GXMGal normally participates in capsule polysaccharide organization, so that its absence yields a looser, and therefore more voluminous, structure. Defects in protein glycosylation may also indirectly cause changes in capsule synthesis, for example via altered enzyme activity or stability.

It is notable that depending on the induction conditions *ugt1*Δ exhibits two distinct capsule phenotypes, being normocapsular in DMEM medium but hypercapsular relative to wild type in di-

lute Sabouraud's broth (Fig. A.6A). Multiple signaling pathways trigger capsule production in response to distinct environmental or chemical conditions, and we are just beginning to understand the complex interplay between them (54-56). *C. neoformans*, furthermore, is a facultative intracellular pathogen that occupies multiple sub-environments within the host, including the nutrient-limited intracellular and blood stream niches, which we model *in vitro* with 10% Sabouraud and DMEM, respectively. Capsule thickness is known to vary between organs in infected hosts (57, 58); our distinct culture conditions may be similarly inducing changes in both size and organization.

The alterations observed in *ugt1*Δ cells were not isolated to capsule synthesis. Mutant cells have a propensity to aggregate (Fig. A.6A); they are also more sensitive to cell wall perturbing reagents (Congo Red, SDS) and less able to tolerate environmental stresses (temperature, H_2O_2) (Fig. A.6) than wild type (12). These phenotypes suggest defects in cell wall synthesis, again potentially due directly to alterations in component glycans or indirectly due to underglycosylated synthetic machinery. However, since galactose and GalNAc modification of protein-linked glycans in *C. neoformans* has not been examined to date, these models remain to be tested.

The absence of Ugt1 also resulted in the inability of mutant cells to mate. In *S. cerevisiae*, mating depends on the interaction of two distinct cell surface glycoproteins (59), which are five times less active when they are not glycosylated (60). Galactosylation of specific determinants may similarly be required for efficient mating to occur in *C. neoformans*. This mechanism also potentially underlies the inability of *Schizosaccharomyces pombe* mutants deficient in UDP-Gal transport to undergo sexual conjugation during nutritional deprivation (61).

Finally, we found that *ugt1*Δ cells are rapidly cleared *in vitro* and *in vivo*, likely facilitated by the increased recognition and phagocytosis of *ugt1*Δ by macrophages (Fig. A.8). This result is somewhat surprising, since internalization of hypercapsular mutants is often reduced, attributed to the overall increase in the antiphagocytic capsule. However, if the enlarged capsule of *ugt1*Δ results from poorly organized GXM, rather than overproduction of capsule material, it may not function normally. In this scenario, changes in surface epitope accessibility may result in better recognition by macrophages while the sensitivity profile facilitates clearance. Together, these would result in the avirulence seen both in our inhalational model and in prior studies using intravenous inoculation with pools of mutants (12).

The pleiotropic defects and general avirulence of cells lacking Ugt1 emphasize the importance of galactose precursor localization to the biology and pathogenicity of *C. neoformans*. Defining the activity of Ugt1 and other NSTs will advance our understanding of glycan biosynthetic pathways, setting the stage for further studies of fundamental glycobiology and cryptococcal pathogenesis.

Materials and methods

Sequence and phylogenetic analysis

UGT1 was identified by BLASTP searches against *C. neoformans* predicted proteins (Broad Institute; *Cryptococcus neoformans var. grubii* H99 database) using known UDP-galactose transporters from *Schizosaccharomyces pombe* (NP_588041), *Arabidopsis thaliana* (NP_565158.1), *Caenorhabditis elegans* (NP_001255676.1), and *Homo sapiens* (NC_000023.11). Alignments were performed using the ClustalW program at Jalview 2.0 Alignment Annotator

(http://www.bioinformatics.org/strap/aa/) with default settings (62). Transmembrane domains of Ugt1 were predicted using TMHMM server v 2.0 (Center for Biological Sequence Analysis, Technical University of Denmark). Protter (http://wlab.ethz.ch/protter/start/) was used to visualize putative protein topology. Multiple sequence alignment (MUSCLE; (63)), phylogenetic analysis (PhyML; (64)), and tree rendering (TreeDyn; (65)) of Ugt1 and characterized human NSTs was done using the online Phylogeny.fr program (http://www.phylogeny.fr/version2_cgi/index.cgi) with default settings (66, 67).

Cell growth

Unless otherwise noted, *C. neoformans* strains (Table A.1) were grown at 30°C in YPD medium (1% [wt/vol] BactoYeast Extract, 2% [wt/vol] BactoPeptone, 2% [wt/vol] dextrose) with shaking (230 rpm). For phenotypic analysis, cells from overnight (O/N) cultures were washed in sterile phosphate buffered saline (PBS), resuspended at 10^7 cells/ml in PBS, and 5 ml aliquots of 5 or 10-fold serial dilutions were plated and grown at 30 or 37°C as indicated. Conditions tested included YPD containing 0.005% SDS, 2 M Sorbitol, 10 mM H_2O_2, or 0.05% Congo Red. Mating was assayed at 25°C on 5% V8 juice agar medium, pH = 5.25 (68).

C. neoformans strains and plasmids

We used a split marker strategy (69) to replace *UGT1* with a nourseothricin (NAT) resistance marker, selecting transformants on NAT-containing plates for PCR verification of gene replacement. We used a similar strategy to complement the *ugt1* deletion strain at the endogenous locus, by replacing the NAT deletion cassette with *UGT1* in tandem with a geneticin (G418) resistance marker. Transformants of interest were identified by resistance to G418 and sensitivity to NAT,

consistent with replacement of the deletion cassette by *UGT1* in tandem with the G418 marker. All complemented strains were verified by PCR (data not shown) and reversal of phenotypes (see Results).

For protein localization, a construct encoding C-terminally HA-tagged Ugt1 (pUGT1-HA) was generated by amplification of *UGT1* from genomic Jec21 DNA with Primers 1-2 (Table A.2) to incorporate sequence encoding the tag, subcloning into pCR2.1 for sequencing, and then PmeI digestion with ligation to pMSC043 to incorporate a NAT resistance marker and place the tagged protein under the actin promoter. pUGT1-HA was linearized with IsceI and transformed into the Cxt1-myc strain (14) by biolistic transformation. Transformants were selected by growth on NAT plates and verified by immunoblotting.

To episomally complement *ugt1*Δ, N- and C- terminally truncated and full-length Ugt1 constructs were generated from Jec21 cDNA by amplification with Primers 3-4, 5-6, and 7-8, respectively (Table A.2). The DNA fragments were then digested with EcoRI/NotI and subcloned into pYEScupFLAG*K* (39) to add an N-terminal FLAG-tag and facilitate sequencing. The resulting FLAG-tagged constructs were amplified with Primers 9-10 or 10-11 (Table A.2) and digested with PmlI/AvrII for ligation into pMSC042-neo to incorporate a G418 resistance marker and place *UGT1* under control of the actin promoter. The plasmids were subsequently linearized with I-SceI and electroporated into *ugt1*Δ. Transformants were selected by growth on G418 plates and verified by PCR.

Localization

JEC21 *CXT1-myc* (33) alone or expressing Ugt1-HA or Gmt1-HA was prepared for microscopy as described in reference (14) with minor modifications. Briefly, cells were grown O/N in YPD before fixation and blocking, and slides were then incubated with high-affinity rat anti-hemagglutinin (anti-HA) monoclonal antibody (Roche Applied Science; 20 ng/ml in blocking buffer), mouse anti-c-Myc (anti-myc) antibody (Abcam; 5μg/ml in blocking buffer) or blocking buffer alone. This was followed by incubation with the appropriate secondary antibody, either AlexaFluor 594-tagged goat anti-rat IgG or Alexa Fluor 488-tagged goat anti-mouse IgG (Invitrogen), at 1 μg/ml in blocking buffer.

For localization studies in MDCKII cells, human SLC35A2 (BAA95615) or cryptococcal *UGT1* (EAL18940) were amplified so as to encode a C-terminal HA-tag, cloned into the PmeI site of pcDNA3.1 (Life Technologies) to form phUGT1-HA or pcUGT1-HA respectively, and verified by sequencing. MDCKII cells seeded to $5x10^4$cells/cm^2 in a 6-well plate then were transiently transfected with 1 μg of pcDNA3.1, pcUGT1-HA, or phUGT1-HA. For transfection the DNA and lipofectamine (Life Technologies) were incubated at room temperature (RT) for 15 min and added to cells for incubation at 37°C/5% CO_2 for 3 h. Cells were then washed and incubated in MEM+10% FCS O/N before being plated on cover slips in a 12-well plate. After 24 h at 37°C/5% CO_2, the cover slips were fixed in 4% formaldehyde/PBS for 20 min and the cells were permeabilized with 5% BSA in 0.3% TX-100 in PBS for 15 min and stained with rabbit anti-Giantin IgG (Abcam; 200 ng/ml in blocking buffer) and rat anti-HA (Invitrogen; 20 ng/ml in blocking buffer). Finally, cells were incubated for 20 min with AlexaFluor 594-tagged goat anti-rat IgG and AlexaFluor 488-tagged goat anti-rabbit IgG (Invitrogen; 1 μg/ml in blocking buffer)

and viewed with a ZEISS Axioskop2 MOT Plus microscope using a 63× objective. Where not specified, all steps were performed at RT.

Lec Cell Complementation

Lec8 cells were transiently transfected with pcDNA3.1, pcUGT1-HA, or phUGT1-HA as described for the MDCKII studies. Cover slips were then fixed with 3.7% formaldehyde for 30 min, washed 2x with PBS, and permeabilized with 0.1% TX-100/PBS for 30 min. After blocking in 1% BSA/PBS for 10 min, cells were stained with fluorescein isothiocyanate (FITC)-conjugated GSII in blocking buffer for 30 min at 37°C, rat anti-HA for 1 h, and AlexaFluor 594-tagged goat anti-rat IgG for 1 h. Samples were viewed with a ZEISS Axioskop2 MOT Plus microscope using a 63× objective. Where not specified steps were performed at RT.

Ugt1 truncations (Table A.3) were assessed in a Lec8 cell line stably transformed with the polyoma virus large T antigen (CHOP8) as described in reference (70). Briefly, CHOP8 cells were transfected with the vector pEFBO encoding the rat β-1,3-glucuronyltransferase (71), and plasmids expressing each Ugt1 variant were generated using the primers in Table A.4. After 3 days at 37°C/5% CO_2, cells were fixed, blocked in 2% milk/TBS, and then stained with rat monoclonal L2-412 (46, 47) followed by goat anti-rat alkaline phosphatase in blocking solution. Samples were then treated with Fast-Red substrate (Sigma-Aldrich) to allow enumeration of red cells per plate by light microscopy.

S. cerevisiae expression and transport assays

Yeast expression experiments were done in *S. cerevisiae* strain YPH500 (*MATα ura3-52 lys2-801 ade2-101 trp1-*Δ *63 his3-*Δ*200 leu2-*Δ*1*). *UGT1* was amplified from JEC21 RNA using primers 10 and 11, cloned into pCR2.1 (TOPO TA, Life Technologies), and sequenced. The fragment was then digested with EcoRI and XbaI, ligated into the copper-inducible expression vector pYEScupFLAG*K*, (39) and transformed into YPH500 cells using lithium acetate (Invitrogen).

S. cerevisiae cells transformed with empty pYEScupFLAG*K* or pYEScupFLAG*K*–UGT1 were grown in 0.5 mM $CuSO_4$-supplemented selective medium (0.67% Bacto yeast nitrogen base without amino acids, L-leucine, L-histidine, L-tryptophan, L-lysine, adenine, 2% glucose) for 2 h to induce protein expression. Golgi membranes were isolated by subcellular fractionation and then assayed for the ability to import radiolabeled nucleotide sugars (NEM Life Science Products) as described in (39). Transport of each assay substrate by strains with empty or Ugt1-expressing vectors was compared by unpaired Student's t-test.

Capsule induction

O/N cultures of *C. neoformans* grown in YPD were collected by centrifugation and washed twice with sterile PBS. Cells were then either resuspended in Dulbecco's Modified Eagle's Medium (DMEM; Sigma-Aldrich) at 10^6 cells/ml in T-75 tissue culture flasks and incubated at 37°C in 5% CO_2 for 24 h or diluted to 5 x 10^6 cells/ml in 10% Sabouraud's medium (4% [wt/vol] dextrose, 2% [wt/vol] peptone, pH = 5.6) in PBS and grown at 30°C with shaking for 48 h. Cells were collected, washed twice in PBS, resuspended in PBS, mixed with 1.5 parts India ink, and viewed with a ZEISS Axioskop2 MOT Plus microscope, 63× objective.

Fungal gene expression

Wild-type cells cultured in YPD were grown in DMEM under capsule-inducing conditions and sampled at 0, 1.5, 3, 8, and 24 h for RNA isolation and sequencing. See reference (56) for details.

Transmission electron microscopy

Strains were grown in Sabouraud's capsule-inducing conditions (72), collected by centrifugation (3,000 x g; 5min), fixed for 1 h at RT with 2% glutaraldehyde (Polysciences Inc.) in 100 mM phosphate buffer (pH 7.2), and then incubated for 1 h in 1% osmium tetraoxide (Polysciences Inc.). Following dehydration with ethanol and propylene oxide, cells were embedded in Eponate 12 resin (Tel Pella Inc.), and 70-90 nm sections were cut with an UCT ultramicrotome (Leica Microsystems Inc.). Sections were stained with uranyl acetate and lead citrate for visualization with a JEOL 1200EX transmission electron microscope (JOEL Ltd.).

Macrophage assays

To assay fungal survival in macrophages, THP-1 monocytes were seeded at 3.5 x 10^5 cells/well in a 96-well plate, treated with 0.2 ug/ml PMA for 72 h to induce differentiation, and incubated with *C. neoformans* at MOI = 0.1 for 1 h at 37°C and 5% CO_2. Plates were washed twice with PBS, and samples incubated for 1 or 24 h before lysis and plating in triplicate on YPD agar for counts of colony forming units (CFU).

Macrophage phagocytosis of fungal strains was quantified using our previously published assay (49) with minor modifications. Briefly, cells were grown in capsule inducing media as above or

in parallel YPD cultures. Cells were then collected by centrifugation, washed, and opsonized with commercial human serum before incubation with differentiated THP-1 macrophages for 1 h. Host cell cytosol and nuclei and fungal walls were stained, and samples were imaged on a Cytation3 plate reader (BioTek) and analyzed using IN Cell Developer Toolbox 1.9.2 (GE Healthcare Life Sciences). Assay results for *ugt1*Δ were compared to those for wild-type and complemented strains by analysis of variance (ANOVA).

Animal studies

Fungal strains to be tested were cultured O/N in YPD, washed in PBS, and diluted to 2.5 x 10^4 cells/ml in sterile PBS. 50 μl aliquots were then inoculated intranasally into six 4- to 6-week-old female C57BL/6 mice (NCI, National Institutes of Health). Groups of two and four mice were sacrificed at 1 h and 7 days post inoculation, respectively. Initial inocula and lung homogenates were plated for CFU, and organ burden was analyzed by ANOVA. All studies were performed in compliance with institutional guidelines for animal experimentation.

Acknowledgements

This work was supported by National Institutes of Health grants GM071007 and AI109623. LXL was partly supported by a Sondra Schlesinger Graduate Fellowship and a National Institute of Allergy and Infectious Diseases award F30AI120339.

We thank Matthew Williams for help with the mouse experiments and Wandy Beatty for performing the EM studies. We also thank June Kwon-Chung (NIAID) for cryptococcal strain Jec21, Joe Heitman (Duke University) for strains KN99 and KN433, Jennifer Lodge (Washing-

ton University School of Medicine) for plasmid pMH12-T, and members of the Doering laboratory for helpful discussions.

References

1. Park BJ, *et al.* (2009) Estimation of the current global burden of cryptococcal meningitis among persons living with HIV/AIDS. *AIDS* 23(4):525-530.

2. Botts MR & Hull CM (2010) Dueling in the lung: how *Cryptococcus* spores race the host for survival. *Curr Opin Microbiol* 13(4):437-442.

3. Doering TL (2009) How sweet it is! Cell wall biogenesis and polysaccharide capsule formation in *Cryptococcus neoformans*. *Annu Rev Microbiol* 63:223-247.

4. Kumar P, Yang M, Haynes BC, Skowyra ML, & Doering TL (2011) Emerging themes in cryptococcal capsule synthesis. *Curr Opin Struct Biol* 21(5):597-602.

5. Yoneda A & Doering TL (2006) A eukaryotic capsular polysaccharide is synthesized intracellularly and secreted via exocytosis. *Mol Biol Cell* 17(12):5131-5140.

6. Reese AJ, *et al.* (2007) Loss of cell wall alpha(1-3) glucan affects *Cryptococcus neoformans* from ultrastructure to virulence. *Mol Microbiol* 63(5):1385-1398.

7. Voelz K & May RC (2010) Cryptococcal interactions with the host immune system. *Eukaryot Cell* 9(6):835-846.

8. Cherniak R, Valafar H, Morris LC, & Valafar F (1998) *Cryptococcus neoformans* chemotyping by quantitative analysis of 1H nuclear magnetic resonance spectra of glucuronoxylomannans with a computer-simulated artificial neural network. *Clin Diagn Lab Immunol* 5(2):146-159.

9. Heiss C, Klutts JS, Wang Z, Doering TL, & Azadi P (2009) The structure of *Cryptococcus neoformans* galactoxylomannan contains beta-D-glucuronic acid. *Carbohydr Res* 344(7):915-920.

10. Heiss C, *et al.* (2013) Unusual galactofuranose modification of a capsule polysaccharide in the pathogenic yeast *Cryptococcus neoformans*. *J Biol Chem* 288(16):10994-11003.

11. Chang YC & Kwon-Chung KJ (1994) Complementation of a capsule-deficient mutation of *Cryptococcus neoformans* restores its virulence. *Mol Cell Biol* 14(7):4912-4919.

12. Moyrand F, Fontaine T, & Janbon G (2007) Systematic capsule gene disruption reveals the central role of galactose metabolism on *Cryptococcus neoformans* virulence. *Mol Microbiol* 64(3):771-781.

13. Olson GM, Fox DS, Wang P, Alspaugh JA, & Buchanan KL (2007) Role of protein O-mannosyltransferase Pmt4 in the morphogenesis and virulence of *Cryptococcus neoformans*. *Eukaryot Cell* 6(2):222-234.

14. Reilly MC, *et al.* (2011) A xylosylphosphotransferase of *Cryptococcus neoformans* acts in protein O-glycan synthesis. *J Biol Chem* 286(30):26888-26899.

15. Park JN, *et al.* (2012) Unraveling unique structure and biosynthesis pathway of N-linked glycans in human fungal pathogen *Cryptococcus neoformans* by glycomics analysis. *J Biol Chem* 287(23):19501-19515.

16. Reese AJ & Doering TL (2003) Cell wall alpha-1,3-glucan is required to anchor the *Cryptococcus neoformans* capsule. *Mol Microbiol* 50(4):1401-1409.

17. Banks IR, *et al.* (2005) A chitin synthase and its regulator protein are critical for chitosan production and growth of the fungal pathogen *Cryptococcus neoformans*. *Eukaryot Cell* 4(11):1902-1912.

18. Gilbert NM, *et al.* (2010) *KRE* genes are required for beta-1,6-glucan synthesis, maintenance of capsule architecture and cell wall protein anchoring in *Cryptococcus neoformans*. *Mol Microbiol* 76(2):517-534.

19. Gilbert NM, Lodge JK, & Specht CA (2011) The Cell Wall of *Cryptococcus*. *Cryptococcus From Human Pathogen to Model Yeast*, eds Heitman J, Kozel TR, Kwon-Chung KJ, Perfect J, & Casadevall A (ASM Press, Washington), pp 67-79.

20. Vincent VL & Klig LS (1995) Unusual effect of *myo*-inositol on phospholipid biosynthesis in *Cryptococcus neoformans*. *Microbiology* 141 (Pt 8):1829-1837.

21. Heise N, *et al.* (2002) Molecular analysis of a novel family of complex glycoinositolphosphoryl ceramides from *Cryptococcus neoformans*: structural differences between encapsulated and acapsular yeast forms. *Glycobiology* 12(7):409-420.

22. Castle SA, *et al.* (2008) Beta1,2-xylosyltransferase Cxt1p is solely responsible for xylose incorporation into *Cryptococcus neoformans* glycosphingolipids. *Eukaryot Cell* 7(9):1611-1615.

23. Rittershaus PC, *et al.* (2006) Glucosylceramide synthase is an essential regulator of pathogenicity of *Cryptococcus neoformans*. *J Clin Invest* 116(6):1651-1659.

24. Varki A, Esko JD, & Colley KJ (2009) Cellular Organization of Glycosylation. *Essentials of Glycobiology*, eds Varki A, Cummings RD, Esko JD, Freeze HH, Stanley P,

Bertozzi CR, Hart GW, & Etzler ME (Cold Spring Harbor Laboratory PRess, Cold Spring Harbor, NY).

25. Abeijon C, Mandon EC, & Hirschberg CB (1997) Transporters of nucleotide sugars, nucleotide sulfate and ATP in the Golgi apparatus. *Trends Biochem Sci* 22(6):203-207.

26. Berninsone PM & Hirschberg CB (2000) Nucleotide sugar transporters of the Golgi apparatus. *Curr Opin Struct Biol* 10(5):542-547.

27. Bar-Peled M, Griffith CL, & Doering TL (2001) Functional cloning and characterization of a UDP- glucuronic acid decarboxylase: the pathogenic fungus *Cryptococcus neoformans* elucidates UDP-xylose synthesis. *Proc Natl Acad Sci U S A* 98(21):12003-12008.

28. Wills EA, *et al.* (2001) Identification and characterization of the *Cryptococcus neoformans* phosphomannose isomerase-encoding gene, *MAN1*, and its impact on pathogenicity. *Mol Microbiol* 40(3):610-620.

29. Bar-Peled M, Griffith CL, Ory JJ, & Doering TL (2004) Biosynthesis of UDP-GlcA, a key metabolite for capsular polysaccharide synthesis in the pathogenic fungus *Cryptococcus neoformans*. *Biochem J* 381(Pt 1):131-136.

30. Griffith CL, Klutts JS, Zhang L, Levery SB, & Doering TL (2004) UDP-glucose dehydrogenase plays multiple roles in the biology of the pathogenic fungus *Cryptococcus neoformans*. *J Biol Chem* 279(49):51669-51676.

31. Beverley SM, *et al.* (2005) Eukaryotic UDP-galactopyranose mutase (*GLF* gene) in microbial and metazoal pathogens. *Eukaryot Cell* 4(6):1147-1154.

32. Moyrand F, Lafontaine I, Fontaine T, & Janbon G (2008) *UGE1* and *UGE2* regulate the UDP-glucose/UDP-galactose equilibrium in *Cryptococcus neoformans*. *Eukaryot Cell* 7(12):2069-2077.

33. Cottrell TR, Griffith CL, Liu H, Nenninger AA, & Doering TL (2007) The pathogenic fungus *Cryptococcus neoformans* expresses two functional GDP-mannose transporters with distinct expression patterns and roles in capsule synthesis. *Eukaryot Cell* 6(5):776-785.

34. Martinez-Duncker I, Mollicone R, Codogno P, & Oriol R (2003) The nucleotide-sugar transporter family: a phylogenetic approach. *Biochimie* 85(3-4):245-260.

35. Berninsone P, Hwang HY, Zemtseva I, Horvitz HR, & Hirschberg CB (2001) SQV-7, a protein involved in *Caenorhabditis elegans* epithelial invagination and early embryogenesis, transports UDP-glucuronic acid, UDP-N- acetylgalactosamine, and UDP-galactose. *Proc Natl Acad Sci U S A* 98(7):3738-3743.

36. Norambuena L, *et al.* (2002) Transport of UDP-galactose in plants. Identification and functional characterization of AtUTr1, an *Arabidopsis thaliana* UDP-galactose/UDP-glucose transporter. *J Biol Chem* 277(36):32923-32929.

37. Segawa H, Kawakita M, & Ishida N (2002) Human and *Drosophila* UDP-galactose transporters transport UDP-N-acetylgalactosamine in addition to UDP-galactose. *Eur J Biochem* 269(1):128-138.

38. Aoki K, Ishida N, & Kawakita M (2003) Substrate recognition by nucleotide sugar transporters: further characterization of substrate recognition regions by analyses of UDP-galactose/CMP-sialic acid transporter chimeras and biochemical analysis of the substrate specificity of parental and chimeric transporters. *J Biol Chem* 278(25):22887-22893.

39. Ashikov A, *et al.* (2005) The human solute carrier gene SLC35B4 encodes a bifunctional nucleotide sugar transporter with specificity for UDP-xylose and UDP-N-acetylglucosamine. *J Biol Chem* 280(29):27230-27235.

40. Segawa H, Soares RP, Kawakita M, Beverley SM, & Turco SJ (2005) Reconstitution of GDP-mannose transport activity with purified *Leishmania* LPG2 protein in liposomes. *J Biol Chem* 280(3):2028-2035.

41. Caffaro CE, *et al.* (2008) A single *Caenorhabditis elegans* Golgi apparatus-type transporter of UDP-glucose, UDP-galactose, UDP-N-acetylglucosamine, and UDP-N-acetylgalactosamine. *Biochemistry* 47(14):4337-4344.

42. Maszczak-Seneczko D, Sosicka P, Majkowski M, Olczak T, & Olczak M (2012) UDP-N-acetylglucosamine transporter and UDP-galactose transporter form heterologous complexes in the Golgi membrane. *FEBS Lett* 586(23):4082-4087.

43. Kwon-Chung KJ & Varma A (2006) Do major species concepts support one, two or more species within *Cryptococcus neoformans*? *FEMS Yeast Res* 6(4):574-587.

44. Deutscher SL & Hirschberg CB (1986) Mechanism of galactosylation in the Golgi apparatus. A Chinese hamster ovary cell mutant deficient in translocation of UDP-galactose across Golgi vesicle membranes. *J Biol Chem* 261(1):96-100.

45. Oelmann S, Stanley P, & Gerardy-Schahn R (2001) Point mutations identified in Lec8 Chinese hamster ovary glycosylation mutants that inactivate both the UDP-galactose and CMP-sialic acid transporters. *J Biol Chem* 276(28):26291-26300.

46. Kruse J, *et al.* (1984) Neural cell adhesion molecules and myelin-associated glycoprotein share a common carbohydrate moiety recognized by monoclonal antibodies L2 and HNK-1. *Nature* 311(5982):153-155.

47. Bakker H, *et al.* (1997) Expression cloning of a cDNA encoding a sulfotransferase involved in the biosynthesis of the HNK-1 carbohydrate epitope. *J Biol Chem* 272(47):29942-29946.

48. Wohlschlager T, *et al.* (2013) Identification of the galactosyltransferase of *Cryptococcus neoformans* involved in the biosynthesis of basidiomycete-type glycosylinositolphosphoceramide. *Glycobiology* 23(11):1210-1219.

49. Srikanta D, Yang M, Williams M, & Doering TL (2011) A sensitive high-throughput assay for evaluating host-pathogen interactions in *Cryptococcus neoformans* infection. *PLoS One* 6(7):e22773.

50. Aoki K, Ishida N, & Kawakita M (2001) Substrate recognition by UDP-galactose and CMP-sialic acid transporters. Different sets of transmembrane helices are utilized for the specific recognition of UDP-galactose and CMP-sialic acid. *J Biol Chem* 276(24):21555-21561.

51. Hadley B, *et al.* (2014) Structure and function of nucleotide sugar transporters: Current progress. *Comput Struct Biotechnol J* 10(16):23-32.

52. Klutts JS & Doering TL (2008) Cryptococcal xylosyltransferase 1 (Cxt1p) from *Cryptococcus neoformans* plays a direct role in the synthesis of capsule polysaccharides. *J Biol Chem* 283(21):14327-14334.

53. Klutts JS, Levery SB, & Doering TL (2007) A beta-1,2-xylosyltransferase from *Cryptococcus neoformans* defines a new family of glycosyltransferases. *J Biol Chem* 282(24):17890-17899.

54. Haynes BC, *et al.* (2011) Toward an integrated model of capsule regulation in *Cryptococcus neoformans*. *PLoS Pathog* 7(12):e1002411.

55. O'Meara TR & Alspaugh JA (2012) The *Cryptococcus neoformans* capsule: a sword and a shield. *Clin Microbiol Rev* 25(3):387-408.

56. Maier EJ, *et al.* (2015) Model-driven mapping of transcriptional networks reveals the circuitry and dynamics of virulence regulation. *Genome Res* 25(5):690-700.

57. Rivera J, Feldmesser M, Cammer M, & Casadevall A (1998) Organ-dependent variation of capsule thickness in *Cryptococcus neoformans* during experimental murine infection. *Infect Immun* 66(10):5027-5030.

58. Garcia-Hermoso D, Dromer F, & Janbon G (2004) *Cryptococcus neoformans* capsule structure evolution in vitro and during murine infection. *Infect Immun* 72(6):3359-3365.

59. Cappellaro C, *et al.* (1991) *Saccharomyces cerevisiae* a- and alpha-agglutinin: characterization of their molecular interaction. *EMBO J* 10(13):4081-4088.

60. Cappellaro C, Baldermann C, Rachel R, & Tanner W (1994) Mating type-specific cell-cell recognition of *Saccharomyces cerevisiae*: cell wall attachment and active sites of a- and alpha-agglutinin. *EMBO J* 13(20):4737-4744.

61. Tanaka N, Konomi M, Osumi M, & Takegawa K (2001) Characterization of a *Schizosaccharomyces pombe* mutant deficient in UDP-galactose transport activity. *Yeast* 18(10):903-914.

62. Waterhouse AM, Procter JB, Martin DM, Clamp M, & Barton GJ (2009) Jalview Version 2--a multiple sequence alignment editor and analysis workbench. *Bioinformatics* 25(9):1189-1191.

63. Edgar RC (2004) MUSCLE: multiple sequence alignment with high accuracy and high throughput. *Nucleic Acids Res* 32(5):1792-1797.

64. Guindon S & Gascuel O (2003) A simple, fast, and accurate algorithm to estimate large phylogenies by maximum likelihood. *Syst Biol* 52(5):696-704.

65. Chevenet F, Brun C, Banuls AL, Jacq B, & Christen R (2006) TreeDyn: towards dynamic graphics and annotations for analyses of trees. *BMC Bioinformatics* 7:439.

66. Dereeper A, *et al.* (2008) Phylogeny.fr: robust phylogenetic analysis for the non-specialist. *Nucleic Acids Res* 36(Web Server issue):W465-469.

67. Dereeper A, Audic S, Claverie JM, & Blanc G (2010) BLAST-EXPLORER helps you building datasets for phylogenetic analysis. *BMC Evol Biol* 10:8.

68. Kwon-Chung KJ, Edman JC, & Wickes BL (1992) Genetic association of mating types and virulence in *Cryptococcus neoformans*. *Infect Immun* 60(2):602-605.

69. Fu J, Hettler E, & Wickes BL (2006) Split marker transformation increases homologous integration frequency in *Cryptococcus neoformans*. *Fungal Genet Biol* 43(3):200-212.

70. Bakker H, *et al.* (2005) Molecular cloning of two *Arabidopsis* UDP-galactose transporters by complementation of a deficient Chinese hamster ovary cell line. *Glycobiology* 15(2):193-201.

71. Terayama K, *et al.* (1997) Cloning and functional expression of a novel glucuronyltransferase involved in the biosynthesis of the carbohydrate epitope HNK-1. *Proc Natl Acad Sci U S A* 94(12):6093-6098.

72. Zaragoza O & Casadevall A (2004) Experimental modulation of capsule size in *Cryptococcus neoformans*. *Biol Proced Online* 6:10-15.

73. Nielsen K, *et al.* (2005) *Cryptococcus neoformans {alpha}* strains preferentially disseminate to the central nervous system during coinfection. *Infect Immun* 73(8):4922-4933.

74. Kwon-Chung KJ, *et al.* (1992) Virulence, serotype, and molecular characteristics of environmental strains of *Cryptococcus neoformans var. gattii*. *Infect Immun* 60(5):1869-1874.

75. Wang ZA, *et al.* (2014) *Cryptococcus neoformans* dual GDP-mannose transporters and their role in biology and virulence. *Eukaryot Cell* 13(6):832-842.

76. Nielsen K, *et al.* (2003) Sexual cycle of *Cryptococcus neoformans var. grubii* and virulence of congenic a and alpha isolates. *Infect Immun* 71(9):4831-4841.

Figures

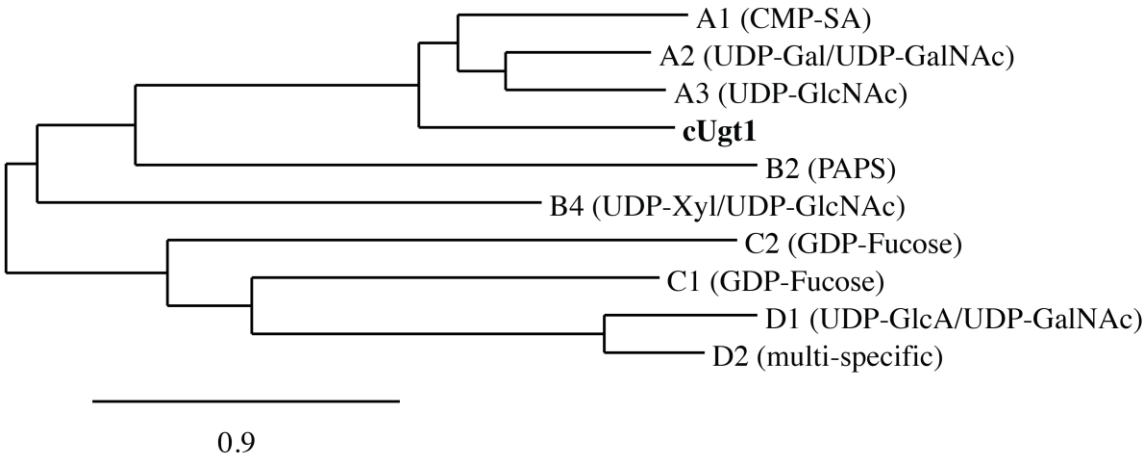

Figure A.1. Phylogenetic relationships of cryptococcal Ugt1 (bold) and human NSTs with known substrates (in parentheses). Tree reconstruction was performed with the Phylogeny.fr web server (66, 67) using MUSCLE, PhyML, and TreeDyn software. Human transporters are denoted by their SLC35 family designation, and distance is expressed as the number of amino acid substitutions per 100 positions.

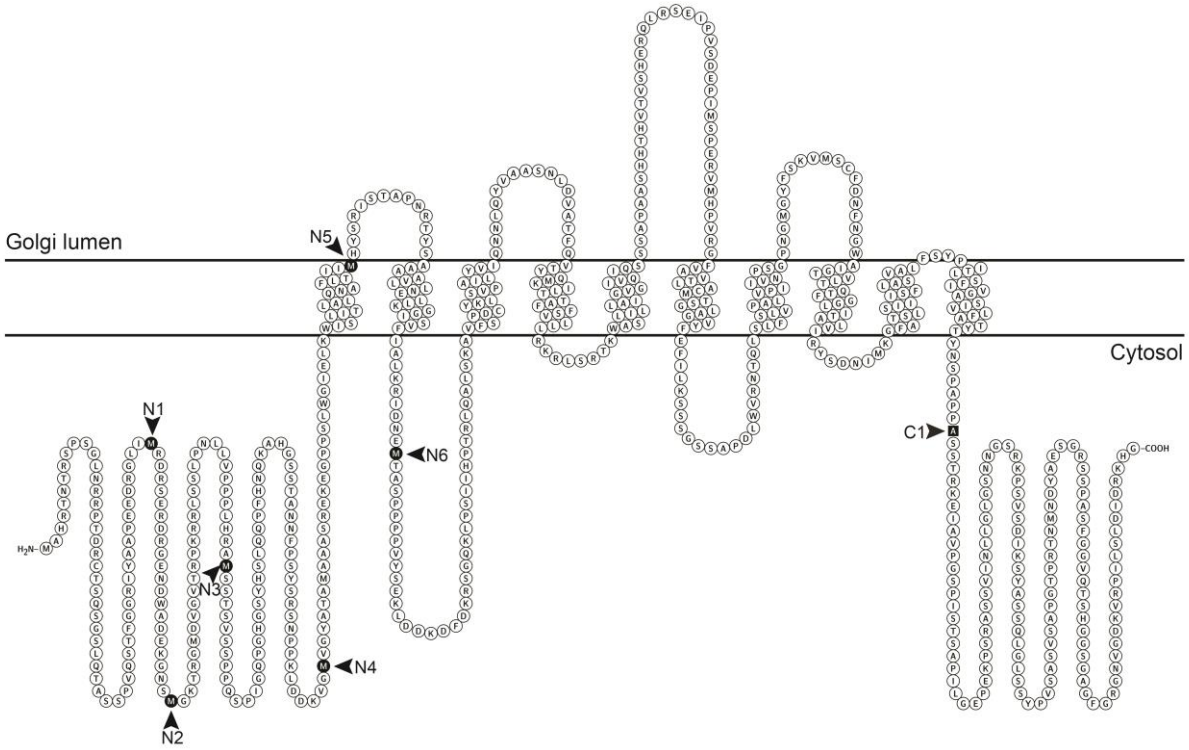

Figure A.2. Topology of *C. neoformans* Ugt1 as predicted by TMHMM server v 2.0, showing 10 putative transmembrane domains and long N- and C- terminal cytosolic tails. Arrowheads indicate the new N-terminus for each N-terminal truncation and the terminal residue of the single C-terminal truncation (C1); see text and Table A.3 for details.

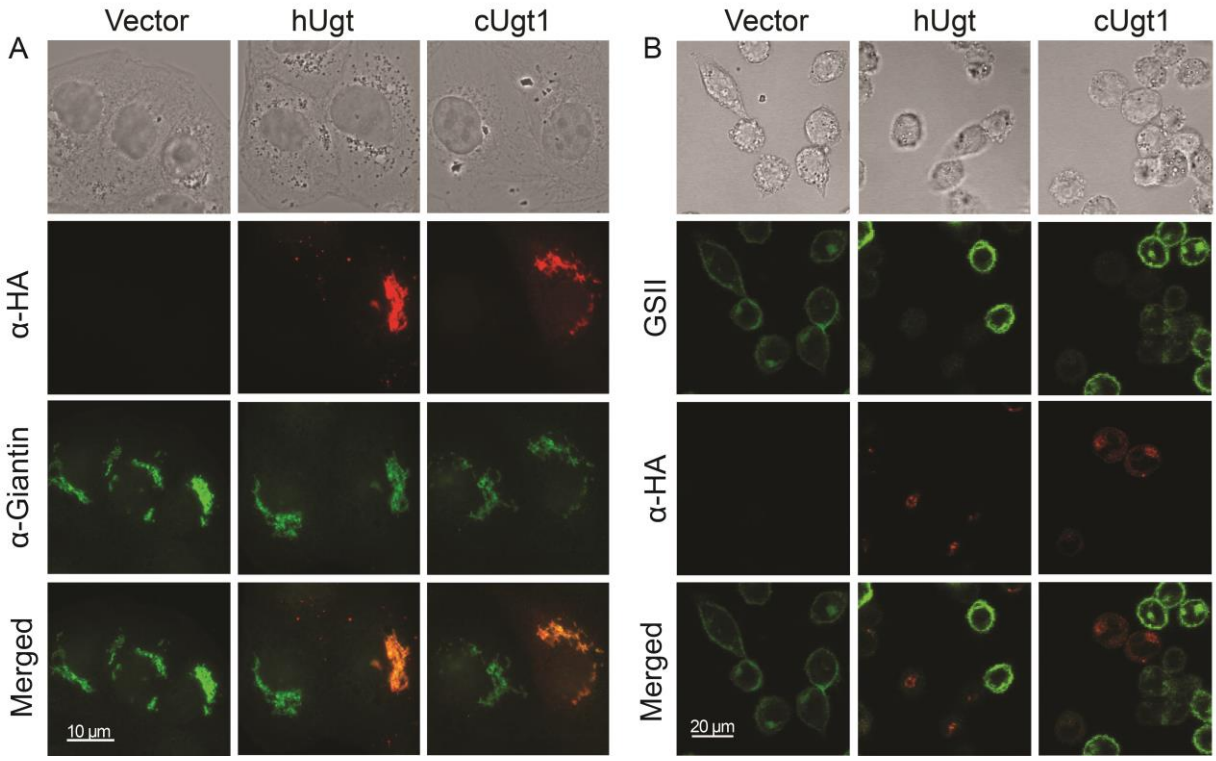

Figure A.3. The cryptococcal UDP-Gal transporter localizes with a Golgi marker and is functional in mammalian cells. (A) MDCKII cells transiently transfected with vector alone (vector) or vector expressing HA-tagged forms of the human UDP-Gal transporter (hUgt) or cryptococcal UDP-Gal transporter (cUgt1) were probed with antibodies to HA (red) and to the Golgi protein giantin (green). As expected, all cells stain with the Golgi marker, while a subset expresses each colocalizing transporter. (B) Lec8 cells were transiently transfected with the same constructs as in Panel A and probed with anti-HA antibody (red) and GSII-FITC (a lectin specific for terminal GlcNAc; green). Terminal galactose modification of cell surface glycans, which prevents the lectin binding, occurs only in cells that express a UDP-Gal transporter. Bright field and merged images are shown (Panel A scale bar, 10 μm; Panel B scale bar, 20 μm).

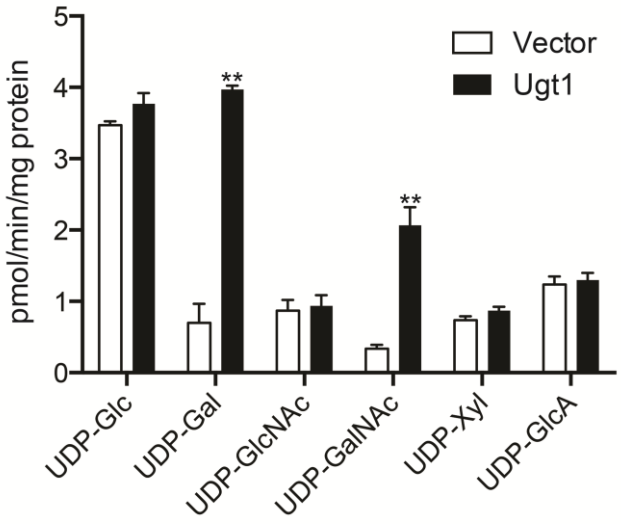

Figure A.4. Ugt1 transports UDP-Gal and UDP-GalNAc. Golgi fractions isolated from *S. cerevisiae* expressing vector alone (white bars) or *UGT1* (black bars) were assayed for transport of the indicated nucleotide sugars. Each value represents the mean and standard deviation of duplicate assays from three independent Golgi preps. **, $p < 0.001$ compared with vector alone.

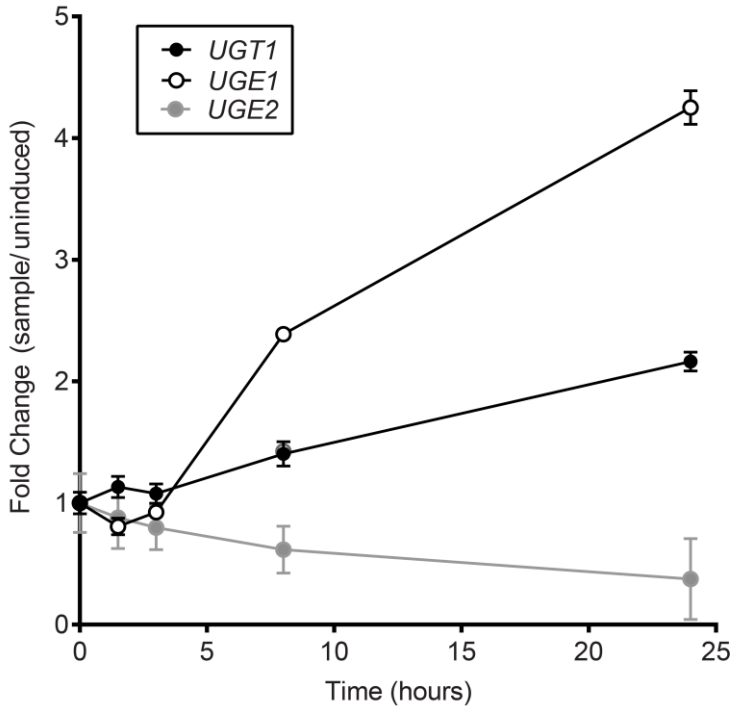

Figure A.5. Transcription of *UGT1* and *UGE1* increases during capsule induction. Reads from RNA-seq data (mean ± SD) were normalized to their levels at t = 0, which were: *UGT1*, 383,949 ± 24,018; *UGE1*, 724,792 ± 19,475; and *UGE2*, 110,719 ±18,909. Values shown are compiled from three independent experiments, each with RNA prepared from three biological replicates.

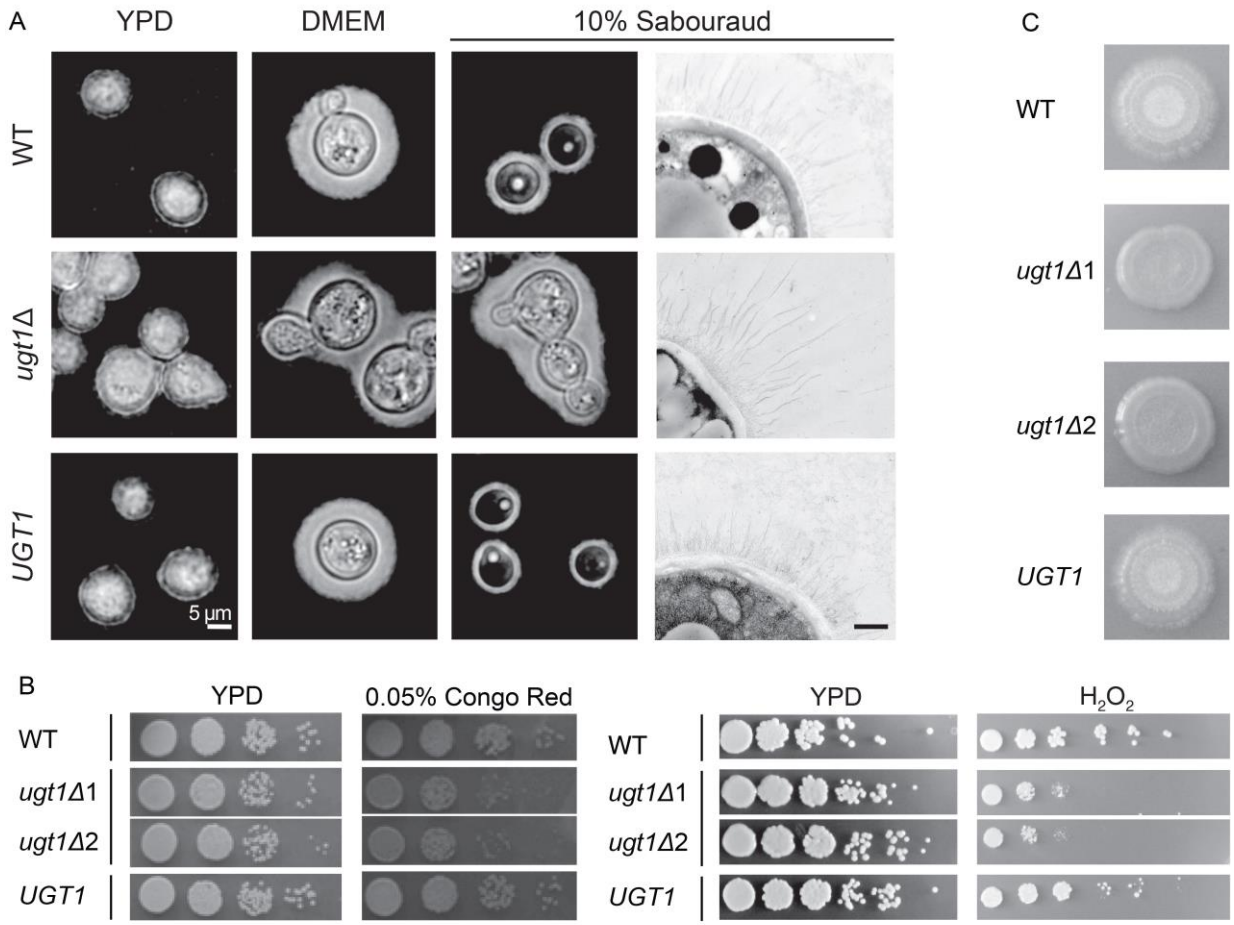

Figure A.6. *ugt1*Δ mutants show altered capsule and cellular morphology, and exhibit growth and mating defects. (A) Wild type (WT), *ugt1*Δ, and complemented *ugt1*Δ (*UGT1*) were grown in the media noted above and visualized by light microscopy after negative staining with India Ink (first three columns, scale bar = 5 μm) or by electron microscopy (last column, scale bar = 500 nm). (B) The indicated strains, including two independent *ugt1*Δ strains, were grown overnight at 30°C in YPD, and 5 μl of serial dilutions were spotted and grown as indicated. Left panel, dilutions were 10-fold starting at 10^6 cells; right panel, dilutions were 5-fold, starting at 10^7 cells. (C) Equal volumes of the indicated MATα strains and KN99a were mixed, spotted on V8 agar, and incubated at RT in the dark. Images were taken two weeks after initial spotting. In three independent experiments, no filamentation of either mutant strain was detected.

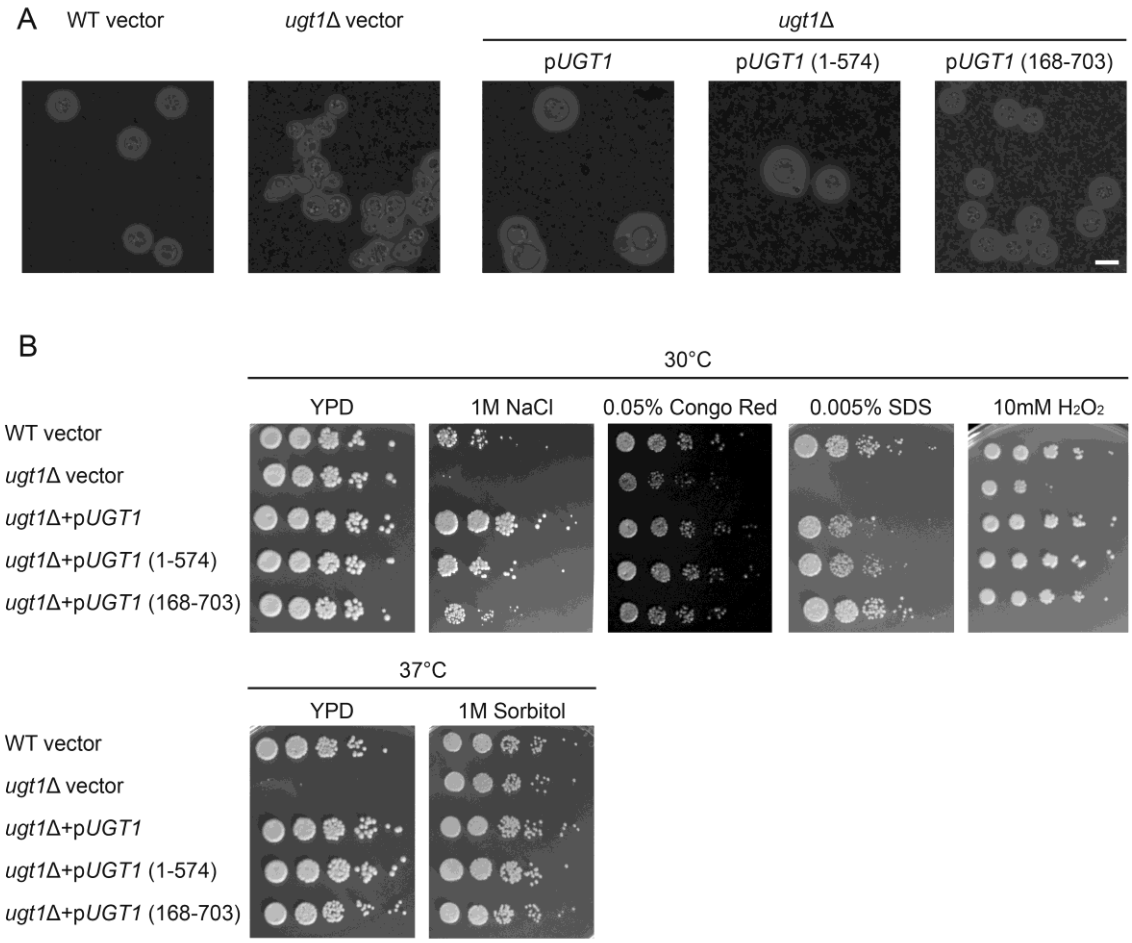

Figure A.7. N- and C- terminal Ugt1 truncations complement capsule and cellular morphology defects in *ugt1*Δ. (A) The strains indicated above the horizontal line, carrying the plasmids shown below the line, were grown in DMEM + G418 and visualized by light microscopy after negative staining with India Ink (scale bar = 5 μm). (B) The indicated strain and plasmid combinations were grown overnight at 30°C in YPD + G418. 5 μl of serial dilutions were spotted and grown as indicated with G418 (except for 0.005% SDS). Dilutions were 5-fold starting at 10^6 cells.

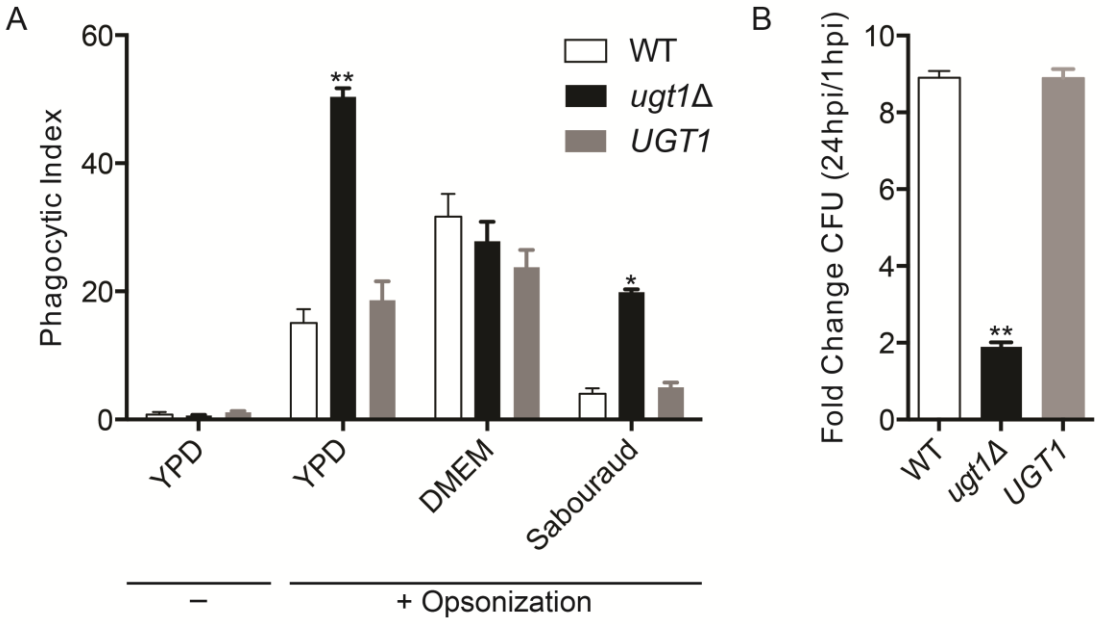

Figure A.8. Cells lacking Ugt1 are more efficiently phagocytosed and killed by THP-1 cells than wild-type *C. neoformans*. (A) Phagocytic index (engulfed fungi/100 host cells) of strains grown in YPD (-/+ opsonization) or in inducing media (+ opsonization). (B) Survival of YPD-grown, opsonized fungi after internalization by THP-1 cells. Data are representative of three independent experiments performed with n = 3 (*, $p < 0.01$; **, $p < 0.001$).

Table A.1. *C. neoformans* strains used in these studies.

C. neoformans strain[i]	Serotype	Origin
KN433	D	(73)
KN433 *ugt1*	D	This study
KN433 *ugt1::UGT1*	D	This study
Jec21	D	(74)
Jec21 *CXT1*-myc	D	(14)
Jec21 *CXT1*-myc *UGT1*-HA	D	This study
Jec21 *CXT1*-myc *GMT1*-HA	D	(75)
KN99**a**	A	(76)

[i]All strains are MATα except for KN99**a**.

Table A.2. Primers used for modification of or expression in *C. neoformans*.

Primer	Sequence (5′-3′)
1	CCGGCGCGCCGTTTAAACTCATGCGTAATCCGGAACGTCGTAGGGGTAAC-CATGCTTTCTATCAATGTCCAAAC
2	CCCTAGCTAGCGTTTAAACATGGCCCATCGAACCAACACTCG
3	GTCACGAAGAATTCGTGGGCTATGCTACTGCGATG
4	TACCTCGGCGCGGCCGCTTAACCATGCTTTCTATC
5	GTCACGAAGAATTCGCCCATCGAACCAACACT
6	GTCACGAACCTAGGCTAGATTGGCGGAGCGGGGCT
7	GTCACGAACCTAGGTCAACCATGCTTTCTATCAATG
8	GTCACGAACACGTGATGGACTACAAGGACGATGACG
9	GTCACGAACCTAGGGATTGGCGAGCGGGGCT
10	GAATTCGCCCATCGAACCAACAT
11	CTCGAGTTAACCATGCTTTCTATC

Table A.3. Ugt1 truncations and their ability to complement UDP-Gal transport.

UGT1 Variant	Amino Acids	CHOP8 Complementation
Full Length	1-703	+
N1	56-703	+
N2	76-703	+
N3	109-703	+
N4	168-703	+
N5	212-703	-
N6	254-703	-
C1	1-571	+
N6/C1	254-571	-

Table A.4. Primers used to generate truncation constructs for Lec8 expression.

UGT1 Variant	Primer Sequence
Full Length	5′-ATCGAATTCGCCCATCGAACCAACACT-3′ 5′-TTAACCATGCTTTCTATC-3′
N1	5′-ACTAGAATTCAGAGATCGAAGCGAGAGA-3′ 5′-TTAACCATGCTTTCTATC-3′
N2	5′-ACTAGAATTCGGGAAGACGCGCGGTATGGA-3′ 5′-TTAACCATGCTTTCTATC-3′
N3	5′-ACTAGAATTCTCCTCTACCTCTGTCAGCT-3′ 5′-TTAACCATGCTTTCTATC-3′
N4	5′-ACTAGAATTCGTGGGCTATGCTACTGCGA-3′ 5′-TTAACCATGCTTTCTATC-3′
N5	5′-ACTAGAATTCCACTATTCACGGATATCTA-3′ 5′-TTAACCATGCTTTCTATC-3′
N6	5′-ACTAGAATTCACTGCATCTCCTCCTC-3′ 5′-TTAACCATGCTTTCTATC-3′
C1	5′-ATCGAATTCGCCCATCGAACCAACACT-3′ 5′-ACACTCGAGACTGGCAGGTGGAGCGGGGCT-3′

Supplementary materials

Figure A.S1. Protein sequence alignment of *C. neoformans* Ugt1 with other UDP-Gal transporters. The Jalview2 alignment includes aa 195-563 of cryptococcal Ugt1 (703 aa total) and the complete sequences of *Schizosaccharomyces pombe* (Sp) Gms1, *Arabidopsis thaliana* (At) UDP-GalT1, *Caenorhabditis elegans* (Ce) Srf3, and *Homo sapiens* (Hs) SLC35A2. Residues conserved in three or more sequences are highlighted in blue with darker color corresponding to a greater number of sequences that share the residue.

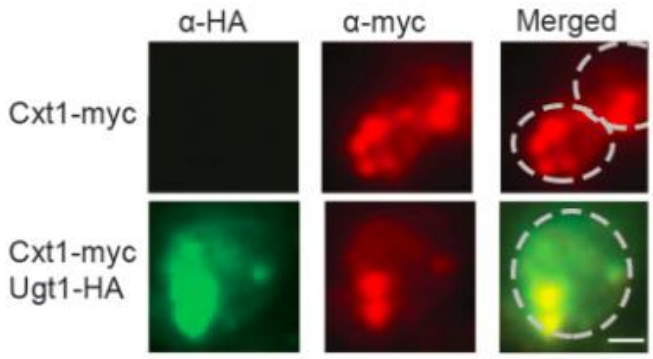

Figure A.S2. Cryptococcal Ugt1 colocalizes with a Golgi enzyme. Cells expressing Cxt1-myc alone (top row) or Cxt1-myc and Ugt1-HA (second row) were probed with antibodies to c-myc (red) and HA (green). Single wavelength and merged images are shown, all to the same scale (scale bar, 1 μm). Cell bodies are outlined with dotted gray lines over the merged image.

Appendix B: Other nucleotide sugar transporter candidates

While the majority of my thesis work focused on Uut1, Uxt1, and Uxt2, I also performed preliminary studies on an additional four NST candidates (G, J, L, and X). Below, I summarize my progress and suggest research directions for these proteins.

B.1 NST_G (CNAG_05674)

NST_G was identified by homology to the human UDP-GlcA transporter (1). Mutants lacking *NST_G* were hypocapsular (Fig. B.1), and expression of *NST_G* was upregulated ~2-fold during capsule induction (Fig. B.2). This initially suggested NST_G transported an activated donor of a capsule component, but prior work (2, 3) and this thesis identified NSTs responsible for all capsule glycan precursors. There were furthermore no detectable changes in capsule epitopes; induced *nst_G*Δ cells were recognized normally by anti-GXM antibodies, including those specific for Xyl and O-acetyl groups (Table B.1). GXM isolated from this strain also demonstrated no compositional differences from WT GXM (Table B.2), which suggested that there was a proportional reduction of all of the capsule monosaccharides.

We next directly assayed transport of a standard panel of 16 nucleotide sugars (as in Fig. 2.4) *in vitro* using proteoliposomes prepared from *S. cerevisiae* expressing NST_G. We did not, however, detect transport activity for any of the nucleotide sugars tested (Joshua Heazlewood, personal communication). Further phylogenetic analysis places NST_G in the same clade as triose phosphate transporters, so it may, instead, be a sugar phosphate transporter (i.e. G6P, F6P, IP6)

Beyond identifying the substrate(s) of NST_G, we were also interested in determining the physiological role of this NST. *nst_G*Δ exhibited only mild sensitivity to high salt and high pH at elevat-

ed temperature (Table B.3). The defects were insufficient to reduce its growth rate in the presence of macrophages *in vitro* (Fig. B.3), and the time of death for mice infected with this mutant was only slightly delayed compared to that of mice infected with control strains (Fig. B.4). There may be functionally redundant NSTs that mask the phenotypes from loss of NST_G although there are no close homologs of this gene in the cryptococcal genome. Alternatively, the luminal roles of the substrate may be dispensable for survival, or we might not have found the conditions under which the substrate is required. Elucidating the biochemical function of NST_G may help distinguish between these scenarios and explain the capsule size defect.

B.2 NST_J (CNAG_02036)

NST_J was initially identified by homology to the *Aspergillus fumigatus* UDP-Gal*f* transporter, GlfB (4). Deletion of nst_J did not affect capsule size or growth on stress plates (Table B.3), which is consistent with loss of Gal*f* in the capsule since loss of the Gal*f* mutase also produces no detectable phenotypes (5). We already have evidence that Uxt1 and Uxt2 transport UDP-Gal*f* (Fig. B.5). NST_J might transport substrate(s), including UDP-Gal*f*, for which there are additional overlapping NSTs. Given the lack of phenotypes, NST_J was a lower priority in our studies, and we did not pursue it in parallel with the other candidates.

B.3 NST_L (CNAG_02355)

NST_L was identified by homology to the human UDP-Xyl/UDP-GlcNAc transporter (6), but since deletion of *UXT1* and *UXT2* (Chapter 3) completely abrogates Xyl incorporation into glycoconjugates, it is unlikely that NST_L transports the same substrate(s). Loss of NST_L did not affect capsule size (Fig. B.1) or GXM shedding (Table B.1), and the mutant stained normally with

capsule antibodies and cell wall stains (Table B.1). NST_L, thus, does not seem to be required for capsule production, and NST_L expression was, in fact, repressed four-fold during capsule induction (Fig. B.2). We furthermore did not detect transport of any nucleotide sugars (standard panel of 16, including capsule donors) when we directly assayed transport *in vitro* using proteoliposomes prepared from *S. cerevisiae* expressing NST_L (Joshua Heazlewood, personal communication).

Mutants lacking NST_L demonstrated only a mild growth delay in response to standard stress assays (Table B.3). $nst_L\Delta$ also proliferated normally in culture (Fig. B.6) and in the presence of macrophages *in vitro* (Fig. B.7). Despite the limited defects *in vitro*, $nst_L\Delta$-infected mice were significantly delayed in time to death (Fig. B.4). We are interested in ascertaining the cause of this delay in virulence given the limited defects *in vitro*; greater insight may result from identification of the NST_L substrate(s).

B.4 NST_X (CNAG_05254)

NST_X was initially identified by homology to the *Arabidopsis thaliana* UDP-glucose transporter (7). $nst_X\Delta$ is hypocapsular (Fig. B.1), but there were no detectable differences in GXM composition compared to WT cells. Mutants were also sensitive to cell wall, cell membrane, and osmotic stress at high temperature (Table B.3) and grew slower than WT in the presence of macrophages *in vitro* (Fig. B.8). This mutant was extremely attenuated in virulence, with clearance from mice by 7 dpi (Fig. B.9).

The growth defects of *nst$_X$*Δ were partially complemented by the human CMP-sialic acid transporter (hCST; Fig. B.10). The presence of sialic acids in *C. neoformans*, however, is controversial. Although sialylated glycoproteins and sialyltransferase activity have been reported in *C. neoformans* (8-10), we have not detected sialic acids in several lab strains tested, and sequenced cryptococcal genomes do not encode homologs of known sialic acid synthetic machinery. Additionally, when we directly assayed transport *in vitro* using proteoliposomes prepared from *S. cerevisiae* expressing NST$_X$, we did not detect transport of any nucleotide sugars assayed, including CMP-sialic acid (standard panel of 16 nucleotide sugars; Josh Heazlewood, personal communication). It may be that the partial complementation is due to the ability of hCST to transport some other, as yet unknown, substrate.

The human homolog hCST appears to have an as yet undefined and transport-independent role in *O*-mannosylation (11). We collaborated with Dr. Dick Lefeber (Netherlands), who has generated a mutant form of hCST with no transport activity but preserved function in O-mannosylation (11). Plasmid-mediated expression of the WT and mutant forms of hCST, under control of an actin promoter, complemented *nst$_X$*Δ to the same extent at 30 °C, suggesting that the role in *O*-mannosylation is enough to achieve this level of complementation. However, neither one restored fungal growth at 37 °C (Fig. B.11). It may be that hCST requires additional interaction partners or protein modifications that are not present in *C. neoformans* to be completely functional as a replacement for NST$_X$, or that it cannot do so because of fundamental differences in activity.

B.5 Future directions

Since assays of these putative NSTs did not yield detectable transport of any nucleotide sugars *in vitro*, our collaborator (Dr. Joshua Heazlewood) is pursuing additional substrates that are structurally similar to nucleotide sugars and are known to be required in the Golgi and/or ER. Further compositional assays will be considered based on the identified substrate(s).

B.6 References

1. Muraoka M, Kawakita M, & Ishida N (2001) Molecular characterization of human UDP-glucuronic acid/UDP-N-acetylgalactosamine transporter, a novel nucleotide sugar transporter with dual substrate specificity. *FEBS Lett* 495(1-2):87-93.

2. Cottrell TR, Griffith CL, Liu H, Nenninger AA, & Doering TL (2007) The pathogenic fungus *Cryptococcus neoformans* expresses two functional GDP-mannose transporters with distinct expression patterns and roles in capsule synthesis. *Eukaryot Cell* 6(5):776-785.

3. Wang ZA, *et al.* (2014) *Cryptococcus neoformans* dual GDP-mannose transporters and their role in biology and virulence. *Eukaryot Cell* 13(6):832-842.

4. Engel J, Schmalhorst PS, Dork-Bousset T, Ferrieres V, & Routier FH (2009) A single UDP-galactofuranose transporter is required for galactofuranosylation in *Aspergillus fumigatus*. *J Biol Chem* 284(49):33859-33868.

5. Heiss C, *et al.* (2013) Unusual galactofuranose modification of a capsule polysaccharide in the pathogenic yeast *Cryptococcus neoformans*. *J Biol Chem* 288(16):10994-11003.

6. Ashikov A, *et al.* (2005) The human solute carrier gene SLC35B4 encodes a bifunctional nucleotide sugar transporter with specificity for UDP-xylose and UDP-N-acetylglucosamine. *J Biol Chem* 280(29):27230-27235.

7. Reyes F, *et al.* (2006) AtUTr1, a UDP-glucose/UDP-galactose transporter from *Arabidopsis thaliana*, is located in the endoplasmic reticulum and up-regulated by the unfolded protein response. *J Biol Chem* 281(14):9145-9151.

8. Rodrigues ML, *et al.* (2002) Sialylglycoconjugates and sialyltransferase activity in the fungus *Cryptococcus neoformans*. *Glycoconj J* 19(3):165-173.

9. Rodrigues ML, *et al.* (1997) Identification of N-acetylneuraminic acid and its 9-O-acetylated derivative on the cell surface of *Cryptococcus neoformans*: influence on fungal phagocytosis. *Infect Immun* 65(12):4937-4942.

10. Hamilton AJ, Jeavons L, Hobby P, & Hay RJ (1992) A 34- to 38-kilodalton *Cryptococcus neoformans* glycoprotein produced as an exoantigen bearing a glycosylated species-specific epitope. *Infect Immun* 60(1):143-149.

11. Riemersma M, *et al.* (2015) Disease mutations in CMP-sialic acid transporter SLC35A1 result in abnormal alpha-dystroglycan O-mannosylation, independent from sialic acid. *Hum Mol Genet* 24(8):2241-2246.

12. Gish SR, *et al.* (2016) Computational analysis reveals a key regulator of Cryptococcal virulence and determinant of host response. *MBio* 7(2):e00313-00316.

B.7 Figures

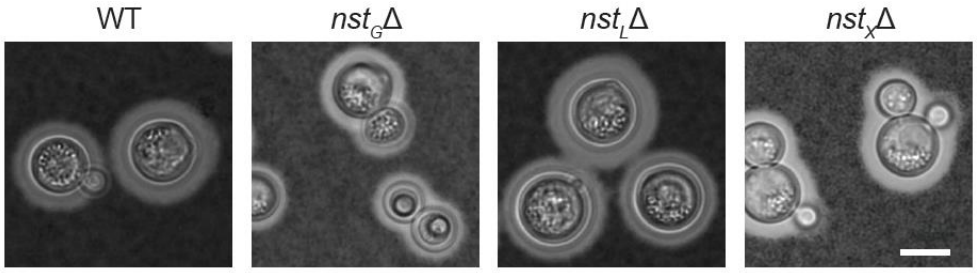

Figure B.1. *NST$_G$* and *NST$_X$* deletion mutants are hypocapsular compared to WT. Shown are light micrographs of WT, *nst$_G$*Δ, *nst$_L$*Δ and *nst$_X$*Δ grown in capsule-inducing conditions and visualized after negative staining with India Ink (scale bar = 5 μm).

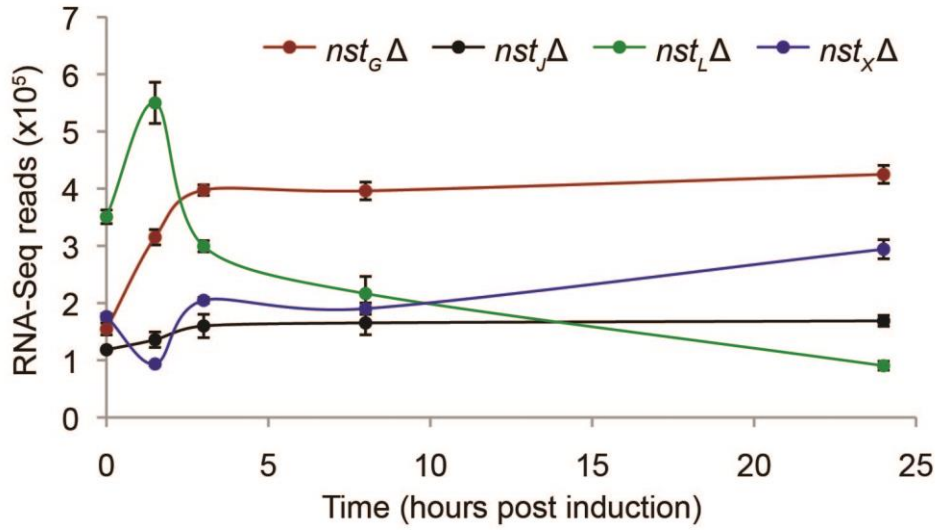

Figure B.2. Transcription of *NST$_G$*, *NST$_J$*, *NST$_L$*, and *NST$_X$* during capsule induction. Reads from RNA-Seq data (mean ± SD) during capsule induction were compiled from three independent experiments, each with RNA prepared from three biological replicates as in (12).

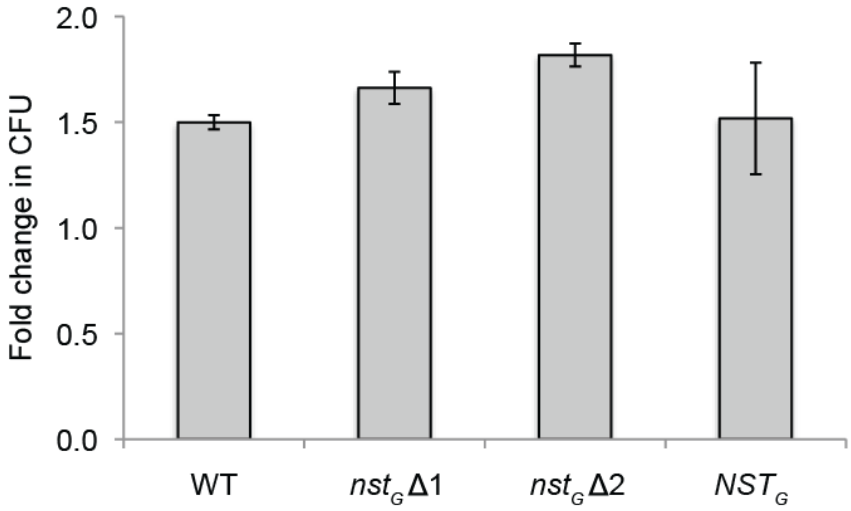

Figure B.3. Intracellular survival of cells lacking *NST$_G$* resembles that of wild-type *C. neoformans*. Fold-change in colony forming units (24 h:0 h) after internalization of opsonized fungi by THP-1 cells. Data are the mean ± SEM of three independent experiments.

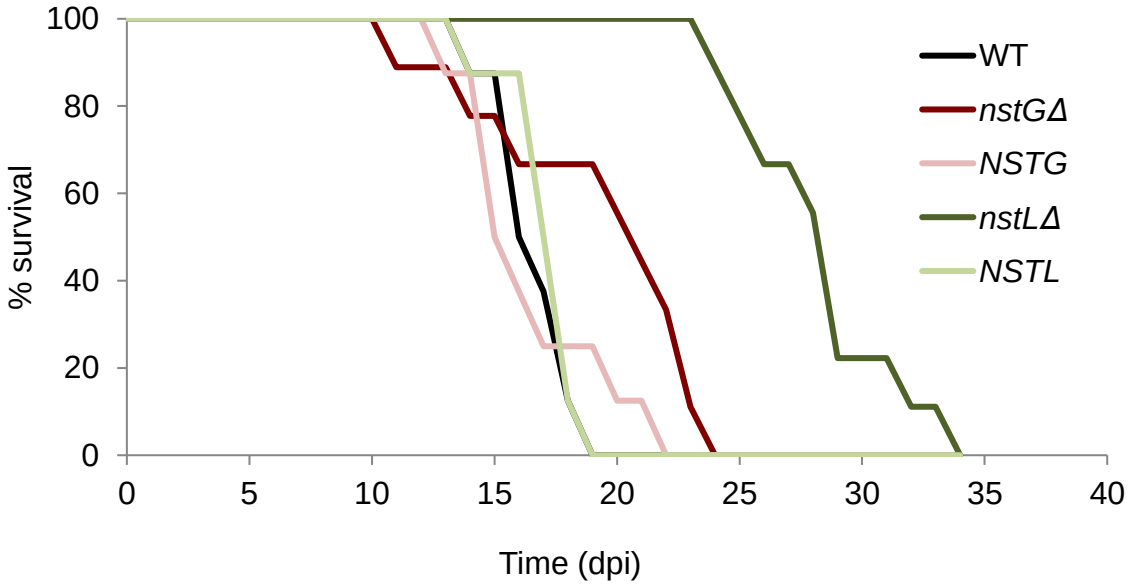

Figure B.4. Mice infected with *nst$_G$*Δ and *nst$_L$*Δ are delayed in time of death compared to those infected with wild-type cryptococci. Shown is survival of mice after intranasal inoculation with 5 × 10^4 cell of the indicated strains (n = 8-9).

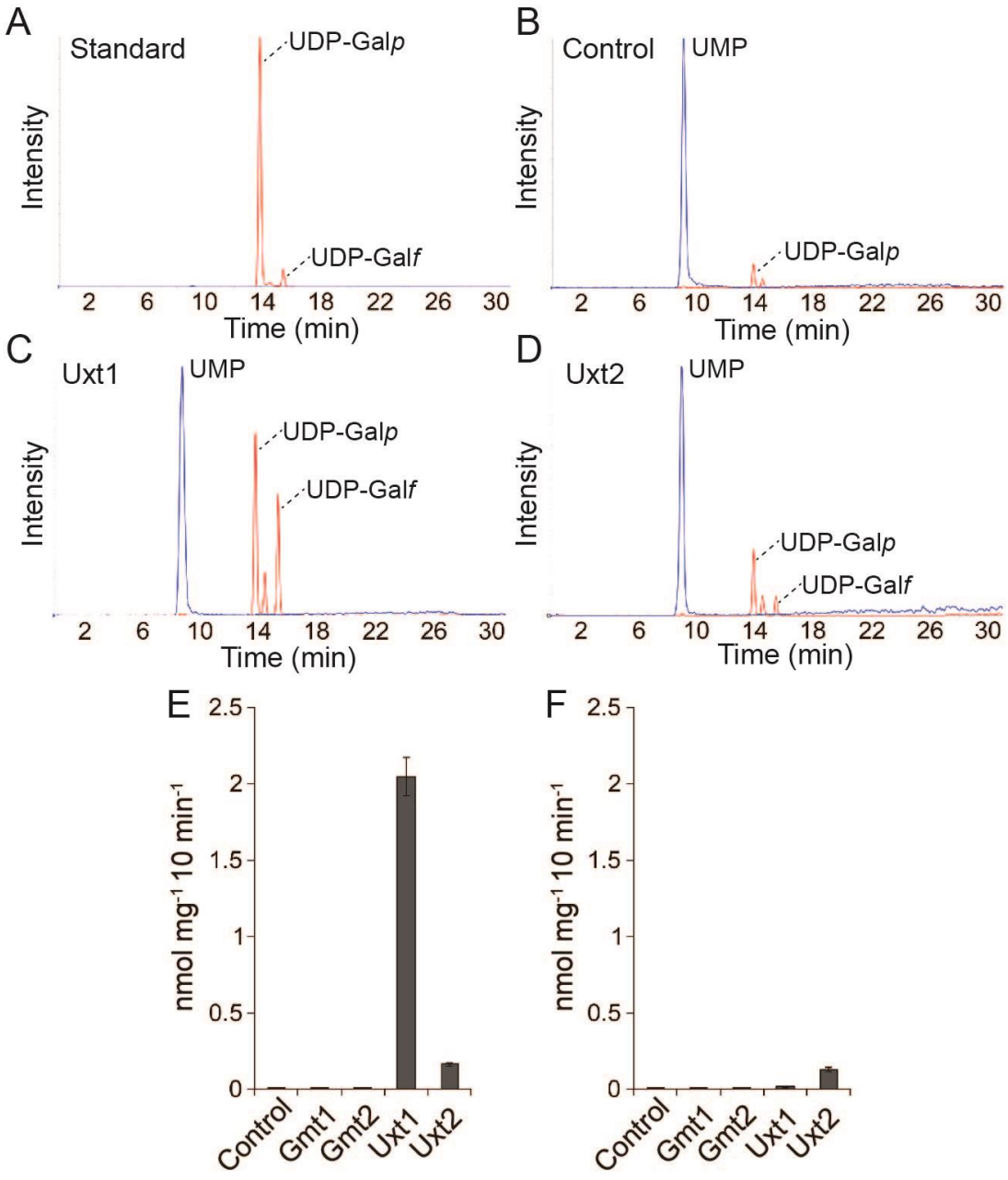

Figure B.5. Uxt1- and Uxt2-mediated UDP-Gal*f* uptake into proteoliposomes. (A) LC-MS/MS analysis of UDP-Gal*f* prepared from UDP-Gal*p* utilizing *E. coli* UDP-galactopyranose mutase (GLF). (B - D) Proteoliposomes prepared from *S. cerevisiae* expressing vector alone (B), Uxt1 (C), or Uxt2 (D) were preloaded with 30 mM UMP and analyzed by LC-MS/MS after a 10 min incubation with 700 mM UDP-Gal*p* and 10 mg purified GLF. (E and F) Quantification of nucle-

otide sugar uptake into proteoliposomes preloaded with (E) 30 mM UMP, or (F) 30 mM GMP. Data were normalized to the total protein content of the proteoliposome preparations (Table 3.S4) and show the mean ± SD of four assays. All assays were performed at 37 °C.

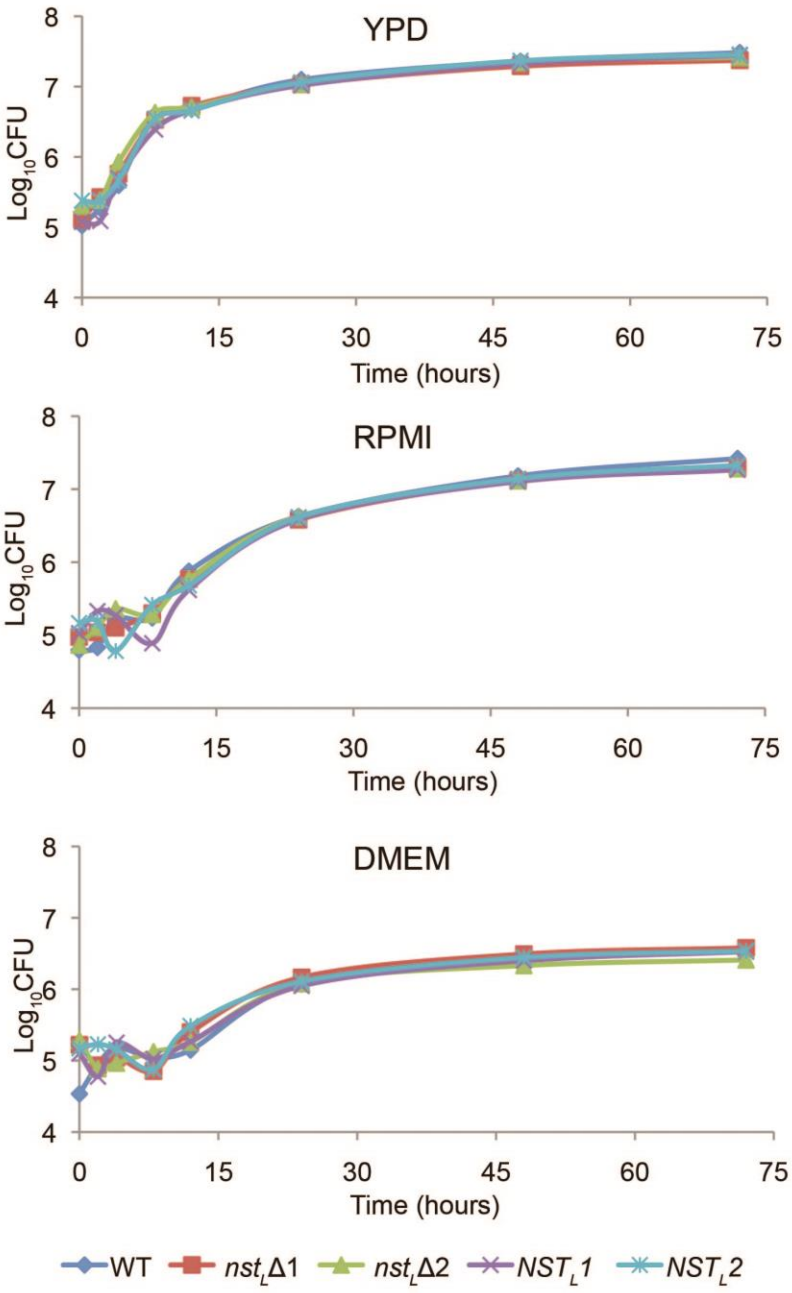

Figure B.6. *nst*$_L$Δ growth is not restricted at 37 °C. The indicated *C. neoformans* strains were grown overnight at 30 °C in YPD, diluted to 10^5 cells/mL in the media indicated, and incubated at 37 °C with 5% CO_2. The results shown are the averages of three measurements.

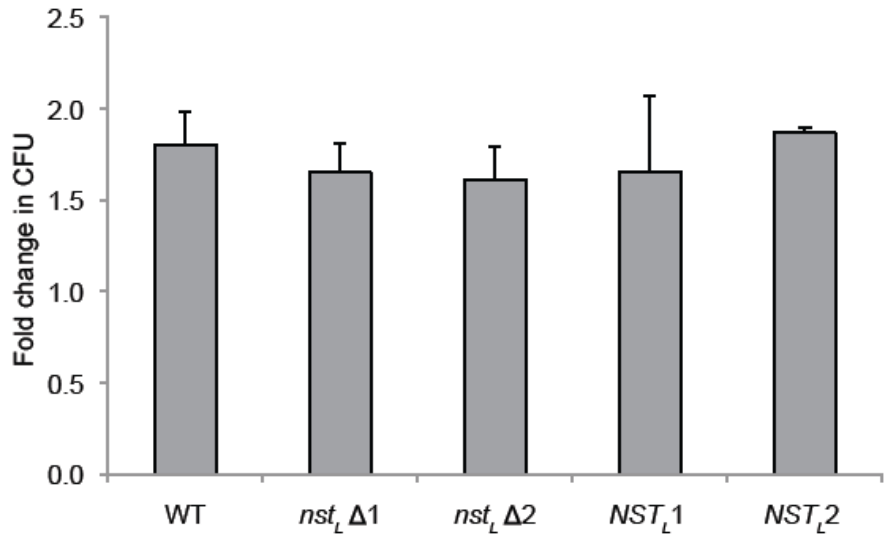

Figure B.7. Intracellular survival of cells lacking *NST*$_L$ resembles that of wild-type *C. neoformans*. Fold-change in colony forming units (24 h:0 h) after internalization of opsonized fungi by THP-1 cells. Data are the mean ± SEM of three independent experiments.

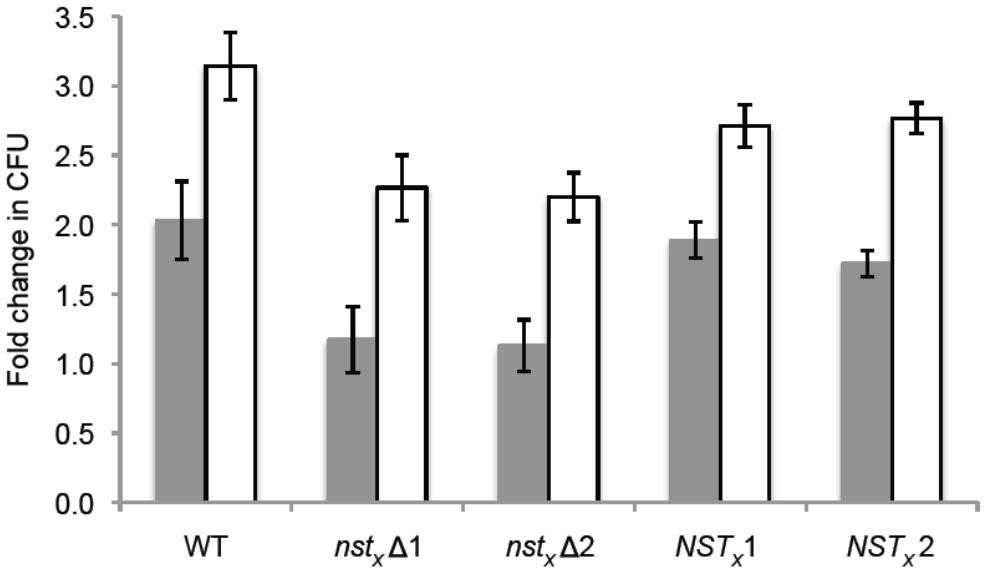

Figure B.8. *nst*$_X$Δ growth is delayed in the presence of THP-1s. Fold-change in colony forming units compared to 0 h after internalization of opsonized fungi by THP-1 cells (grey bars, 24 hpi; white bars, 48 hpi). Data are the mean ± SD (n = 3) from one representative experiment (of two independent experiments).

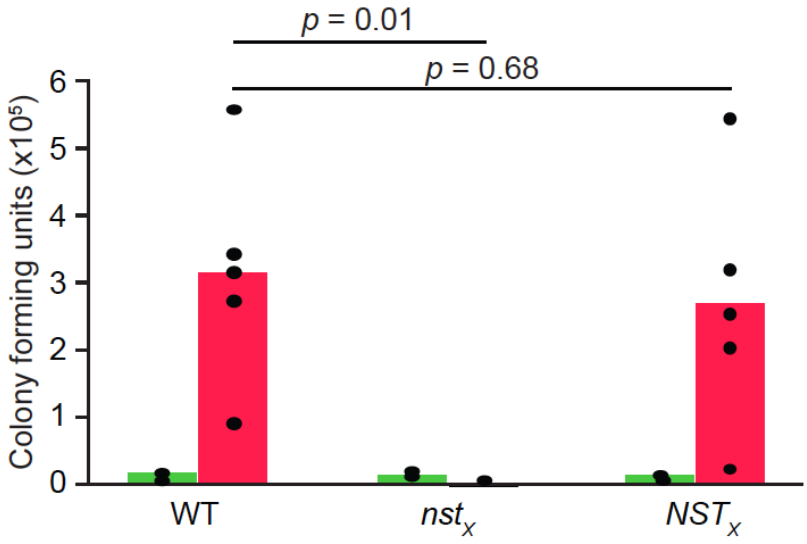

Figure B.9. *nst*$_X$Δ is cleared by 7 dpi in mice. Colony forming units in the lung 1 h (green bars) or 1 week (red bars) after intranasal inoculation of 10^4 cells of the indicated strains. Average and each value for groups of 5 mice are shown, with *p* values shown above.

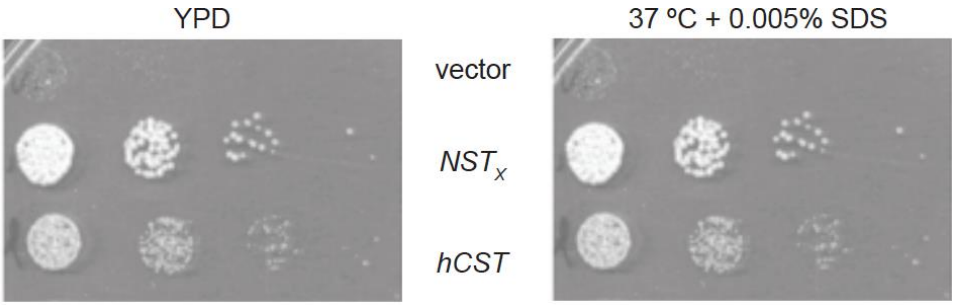

Figure B.10. hCST partially rescues *nst*$_X$Δ growth on SDS. Serial 5-fold dilutions on rich medium of *nst*$_X$Δ complemented with vector alone (v), NST_X, or the human CMP-sialic acid transporter (hCST). Left, 30 °C YPD; right, 37 °C + SDS.

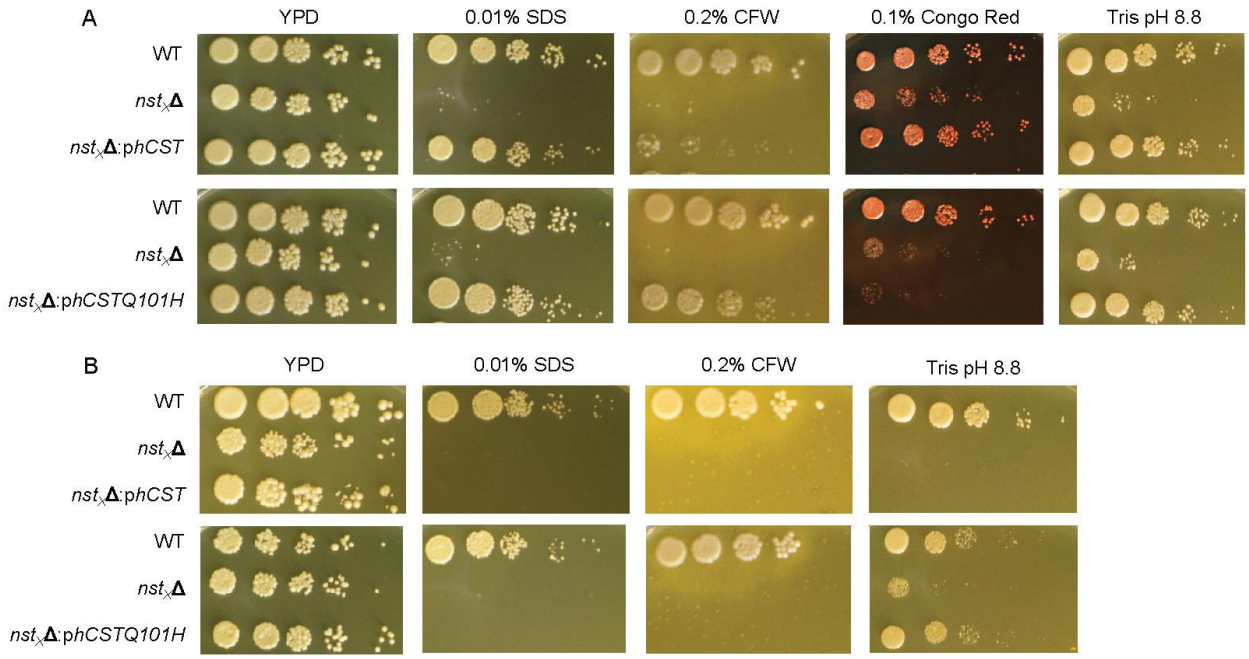

Figure B.11. Transport activity of hCST is not required to rescue *nst*$_X$Δ growth at 30 °C. Serial 5-fold dilutions on indicated medium of *nst*$_X$Δ complemented with vector alone (v), hCST, or the mutant hCST that lacks transport (Q101H) at (A) 30 °C and (B) 37 °C. Note that plasmid complementation may yield higher protein expression.

Table B.1. Capsule and cell wall phenotypes.

	Capsule size	GXM shedding	Capsule staining			Cell wall staining[a]				
Strain		339 + F12D2	339	302	F12D2	CFW	Pont	LY	EY	ConA
nst$_G$Δ	Hypo	NT[b]	+	+	+	NT	NT	NT	NT	NT
nst$_J$Δ	Normal	NT	NT	NT	NT	NT	NT	NT	NT	NT
nst$_L$Δ	Normal	Normal	+	+	+	+	+	+	+	+
nst$_X$Δ	Hypo	NT	+	NT	NT	NT	NT	NT	NT	NT

[a]CFW (binds chitin), Concanavalin A (ConA, binds mannoproteins), Eosin Y (EY, binds chitosan), and Lucifer yellow (LY, binds unspecified cell wall components), and Pontamine (Pont, binds unspecified cell wall components)
[b]NT, not tested

Table B.2. Glycosyl composition analysis of GXM.

	WT[a]	*nstG*Δ
Xylose[b]	28.1	24.1
Glucuronic acid	9.9	11.2
Mannose	61.9	64.6

[a] Jec21 is the wild-type strain for these studies.
[b] Values are reported as mole percent.

Table B.3. Dot plating phenotypes.[a]

	G		J		L		X	
	30 °C	37 °C	30 °C	37 °C	30 °C	37 °C	30 °C	37 °C
YPD								
Tris pH 8.8								
1.2 M NaCl								NT[b]
1.2 M KCl								NT
1.5 M Sorbitol							NT	NT
0.2% CR						NT		
2 mg/mL CFW								
0.2% Caffeine							NT	NT
0.01% SDS								
YNB							NT	NT
10 mM H_2O_2						NT	NT	NT
10 mM $NaNO_2$						NT	NT	NT

[a] Yellow, no difference from WT; Blue, reduced growth compared to WT; Dark blue, no growth.
[b] NT, not tested